Year : 2023

Evolution of olfactory pathways in drosophilids

Álvarez-Ocaña Raquel

Álvarez-Ocaña Raquel, 2023, Evolution of olfactory pathways in drosophilids

Originally published at : Thesis, University of Lausanne

Posted at the University of Lausanne Open Archive http://serval.unil.ch
Document URN : urn:nbn:ch:serval-BIB_39B43BE8A0F34

UNIL | Université de Lausanne
Faculté de biologie
et de médecine

Center for Integrative Genomics (CIG)

Evolution of olfactory pathways in drosophilids

Doctoral thesis in Life Sciences

Presented to:

Faculty of Biology and Medicine
of the University of Lausanne

by:

RAQUEL ÁLVAREZ-OCAÑA
Master from the University of Lausanne

Jury

Prof. CHRISTIAN WIDMANN, President
Prof. RICHARD BENTON, Director
Prof. BRUNO LEMAITRE, Expert
Prof. EMI NAGOSHI, Expert
Prof. SIMON SPRECHER, Expert

Lausanne
2023

UNIL | Université de Lausanne
Faculté de biologie
et de médecine

Center for Integrative Genomics (CIG)

Evolution of olfactory pathways in drosophilids

Doctoral thesis in Life Sciences

Presented to:

Faculty of Biology and Medicine
of the University of Lausanne

by:

RAQUEL ÁLVAREZ-OCAÑA
Master from the University of Lausanne

Jury

Prof. CHRISTIAN WIDMANN, President
Prof. RICHARD BENTON, Director
Prof. BRUNO LEMAITRE, Expert
Prof. EMI NAGOSHI, Expert
Prof. SIMON SPRECHER, Expert

Lausanne
2023

UNIL | Université de Lausanne
Faculté de biologie
et de médecine

Ecole Doctorale
Doctorat ès sciences de la vie

Imprimatur

Vu le rapport présenté par le jury d'examen, composé de

Président·e	Monsieur	Prof.	Christian	**Widmann**
Directeur·trice de thèse	Monsieur	Prof.	Richard	**Benton**
Expert·e·s	Monsieur	Prof.	Bruno	**Lemaitre**
	Madame	Prof.	Emi	**Nagoshi**
	Monsieur	Prof.	Simon	**Sprecher**

le Conseil de Faculté autorise l'impression de la thèse de

Raquel Álvarez Ocaña

Master en biologie médicale, Université de Lausanne

intitulée

Evolution of olfactory pathways in drosophilids

Lausanne, le 19 janvier 2023

pour le Doyen
de la Faculté de biologie et de médecine

Prof. Christian Widmann

TABLE OF CONTENTS

ACKNOWLEDGEMENTS

Closing this chapter wouldn't have been possible without the support of a lot of people that made me enjoy every step of the journey.

Richard Benton, thank you. Thank you for trusting me and giving me the opportunity of becoming a better scientist. Thank you for pushing me to be independent but also for teaching me that help is always at reach when you ask for it. Thank you for the long scientific (and less scientific) discussions we had. Thank you for your support and understanding when things were wobbling around me. I couldn't have asked for a better PhD supervisor to look up to.

Thank you to the former and past members of the Benton Lab. It has been incredible being surrounded by so many different cultural and scientific backgrounds from which I could learn.

Thanks to the members of my thesis committee for their time, feedback and suggestions on my always evolving thesis project.

Thanks to Iris Marouani for her always essential administrative help.

Another big thanks to Thomas Auer and Roman Arguello. From the beginning of my master thesis to the end of my PhD they have always been of extreme support and help. I consider them two walking encyclopedias.

Thanks to Liliane Abuin. She has been like an aunt to me.

Thank you to Jan Armida and Juan Sánchez Alcañiz. They clearly knew how to make me laugh even about my own mistakes (like when I rushed into running a gel with undigested plasmid mix because there was an important seminar I needed to attend).

Thanks to Michael Shahandeh and Daehan Lee for mediating in between my hate-love relationship with R Studio and statistics.

Gracias, Andrea. Siempre fuiste la hermana que nunca tuve y todos quisieran tener.

Gracias, abuelo. Gracias, abuela. Vuestro cariño y amor siempre han estado presentes.

Gracias, hermano. Aún recuerdo el momento en el que decidí embarcarme en esta aventura y tu sorpresa, mezcla de admiración y pena, cuando dijiste “sabía que algún día te marcharías de casa, pero no pensé que fuera tan pronto”. Aún así, siempre te he sentido cerca.

Gracias, mamá. Gracias, papá. Por vuestro apoyo y amor incondicional en cada una de las etapas de mi vida. Gracias por darme alas y hacerme saber que todo es posible cuando uno lucha por lo que quiere. Gracias por luchar siempre conmigo.

Thanks to the furry members of my family for their unconditional love and for brightening up every day of my life with their fluffiness.

Thank you Ágata for making me see the huge amount of love I can give, for helping me realize how patient I can be and for improving my project management skills. Thanks for all the sleep-full nights that made my daily life way easier. But most of all, thank you for every cooing, every giggle, every smile and every laugh that made me feel fulfilled. You are my most important project.

And finally, but not least, thanks to my best friend, Christopher. Thank you for your patience and support. Thank you for knowing me even better than I know myself. Thank you for every hug. Thank you for picking up every tear I had and making a piña colada cocktail with it. Thank you for being my #1 fan and always believing in my capacity. You have been essential for this success.

I always joked about the PhD being a very long pregnancy. What a surprise when I found out that 2022 would be the double-delivery year.

ABSTRACT

Animal's behaviors are governed by complex signaling pathways that diverge in their function and architecture. This is evident when analyzing the enormous diversity of brain sizes and brain structures across the animal kingdom (Herculano-Houzel 2012). However, the molecular mechanisms responsible for these changes are nor very well understood. To shed some light on the genetic and neural mechanisms that drive behavioral adaptations in animals, I have examined the olfactory system of *Drosophila melanogaster* and its closely related species as model systems to tackle evolutionary questions. *D. melanogaster*'s well-described neuroanatomy, accessibility, and easy manipulation, as well as its mapped olfactory pathways (Couto, Alenius and Dickson 2005, Grabe et al. 2016), make this organism a preeminent model for sensory neurobiology and evolutionary genetic studies.

During the time course of my thesis, I have worked on the following topics:

- The evolution of peripheral organs, including Odorant receptor (*Or*) gene copy number variations, Or tuning and variations in Olfactory Sensory Neurons (OSNs) population size (Chapter 2). In this work, I and my co-authors have described a novel species-specific olfactory sensory adaptation driven by changes in *Or* gene copy number.
- The evolution of olfactory processing centers, including changes in the representation of the olfactory information in the central brain (Chapter 3). In this section, I analyze species-specific expression pattern of neuromodulators and describe species-specific odorant representation in the central brain.

- The behavioral consequences of species-specific olfactory system adaptations using *Drosophila*'s egg lying behavior as read-out (Chapter 4). With the help of some collaborators, in this chapter I show species-specific oviposition behavioral adaptations that required the acquisition of novel response profiles of a (at least one) olfactory receptor gene.

Overall, I have learned that behavioral evolution is governed by complex and multiple mechanisms that exert evolutionary pressures at different levels on the fly's olfactory system (periphery and central brain) to control species-specific behaviors.

RÉSUMÉ EN FRANÇAIS

Le comportement des animaux est régi par des voies de signalisation complexes qui divergent dans leur fonction et leur organisation. Cela est évident lors de l'analyse de l'énorme diversité des tailles de cerveaux et des structures cérébrales à travers le règne animal (Herculano-Houzel 2012). Cependant, les mécanismes moléculaires responsables de ces changements ne sont pas très bien compris. Pour mieux comprendre les mécanismes génétiques et neuronaux qui déterminent les adaptations comportementales chez les animaux, j'ai examiné le système olfactif de la *Drosophila melanogaster* et de ses espèces étroitement apparentées en tant que modèles pour aborder les questions évolutives. La neuroanatomie, l'accessibilité et la facilité de manipulation bien décrites de *D. melanogaster*, ainsi que ses voies olfactives cartographiées (Couto, Alenius et Dickson 2005, Grabe et al. 2016), font de cet organisme un modèle prééminent pour la neurobiologie sensorielle et les études génétiques évolutives.

Au cours de ma thèse, j'ai travaillé sur les sujets suivants :

- L'évolution des organes périphériques, y compris les variations du nombre de copies du gène du récepteur odorant (Or), l'ajustement de l'Or et les variations de la taille de la population des neurones sensoriels olfactifs (OSN) (chapitre 2). Dans ce travail, moi et d'autres co-auteurs avons décrit une nouvelle adaptation sensorielle olfactive propre à chaque espèce, entraînée par des changements dans le nombre de copies du gène Or.

- L'évolution des centres de traitement olfactif, y compris les changements dans la représentation de l'information olfactive dans le système nerveux central (Chapitre 3). Dans cette section, j'analyse l'expression des neuromodulateurs propre à chaque espèce et décris leur représentation odorante correspondante dans le système nerveux central.

- Les conséquences comportementales des adaptations du système olfactif propres à chaque espèce en utilisant la ponte des œufs de la drosophile comme paramètre de mesure (chapitre 4). Avec l'aide de quelques collaborateurs, je montre dans ce chapitre des adaptations comportementales de ponte spécifiques à chaque espèce qui ont nécessité l'acquisition de nouveaux profils de réponse d'au moins un gène du récepteur olfactif.

Dans l'ensemble, j'ai appris que l'évolution comportementale est régie par des mécanismes complexes et multiples qui déploi des pressions évolutives à différents niveaux sur le système olfactif de la mouche (au niveau périphérique et système nerveux central) pour contrôler les comportements spécifiques à chaque espèce.

CHAPTER 1: GENERAL INTRODUCTION

In this chapter, I will describe basic concepts regarding behavioral evolution, and I will highlight examples of behavioral adaptation across related animal species.

1.1. What is behavior and how do behaviors evolve?

The word “behavior” refers to the way animals, including humans, act in a particular situation or under certain conditions, ranging from simple reflexes to complex sequences of actions. Behaviors are generally triggered by sensory perception, and they are the result of the interaction of external stimuli and the animal’s internal motivation state (i.e., starved animals will seek food sources more persistently, and sexually mature animals will court potential mating partners). When studying animal behavior, researchers are interested in understanding how animals move in their environment, the way they socially interact and how they learn from the stimuli that surround them.

The genetic information controlling sensory perception and the way it is processed, motivation, and neuronal development and plasticity, are important for determining behavior. At the same time, the morphological and physiological features intrinsic to each species will be instrumental for an adaptive behavioral output.

Animal’s behaviors must evolve (change over time in response to selective pressures) and adapt (to be better suited to its environment and increase their fitness) to the ever-changing conditions where animals live. Adaptations can occur through changes at different levels, such as sensory perception, processing of internal information (given by the feeding or reproductive state, for

example), or by modulating motor outputs. From Charles Darwin and his theory of evolution (Darwin 1859) – built through the systematic observation and annotation of interspecific behavioral differences – to nowadays, the way to study evolutionary adaptations have changed. Thanks to the development of new tools to study changes over time across animal species, evolutionary biologists are now capable to relate single genetic mutations with behavioral adaptive traits in animals.

1.2. Genetic approaches to study the evolution of behavioral traits

Generally, the first step towards understanding behavioral evolution is to compare closely related species that display marked differences in at least one of their behaviors. The more similar their genomes, the easier it will be to spot genetic variations by genomic alignments of regions of interest (such as the loss of sweet gustatory receptor in cats (Li et al. 2006)) and subsequent mutagenesis experiments (methodology used, for example, in flies (Auer et al. 2020, Prieto-Godino et al. 2017)).

Genomic-wide association studies (GWAS) are observational studies that help scientist identify genes associated to a particular trait. Through the analysis of the entire genome in a broad group of individuals having varying phenotypes, they can identify single nucleotide polymorphisms (SNPs) – or genomic variants – that can be linked to an observed trait (Hardy and Singleton 2009).

Another broad linkage-based mapping technique used is Quantitative Trait Locus (QTL). Through the generation of hybrid individuals that are unilaterally back crossed to the parental lines, QTL allows the genetic characterization (or mapping) of certain phenotypic traits that vary to a certain extent and can be associated to monogenic or polygenic effects, as well as to changes in the

environment. Extensive QTL approaches both in fruit flies and mice have revealed a high complexity in the genetic architecture of behavioral traits meaning that, although there are exceptions, behaviors are far from being explained by single-gene mutations (Edwards and Mackay 2009, Flint 2003, Jordan, Morgan and Mackay 2006). While these genetic methods can provide high-resolution mapping of candidate genes, the next steps necessary to describe the causality of gene expression are rarely taken. Furthermore, these studies have their limitations: small sample sizes, lack and not so well-defined controls, or a low reproducibility are the main caveats (Tabor, Risch and Myers 2002).

Candidate-gene approaches, on the other hand, constrain the analysis to relatively fewer numbers of genes based on prior hypothesis and focus on describing gene function. There are at least three tests that provide information about the phenotypic variation harbored by a candidate gene (Stern 2014). One of them is the homologous recombination (= gene targeting) test, that consists in the genetic replacement of a genomic region of interest with its orthologous genomic region from another strain or species. Although less precise, transgenesis has also been employed to explain the causality of gene differences between organisms. Generally, loci of interest from different species are transferred into a model organism in which transgenesis is more efficient and simpler. A third method is the reciprocal hemizygosity test, easier to use than the homologous recombination test and sorts some of the limitations of transgenesis. In brief, this test compares genetically identical hybrids that only differ on the locus of interest, which is formed by the two parental alleles – therefore hemizygous – (Stern 2014). If differences between the two reciprocal hemizygous

genotypes are observed, this can be explained by the evolution of the two parental alleles.

Although the genetic tests previously mentioned serve of general use to address gene-phenotype associations, many behaviors are far from being mono-allelic and alternative approaches are needed. Thanks to the increasing understanding of the phenotype, architectural organization of tissues, and genes and proteins' function, we can now perform more direct evolutionary analysis by performing comparative neuroanatomy and comparative neurophysiology studies. In fact, these types of studies are the ones I have employed during my thesis work, and they will be explained throughout the chapters of this thesis.

In the next section (1.3.) I will discuss several examples of behavioral evolution that have been studied using (some) of the methodologies mentioned above.

1.3. Examples of behavioral evolution in closely related species

Below, I highlight some of the most studied cases of interspecific behavioral evolution, which have (partially) identified the underlying genetic mechanisms.

1.3.1. Burrowing behavior in deer mouse species

Burrowing is an ecologically relevant behavior that greatly varies across related species of deer mouse in North America (Metz et al. 2017). For example, *Peromyscus polionotus* individuals show precocious digging behaviors, starting at 17 days after birth, building deeper and longer tunnels an incorporating an escape tunnel that projects back towards the surface away from the main burrow entrance. By contrast, *P. maniculatus*, starts its burrowing activity 10 days later,

excavating more superficial and shorter tunnels that lack an escape path. After comparing morphology, size and activity rate among these two species, it was concluded that the precocious burrowing in *P. polionotus*, as well as the length of the tunnels, reflected a behavioral difference that was not due to physiological or morphological advantages (such as bigger or stronger limbs) in *P. polionotus* pups (Metz et al. 2017, Weber, Peterson and Hoekstra 2013).

This study also disentangles the effects of genetics from environment by reciprocally cross-fostering pups of the two species of deer mouse. After analyzing burrowing onset, length and depth of the tunnels, they found no differences in burrowing behavior across the cross-fostered individuals. These data suggest that the parental phenotype does not influence pups' behavior, revealing a strong genetic component to the development of burrowing behavior.

F1 hybrid crosses between the sibling species revealed a dominant genetic contribution from *P. polionotus* to burrowing behavior. The subsequent generation of hybrid backcrosses accompanied by QTL data showed that a common genetic region – formed by a single pleiotropic gene or a group of genes – was linked to precocious burrowing as well as to variation in tunnel length (Hu et al. 2022). In fact, it has been described that the behavioral differences observed in these species of mice can be explained by distinct *cis*-regulatory networks controlling locomotor-related genes' expression (Hu et al. 2022).

1.3.2. Schooling behavior in marine and freshwater sticklebacks

Schooling is a complex social grouping behavior in which many fish get together maintaining a coordinated body position and display a synchronized swimming appearing to act as a single organism. Group behaviors provide

several benefits, such as safety for the individual, but it can also be detrimental in some cases, so the frequency of schooling will vary depending on the ecological context. This behavior is commonly observed in clupeiform fish such as sticklebacks (*Gasterosteus aculeatus*). Populations of sticklebacks from marine environments or from freshwater regions display divergent schooling behavior. Lab-raised marine sticklebacks show strong schooling while lab-raised benthic sticklebacks have considerably reduced their schooling capacity (Wark et al. 2011).

First, to reveal the genetic basis of schooling behavior diversity in sticklebacks, a model school assay and a parallel QTL analysis with 229 benthic-marine F2 hybrids were developed. Two genetically separated fundamental components of schooling were described at first: schooling tendency (referring to the time, latency and the number of schooling sessions) and schooling position (referring to the body and head disposition). While they were able to identify two QTL associated with schooling position, they could not identify any QTL for schooling tendency, suggesting a multigenic regulation of these features or an important environmental component over it (Greenwood et al. 2013).

Second, the neurosensory phenotypes associated with schooling behavior were analyzed, and visual cues and the lateral line (a mechanoreceptive sensory system consisting of hair cells that detect changes in the water flow) were strong candidates to influence position and orientation during schooling. However, while vision differences across populations of sticklebacks were discarded, benthic sticklebacks display a very superficial lateral line. Interestingly, a common QTL for both schooling position and aspects of the lateral line anatomy was detected

(Wark et al. 2012), which favors the hypothesis that the differences observed on schooling behaviors are due to sensory modifications of the lateral line.

1.3.3. Courtship song behavior in fruit flies

During courtship behavior in fruit flies, males vibrate their wings producing songs that are attractive for females. Interestingly, the courtship songs are species-specific, and they are relatively easy to quantify (Greenspan and Ferveur 2000), making them powerful candidate behaviors for evolutionary genetics studies. Two different components can be differentiated in within the courtship song: sine song (continuous sound at a certain frequency) and pulse song (series of pulses separated by intervals) (Greenspan and Ferveur 2000). In the close-related species *D. simulans* and *D. mauritiana* some courtship song components have diverged, such as the carrier frequency of sine song (Ding et al. 2016).

The *slowpoke* gene encodes a calcium-activated potassium channel and regulates male's singing performance during mating (Atkinson, Robertson and Ganetzky 1991). Through QTL mapping and reciprocal hemizygosity tests (Stern 2014), a genetic difference in the *slowpoke* locus – caused by a retrotransposon – could explain why certain strains of *D. simulans* males sing lower frequencies of sine song compared to *D. mauritiana* males (Ding et al. 2016). This study illustrates how a highly pleiotropic gene can modulate species-specific behaviors in flies.

1.3.4. Mate preference in flies

Among the different decisions that animals make, the choice of a mating partner will directly impact their evolutionary success (Arbuthnott et al. 2017).

During speciation, reproductive isolation is driven by genetic and behavioral differences that will reinforce the species identity and will minimize interspecies sexual encounters. As an example, *D. melanogaster* and *D. simulans* are two co-occurring cosmopolitan species and yet they rarely or never hybridize. How are they capable of selecting conspecific mates? One mechanism is directed using sexual species-specific pheromones that control courtship attraction between different sexes of the same species and mediates courtship avoidance between individuals of the same sex or between different species (Jallon and David 1987).

D. melanogaster females produce 7,11-heptacosadiene (7,11-HD), a pheromone that elicits courtship in *D. melanogaster* males but keeps *D. simulans* males from courting (Jallon and David 1987). Through the comparison of pheromone information processing pathways in males, the mechanism by which *D. melanogaster* and *D. simulans* endow 7,11-HD with the opposite behavioral valence to allow inter-species discrimination was described (Seeholzer et al. 2018). In brief, homologous peripheral sensory pathways $Ppk23^{+}$ (Ppk23 DEG/ENaC channel) in males of both species similarly detected 7,11-D (Lu et al. 2012). However, this information was differentially transduced to P1 neurons – neurons that form the central node of the Fru^{+} (*fruitless*-expressing neurons) circuitry and initiate courtship behavior in *D. melanogaster* (Kallman, Kim and Scott 2015) – due to alternative excitability of GABAergic interneurons (Seeholzer et al. 2018) that antagonize the excitatory input elicited by 7,11-D in *D. simulans* males. With this study the authors revealed how alterations in synaptic excitability, and not necessarily circuitry architecture modifications, led to behavior diversification.

Overall, these studies provide valuable genetic and behavioral information on the evolution of innate behaviors and reveal strong genetic components across closely related species. In my thesis projects, I wanted to further investigate behavioral evolution using the olfactory system of flies as model system.

1.4. Olfaction as a model system to understand behavioral evolution

Chemosensory systems, such as olfaction, have been of great help to study evolutionary mechanisms since chemoreceptor gene families are characterized for rapid gene number changes (Arguello et al. 2016, Auer, Shahandeh and Benton 2021, D'Oliveira Albanus et al. 2014, Hansson and Stensmyr 2011, McBride, Arguello and O'Meara 2007, Niimura, Matsui and Touhara 2014, Robertson 2019, Robertson and Wanner 2006).

Odors can either be attractive cues to recognize mates, feeding or mating substrates, or repulsive cues to avoid predators and other hazardous organisms. When the environmental conditions change, the chemical inputs and therefore how they are perceived by animals will also change. Because olfactory systems mediate in between the external chemical cues and the internal state of the organism, olfactory systems are believed to be under strong selective pressures making olfaction evolve rapidly (Arguello et al. 2016). A well characterized example displaying fast sensory evolution is the nematode *Caenorhabditis*. In the context of social interactions, two species of *Caenorhabditis* have exhibit parallel evolution of their pheromone receptor genes repertoire to adapt to high density growth. Two strains of *C. elegans*, when raised in high density environments in laboratory conditions, have acquired multigenic resistance to a pheromone responsible for inducing dauer formation – a long-lived but not-reproductive state

– (Golden and Riddle 1984b, Golden and Riddle 1984a, McGrath et al. 2011). QTL mapping described a deletion that disturbs the *serpentine receptor class g (srg)-36* and *37* genes causing resistance to the pheromone ascaroside C3 controlling this behavior. Similarly in *C. briggsae*, multigenic resistance has also arisen due (in part) to a deletion in the paralogous *srg* gene. These events argue for the fact that variations in the environment can cause repeated modifications in the chemosensory gene repertoire.

1.5. *Drosophila* species as model system to understand the evolution of olfactory systems in insects

Drosophilids represent one of the most extensively characterized examples of peripheral olfactory circuit evolution (Zhao and McBride 2020). They have recently emerged as interesting models to study the genetic basis of olfactory evolution due to the species-specific odor-driven behaviors that include foraging, mating and oviposition (Dekker et al. 2006, Linz et al. 2013, Markow, Beall and Matzkin 2009, Prieto-Godino et al. 2017).

In nature, instances of drosophilids with very diverse ecologies have been reported. Some of them are considered generalists, which are species capable of exploiting a large diversity of food substrates for feeding or reproduction, such as *D. melanogaster* and *D. simulans* (Markow et al. 2009) or *D. mauritiana* (Garrigan et al. 2012, Stensmyr, Dekker and Hansson 2003). Others are considered specialists, which are species with very stringent adaptations to certain fruits/plants such as *D. sechellia* and its high specialization to the – toxic for other species – *Morinda citrifolia* fruit in the Seychelles islands (Auer et al.

2021, Dekker et al. 2006, Markow et al. 2009), or the cactophilic *D. mojavensis* in the Sonoran Desert (Matzkin et al. 2006). A third group is formed by species of flies with intermediate phenotypes, such as the seasonal specialism of *D. erecta* to the *Pandanus* fruit. While some species exploit rotten fruits and are attracted to their fermented compounds, other species such as the agricultural pest *D. suzukii* have developed phenotypical adaptations (a serrated ovipositor) that allows them the exploitation of sugar-enriched ripening fruits (Akutsu and Matsuo 2022, Dweck et al. 2021, Karageorgi et al. 2017, Keesey, Knaden and Hansson 2015).

Evolutionary analyses are possible with these – and many other – drosophilid olfactory systems since, first, they have a simple neuronal architecture that has been thoroughly described (Dekker et al. 2006, Linz et al. 2013, Prieto-Godino et al. 2017). Second, there is extensive knowledge about the olfactory function which can be easily monitored by physiological techniques such as electrophysiology (in the periphery) or calcium imaging (in the central brain). Third, we can take advantage of the recent and rapidly increasing number of genetic tools available across drosophilids. Finally, their genomes have been sequenced, making genetic inter-species comparisons and genotype-phenotype associations easier (Drosophila 12 Genomes et al. 2007).

1.6. Organization of the olfactory system in *Drosophila*

The periphery of the olfactory sensory system in *Drosophila* consists of a pair of antennae and maxillary palps. Each antenna consists of three different segments ((a1-a3) also known as the scape, pedicel and funiculus, respectively). The third segment of the antenna contains many OSNs (Couto et al. 2005) and mediates both long- and short-range behaviors (Auer et al. 2020). The maxillary

palps consist of a single segment that contains olfactory neurons displaying overlapping functions to the antenna (de Bruyne, Clyne and Carlson 1999, Shiraiwa 2008, Vosshall and Stocker 2007), probably necessary to discriminate feeding substrates in combination with the gustatory neurons situated in the mouth parts (Shiraiwa 2008).

In *Drosophila*, many chemosensory receptors involved in the recognition of chemical volatiles are members of the Odorant receptor (Or) and Ionotropic receptor (Ir) families (Benton et al. 2006, Benton et al. 2009, Vieira and Rozas 2011, Vosshall et al. 1999, Vosshall and Stocker 2007). Ors are seven-transmembrane domain odor-gated ion channels unrelated to the mammalian GPCR-family Ors (Benton et al. 2006). Irs have evolved from ionotropic glutamate receptors (iGluRs) and generally occupy different locations in the antenna (Benton et al. 2009, Rytz, Croset and Benton 2013)). Olfactory receptors are expressed by OSNs whose ciliated sensory dendrites are protected from the external environment by porous cuticular hairs, called sensilla, projecting from the surface of the olfactory organs. Sensilla can be classified into four morphological groups: basiconic, coeloconic, trichoid and intermediate sensilla (Couto et al. 2005, Lin and Potter 2015, Vosshall and Stocker 2007). OSNs send axonal projections from the antenna to the antennal lobes in the central brain (Figure 1B-C). Generally, OSNs express only one type of Or, although a few exceptions have been described (Couto et al. 2005, Grabe et al. 2016). OSNs expressing the same Or extend axonal projections to one of the 58 regions of neuropil (glomeruli) in the antennal lobe (Barish and Volkan 2015, Couto et al. 2005, Grabe et al. 2016, Schlegel et al. 2021, Vosshall and Stocker 2007).

OSNs synapse with both local interneurons (LNs), which regulate interglomerular communication compiling different olfactory information valences to create elaborate responses, and projection neurons (PNs), that carry sensory information to higher brain centers, such as the mushroom bodies and the lateral horn (Figure 1B-C), which are responsible for learned and innate behaviors, respectively (Jefferis et al. 2001, Ramdya and Benton 2010, Schlegel et al. 2021, Vosshall and Stocker 2007). Depending on the internal state of the fly and on its physiological requirements, such as nutritional or reproductive state, synaptic transmission within glomeruli can be shaped by neuromodulatory molecules (Carlsson et al. 2010, Kim, Su and Wang 2017, Martelli et al. 2017, Su and Wang 2014, Wang and Wang 2019, Zandawala et al. 2018).

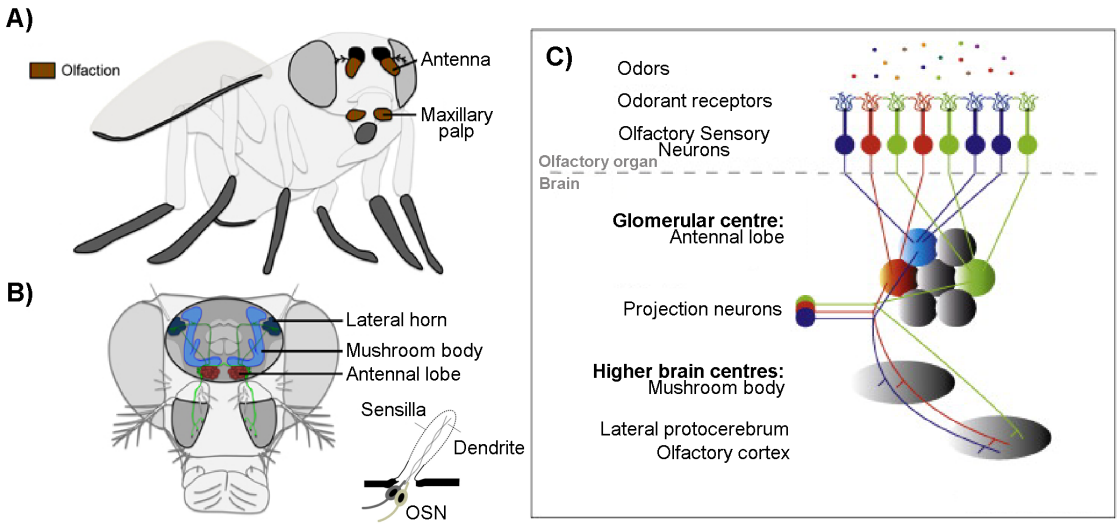

Figure 1. The *Drosophila* olfactory system. A) Schematic of a *Drosophila* adult with olfactory organs shown in brown (modified from (Ziegler, Berthelot-Grosjean and Grosjean 2013)). B) Olfactory sensory neurons (OSNs) are mainly located in the antenna housed by modifications of the cuticle called sensilla. First and second level brain processing centres of olfaction include the antennal lobes, where the odor information experiences its first processing, and the mushroom bodies and the lateral horn involved in stimulus-related learned behaviors or innate behaviors, respevtively. C) OSNs send axonal projections from the third antennal segment to the antennal lobes from where projection neurons send the information to higher brain centres. OSNs that express the same receptor send axonal projections to the same glomerulus (modified from (Ramdya and Benton 2010)).

1.7. Evolution of olfactory systems

In this section, I describe and compile information about the different levels at which olfactory systems have evolved in drosophilids.

1.7.1. Evolution of the periphery of olfactory circuits

Changes at the peripheral level can occur through: (a) changes in OSN tuning as a consequence of mutations in the Or gene sequences; (b) changes in OSN number as a result of the adjustment of the number of neurons in preexisting neuronal populations; (c) the expansion and contraction of Or gene families (by duplications or deletions); or (d) the expansion and contraction of OSN population types due to changes in developmental processes.

(a) Changes in OSN tuning is probably one of the most common ways in which peripheral olfactory systems can evolve with several examples in the literature (Hansson and Stensmyr 2011, Mansourian et al. 2018, Zhao and McBride 2020). Modifications of OSN tuning reflect increased sensitivity or reduced attraction towards compounds with new ecological relevance. While most OSNs show conserved tuning across the melanogaster subgroup (Stensmyr et al. 2003), the antennal basiconic 3A (ab3A, Or22a) neuron tuning rapidly switched across sibling species producing main shifts in neuronal response properties (Keesey et al. 2022). In *D. melanogaster*, ab3 sensilla housing the broadly tuned Or22a receptor is tuned towards ethyl esters. In *D. sechellia*, the Or22a channel has shifted its sensitivity towards methyl esters characteristics of the noni fruit (Auer et al. 2020, Dekker et al. 2006). This sensory adaptation is caused mainly, but not only, by the exchange of a single amino acid

in the predicated ligand-binding pocket (Auer et al. 2020). *D. erecta*, another close relative of *D. melanogaster*, has shifted Or22a's tuning towards the *Pandanus*-derived volatile 3-methyl-2-butenyl in a very specific manner (Linz et al. 2013), picturing the Ab3A channel as a pre-eminent olfactory pathway to drive species-specific ecological adaptations.

Another well described case of OSN re-tuning is observed in the antennal coeloconic 3I (ac3I) housing the acid sensing Ir75b receptor. In *D. sechellia*, Ir75b has evolved hexanoic acid sensitivity (compared to *D. melanogaster*'s Ir75b receptor tunned to butyric acid) principally through a single residue exchange in its ligand-binding domain (Prieto-Godino et al. 2017).

(b) Generally, Or gene evolution is considered a continuous "birth and death" process as genes undergo duplications or deletions (Sanchez-Gracia, Vieira and Rozas 2009). There are instances of novel Or genes originating as well as instances of rapid reduction in size of Or subfamilies (Albalat and Canestro 2016, Guo and Kim 2007, Niimura 2009, Ramdya and Benton 2010). A particularly interesting Or subfamily that contains examples of both of these phenomena is the Or67a subfamily (Arguello et al. 2016, McBride et al. 2007). Closely related species show remarkable differences in terms of Or67a gene copy number. For instance, *D. melanogaster* and *D. sechellia* only have one intact copy of this gene. Conversely, *D. simulans* and *D. mauritiana* present three intact copies of the *Or67a* gene. These properties prompted the work described in Chapter 2.

(c) Changes in OSNs number is another way in which pre-existing neural circuits can evolve. Increasing or decreasing the number of neurons that respond to certain compounds can also help to increase or diminish detection of ecologically relevant (or not) volatiles. Although these changes have been less reported in the literature, they still occur, and they accompany receptor tuning adaptations. Two well-known evolutionary mechanisms that drove adaptation towards noni fruit involve augmentations of the size of the ab3A (Or22a) and ac3I (Ir75b) olfactory sensory neuron populations in *D. sechellia* (Auer et al. 2020, Dobritsa et al. 2003, Prieto-Godino et al. 2017). The increase in sensitivity towards 3-methyl-2-butenyl described in *D. erecta* has also been correlated to the increase in Or22a neuron numbers (Linz et al. 2013).

(d) OSN population changes due to developmental processes. As described above, OSNs are contained in sensory sensilla. The cells of each sensillum derives from a single sensory organ precursor (SOP) harbored in the larval antennal imaginal disc. After asymmetric cell divisions, each SOP produces eight cells. Out of them four cells will adopt a non-neural fate becoming the "support cells" determining the structure of the sensilla, while the other four cells will have the potential of developing into OSNs (Endo et al. 2011). In most sensilla, 1-3 of those cells will be removed through programmed cell death (or apoptosis) (Endo et al. 2007). It is reasonable to hypothesise that altered patterns of apoptosis will affect the final number of OSNs in animals. Indeed, artificial apoptosis blockage during *Drosophila* pupal development resulted in an increased number of OSNs present in the antenna (Prieto-Godino et al. 2020). Furthermore, these "undead" OSNs could express selected Ors, showed odor-

evoked responses and integrated into the pre-existent olfactory circuitry forming and reorganizing previous synapsis (Prieto-Godino et al. 2020).

1.7.2. Evolution of olfactory processing centers

Evolution of the olfactory processing centers can occur at the level of the (a) antennal lobe, (b) lateral horn, (c) mushroom bodies or (d) by modifying the neuromodulatory systems (Figure 1B).

(a) The antennal lobe is the first processing center in the central brain of olfactory information. Here, the sensory information carried out by OSNs is processed and transformed before being sent to higher brain centers. It is expected that changes at the peripheral level will be reflected in the antennal lobe. For example, Or22a and Ir75b OSN population enlargements in *D. sechellia* caused an increased volume of their corresponding glomeruli in the antennal lobe, DM2 and DL2d, respectively (Auer et al. 2020, Dekker et al. 2006, Prieto-Godino et al. 2017).

(b) The lateral horn is a sexually dimorphic high olfactory center that coordinates innate and learnt olfactory behavioral responses (Hansson and Stensmyr 2011, Schultzhaus et al. 2017). Interestingly, PNs have very stereotyped projection patterns in the lateral horn, where OSNs-derived connections proceeding from different sensilla groups are clustered. Furthermore, fruit odor-responsive PNs generally project to the posterior-dorsal region of the lateral horn, while pheromones are mostly represented in the anterior-ventral part (Jefferis et al. 2002, Jefferis et al. 2007). Presumably,

modifications of its stereotyped organization by the appearance (or disappearance) of projection neuron branches can, potentially, affect innate responses. Indeed, a novel axonal branch from the DM2 PNs has been described in *D. sechellia* flies compared to *D. melanogaster*'s DM2 PNs axonal pattern (Auer et al. 2020). If and how this brain structural modification leads to alternative processing of the odorant information across species and how it affects behavioral outputs is, however, unknown.

(c) The mushroom bodies (MBs) are the primary high olfactory center for olfactory learning and memory in insects, including *Drosophila* (Heisenberg 2003), It is formed by Kenyon cells that can be subdivided in three different groups: α/β and α'/β' neurons which project to medial and vertical lobes, and γ neurons that only project medially (Lee, Lee and Luo 1999). MB's size varies across insect species, including *Drosophila melanogaster*, although little is known about the effect that changes in MB lobes' size have on behavioral evolution. Using the *Drosophila* Genetic Reference Panel (Mackay et al. 2012) intra-species natural genetic variation in lobes' size were described and negative correlations between MB morphology/dimensions and behaviors such as aggression, sleep and lifespan have been reported (Zwarts et al. 2015). However, no structural or physiological adaptations that could explain olfactory changes across strains or species of flies have so far been described.

(d) The activity of most or all the neuronal classes described above is systematically regulated to match the organism's internal state by neuromodulatory cells that release neuropeptides and biogenic amines. While

the role of several of them has been extensively characterized in *D. melanogaster* (discussed further in Chapter 3), little is known about how they contribute to the evolution of olfactory systems in flies.

1.8. Thesis "road map"

In this thesis, I present several research projects to address different aspects of olfactory evolution across four *Drosophila* species: *D. melanogaster*, *D. simulans*, *D. sechellia* and *D. mauritiana*. They share a common ancestor 3 million years ago (Garrigan et al. 2012, Lachaise and Silvain 2004) and some aspects of their ecology have already been mentioned. Despite their evolutionary relative proximity, in within these four species important differences exist related (among others) with their fruit host exploitation adaptations. *D. melanogaster* and *D. simulans* are generalist species distributed worldwide. In nature, these species are commonly found feeding on several types of overripe fruits that lie on the ground and coexisting with larvae and other drosophilids (Markow et al. 2009). *D. mauritiana* is endemic to the Mauritius island and is also considered a generalist fly species (Garrigan et al. 2012). Remarkably, *D. sechellia*'s stringent specialization on the fruit of *Morinda citrifolia*, noni fruit, in the Seychelles Islands has supposed a sensory and metabolic adaptation. From the sensory perspective, several cases of re-tunned olfactory receptors (and probably gustatory as well, although this needs to be confirmed) have been described (Auer et al. 2020, Dekker et al. 2006, Prieto-Godino et al. 2017). Noni fruit is toxic for all tested drosophilids, including *D. melanogaster*, *D. simulans* and *D. mauritiana* (although resistance to this fruit has also been seen in the substrain *D. yakuba mayottensis* (Yassin et al. 2016)). For this reason, metabolic adaptations must have occurred in the *D. sechellia* lineage to survive the toxic

acids of noni fruit (Huang and Erezyilmaz 2015, Lavista-Llanos et al. 2014, McBride 2007, Shiao et al. 2015). The intriguing adaptation of *D. sechellia* to its host has prompted several questions I tried to answer in Chapters 3 and 4 of this thesis.

This work is organized into four chapters that tackle different evolutionary questions – at the level of olfactory-related circuits' architecture, circuits' function and odor-related behavior – and resulted into two publications and one submitted pre-print.

Chapter 2 describes a collaborative effort to study the impact that changes in olfactory receptor numbers have on fly's olfactory adaptations.

Chapter 3 describes data from two main evolutionary questions: first, how odorant representations vary across drosophilids with different ecological niches and, second, the role of neuromodulation in controlling odorant-derived excitability in the central brain across species.

Chapter 4 describes my investigations of the evolution of olfactory regulation of oviposition behavior in *D. sechellia* during its stringent specialization the noni fruit.

Chapter 5 contains a general discussion that englobes the three different evolutionary approaches I have taken to answer evolutionary questions during my thesis work and includes challenges encountered and future perspectives of my thesis research.

CHAPTER 2: Copy number changes in co-expressed odorant receptor genes enable selection for sensory differences in drosophilids species

Summary of the results

This chapter describes the result of a collaborative effort from past and current members of the Richard Benton's lab (Auer*, Álvarez-Ocaña*, Cruchet, Benton and Arguello; *equal contribution), published in Nature Ecology and Evolution (Auer et al. 2022). In this work, we used *Drosophila*'s evolutionary dynamic Or67a olfactory receptor subfamily to study OSN evolution. While the common ancestor of the *Drosophila* trio (*D. melanogaster*, *D. simulans* and *D. sechellia*) had three *Or67a* paralogs that diverged in their odor-evoked responses, following their speciation, two *Or67a* paralogs were lost in *D. melanogaster* and *D. sechellia*. Comparative and population genomic analyses revealed ongoing positive selection (the conservation of novel traits that lead to evolutionary adaptations) acting on the intact genes. Unexpectedly, the three *Or67a* paralogs were co-expressed in the same neuron population in *D. simulans* and *D. mauritiana*, which deviates from the "one neuron–one receptor" general rule (although some other exceptions have already been reported). Therefore, while peripheral neuroanatomical properties of these pathways are conserved across species, independent selection on co-expressed receptor has contributed to species-specific peripheral coding of olfactory information.

My contribution to this work

During my master thesis, and continuing into my PhD research, I worked on the evolution of the Or67a receptor subfamily across *Drosophila* species through the analysis of the expression pattern of *Or67a* orthologs in *D.*

melanogaster, *D. simulans*, *D. sechellia* and *D. mauritiana*. I described the expression of a single *Or67a* gene in *D. melanogaster* and *D. sechellia* and the expression of three *Or67a* paralogs in *D. simulans* and *D. mauritiana* using RNA FISH probes and GFP reporter lines (Figure 3 and Supplementary Figure 5). I discovered that *D. simulans Or67a* paralogs were all expressed in the same population of OSNs and showed that these neurons project to the DM6 glomerulus in the antennal lobe (Figure 3). I analyzed the promoter regions across orthologs and paralogs revealing a degree of conservation inferior to 50% (Supplementary Table 6). Finally, and in order to have a broader idea about the natural genetic variation segregating within the *Or67a* paralogs, I sequenced these loci in 13 *D. simulans* strains. In three of the strains (07, 09 and 13) a premature stop codon possibly indicated the presence of a truncated protein (Supplementary Table 5). I also contributed to the preparation of Figures 3a-d and S5b-d, wrote a first draft of the results contained in Figures 3 and S5 and helped with comments and corrections throughout the manuscript.

2.1. Article: Copy number changes in co-expressed odorant receptor genes enable selection for sensory differences in drosophilids species

nature ecology & evolution

ARTICLES

https://doi.org/10.1038/s41559-022-01830-y

Copy number changes in co-expressed odorant receptor genes enable selection for sensory differences in drosophilid species

Thomas O. Auer[1,4], Raquel Álvarez-Ocaña[1,4], Steeve Cruchet[1], Richard Benton[1] and J. Roman Arguello[2,3]✉

Despite numerous examples of chemoreceptor gene family expansions and contractions, how these relate to modifications in the sensory neuron populations in which they are expressed remains unclear. *Drosophila melanogaster*'s odorant receptor (Or) family is ideal for addressing this question because most Ors are expressed in distinct olfactory sensory neuron (OSN) types. Between-species changes in *Or* copy number may therefore indicate increases or reductions in the number of OSN populations. Here we investigated the *Or67a* subfamily, which exhibits copy number variation in *D. melanogaster* and its closest relatives: *D. simulans*, *D. sechellia* and *D. mauritiana*. These species' common ancestor had three *Or67a* paralogues that had already diverged adaptively. Following speciation, two *Or67a* paralogues were lost independently in *D. melanogaster* and *D. sechellia*, with ongoing positive selection shaping the intact genes. Unexpectedly, the functionally diverged *Or67a* paralogues in *D. simulans* are co-expressed in a single neuron population, which projects to a glomerulus homologous to that innervated by Or67a neurons in *D. melanogaster*. Thus, while sensory pathway neuroanatomy is conserved, independent selection on co-expressed receptors has contributed to species-specific peripheral coding. This work reveals a type of adaptive change largely overlooked for olfactory evolution, raising the possibility that similar processes influence other cases of insect Or co-expression.

The evolution of animal chemoreceptor families is characterized by rapid changes in gene copy number[1–6]. Numerous studies have correlated expansions and contractions of these families to known ecological shifts (for example, dietary change or host-plant specialization), reflecting their capacity to quickly respond to environmental variation and to contribute to adaptive modifications[3,6–9]. The evolution of chemoreceptor gene repertoires has raised considerable interest from a molecular evolutionary perspective, where it is often modelled as a stochastic birth-and-death process[10,11]. Receptor gene deletion and duplication events are particularly compelling in light of their roles in establishing the peripheral coding of chemical stimuli and because of their highly selective expression patterns: only one or a small number of receptor genes are expressed in a given sensory neuron population. Whether and how chemoreceptor duplicates evolve cell type-specific expression, and how chemoreceptor gains and losses functionally impact the sensory cells in which they are expressed, remain unclear.

A challenge to addressing these questions is the need for experimentally tractable systems with which to link changes at the level of the genome to physiology and neuroanatomy. *Drosophila melanogaster* and its closely related drosophilid species have emerged as an outstanding group for functional comparative studies of nervous systems. The extensive knowledge and resources that are available for *D. melanogaster*[12–15] are driving the development of genetic reagents in its ecologically diverse sister species[16–20]. Additionally, the short evolutionary distances between multiple species in the *D. melanogaster* species group help to identify key mutational events and in inferring the evolutionary processes that underly the changes of interest.

Drosophila's odorant receptor (Or) family is advantageous for relating between-species changes in chemoreceptor gene copy number to expression and neuronal response evolution. As in many other insects, Ors are expressed in olfactory sensory neurons (OSNs) housed in the sensilla of two olfactory organs in adults, the antennae and the maxillary palps. Importantly, a large majority of Ors are uniquely expressed in individual OSN populations (together with the broadly expressed co-receptor Orco[21]), which is analogous to the singular expression of vertebrate olfactory receptor genes[22,23]. The axons of OSNs expressing the same receptor converge onto a discrete, stereotypically positioned glomerulus in the primary olfactory centre, the antennal lobe[24]. The distinct pattern of *Or* expression raises the possibility that between-species changes in *Or* copy number reflect the evolution of new OSN populations or the loss of sensory pathways, in coordination with *Or* duplication and deletion events, respectively. Here we investigate a drosophilid *Or* subfamily, *Or67a*, to examine the relationship between sequence, function and expression evolution of olfactory receptors across species.

Results

***Or67a* copy number is evolutionarily dynamic.** *Or67a* is one of the few olfactory receptor genes that differ in copy number among the closely related *D. melanogaster* subgroup species[3,10,25], which share a common ancestor ~3.4 million years ago[26]. The *Or67a* subfamily has also experienced remarkable expansions in more distantly related species: for example, *D. suzukii*, which shares a last common ancestor with *D. melanogaster* ~15 million years ago[27], has five paralogues (Fig. 1a)[10,25,28]. *D. melanogaster* Or67a is the most broadly responding antennal Or when presented with headspace

[1]Center for Integrative Genomics, Faculty of Biology and Medicine, University of Lausanne, Lausanne, Switzerland. [2]Department of Ecology & Evolution, Faculty of Biology and Medicine, University of Lausanne, Lausanne, Switzerland. [3]Swiss Institute of Bioinformatics, Lausanne, Switzerland. [4]These authors contributed equally: Thomas O. Auer, Raquel Álvarez-Ocaña. ✉e-mail: roman.arguello@unil.ch

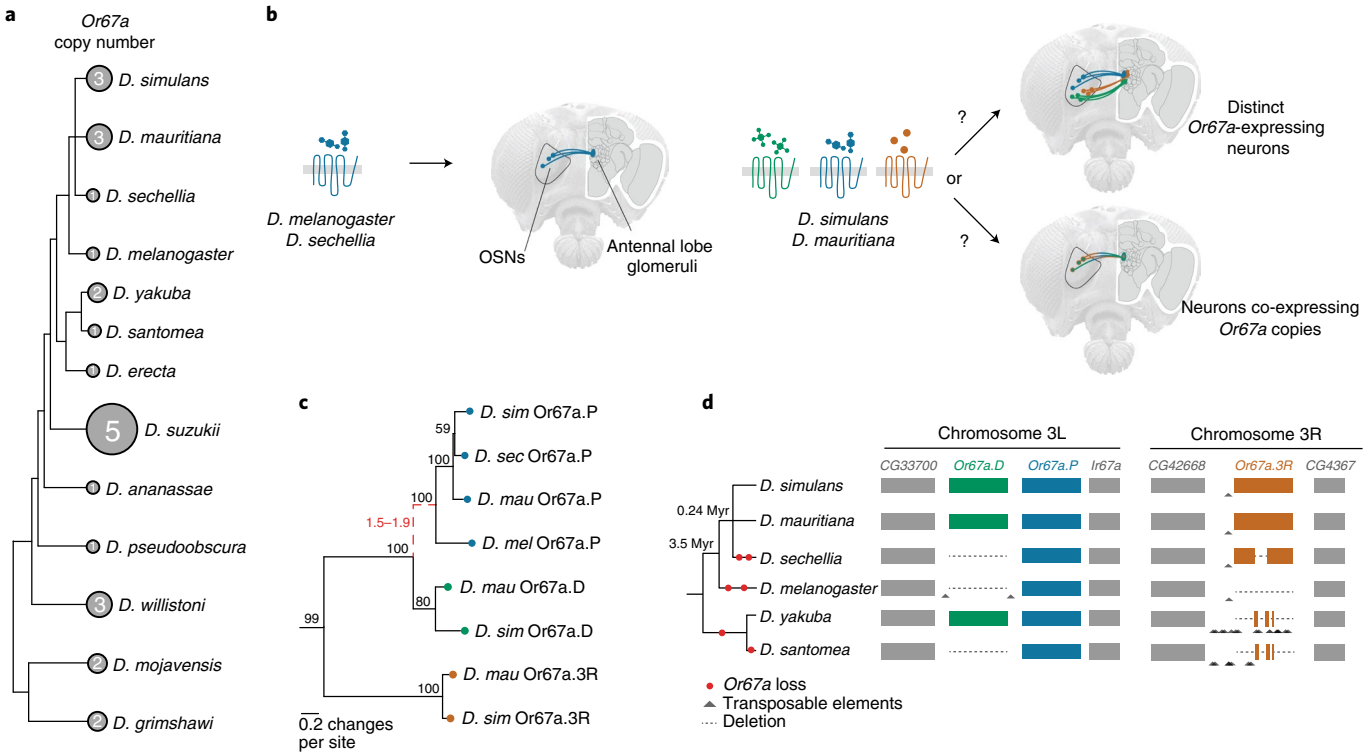

Fig. 1 | Molecular evolution of the *Or67a* subfamily in *Drosophila*. a, *Drosophila* species tree (branches not to scale) illustrating *Or67a* copy number changes in a subset of available genome assemblies that is[3,10,25,28]. These numbers exclude pseudogenes that are recognizable *Or67a* family members. **b**, Illustration of the evolutionary scenarios that are being investigated for the *Or67a* family. To what extent are the receptors tuned to different ligands within (and between) species? For *D. simulans* and *D. mauritiana*, are the three *Or67a* paralogues expressed in distinct neuron populations that project to different regions (glomeruli) of the antennal lobe, or are they co-expressed in the same neuron population(s)? An intermediate scenario (not shown) is the co-expression of two receptors in one OSN population and singular expression of the third receptor in a second population. **c**, Bayesian protein tree inferred for the intact Or67a subfamily members. The black numbers near the nodes indicate posterior support. The branch with a dashed line was inferred to have a significant elevation in protein evolution (dN/dS = 1.5–1.9, red text); the remaining branches were inferred to have been under functional constraint (dN/dS < 0.5). **d**, Overview of the parallel loss of the *Or67a.D* and *Or67a.3R* genes in *D. melanogaster* and the *simulans* group, using *D. yakuba* and *D. santomea* as outgroup species. On the left is a species tree for the samples included in the analyses (branches not to scale). The numbers at the tree nodes indicate divergence dates in millions of years for *D. melanogaster* and the *D. simulans* group[30,31]. To the right of the tree are schematics of the alignments of the *Or67a*-containing chromosomal regions. Shown are the conserved genes (grey rectangles) that flank the *Or67a*-containing regions (coloured rectangles) and the independent deletions of the *Or67a.D* and *3R* genes (dashed lines). The deletions are mapped onto the species tree with red dots. Many remnants of transposable elements were identified within these intervals, illustrated with grey triangles (the schematic is not to scale, but see Extended Data Figs. 1 and 2).

odours from an extensive collection of fruits[29], suggesting that evolution of the Or67a subfamily is related to species-specific olfactory responses to food. In this study, we focused on *D. melanogaster* and its sister species in the *simulans* complex (*D. simulans*, *D. sechellia* and *D. mauritiana*), which share a common ancestor ~0.24 million years ago[30,31], to connect between-species differences in *Or* copy number and potential differences in the function and/or organization of the sensory neurons in which they are expressed (Fig. 1b). *D. sechellia* and *D. melanogaster* have a single intact *Or67a* gene, while *D. simulans* and *D. mauritiana* have three (Fig. 1a,b). We refer to these three *Or67a* genes as *Or67a.P* (the 3L copy proximal to the centromere), *Or67a.D* (the 3L copy distal to the centromere) and *Or67a.3R* (the copy on the right arm of the third chromosome).

To determine the evolutionary history of this *Or67a* subfamily, we first inferred a protein tree for the eight receptors from these four species. The well-supported tree clusters each of the Or67a.P, Or67a.D and Or67a.3R members together, indicating that the three paralogues existed prior to this group's speciation events and that the *Or67a.D* and *Or67a.3R* genes were lost independently along *D. melanogaster*'s and *D. sechellia*'s branches (Fig. 1c). The scenario involving two independent *Or67a.D* and *Or67a.3R* losses is further supported by inspecting alignments of the homologous chromosomal regions and polarizing the changes using the outgroup species *D. yakuba* and *D. santomea*. The genes flanking the *Or67a* paralogues are conserved across the six species, verifying that the chromosomal regions are homologous (Fig. 1d and Supplementary Data 1 and 2). However, considerable nucleotide and indel differences have arisen between species within the intervals containing the *Or67a* paralogues, as have remnants of transposable elements, particularly for the *Or67a.3R*-containing region in *D. yakuba* and *D. santomea* (Fig. 1d and Extended Data Figs. 1 and 2). These alignments clarify that independent deletions have completely removed the *Or67a.D* orthologue in *D. sechellia* (*secOr67a.D*), *D. melanogaster* (*melOr67a.D*) and *D. santomea*, although it remains intact in *D. yakuba*. Deletions have also entirely removed the *melOr67a.3R* orthologue and a portion of the coding region in the *D. sechellia* orthologue (*secOr67a.3R*), eliminating sequences encoding two transmembrane domains that are required for forming the ion channel of the receptor[32,33]. Short remnants of the *Or67a.3R* orthologues are still detectable in *D. yakuba* and *D. santomea*, additionally indicating that the orthologue was present in these more distant species. In combination, these data support a history in which three

Table 1 | Functional constraint on *Or67a* paralogues

Species	Gene	*n*	π_{rep}/π_{sil}
D. melanogaster	*Or67a.P*	84	0.083
D. simulans	*Or67a.P*	210	0.13
D. simulans	*Or67a.D*	210	0.129
D. simulans	*Or67a.3R*	208	0.134

Constraint has been measured by π_{rep}/π_{sil}. All copies have $\pi_{rep}/\pi_{sil} < 0.5$, indicating ongoing purifying selection. Sample size is indicated by *n*.

Or67a paralogues existed in the common ancestor of *D. melanogaster* and the *simulans* group and that *D. sechellia* and *D. melanogaster* have recently lost the *Or67a.D* and *Or67a.3R* copies in parallel. The rapid change in *Or67a* copy number is probably related to past transposable element insertions and deletions in these loci.

Recurrent positive selection on Or67a paralogues. The observation of recent parallel gene losses among these closely related species raises questions about the selective constraints acting on the intact receptors. We tested models of protein evolution by fitting rates of amino-acid-changing (dN) and silent (dS) substitutions along the branches of the Or67a tree (Fig. 1c). Among the models we investigated, those that fit best consistently resulted in strong selective constraint along nearly all branches (dN/dS < 0.45). The branch leading to the *Or67a.P* clade was the only exception, with an elevated rate of amino acid change that is consistent with positive selection acting on the *Or67a.P* coding sequence following the *Or67a.D*/*Or67a.P* tandem duplication event (dN/dS = 1.5–1.9; Supplementary Tables 1 and 2). Using available population genomic datasets for *D. melanogaster* and *D. simulans*, we carried out more sensitive tests of ongoing purifying selection based on the ratio of nucleotide diversity at amino-acid-replacement positions (π_{rep}) to nucleotide diversity at silent positions (π_{sil}). These measures lent additional support for functional constraint currently acting on the intact *Or67a* genes for these two species, with all $\pi_{rep}/\pi_{sil} < 0.2$ (Table 1 and Supplementary Data 3). The alignment of the *Or67a.P/D* paralogues suggests that gene conversion has not been an ongoing force homogenizing the two genes. Sequence identity between the paralogues (82.5%) is lower than what would be expected if conversion had occurred recently or was ongoing (closer to 100%), and patterns of shared polymorphism did not uncover signals of conversion tracts.

Combining our polymorphism datasets with between-species alignments, we applied McDonald–Kreitman tests[34] of adaptive protein changes and estimated the fraction of amino acid substitutions that have been fixed within a species by positive selection (α)[35]. These analyses also identified signals of adaptive protein evolution for the *Or67a.P* copies in both *D. melanogaster* and *D. simulans*, where 69% and 55%, respectively, of the protein changes were estimated to have been fixed by positive selection (Table 2). By contrast, the *simOr67a.D* and *simOr67a.3R* copies did not carry signatures of adaptation. This *D. melanogaster* result is consistent with previous population genomic studies that identified *melOr67a.P* as evolving adaptively between species, as well as experiencing very recent positive selection between extant populations[36,37], and further underscores past and ongoing adaptive changes in *melOr67a.P*. Adaptive receptor gene loss may be an important route for sensory change within chemosensory systems[38]. If the two *D. melanogaster* deletions were adaptive and swept to fixation in the recent past, reduced genetic variation (and a negative Tajima's *D*[39]; may be detectable[40]. However, analyses of the polymorphism at the loci containing these deletions did not provide evidence of adaptive loss, as the genetic variation was not different from the larger surrounding chromosomal regions (Extended Data Fig. 3). These results provide evidence that the intact *Or67a* genes are currently under functional constraint, despite parallel gene losses in the recent history of the subfamily. They additionally highlight recurrent bouts of positive selection that presumably diversified receptor function, particularly for the *Or67a.P* clade.

Positive selection has diversified Or67a receptor tuning. To test the hypothesis that positive selection has contributed to the diversification of receptor function within the Or67a subfamily, we performed in vivo electrophysiological recordings of odour-evoked activity of Or67a paralogues and orthologues. We expressed individual Or67a receptors in a *D. melanogaster* 'decoder' neuron—the antennal basiconic sensillum 3A (ab3A) neuron that lacks its endogenous tuning receptor (Or22a) but still expresses Orco[41] (Fig. 2a,b)—and quantified neuronal responses to a panel of nine odours. These odours were selected to cover a range of strong to weak Or67a.P ligands on the basis of previous work in *D. melanogaster*[42–44]. Globally, we observed highly significant evolutionary changes in odour response profiles across the tested receptors (global Wilks' Λ, 15.06; $P \ll 0.01$; Fig. 2c). When we tested for differences across the Or67a.P/D/3R paralogues within *D. mauritiana* or *D. simulans*, all comparisons were significantly different ($P < 0.01$). When we tested for differences among orthologues across species (between all four species for Or67a.P or between *D. simulans* and *D. mauritiana* for Or67a.D and Or67a.3R), all comparisons were again significant ($P < 0.01$), except for the responses measured for Or67a.3R orthologues of *D. simulans* and *D. mauritiana* ($P > 0.01$). The statistical approach used to test for differences in odour responses[45] also allowed us to calculate the relative effects that the odours have on the receptor responses, thereby highlighting key odour combinations that drove these significant orthologue/paralogue differences (Fig. 2d and Supplementary Table 3). For example, the relative effect of geraniol on *sim*Or67a.3R is 86%, indicating a high probability of this receptor responding the strongest to this odour given a random sample from the full set of recordings (a comparable effect (85%) exists for *mau*Or67a.3R). Similarly, *sim*Or67a.D has a 97% probability of having the strongest responses to ethyl hexanoate that, together with the large relative effects of pentanoic acid, methyl hexanoate and 2-heptanone, strongly differentiate it from its *mau*Or67a.D orthologue. Clustering these response data using principal component analysis further highlights the evolutionary changes among receptors (Fig. 2e). In particular, the variation among Or67a.P orthologues is readily apparent, as is the distinct separation of the two Or67a.3R copies (together with *sec*Or67a.P) from the other receptors.

We tested for differences in sensitivity to our panel of odours by generating dose–response curves for the five odours that resulted in the strongest responses at the highest concentration (10^{-2} (v/v)). These experiments revealed numerous differences in sensitivity among both paralogues and orthologues, but the differences were the most pronounced in Or67a.P and Or67a.D, concordant with the elevated diversity in response profiles to the full odour panel at the 10^{-2} concentration (Fig. 2f and Extended Data Fig. 4). For example, *sim*Or67a.D is significantly more sensitive across concentrations of ethyl hexanoate than *mau*Or67a.D ($P < 0.01$; Supplementary Table 4), while the opposite is the case for 6-methyl-5-hepten-2-one ($P < 0.01$; Supplementary Table 4). Other notable differences are the Or67a.P responses to 6-methyl-5-hepten-2-one, where *sec*Or67a.P has high sensitivity across all concentrations, with additional species differences increasing with concentration (Fig. 2f and Supplementary Table 4). These data demonstrate widespread evolution of ligand response profiles within the Or67a subfamily, supporting our molecular evolutionary inferences that positive selection has contributed to functional changes.

The three *D. simulans Or67a* paralogues are co-expressed. Our evolutionary genetic analyses and electrophysiological experiments

Table 2 | McDonald–Kreitman tests for adaptive protein evolution

Species	Gene	*n*	D_{rep}	D_{sil}	π_{rep}	π_{sil}	*P*	α
D. melanogaster	*Or67a.P*	84	65	56	20	42	0.0015	0.69
D. simulans	*Or67a.P*	210	30	24	28	50	0.0325	0.55
D. simulans	*Or67a.D*	210	53	70	19	33	0.5021	0.24
D. simulans	*Or67a.3R*	208	19	39	24	67	0.4597	0.26

The *Or67a.P* copies were found to have experienced adaptive protein evolution in both *D. melanogaster* and *D. simulans*, while signatures of adaptation were not found in *simOr67a.D* or *simOr67a.3R*. D_{rep}, number of amino-acid-replacement substitutions; D_{sil}, number of silent substitutions.

uncovered adaptive functional diversification in the Or67a subfamily. The three *D. simulans* receptors could either define different populations of OSNs (some of which were lost in *D. melanogaster* and *D. sechellia*) or be co-expressed in a single neuron population (Fig. 1b). To investigate these possibilities, we first examined receptor expression using RNA fluorescence in situ hybridization (FISH). For all four species, we detected *Or67a*-expressing neurons within a comparable spatial domain of the antenna (Fig. 3a). Quantification of neuron numbers indicates similar numbers of cells expressing *Or67a.P* and *Or67a.D* in *D. simulans*. We observed very few *Or67a.3R*-positive cells (possibly because of lower expression levels of this receptor); similarly, *mauOr67a.P* and *mauOr67a.3R* expression was weak but detectable.

One caveat to interpreting these experiments is that the level of sequence identity across paralogues (Supplementary Table 5) may result in cross-reactivity of RNA FISH probes; this issue also precluded double RNA FISH experiments to examine receptor co-expression. To circumvent this limitation, we generated paralogue-specific transgenic transcriptional reporters in *D. simulans*. We used CRISPR–Cas9 to integrate Gal4 at the *simOr67a.3P* and *simOr67a.3R* loci ($simOr67a.P^{Gal4}$ and $simOr67a.3R^{Gal4}$) (Extended Data Fig. 5a) and combined these alleles with a fluorescent reporter (*UAS–GCaMP6s*) to visualize promoter activity. Our attempts to generate an equivalent *simOr67a.D* Gal4 insertion were unsuccessful, so we generated a transgenic promoter reporter for this gene (similar to a *melOr67a.P* reporter[24]; Extended Data Fig. 5b) using the upstream sequence of *simOr67a.D* to drive RFP expression (*simOr67a.D–RFP*). Using these tools, together with RNA FISH, we confirmed that transcription from the *simOr67a.3R* locus overlaps with *simOr67a.P*, and transcription from the *simOr67a.P* locus overlaps with *simOr67a.D* RNA expression (Fig. 3b).

In *D. melanogaster*, the axons of *mel*Or67a.P neurons innervate the DM6 glomerulus in the antennal lobe[24] (Fig. 3c). Similarly, in *D. simulans*, the neurons labelled by either $simOr67a.P^{Gal4}$ or $simOr67a.3R^{Gal4}$, as well as the *simOr67a.D–RFP* promoter transgenic reporter, all targeted the same glomerulus, which is located in the identical location of the antennal lobe to that of DM6 in *D. melanogaster* (Fig. 3c). These results collectively argue for the co-expression of the three *D. simulans Or67a* paralogues in a neuron population that is homologous to *D. melanogaster* Or67a neurons.

The evolutionary stability of the co-expression of *D. simulans* paralogues is notable, given the nucleotide sequence divergence between their putative regulatory regions (Supplementary Table 6). To investigate the transcriptional activity of these sequences outside of their endogenous genomic context, we generated promoter transgenic transcriptional reporters containing the upstream sequences of each *D. simulans Or67a* paralogue and inserted them into an identical genomic site within a common *D. melanogaster* genetic background. All three reporters displayed neuronal expression patterns in the antenna that are consistent with that of endogenous *melOr67a.P* RNA (Extended Data Fig. 5b,c), and they paired with Or49a/Or85f-expressing neurons within the ab10 sensillum class (Extended Data Fig. 5d)[24]. Moreover, all three labelled neuron populations target DM6 (Fig. 3d). Computational searches for putative regulatory motifs within these upstream sequences identified different degrees of overlap across the *Or67a* genes in *D. melanogaster* and *D. simulans*. Consistent with their sequence identity (Supplementary Table 6), more motifs were shared between the upstream sequences of *simOr67a.P* and *simOr67a.D* than either shared with *simOr67a.3R* (Fig. 3e and Supplementary Table 7). This observation suggests that co-expression of the three receptors has probably been maintained by common transcriptional regulators of *Or* expression; the higher sequence identity between the regulatory regions of the *Or67a.P* and *Or67a.D* paralogues presumably reflects their more recent divergence.

Co-expressed *Or67a* paralogues have unique but overlapping contributions. The observation that the three *Or67a* paralogues are co-expressed in *D. simulans* led us to investigate the correspondence between the decoder neuron responses (Fig. 2b,c) and those from endogenous neurons (housed in ab10 sensilla) in *D. melanogaster* and *D. simulans*. To facilitate unambiguous targeting of ab10 sensilla in *D. simulans*, we generated a *simOr67a.P–GFP* promoter reporter in *D. simulans* (similar to that in *D. melanogaster*; Fig. 3c and Extended Data Fig. 5b) for fluorescent-guided electrophysiological recordings. In *D. melanogaster*, the wild-type ab10 response profile to the nine odours was qualitatively similar to that obtained from the decoder neuron (Figs. 2c and 4a). In *D. simulans*, the relative responses across the odour panel of wild-type ab10 neurons globally matched the profile predicted from the individual contributions of the three receptors in the decoder neuron, though with overall lower absolute responses (Fig. 4b). For example, ethyl hexanoate, which evoked the strongest responses across any of the three *sim*Or67a paralogues in the decoder neuron, was the strongest ligand in *D. simulans* ab10 Or67a neurons (Fig. 4a), while geraniol, which evoked a response only by *sim*Or67a.3R in the decoder neuron, evoked a more modest response in ab10 neurons.

To investigate contributions of the individual *D. simulans* Or67a paralogues to the overall response profile in their endogenous neurons, we measured odour-evoked activity in ab10 sensilla in a $simOr67a.3R^{RFP}$ loss-of-function mutation (produced during the generation of $simOr67a.3R^{Gal4}$ (Extended Data Fig. 5)), as well as our $simOr67a.P^{Gal4}$ knock-in allele. The $simOr67a.3R^{RFP}$ mutation led to a loss of Or67a neuron responses to geraniol and a significant reduction in responses to phenethyl alcohol (both Wilcoxon rank sum tests, $P<0.01$), but no modification in the responses to the other odours, consistent with *sim*Or67a.3R contributing uniquely to the global response profile (Fig. 4c; one-way multivariate analysis of variance, $F=5.45$, $P>0.05$; only the pairwise Wilcoxon rank sum tests for geraniol and phenethyl alcohol were significant). Unexpectedly, the overall response profile of the $simOr67a.P^{Gal4}$ mutant was not significantly different from that of wild-type ab10 sensilla (Fig. 4c; one-way multivariate analysis of variance, $F=2.42$, $P>0.05$), including responses to this receptor's best ligand, 6-methyl-5-hepten-2-one (Wilcoxon rank sum test, $P>0.05$). The absence of phenotype of this receptor mutant (for at least the tested odour panel) is probably because *sim*Or67a.D and *sim*Or67a.3R also

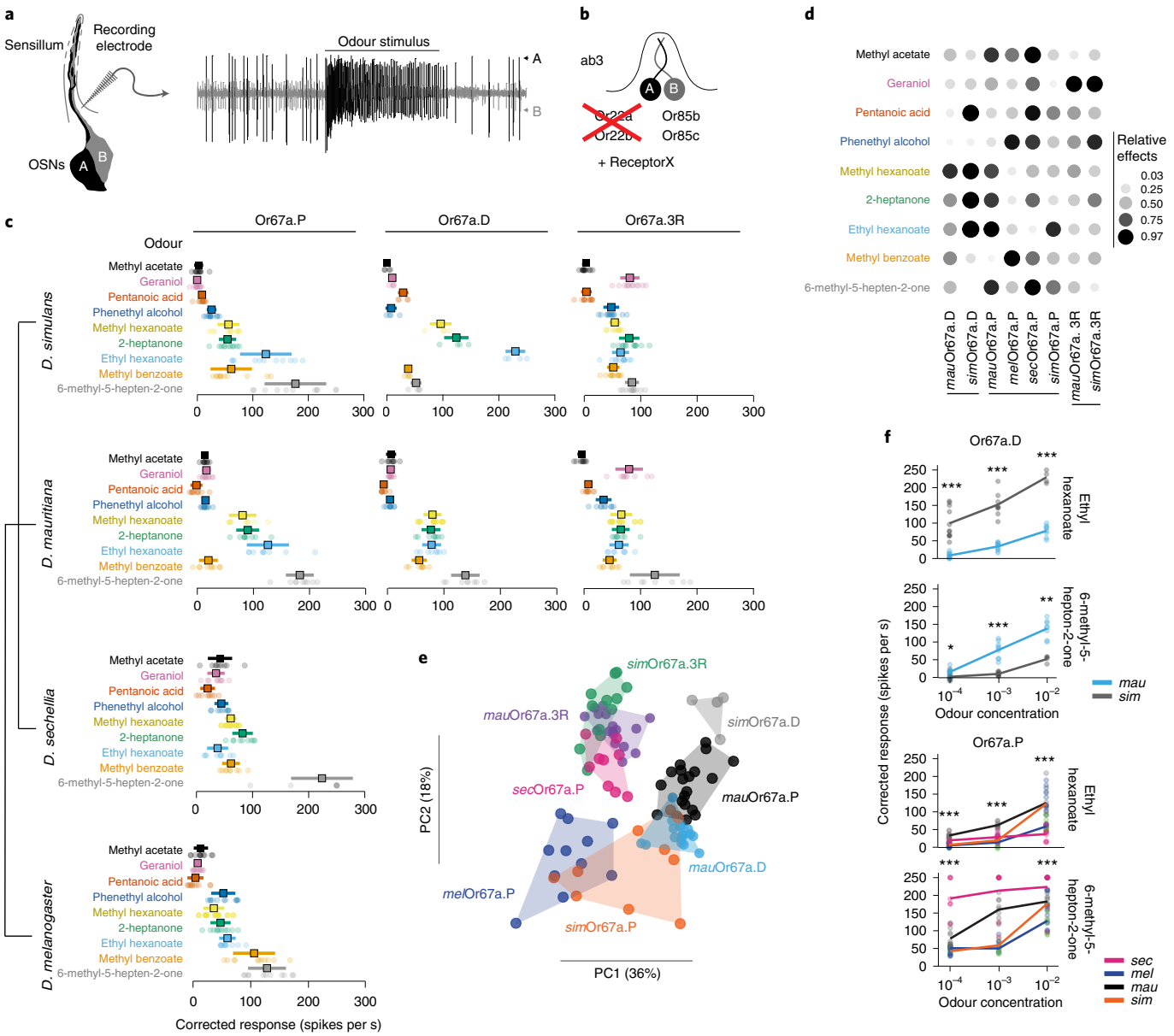

Fig. 2 | Evolutionary changes in Or67a orthologue and paralogue odour responses. a, Schematic for single-sensillum recordings from a sensillum housing two OSNs (A and B), differentiable by spike amplitudes. **b**, Illustration of the *D. melanogaster* 'decoder' system[41] used to screen the response profiles of Or67a orthologues and paralogues. **c**, Quantification of Or67a.P/D/3R responses to nine odours at 10^{-2} (v/v) concentration delivered in 1 s pulses (the tree is not to scale). The circles are individual data points, the squares indicate the means and the error bars display the standard deviations. The number of independent sensilla recorded per odour–receptor combination is: for *D. melanogaster*, Or67a.P = 11; for *D. sechellia*, Or67a.P = 9; for *D. mauritiana*, Or67a.P = 9, Or67a.D = 8 and Or67a.3R = 8; and for *D. mauritiana*, Or67a.P = 11, Or67a.D = 4 and Or67a.3R = 12. **d**, Relative effects of the odours on Or67a.P/D/3R responses at 10^{-2} (v/v) concentration. These values provide the probability that a given odour-receptor response will be the largest given the full dataset. **e**, Principal component analyses based on the data from Fig. 2b. The percentages along the axes indicate the amount of variation explained by the principal components. Species names have been abbreviated to the first three letters. **f**, The two odour-receptor combinations that resulted in the largest dose-response differences among the Or67a.P/D/3R orthologues (see Extended Data Fig. 4 for the other odours). For simplicity, the level of significance indicated above each concentration's comparison is only for the single species comparison with the largest difference (see Supplementary Table 4 for the full set of tests; $*P < 0.05$; $**P < 0.01$; $***P < 0.001$). The *P* values were calculated with a two-sided Dunn test; correction for multiple comparisons was done using the Holm method. The number of independent sensilla recorded for Or67a.D responses to ethyl hexanoate and 6-methyl-5-hepten-2-one is (low to high concentrations): for *D. simulans*, 11, 8 and 4; and for *D. mauritiana*, 9, 9 and 8. The sample sizes for Or67a.P responses to ethyl hexanoate and 6-methyl-5-hepten-2-one are: for *D. simulans*, 11, 8 and 11; for *D. mauritiana*, 10, 9 and 9; for *D. melanogaster*, 10, 9 and 11; and for *D. sechellia*, 8, 8 and 9.

respond to most or all of its ligands (Fig. 2c). Together, these results highlight both specific and overlapping contributions that the Or67a paralogues make to the odour response profile of their endogenous OSNs.

Discussion

Analyses of odour responses of homologous OSNs across species have identified many instances of evolutionary change[16,18,46–49]. Such changes are generally assumed to be due to modifications in the

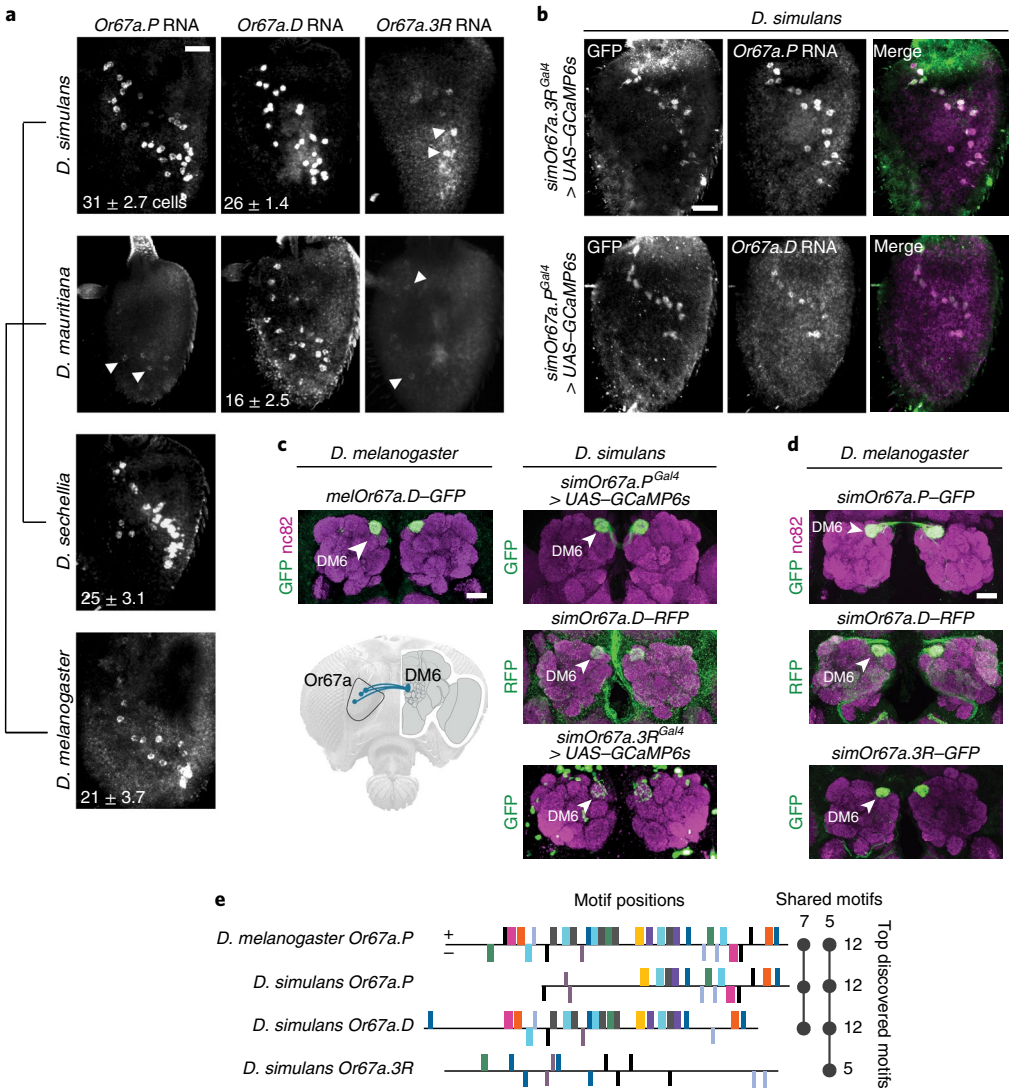

Fig. 3 | Evolutionary analyses of *Or67a* expression and circuit neuroanatomy. a, Whole-mount antennal RNA expression of *Or67a* paralogues and orthologues in *D. simulans* (*Drosophila* Species Stock Center (DSSC) 14021-0251.004), *D. mauritiana* (DSSC 14021-0241.151), *D. sechellia* (DSSC 14021-0248.07) and *D. melanogaster* (CantonS) (top to bottom). Scale bar, 25 µm. The number of *Or67a*-expressing OSNs (±standard deviation) is indicated at the bottom left corner (*simOr67a.P*, $n=12$ antennae; *simOr67a.D*, $n=12$; *mauOr67a.P*, $n=10$; *secOr67a.P*, $n=11$; *melOr67a.P*, $n=11$). Weak staining prevented the quantification of OSN numbers expressing *Or67a.3R* in *D. simulans* and *Or67a.3R* and *Or67a.P* in *D. mauritiana*. The arrowheads indicate weakly labelled cells. **b**, Antennal co-expression of knock-in *Gal4* transcriptional reporters (*simOr67a.P*^{Gal4} and *simOr67a.3R*^{Gal4}, visualized by *UAS–GCaMP6s*; GCaMP6s detected by anti-GFP) and *Or67a.P* (top) and *Or67a.D* (bottom) RNA in *D. simulans*. Scale bar, 25 µm. **c**, Top, antennal lobe innervation of neurons labelled by a previously described[24] promoter transcriptional reporter for *Or67a* in *D. melanogaster* (Bloomington *Drosophila* Stock Center (BDSC) no. 52633); neuropil is visualized with nc82 (magenta). Bottom, schematic illustrating the innervation of DM6 by Or67a-expressing neurons. Right, *Gal4* and promoter transcriptional reporters for *Or67a* paralogues in *D. simulans*. All reporter lines label neurons innervating the glomerulus that is homologous to *D. melanogaster*'s DM6 (arrowheads). Scale bar, 25 µm. **d**, Antennal lobe innervation of promoter transcriptional reporters for all three *D. simulans* paralogues in *D. melanogaster* (the arrowheads point to DM6); neuropil is visualized with nc82 (magenta). Scale bar, 25 µm. In **a**–**d**, the experiments were repeated at least three times for each staining on independent days, and the pictures show representative examples for each condition. **e**, Putative regulatory motifs identified in the 5′ DNA sequences of the *Or67a* paralogues in *D. simulans* and *melOr67a.P* (1.5–2 kb; Methods). The boxes indicate the placement of candidate motifs, with colours illustrating the same motif sequence. Positive-strand motifs are above the horizontal line, and negative-strand motifs are below. The sequences have been arranged to approximate a DNA alignment without gaps. The plot to the right summarizes the number of motifs per sequence and the overlap of motifs between the four sequences.

tuning of singularly expressed receptors, which has been supported by the direct assessment of receptor responses in heterologous expression systems[18,41]. In a few cases, amino acid substitutions that underlie the tuning differences between orthologous receptors have been mapped[16,18]. Our study of the *Or67a* subfamily reveals an additional mechanism of tuning evolution of OSNs, in which neurons stably co-express multiple receptors that independently diversify under positive selection.

Although we have found signatures of selection within the *Or67a* subfamily, one important open question is the ecological basis of the changes in tuning properties of Or67a neurons across the four *Drosophila* species. *D. melanogaster* and *D. simulans* are both human-commensal cosmopolitans, while *D. sechellia* and *D. mauritiana* are endemic to the Seychelles archipelago and Mauritius, respectively. *D. sechellia* is an extreme specialist, spending most of its life cycle on a single host fruit[50], but less is known about the

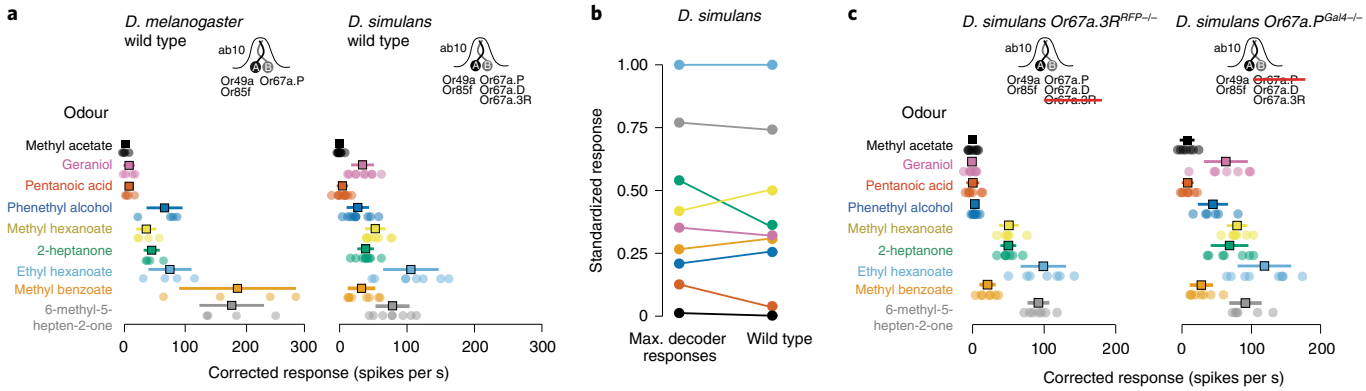

Fig. 4 | Unique but overlapping contributions of *Or67a* paralogues to endogenous neuronal responses. a, Quantification of wild-type ab10 sensilla recordings for *D. melanogaster* (left) and *D. simulans* (right) to a panel of nine odours (as in Fig. 2c). For *D. melanogaster*, $n = 4$ for all odours; for *D. simulans*, $n = 8$ (6-methyl-5-hepten-2-one, methyl benzoate, ethyl hexanoate and methyl acetate), 9 (methyl hexanoate and geraniol) and 10 (2-heptanone, phenethyl alcohol and pentanoic acid). The circles represent individual data points, the squares indicate the means and the error bars display the standard deviations. **b**, Comparison between the standardized odour responses from the 'decoder' neuron and the wild-type *D. simulans* ab10 sensilla. On the left are the standardized (to the strongest odour-evoked response) mean responses for the Or67a paralogue that produced the maximum response to a given odour; on the right are the standardized mean responses from the wild-type recordings (as plotted in **a**). The colour code matches that in **a**. **c**, Right, quantification of *simOr67a.3R* loss-of-function responses to the panel of nine odours; $n = 6$ for all odours. Left, quantification of *simOr67a.P* loss-of-function responses to the panel of nine odours; $n = 6$ (6-methyl-5-hepten-2-one and phenethyl alcohol), 7 (2-heptanone, methyl hexanoate, geraniol and methyl acetate), 8 (methyl benzoate and pentanoic acid) and 9 (ethyl hexanoate). The circles represent individual data points, the squares indicate the means and the error bars display the standard deviations.

chemical ecology of the other drosophilids (although all three are thought to be generalists)[51,52]. Given *mel*Or67a's broad tuning towards fruit esters[29], an expanded survey of fruit odour bouquets via single-sensillum recording coupled to gas chromatography–mass spectrometry will be instrumental to characterizing species-specific receptor tuning in more detail. Such an analysis will be particularly insightful for *sim*Or67a.P, which has diverged adaptively yet displays a relatively similar response profile to *sim*Or67a.D, indicating that ecologically relevant, receptor-specific odour ligands remain to be discovered. Similarly, our observation that *sim*Or67a.3R responses are generally lower than those of *sim*Or67a.D and *sim*Or67a.P suggests that we have not identified its most potent ligands. Behavioural studies will also be necessary to understand how species-specific Or67a OSN tuning relates to an animal's actions in nature. Even in *D. melanogaster*, the behavioural role of the Or67a sensory pathway is unclear: the correlation of odour-evoked neuronal activity across the Or repertoire with odour preference assays suggests (indirectly) that Or67a contributes to behavioural aversion[29], while the optogenetic activation of Or67a neurons in this species induces oviposition site preference[53]. Our analysis of the projections of the Or67a-expressing neurons to the DM6 glomerulus in *D. melanogaster* and *D. simulans* argues that they synapse with homologous projection neurons that carry olfactory information to higher brain centres. However, we cannot exclude that anatomical changes have occurred in central circuit elements, as has been observed in other olfactory pathways in *D. sechellia*[16]. Moreover, it remains possible that the evolution of Or67a paralogues in other lineages has been accompanied by the formation of new OSN populations with novel glomerular targets. Future work examining the expression of *Or67a* paralogues in more divergent species (such as *D. suzukii* (Fig. 1a))[54] may provide different snapshots of evolutionary outcomes and stages in the diversification of OSNs and olfactory circuits.

The one-receptor–one-neuron model has been pervasive in our understanding of olfactory coding in insects, emphasizing a parallel with vertebrate olfactory systems[55]. However, non-insect invertebrates (notably nematode worms) express multiple receptors in olfactory neurons[56], and the insect Or family itself evolved from the gustatory receptor (Gr) family, whose members display widespread receptor co-expression in contact chemosensory neurons[57–65]. Why are *D. melanogaster Or* genes (and probably those of other drosophilids) mostly expressed individually in sensory neurons? We speculate that this property reflects a biochemical constraint of olfactory receptor function, because tuning Ors (but not Grs) act together with the broadly expressed Orco[21]; singular Or expression may prevent multiple types of tuning receptors from forming non-functional complexes that lack the co-receptor subunit. For co-expressed Or67a paralogues in *D. simulans*, it remains unclear whether they function with Orco in independent complexes, or—given the likely heterotetrameric nature of Or complexes[32,33]—form complexes comprising two distinct tuning receptor subunits together with Orco. Alternatively, or additionally, the singular expression of Ors may reflect a difference in the neuronal coding properties of the olfactory system. Current models propose that many (though not all) odours are encoded by the activity of combinations of multiple populations of OSNs[66]. Given this partial redundancy in sensory coding of odour-evoked behaviours, further redundancy by co-expression of functionally similar Ors (if they arose by gene duplication) may have little selective advantage. By contrast, in the gustatory system, individual sensory channels are more closely tied to behavioural responses (for example, attraction by sugar-sensing neurons or aversion by bitter-sensing neurons)[63], so co-expressed receptors may still individually have a substantial behavioural impact—for example, by broadening neuronal tuning to a greater diversity of sugars or toxic compounds. Whatever the reason for singular olfactory receptor expression, its importance is supported by recent studies in *D. melanogaster* and *Anopheles gambiae* indicating the existence of feedback mechanisms ensuring that insect OSNs express only single types of olfactory receptor[67–69].

Adaptive changes in peripheral tuning via receptor co-expression are unlikely to be unique to the *Or67a* subfamily. Copy number changes for other olfactory receptor subfamilies exist, as do several cases of receptor co-expression[70–73]. For example, another fruit odour receptor, Or22a, and a tandem duplicate, Or22b, are thought to be co-expressed in *D. melanogaster*, and paralogues of these receptors vary substantially in copy number between drosophilid species[3,10,16,41,74,75]. Additionally, the highly divergent Or33c and

Or85e are co-expressed in several drosophilids[70]. While physiological data suggest that some examples of endogenous co-expression impact neuron response properties[16,48,75,76], more detailed evolutionary and expression studies are needed to determine whether similar processes as described here for the Or67a subfamily are shaping other olfactory channels. Furthermore, *D. melanogaster* is the only insect for which receptor expression has been comprehensively analysed[24,77,78], and it is possible that this species offers a biased view into the molecular logic of peripheral coding in insects[79]. Indeed, recent studies of receptor expression in other insect species have revealed several cases of co-expression[80–82]. For example, in *A. gambiae*, RNAs encoded by six clustered *Or* genes have been detected in the same OSN population, which is probably the result of these loci being transcribed polycistronically[81]. If multiple types of functional Ors are translated from such transcripts, the tuning of the OSNs may depend on the combined activities of these receptors. In addition, recent single-nucleus RNA-sequencing analyses of *Aedes aegypti* OSNs revealed many cases of co-expression of Ors and members of a different family of olfactory receptor, the ionotropic receptors[82]. While the contribution of tuning receptor co-expression to OSN response properties remains to be elucidated in this mosquito, electrophysiological analysis of neurons lacking Or or ionotropic receptor co-receptors provided evidence for the participation of different receptor families in odour-evoked signalling[82] (similar observations have been made in *D. melangaster*[83]). The existence of receptor co-expression in OSNs may help explain why more receptor genes are expressed in the olfactory organs of *A. aegypti* than there are OSN classes (as estimated by the number of glomeruli in the antennal lobe), a discrepancy also noted in other insect species[82,84]. These studies, together with our present work, raise the possibility that evolutionarily stable receptor co-expression in sensory neurons may be a more widespread feature of insect olfactory systems than currently appreciated.

Methods

***Drosophila* stocks.** *Drosophila* stocks were maintained on standard wheat flour/yeast/fruit juice medium under a 12 h light:12 h dark cycle at 25 °C. For *D. sechellia* strains, a few grams of Formula 4-24 Instant *Drosophila* Medium, Blue (Carolina Biological Supply Company), soaked in noni juice (nu3 GmbH), were added on top of the standard food. The wild-type strains that we used were *D. simulans* (DSSC 14021-0251.004, DSSC 14021-0251.005, DSSC 14021-0251.006, DSSC 14021-0251.007, DSSC14021-0251.008, DSSC 14021-0251.009, DSSC 14021-0251.013, DSSC 14021-0251.014, DSSC 14021-0251.016, DSSC 14021-0251.019, DSSC 14021-0251.165, DSSC 14021-0251.192, DSSC 14021-0251.195, DSSC 14021-0251.196 and DSSC 14021-0251.198), *D. mauritiana* (DSSC 14021-0241.151), *D. sechellia* (DSSC 14021-0248.07) and *D. melanogaster* (CantonS, w^{1118}). To generate transgenic *D. melanogaster* strains for the decoder neuron experiments and for promoter transgenic reporters, we used BDSC no. 24749 (*M{3xP3-RFP.attP}ZH-86Fb)* flies for phiC31-mediated transgenesis. Transgenes in *D. simulans* were integrated into the *attP* landing site of *Dsim#2178* and *Dsim#2176* (ref. [20]; gift from D. Stern) to generate the *simOr67a.D–RFP* and *simOr67a.P–GFP* promoter reporter lines, respectively. Genome engineering in *D. simulans* (described below) was performed in DSSC 14021-0251.195. To visualize Gal4 expression in *D. simulans*, we combined *Gal4* alleles ($simOr67a.3R^{Gal4}$ and $simOr67a.P^{Gal4}$) with *D. simulans UAS–GCaMP6s* transgenics[19] (gift from D. Stern). For the decoder neuron experiments, we combined $DmelOr22a/b^{\Delta halo}$ flies[41] (gift from J. R. Carlson) with *Or22a-Gal4* (ref. [85], BDSC no. 9952) and the respective *UAS–Or67a* transgenics. *DmelOr67a–GFP* transgenic flies[24] (BDSC no. 52633) were used to visualize *Or67a*-expressing neurons, and *DmelOr85f–Gal4* (ref. [77], BDSC no. 23136) and *UAS–RFP* (BDSC no. 35841) transgenic flies were used to visualize *Or85f*-expressing neurons in *D. melanogaster*.

CRISPR–Cas9-mediated genome engineering. *Single guide RNA expression vectors.* To express multiple sgRNAs from the same vector backbone, oligonucleotide pairs (Supplementary Table 8) were used for PCR, and the amplicons were inserted into *pCFD5* (Addgene no. 73914) via Gibson Assembly, as previously described[86]. For single sgRNA expression, oligonucleotide pairs (Supplementary Table 8) were annealed and cloned into BbsI-digested *pCFD3–dU6–3gRNA* (Addgene no. 49410), as previously described[87].

Donor vectors for homologous recombination. Homology arms (1–1.6 kb) for *simOr67a.3R* were amplified from *D. simulans* (DSSC 14021-0251.195) genomic DNA and inserted into *pHD–DsRed–attP*[88] via restriction cloning. The oligonucleotide sequences are listed in Supplementary Table 8. For endogenous tagging of *simOr67a.P*, we generated a *T2A–Gal4* targeting vector flanked by homology arms (1–1.1 kb) via gene synthesis (GenScript Biotech) as previously described[89].

Generation of Gal4 reporter alleles. To target the *D. simulans Or67a.3R* locus, we used three guide RNAs binding within the first exon to integrate an *attP* site and a *3P3–DsRed* reporter cassette, resulting in a loss-of-function allele. Subsequently, we employed phiC31-mediated transgenesis to insert a *Gal4* reporter cassette in the newly created *attP* site as described previously[16]. For *D. simulans Or67a.P*, we used two sgRNAs binding within the first coding exon to directly integrate a *T2A–Gal4* reporter cassette (labelled with *3P3–DsRed*) into the locus. In both cases, parts of the coding sequence of the respective *Or* genes intercalating the sgRNA cutting sites were removed.

Molecular cloning and sequencing. *UAS expression vectors.* To express the different Or67a receptors in the decoder neuron system, open reading frames were amplified from genomic DNA of the respective species via PCR, digested with restriction enzymes (BglII, EcoRI and/or KpnI) and integrated into *pUAST–attB*[90]. The oligonucleotide sequences are listed in Supplementary Table 8.

OrX reporter vectors. Promoter fragments for transcriptional reporters were amplified from *D. simulans* (DSSC 14021-0251.195) genomic DNA by PCR and inserted into *pDONR221–MCS*[16] via restriction cloning, and the resulting vector was combined with *pDEST–HemmarG* or *pDEST–HemmarR*[91] via LR recombination (Gateway, Thermo Fisher Scientific). The oligonucleotide sequences are listed in Supplementary Table 8.

The oligonucleotides used for Sanger sequencing of *D. simulans* paralogues from multiple strains are listed in Supplementary Table 8. The FASTA sequences for these samples are provided in Supplementary Data 7–9.

***Drosophila* microinjections.** Transgenesis of *D. simulans* and *D. melanogaster* was performed in-house following standard protocols (http://gompel.org/methods), except for *simOr67a.D–RFP* transgenics (generated by Rainbow Transgenic Flies). The respective fly strains used are listed above in '*Drosophila* stocks'. For CRISPR–Cas9-mediated homologous recombination, we injected a mix of an sgRNA-encoding construct (150 ng µl^{-1}), donor vector (400 ng µl^{-1}) and *pHsp70–Cas9* (400 ng µl^{-1}) (Addgene no. 45945)[88]. Site-directed integration into *attP* sites was achieved by co-injection of an *attB*-containing vector (400 ng µl^{-1}) and *pBS130* (encoding phiC31 integrase under control of a heat shock promoter (Addgene no. 26290)[92]). All concentrations are given as final values in the injection mix.

Electrophysiology. Single-sensillum electrophysiological recordings in the decoder neuron were performed as described previously[93] using chemicals of the highest purity available from Sigma-Aldrich. Spike visualization and quantification were performed using AutoSpike32 (Syntech). To target wild-type ab10 sensilla in *D. melanogaster*, we used (*R*)-actinidine, which is a diagnostic odour for the neighbouring *Or85f*-expressing neuron[94]. To target ab10 sensilla in *D. simulans*, we carried out fluorescent-guided recordings[95] with GFP fluorescence using a Nikon Eclipse FN1 with a C-FLED2 LED light source. For wild-type recordings, we used the *simOr67a.P–GFP* reporter; for *Or67a* mutants, we combined either the $simOr67a.P^{Gal4}$ allele in homozygosity with *UAS–GCaMP6s* or the *simOr67a.P–GFP* reporter with $simOr67a.3R^{RFP}$ in homozygosity. Spike visualization and quantification for these data were performed using the Spike2 software (CED). Generally, we observed a lower response rate in *D. simulans* ab10 recordings than in the recordings from the individually expressed receptors in the *D. melanogaster* ab3A 'decoder' neurons (Fig. 4a). This might be related to differences between the two recording rigs used for the experiments, but it may also reflect a biological difference between natively expressed receptors and the misexpressed receptors. Odorants (6-methyl-5-hepten-2-one (CAS 110-93-0), methyl benzoate (CAS 93-58-3), ethyl hexanoate (CAS 123-66-0), 2-heptanone (CAS 110-43-0), methyl hexanoate (CAS 106-70-7), phenethyl alcohol (CAS 60-12-8), pentanoic acid (CAS 109-52-4), geraniol (CAS 106-24-1) and methyl acetate (CAS 79-20-9)) were used at 10^{-2} (v/v) in all experiments (unless noted otherwise in the figures or figure legends) and diluted in double-distilled water (for pentanoic acid) or paraffin oil (for all other odours). The odours were presented in 1 s pulses using Syntech's CS55 stimulus controller. Corrected responses were calculated as the number of spikes in a 0.5 s window at stimulus delivery (200 ms after stimulus onset to account for the delay due to the air path), minus the number of spontaneous spikes in a 0.5 s window 2 s before stimulation, multiplied by two to obtain spikes per s. The amplitude of the A and B spikes in *D. simulans*'s ab10 did not differ greatly, and when the A cell fired upon odour stimulus, the amplitude would 'pinch' such that spike sorting by amplitude was not possible. As a result, the number of spikes for these recordings included both cells during the 0.5 s stimulation window. Odours that resulted in saturated bursts of spiking that were too numerous to count were replaced with the maximum value from those that were countable. The solvent-corrected responses shown in the figures were calculated by subtracting from the response to each diluted odour the response obtained when stimulating

with the corresponding solvent. Recordings were performed on a maximum of three sensilla per fly. The response data were plotted using R's (v.4.1.0)[96] ggplot2 library (v.3.3.0)[97]. To test for differences between Or67a.P/D/3R responses, we carried out a non-parametric multivariate approach implemented in the npmv library (v.2.4)[45] in R (see the GitLab repository, https://gitlab.com/roman.arguello/or67a_dsim_trio). Principal component analyses were carried out with the prcomp function within R's (v.4.1.0) stats library and plotted with the scatterplot3d library (v.0.3.41)[98]. Missing data were imputed using the non-parametric approach implemented in R's missForest (v.1.4)[99] on a per-odour basis. The full odour response datasets for all single-sensillum recordings are provided in Supplementary Data 4–6, and an R markdown file with analyses and plotting code are provided in the GitLab repository (https://gitlab.com/roman.arguello/or67a_dsim_trio).

Immunohistochemistry. RNA FISH using digoxigenin- or fluorescein-labelled probes and immunofluorescence on whole-mount antennae were performed essentially as previously described[100,101] using a rabbit anti-GFP 1:500 (Invitrogen) and a chicken anti-GFP 1:500 (Abcam) polyclonal antibody. *D. simulans* probe templates were generated by amplification of regions of genomic DNA (DSSC 14021-0251.004) using the primer pairs listed in Supplementary Table 8; these were cloned into *pCR–Blunt II–TOPO* and sequenced. Species-specific in situ probes were generated for *D. melanogaster*, *D. sechellia* and *D. mauritiana* but did not show better staining quality than *D. simulans* probes. Immunofluorescence on adult brains was performed as previously described[102] using mouse monoclonal antibody nc82 1:10 (Developmental Studies Hybridoma Bank), rabbit anti-GFP 1:500 (Invitrogen), rabbit anti-RFP 1:500 (Abcam) and chicken anti-GFP 1:500 (Abcam). Alexa488- and Cy5-conjugated goat anti-rabbit and goat anti-mouse IgG (Molecular Probes; Jackson Immunoresearch) and Alexa488-conjugated goat anti-chicken (Abcam) secondary antibodies were used at 1:500.

Image acquisition and processing. Confocal images of antennae and brains were acquired on an inverted confocal microscope (Zeiss LSM 710) equipped with an oil immersion 40× objective (Plan Neofluar 40× oil immersion DIC objective; 1.3 NA), unless stated otherwise. The images were processed in Fiji[103]. OSN numbers were counted using the Cell Counter Plugin in Fiji or Imaris (v.9.8.2, Bitplane).

Molecular evolution and polymorphism analyses. To infer the protein tree, Or67a.P/D/3R amino acid sequences were aligned using Clustal Omega with the default settings[104]. The Or67a protein tree was inferred using Mr.Bayes (v.3.2.7a)[105] with the following settings: lset nucmodel, protein; mcmc nchains, 6; ngen, 10,000; samplefreq, 500; printfreq, 100; diagnfreq, 1,000; burnin, 500. To estimate dN/dS ratios over the branches of the Or67a subfamily tree, we used maximum likelihood estimation implemented in PAML's CODEML (v.4.8)[106], using the pamlX GUI (v.1.3.1)[107]. Model testing was carried out using likelihood ratio tests on the outputted likelihoods of the models provided in Supplementary Table 1. For the analyses of *D. simulans* polymorphism data in Fig. 1, we used an existing dataset[108] and the sequences from 15 additional wild-type strains (listed in '*Drosophila* stocks'). For the dataset of Signor et al.[108], we extracted *Or67a.P/D/3R* regions from the full VCF file using VCFtools (v.0.1.17)[109], requiring a minimum mean depth of 5 (min-meanDP, 5) and sites that have a proportion of missing data greater than 0.5 (max-missing, 0.5). We converted these gene region VCF files to FASTA format using the custom script vcf2fasta_remove_het.py, where nucleotides at heterozygous positions were sampled randomly. These FASTA sequences were combined with the 15 Sanger-sequenced samples for the results shown in Tables 1 and 2. For *melOr67a.P*, we extracted the gene region for the prefilter VCF provided in ref. [110]. For calculating silent and replacement diversity estimates, we used a custom script, calc_N_S.py, together with the paralogue-specific GTF file. Similarly, for calculating silent and replacement divergence for the *Or67a.D* and *Or67a.3R* genes, we used a custom script, Div_N_S.py. The custom scripts can be found in the GitLab repository at https://gitlab.com/roman.arguello/or67a_dsim_trio. For estimating the lineage-specific divergence between *Or67a.P* orthologues in *D. melanogaster* and *D. simulans*, we first inferred the ancestral sequence using FastML[111] and then counted branch-specific silent and replacement changes on the basis of an alignment of the three sequences. The reference genomes used to make the alignments in Fig. 1d were as follows: for *D. melanogaster*, v.6.4 from Flybase.org; for *D. sechellia* and *D. simulans*, from ref. [112]; for *D. mauritiana* and *D. yakuba*, from ref. [113]; and for *D. santomea*, Prin_Dsan_1.0 (https://www.ncbi.nlm.nih.gov/assembly/GCF_016746245.1). The alignments of the *Or67a*-containing regions were generated with Clustal Omega (v.1.2.3)[104]. Annotations of the transposable element fragments used RepeatMasker (v.4.1.2-p1)[114], with Dfam_3.0 and rmblastn v(2.9.0+), and existing annotations within Flybase's JBrowse.

Regulatory motif searches. We used the MEME programs within the MEME package (v.5.4.1)[115,116] to search for putative regulatory motifs within the 5′ promoter regions of the *D. simulans* and *D. melanogaster Or67a* copies. We inputted 2 kb for each gene, except for *simOr67a.P*, where only ~1.5 kb exists between it and the upstream *simOr67a.D* copy. We limited the total number of significant motifs to 12 for the comparative analysis.

Reporting summary. Further information on research design is available in the Nature Research Reporting Summary linked to this article.

Data availability

All raw data generated for this study are available in the supplementary files or in the GitLab repository at https://gitlab.com/roman.arguello/or67a_dsim_trio.

Code availability

The code for this study is available in the GitLab repository at https://gitlab.com/roman.arguello/or67a_dsim_trio.

Received: 10 January 2022; Accepted: 15 June 2022;
Published online: 21 July 2022

References

1. Gilad, Y., Wiebe, V., Przeworski, M., Lancet, D. & Pääbo, S. Loss of olfactory receptor genes coincides with the acquisition of full trichromatic vision in primates. *PLoS Biol.* **2**, E5–E5 (2004).
2. Hughes, G. M. et al. The birth and death of olfactory receptor gene families in mammalian niche adaptation. *Mol. Biol. Evol.* **35**, 1390–1406 (2018).
3. McBride, C. S. & Arguello, J. R. Five *Drosophila* genomes reveal nonneutral evolution and the signature of host specialization in the chemoreceptor superfamily. *Genetics* **177**, 1395–1416 (2007).
4. Niimura, Y., Matsui, A. & Touhara, K. Extreme expansion of the olfactory receptor gene repertoire in African elephants and evolutionary dynamics of orthologous gene groups in 13 placental mammals. *Genome Res.* **24**, 1485–1496 (2014).
5. Robertson, H. M. Molecular evolution of the major arthropod chemoreceptor gene families. *Annu. Rev. Entomol.* **64**, 227–242 (2019).
6. Robertson, H. M. & Wanner, K. W. The chemoreceptor superfamily in the honey bee, *Apis mellifera*: expansion of the odorant, but not gustatory, receptor family. *Genome Res.* **16**, 1395–1403 (2006).
7. McKenzie, S. K. et al. The genomic basis of army ant chemosensory adaptations. *Mol. Ecol.* https://doi.org/10.1111/mec.16198 (2021).
8. Zhao, H., Li, J. & Zhang, J. Molecular evidence for the loss of three basic tastes in penguins. *Curr. Biol.* **25**, R141–R142 (2015).
9. Zhao, H., Yang, J. R., Xu, H. & Zhang, J. Pseudogenization of the umami taste receptor gene *Tas1r1* in the giant panda coincided with its dietary switch to bamboo. *Mol. Biol. Evol.* **27**, 2669–2673 (2010).
10. Guo, S. & Kim, J. Molecular evolution of *Drosophila* odorant receptor genes. *Mol. Biol. Evol.* **24**, 1198–1207 (2007).
11. Nei, M. & Rooney, A. P. Concerted and birth-and-death evolution of multigene families. *Annu. Rev. Genet.* **39**, 121–152 (2005).
12. Allen, A. M. et al. A single-cell transcriptomic atlas of the adult *Drosophila* ventral nerve cord. *eLife* https://doi.org/10.7554/eLife.54074 (2020).
13. Eschbach C. et al. Circuits for integrating learned and innate valences in the insect brain eLife 10:e62567 (2021).
14. Li, H. et al. Fly Cell Atlas: a single-nucleus transcriptomic atlas of the adult fruit fly. *Science* **375**, eabk2432 (2022).
15. Zheng, Z. et al. A complete electron microscopy volume of the brain of adult *Drosophila melanogaster*. *Cell* **174**, 730–743.e722 (2018).
16. Auer, T. O. et al. Olfactory receptor and circuit evolution promote host specialization. *Nature* **579**, 402–408 (2020).
17. Ding, Y. et al. Neural evolution of context-dependent fly song. *Curr. Biol.* **29**, 1089–1099.e1087 (2019).
18. Prieto-Godino, L. L. et al. Evolution of acid-sensing olfactory circuits in drosophilids. *Neuron* **93**, 661–676.e666 (2017).
19. Seeholzer, L. F., Seppo, M., Stern, D. L. & Ruta, V. Evolution of a central neural circuit underlies *Drosophila* mate preferences. *Nature* https://doi.org/10.1038/s41586-018-0322-9 (2018).
20. Stern, D. L. et al. Genetic and transgenic reagents for *Drosophila simulans*, *D. mauritiana*, *D. yakuba*, *D. santomea*, and *D. virilis*. *G3 (Bethesda)* **7**, 1339–1347 (2017).
21. Larsson, M. C. et al. *Or83b* encodes a broadly expressed odorant receptor essential for *Drosophila* olfaction. *Neuron* **43**, 703–714 (2004).
22. Lewcock, J. W. & Reed, R. R. A feedback mechanism regulates monoallelic odorant receptor expression. *Proc. Natl Acad. Sci. USA* **101**, 1069–1074 (2004).
23. Serizawa, S. et al. Negative feedback regulation ensures the one receptor–one olfactory neuron rule in mouse. *Science* **302**, 2088–2094 (2003).
24. Couto, A., Alenius, M. & Dickson, B. J. Molecular, anatomical, and functional organization of the *Drosophila* olfactory system. *Curr. Biol.* **15**, 1535–1547 (2005).
25. Gardiner, A., Barker, D., Butlin, R. K., Jordan, W. C. & Ritchie, M. G. *Drosophila* chemoreceptor gene evolution: selection, specialization and genome size. *Mol. Ecol.* **17**, 1648–1657 (2008).
26. Obbard, D. J. et al. Estimating divergence dates and substitution rates in the *Drosophila* phylogeny. *Mol. Biol. Evol.* **29**, 3459–3473 (2012).

27. Ometto, L. et al. Linking genomics and ecology to investigate the complex evolution of an invasive *Drosophila* pest. *Genome Biol. Evol.* **5**, 745–757 (2013).
28. Ramasamy, S. et al. The evolution of olfactory gene families in *Drosophila* and the genomic basis of chemical–ecological adaptation in *Drosophila suzukii*. *Genome Biol. Evol.* **8**, 2297–2311 (2016).
29. Dweck, H. K. M. et al. The olfactory logic behind fruit odor preferences in larval and adult *Drosophila*. *Cell Rep.* **23**, 2524–2531 (2018).
30. Garrigan, D. et al. Genome sequencing reveals complex speciation in the *Drosophila simulans* clade. *Genome Res.* **22**, 1499–1511 (2012).
31. Schrider, D. R., Ayroles, J., Matute, D. R. & Kern, A. D. Supervised machine learning reveals introgressed loci in the genomes of *Drosophila simulans and D. sechellia*. *PLoS Genet.* **14**, e1007341 (2018).
32. Butterwick, J. A. et al. Cryo-EM structure of the insect olfactory receptor Orco. *Nature* **560**, 447–452 (2018).
33. Del Mármol, J., Yedlin, M. A. & Ruta, V. The structural basis of odorant recognition in insect olfactory receptors. *Nature* https://doi.org/10.1038/s41586-021-03794-8 (2021).
34. McDonald, J. H. & Kreitman, M. Adaptive protein evolution at the *adh* locus in *Drosophila*. *Nature* **351**, 652–654 (1991).
35. Smith, N. G. C. & Eyre-Walker, A. Adaptive protein evolution in *Drosophila*. *Nature* **415**, 1022–1024 (2002).
36. Arguello, J. R. et al. Extensive local adaptation within the chemosensory system following *Drosophila melanogaster*'s global expansion. *Nat. Commun.* https://doi.org/10.1038/ncomms11855 (2016).
37. Mansourian, S. et al. Wild African *Drosophila melanogaster* are seasonal specialists on marula fruit. *Curr. Biol.* https://doi.org/10.1016/j.cub.2018.10.033 (2018).
38. Albalat, R. & Cañestro, C. Evolution by gene loss. *Nat. Rev. Genet.* **17**, 379–391 (2016).
39. Tajima, F. Statistical method for testing the neutral mutation hypothesis by DNA polymorphism. *Genetics* **123**, 585–595 (1989).
40. Hohenlohe, P. A., Phillips, P. C. & Cresko, W. A. Using population genomics to detect selection in natural populations: key concepts and methodological considerations. *Int. J. Plant Sci.* **171**, 1059–1071 (2010).
41. Dobritsa, A. A., van der Goes van Naters, W., Warr, C. G., Steinbrecht, R. A. & Carlson, J. R. Integrating the molecular and cellular basis of odor coding in the *Drosophila* antenna. *Neuron* **37**, 827–841 (2003).
42. Galizia, C. G., Münch, D., Strauch, M., Nissler, A. & Ma, S. Integrating heterogeneous odor response data into a common response model: a DoOR to the complete olfactome. *Chem. Senses* **35**, 551–563 (2010).
43. Hallem, E. A. & Carlson, J. R. Coding of odors by a receptor repertoire. *Cell* **125**, 143–160 (2006).
44. Hallem, E. A., Ho, M. G. & Carlson, J. R. The molecular basis of odor coding in the *Drosophila* antenna. *Cell* **117**, 965–979 (2004).
45. Burchett, W. W., Ellis, A. R., Harrar, S. W. & Bathke, A. C. Nonparametric inference for multivariate data: the R package npmv. *J. Stat. Softw.* https://doi.org/10.18637/jss.v076.i04 (2017).
46. Khallaf, M. A. et al. Mate discrimination among subspecies through a conserved olfactory pathway. *Sci. Adv*. https://doi.org/10.1126/sciadv.aba5279 (2020).
47. Khallaf, M. A. et al. Large-scale characterization of sex pheromone communication systems in *Drosophila*. *Nat. Commun.* **12**, 4165 (2021).
48. Stensmyr, M. C., Dekker, T. & Hansson, B. S. Evolution of the olfactory code in the *Drosophila melanogaster* subgroup. *Proc. Biol. Sci.* **270**, 2333–2340 (2003).
49. Stensmyr, M. C. et al. A conserved dedicated olfactory circuit for detecting harmful microbes in *Drosophila*. *Cell* **151**, 1345–1357 (2012).
50. Auer, T. O., Shahandeh, M. P. & Benton, R. *Drosophila sechellia*: a genetic model for behavioral evolution and neuroecology. *Annu. Rev. Genet.* https://doi.org/10.1146/annurev-genet-071719-020719 (2021).
51. Lachaise, D. et al. in *Evolutionary Biology* Vol. 22 (eds Hecht, M. K. et al.) Springer US. 159-225 (1988).
52. David, J. R., McEvey, S. F., Solignac, M. & Tsacas, L. *Drosophila* communities on Mauritius and the ecological niche of *D. mauritiana* (Diptera, Drosophilidae). *Rev. Zool. Afr. J. Afr. Zool.* **103**, 107–116 (1989).
53. Wu, S. T. et al. Valence opponency in peripheral olfactory processing. *Proc. Natl Acad. Sci. USA* https://doi.org/10.1073/pnas.2120134119 (2022).
54. Hickner, P. V. et al. The making of a pest: insights from the evolution of chemosensory receptor families in a pestiferous and invasive fly, *Drosophila suzukii*. *BMC Genomics* **17**, 648 (2016).
55. Monahan, K. & Lomvardas, S. Monoallelic expression of olfactory receptors. *Annu. Rev. Cell Dev. Biol.* **31**, 721–740 (2015).
56. Rengarajan, S. & Hallem, E. A. Olfactory circuits and behaviors of nematodes. *Curr. Opin. Neurobiol.* **41**, 136–148 (2016).
57. Dahanukar, A., Lei, Y.-T., Kwon, J. Y. & Carlson, J. R. Two Gr genes underlie sugar reception in *Drosophila*. *Neuron* **56**, 503–516 (2007).
58. Dweck, H. K. M. & Carlson, J. R. Molecular logic and evolution of bitter taste in *Drosophila*. *Curr. Biol.* **30**, e13 (2020).
59. Fujii, S. et al. *Drosophila* sugar receptors in sweet taste perception, olfaction, and internal nutrient sensing. *Curr. Biol.* **25**, 621–627 (2015).
60. Ganguly, A. et al. A molecular and cellular context-dependent role for Ir76b in detection of amino acid taste. *Cell Rep.* **18**, 737–750 (2017).
61. Jiao, Y., Moon, S. J., Wang, X., Ren, Q. & Montell, C. Gr64f is required in combination with other gustatory receptors for sugar detection in *Drosophila*. *Curr. Biol.* **18**, 1797–1801 (2008).
62. Kwon, J. Y., Dahanukar, A., Weiss, L. A. & Carlson, J. R. Molecular and cellular organization of the taste system in the *Drosophila* larva. *J. Neurosci.* **31**, 15300–15309 (2011).
63. Scott, K. Gustatory processing in *Drosophila melanogaster*. *Annu. Rev. Entomol.* **63**, 15–30 (2018).
64. Slone, J., Daniels, J. & Amrein, H. Sugar receptors in *Drosophila*. *Curr. Biol.* **17**, 1809–1816 (2007).
65. Tauber, J. M. et al. A subset of sweet-sensing neurons identified by IR56d are necessary and sufficient for fatty acid taste. *PLoS Genet.* **13**, 1–18 (2017).
66. Wilson, R. I. Early olfactory processing in *Drosophila*: mechanisms and principles. *Annu. Rev. Neurosci.* **36**, 217–241 (2013).
67. Jafari, S., Henriksson, J., Yan, H. & Alenius, M. Stress and odorant receptor feedback during a critical period after hatching regulates olfactory sensory neuron differentiation in *Drosophila*. *PLoS Biol.* **19**, e3001101 (2021).
68. Maguire, S. E., Afify, A., Goff, L. A. & Potter, C. J. Odorant-receptor-mediated regulation of chemosensory gene expression in the malaria mosquito *Anopheles gambiae*. *Cell Rep.* **38**, 110494 (2022).
69. Mika, K. et al. Olfactory receptor-dependent receptor repression in *Drosophila*. *Sci. Adv.* https://doi.org/10.1126/sciadv.abe3745 (2021).
70. Goldman, A. L., der Goes van Naters, W., Lessing, D., Warr, C. G. & Carlson, J. R. Coexpression of two functional odor receptors in one neuron. *Neuron* **45**, 661–666 (2005).
71. Ray, A., van Naters, W. V. D. G. & Carlson, J. R. A regulatory code for neuron-specific odor receptor expression. *PLoS Biol.* **6**, e125 (2008).
72. Ray, A., van Naters, W. V. D. G., Shiraiwa, T. & Carlson, J. R. Mechanisms of odor receptor gene choice in *Drosophila*. *Neuron* **53**, 353–369 (2007).
73. Vosshall, L. B. & Stocker, R. F. Molecular architecture of smell and taste in *Drosophila*. *Annu. Rev. Neurosci.* **30**, 505–533 (2007).
74. Aguadé, M. Nucleotide and copy-number polymorphism at the odorant receptor genes *Or22a* and *Or22b* in *Drosophila melanogaster*. *Mol. Biol. Evol.* **26**, 61–70 (2009).
75. Lebreton, S. et al. A *Drosophila* female pheromone elicits species-specific long-range attraction via an olfactory channel with dual specificity for sex and food. *BMC Biol.* **15**, 88 (2017).
76. de Bruyne, M., Smart, R., Zammit, E. & Warr Coral, G. Functional and molecular evolution of olfactory neurons and receptors for aliphatic esters across the *Drosophila* genus. *J. Comp. Physiol. A* **196**, 97–109 (2010).
77. Fishilevich, E. & Vosshall, L. B. Genetic and functional subdivision of the *Drosophila* antennal lobe. *Curr. Biol.* **15**, 1548–1553 (2005).
78. McLaughlin, C. N. et al. Single-cell transcriptomes of developing and adult olfactory receptor neurons in *Drosophila*. *eLife* https://doi.org/10.7554/eLife.63856 (2021).
79. Mika, K. & Benton, R. Olfactory receptor gene regulation in insects: multiple mechanisms for singular expression. *Front. Neurosci.* **15**, 738088 (2021).
80. Koutroumpa, F. A. et al. Shifts in sensory neuron identity parallel differences in pheromone preference in the European corn borer. *Front. Ecol. Evol.* https://doi.org/10.3389/fevo.2014.00065 (2014).
81. Karner, T., Kellner, I., Schultze, A., Breer, H. & Krieger, J. Co-expression of six tightly clustered odorant receptor genes in the antenna of the malaria mosquito *Anopheles gambiae*. *Front. Ecol. Evol.* https://doi.org/10.3389/fevo.2015.00026 (2015).
82. Younger, M. A. et al. Non-canonical odor coding in the mosquito. Preprint at *bioRxiv* https://doi.org/10.1101/2020.11.07.368720 (2022).
83. Task, D. et al. Chemoreceptor co-expression in *Drosophila melanogaster* olfactory neurons. *eLife* https://doi.org/10.7554/eLife.72599 (2022).
84. Dippel, S. et al. Morphological and transcriptomic analysis of a beetle chemosensory system reveals a gnathal olfactory center. *BMC Biol.* **14**, 90 (2016).
85. Vosshall, L. B., Wong, A. M. & Axel, R. An olfactory sensory map in the fly brain. *Cell* **102**, 147–159 (2000).
86. Port, F. & Bullock, S. L. Augmenting CRISPR applications in *Drosophila* with tRNA-flanked sgRNAs. *Nat. Methods* **13**, 852–854 (2016).
87. Port, F., Chen, H.-M., Lee, T. & Bullock, S. L. Optimized CRISPR/Cas tools for efficient germline and somatic genome engineering in *Drosophila*. *Proc. Natl Acad. Sci. USA* **111**, E2967–E2976 (2014).
88. Gratz, S. J. et al. Highly specific and efficient CRISPR/Cas9-catalyzed homology-directed repair in *Drosophila*. *Genetics* **196**, 961–971 (2014).
89. Kondo, S. et al. Neurochemical organization of the *Drosophila* brain visualized by endogenously tagged neurotransmitter receptors. *Cell Rep.* **30**, 284–297.e285 (2020).

90. Bischof, J., Maeda, R. K., Hediger, M., Karch, F. & Basler, K. An optimized transgenesis system for *Drosophila* using germ-line-specific phiC31 integrases. *Proc. Natl Acad. Sci. USA* **104**, 3312–3317 (2007).
91. Han, C., Jan, L. Y. & Jan, Y.-N. Enhancer-driven membrane markers for analysis of nonautonomous mechanisms reveal neuron–glia interactions in *Drosophila*. *Proc. Natl Acad. Sci. USA* **108**, 9673–9678 (2011).
92. Gohl, D. M. et al. A versatile in vivo system for directed dissection of gene expression patterns. *Nat. Methods* **8**, 231–237 (2011).
93. Benton, R. & Dahanukar, A. Electrophysiological recording from *Drosophila* olfactory sensilla. *Cold Spring Harb. Protoc.* https://doi.org/10.1101/pdb.prot5630 (2011).
94. Ebrahim, S. A. M. et al. *Drosophila* avoids parasitoids by sensing their semiochemicals via a dedicated olfactory circuit. *PLoS Biol.* **13**, 1–18 (2015).
95. Lin, C.-C. & Potter, C. J. Re-classification of *Drosophila melanogaster* trichoid and intermediate sensilla using fluorescence-guided single sensillum recording. *PLoS ONE* **10**, e0139675 (2015).
96. R Core Team R: A Language and Environment for Statistical Computing v.4.1.0 https://www.R-project.org/ (R Foundation for Statistical Computing, 2021).
97. Wickham, H. ggplot2: Elegant graphics for data analysis. R package v.3.3.0 (2016).
98. Ligges, U. & Mächler, M. Scatterplot3d—an R package for visualizing multivariate data. *J. Stat. Softw.* **8**, 1–20 (2003).
99. Stekhoven, D. J. & Bühlmann, P. MissForest—non-parametric missing value imputation for mixed-type data. *Bioinformatics* **28**, 112–118 (2012).
100. Saina, M. & Benton, R. Visualizing olfactory receptor expression and localization in *Drosophila*. *Methods Mol. Biol.* **1003**, 211–228 (2013).
101. Silbering, A. F. et al. Complementary function and integrated wiring of the evolutionarily distinct *Drosophila* olfactory subsystems. *J. Neurosci.* **31**, 13357–13375 (2011).
102. Sánchez-Alcañiz, J. A., Zappia, G., Marion-Poll, F. & Benton, R. A mechanosensory receptor required for food texture detection in *Drosophila*. *Nat. Commun.* **8**, 14192 (2017).
103. Schindelin, J. et al. Fiji: an open-source platform for biological-image analysis. *Nat. Methods* **9**, 676–682 (2012).
104. Sievers, F. et al. Fast, scalable generation of high-quality protein multiple sequence alignments using Clustal Omega. *Mol. Syst. Biol.* **7**, 539 (2011).
105. Ronquist, F. & Huelsenbeck, J. P. MrBayes 3: Bayesian phylogenetic inference under mixed models. *Bioinformatics* **19**, 1572–1574 (2003).
106. Yang, Z. PAML 4: phylogenetic analysis by maximum likelihood. *Mol. Biol. Evol.* **24**, 1586–1591 (2007).
107. Xu, B. & Yang, Z. PAMLX: a graphical user interface for PAML. *Mol. Biol. Evol.* **30**, 2723–2724 (2013).
108. Signor, S. A., New, F. N. & Nuzhdin, S. A large panel of *Drosophila simulans* reveals an abundance of common variants. *Genome Biol. Evol.* **10**, 189–206 (2018).
109. Danecek, P. et al. The variant call format and VCFtools. *Bioinformatics* **27**, 2156–2158 (2011).
110. Grenier, J. K. et al. Global diversity lines—a five-continent reference panel of sequenced *Drosophila melanogaster* strains. *G3 (Bethesda)* https://doi.org/10.1534/g3.114.015883 (2015).
111. Pupko, T., Pe'er, I., Shamir, R. & Graur, D. A fast algorithm for joint reconstruction of ancestral amino acid sequences. *Mol. Biol. Evol.* **17**, 890–896 (2000).
112. Chakraborty, M. et al. Evolution of genome structure in the *Drosophila simulans* species complex. *Genome Res.* **31**, 380–396 (2021).
113. Miller, D. E., Staber, C., Zeitlinger, J. & Hawley, R. S. Highly contiguous genome assemblies of 15 *Drosophila* species generated using nanopore sequencing. *G3 (Bethesda)* **8**, 3131–3141 (2018).
114. Smit, AFA, Hubley, R & Green, P. RepeatMasker Open-4.0.2013-2015. http://www.repeatmasker.org
115. Bailey, T. L. et al. MEME SUITE: tools for motif discovery and searching. *Nucleic Acids Res.* **37**, W202–W208 (2009).
116. Bailey, T. L., Williams, N., Misleh, C. & Li, W. W. MEME: discovering and analyzing DNA and protein sequence motifs. *Nucleic Acids Res.* **34**, W369–W373 (2006).

Acknowledgements

We thank M. Cardoso-Moreira, L.L. Prieto-Godino, J. A. Sánchez-Alcañiz, L. Keller, M. Long and members of the Arguello lab for comments on earlier versions of the manuscript; M. Khallaf, M. Knaden, A. Svatos and J. Weissflog at the Max Planck Institute for Chemical Ecology for the synthesized (*R*)-actinidine; and J. Carlson and D. Stern for sharing transgenic fly lines. T.O.A. was supported by a Human Frontier Science Program Long-Term Fellowship (no. LT000461/2015-L) and a Swiss National Science Foundation Ambizione Grant (no. PZ00P3 185743). Research in R.B.'s laboratory was supported by ERC Consolidator and Advanced Grants (nos 615094 and 833548, respectively) and the Swiss National Science Foundation. Research in J.R.A.'s lab is supported by the Swiss National Science Foundation grants no. PP00P3_176956 and no. 310030_201188.

Author contributions

J.R.A. conceived the study. J.R.A., T.O.A. and R.A.-O. designed the experiments with input from R.B. J.R.A., T.O.A., R.A.-O. and S.C. carried out the experiments. J.R.A., T.O.A. and R.A.-O. analysed the data. J.R.A and T.O.A. prepared the original draft of the manuscript with revisions from R.A.-O. and R.B. All authors read and approved the final version of the manuscript.

Competing interests

The authors declare no competing interests.

Additional information

Extended data is available for this paper at https://doi.org/10.1038/s41559-022-01830-y.

Supplementary information The online version contains supplementary material available at https://doi.org/10.1038/s41559-022-01830-y.

Correspondence and requests for materials should be addressed to J. Roman Arguello.

Peer review information *Nature Ecology & Evolution* thanks Jean-Christophe Billeter, Carolyn McBride and Coral Warr for their contribution to the peer review of this work.

Reprints and permissions information is available at www.nature.com/reprints.

Publisher's note Springer Nature remains neutral with regard to jurisdictional claims in published maps and institutional affiliations.

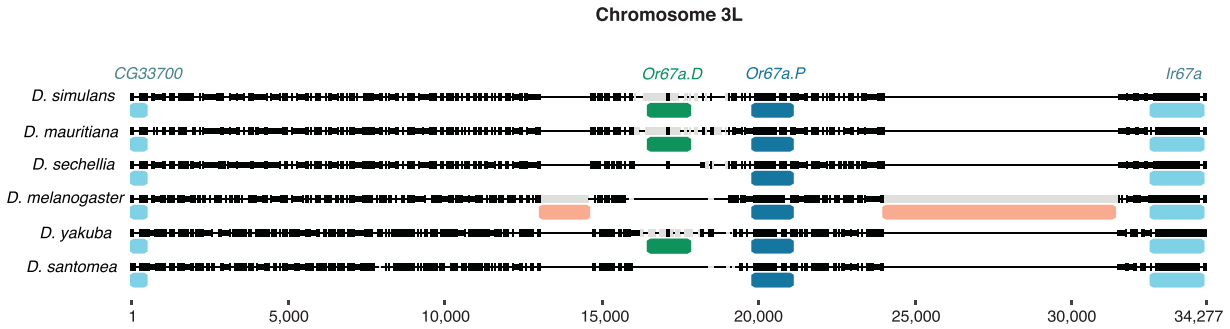

Extended Data Fig. 1 | Microsynteny for chromosomal regions containing *Or67a.D* and *Or67a.P*. Alignment for the chromosome 3L interval containing *Or67a.D* and *Or67a.P* (and flanking genes, light blue) for six species. High sequence identity is indicated with black alignment blocks with low sequence identity indicated with light grey alignment blocks. Thin horizontal lines are alignment gaps. Red annotations indicate locations of transposable elements. Chromosome position on the horizontal axis are relative to the extracted interval. See Supplementary Files 1 for the alignment in a flat file.

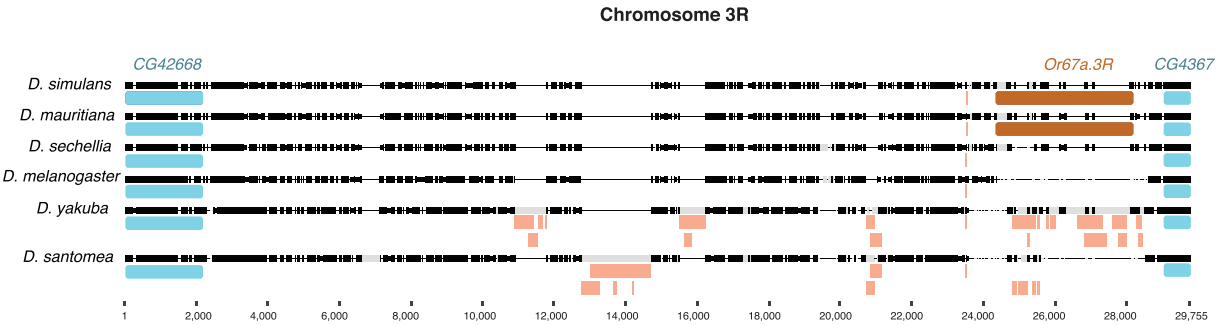

Extended Data Fig. 2 | Microsynteny for chromosomal region containing *Or67a.3R*. Alignment for the chromosome 3R interval containing *Or67a.3R* (and flanking genes, light blue) for six species. High sequence identity is indicated with black alignment blocks with low sequence identity indicated with light grey alignment blocks. Thin horizontal lines are alignment gaps. Red annotations indicate locations of transposable elements. Chromosome position on the horizontal axis are relative to the extracted interval. See Supplementary Files 2 for the alignment in a flat file.

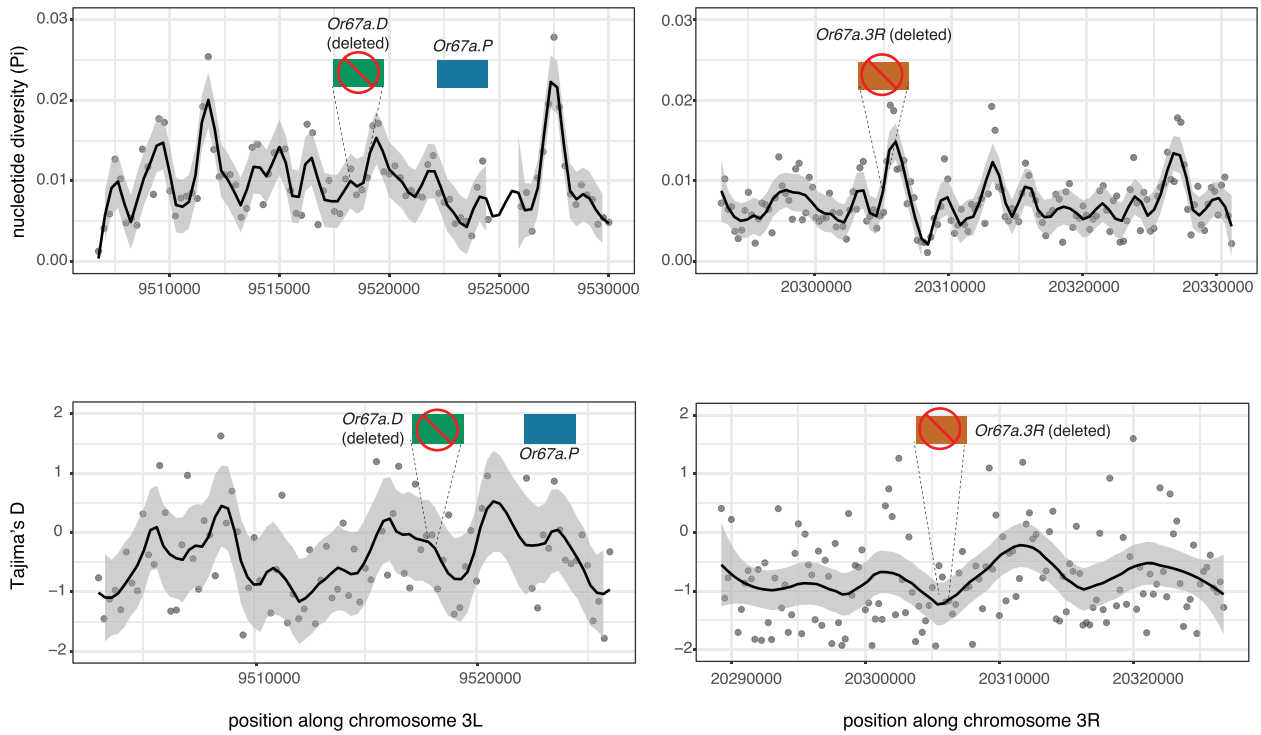

Extended Data Fig. 3 | Genetic diversity in regions containing *D. melanogaster*'s *Or67a.D and Or67a.3R* deletions. Nucleotide diversity (Π) and Tajima's *D* over *D. melanogaster*'s chromosomal regions containing the intact *Or67a.P* gene and the deleted *Or67a.D* and *Or67a.3R*. The regions containing the deleted *Or67a* paralogs do not show differences in genetic diversity in comparison to the surrounding regions, as would be expected if the deletions were adaptive and swept in the population. The black line in each panel is the smoothed curve fit with LOESS, with the grey ribbon around it displaying the standard error. The sample size (number of genomes) = 84.

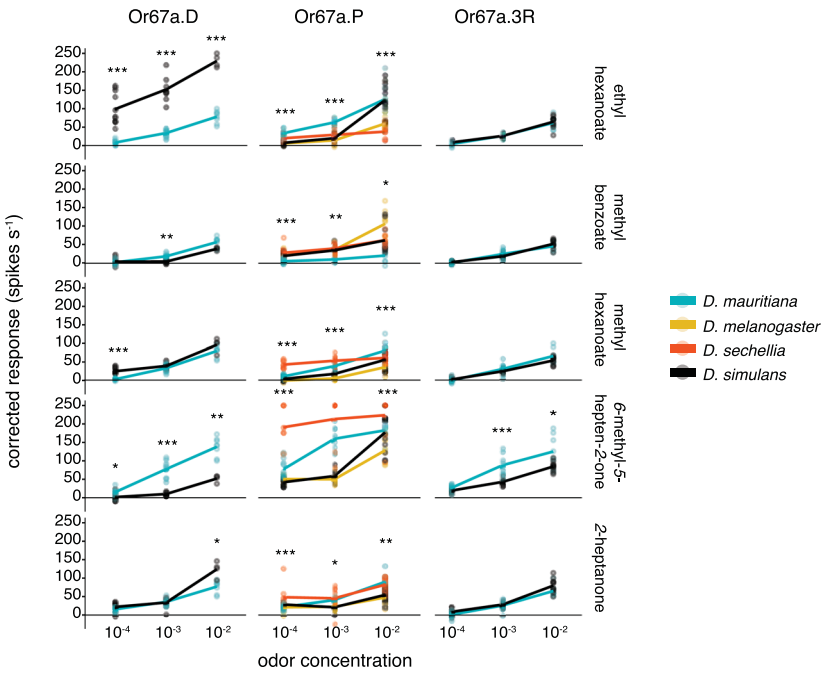

Extended Data Fig. 4 | Evolution of odour sensitivity across Or67a orthologs. The full set of dose-response experiments for the subset of odours that evoked high or intermediate responses in our initial screen of nine odours (Fig. 2b). For simplicity, the level of significance indicated above each concentration's comparison is only for the single comparison with the largest difference (see Supplementary Table 4 for the full set of tests; $*p < 0.05$, $**p < 0.01$, $***p < 0.001$). Colours correspond to those in Fig. 2d. *p*-values were calculated with a two-sided Dunn test; correction for multiple comparisons was done using the Holm method. For sample sizes and all test results see Supplementary Table 4.

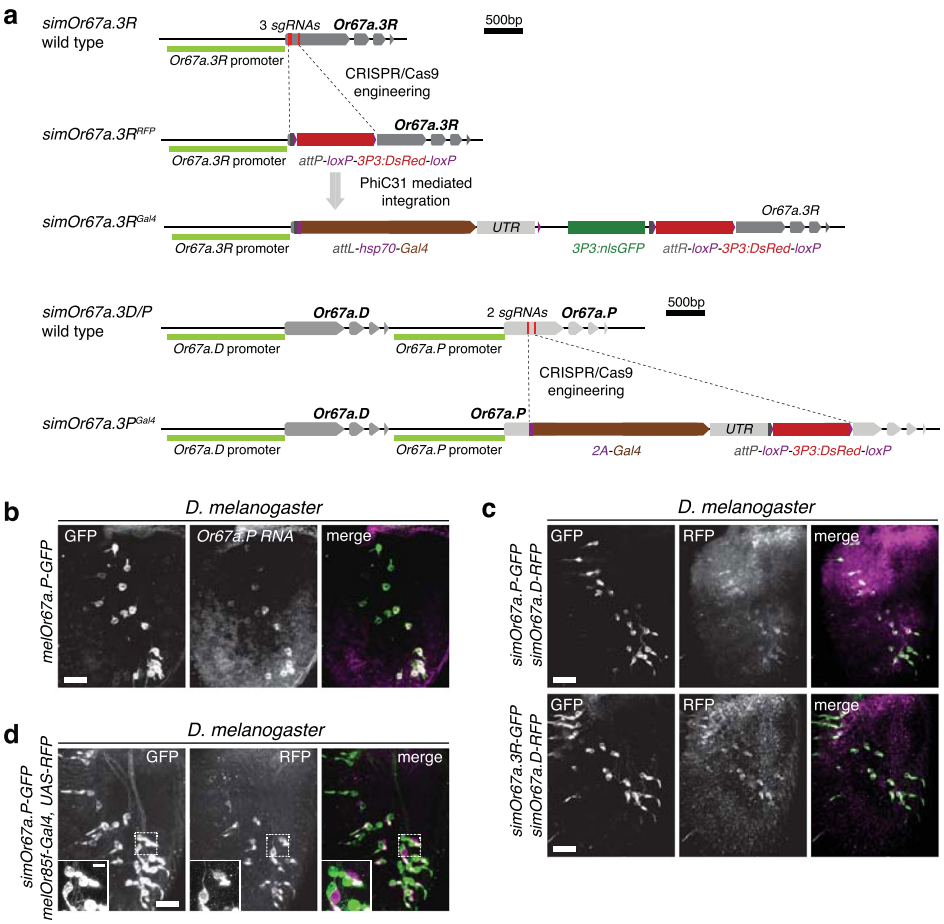

Extended Data Fig. 5 | Transgenic tools for Or67a expression analyses in *D. simulans* and *D. melanogaster*. a, Schematics of the wild-type and knock-in Gal4 transcriptional reporter alleles at the *DsimOr67a.3R* (top) and *DsimOr67a.D/P* (bottom) loci. The first was created via a two-step process (CRISPR/Cas9 engineering + PhiC31 mediated integration) while the latter was resulting from a direct CRISPR/Cas9 mediated insertion. The red lines indicate sgRNA cutting sites; three and two sgRNAs were used to target the *Or67a.3R* and *Or67a.P* locus, respectively. Note that the intercalated sequence was removed upon donor vector integration. **b**, Antennal co-expression of the *melOr67a.P-GFP* transcriptional reporter and *Or67a.P* RNA in *D. melanogaster*. Scale bar = 25 µm. **c**, Antennal co-expression of the *simOr67a.P-GFP* and *simOr67a.D-RFP* transcriptional reporters (top) and the *simOr67a.3R-GFP* and *simOr67a.D-RFP* transcriptional reporters (bottom) in *D. melanogaster*. Scale bar = 25 µm. **d**, Pairing of the *simOr67a.P-GFP* promoter transcriptional reporter and *melOr85f-Gal4*, *UAS-RFP* expression in neighboring neurons in the antenna of *D. melanogaster*. Scale bar = 25 µm. Inset scale bar = 5 µm. (**b**-**d**) Experiments were repeated at least three times for each staining on independent days and pictures show representative examples for each condition.

nature portfolio

Corresponding author(s): J. Roman Arguello

Last updated by author(s): May 24, 2022

Reporting Summary

Nature Portfolio wishes to improve the reproducibility of the work that we publish. This form provides structure for consistency and transparency in reporting. For further information on Nature Portfolio policies, see our Editorial Policies and the Editorial Policy Checklist.

Statistics

For all statistical analyses, confirm that the following items are present in the figure legend, table legend, main text, or Methods section.

n/a	Confirmed	
☐	☒	The exact sample size (*n*) for each experimental group/condition, given as a discrete number and unit of measurement
☐	☒	A statement on whether measurements were taken from distinct samples or whether the same sample was measured repeatedly
☐	☒	The statistical test(s) used AND whether they are one- or two-sided *Only common tests should be described solely by name; describe more complex techniques in the Methods section.*
☒	☐	A description of all covariates tested
☐	☒	A description of any assumptions or corrections, such as tests of normality and adjustment for multiple comparisons
☐	☒	A full description of the statistical parameters including central tendency (e.g. means) or other basic estimates (e.g. regression coefficient) AND variation (e.g. standard deviation) or associated estimates of uncertainty (e.g. confidence intervals)
☐	☒	For null hypothesis testing, the test statistic (e.g. *F*, *t*, *r*) with confidence intervals, effect sizes, degrees of freedom and *P* value noted *Give P values as exact values whenever suitable.*
☒	☐	For Bayesian analysis, information on the choice of priors and Markov chain Monte Carlo settings
☒	☐	For hierarchical and complex designs, identification of the appropriate level for tests and full reporting of outcomes
☐	☒	Estimates of effect sizes (e.g. Cohen's *d*, Pearson's *r*), indicating how they were calculated

Our web collection on statistics for biologists contains articles on many of the points above.

Software and code

Policy information about availability of computer code

Data collection	For physiology, SynTech's Autospike 32 and CED's Spike2 were used. For more details refer to the respective sections of the "Methods".
Data analysis	For image data analyses we used ImageJ Version 2.0.0-rc-65/1.52a and Imaris (version 9.8.2, Bitplane). For evolutionary genetic and related analyses, Mr.Bayes (v3.2.7a), Clustal Omega, PAML's CODEML (v4.8), pamlX GUI (v1.3.1), VCFtools (v0.1.17), FastML, RepeatMasker (v4.1.2-p1), rmblastn v(2.9.0+), MEME (v5.4.1). For statistical analyses we used R (v4.1.0). For more details see "Methods" section.

For manuscripts utilizing custom algorithms or software that are central to the research but not yet described in published literature, software must be made available to editors and reviewers. We strongly encourage code deposition in a community repository (e.g. GitHub). See the Nature Portfolio guidelines for submitting code & software for further information.

Data

Policy information about availability of data

All manuscripts must include a data availability statement. This statement should provide the following information, where applicable:

- Accession codes, unique identifiers, or web links for publicly available datasets
- A description of any restrictions on data availability
- For clinical datasets or third party data, please ensure that the statement adheres to our policy

All data has been submitted with the manuscript, available on our GitLab repository: https://gitlab.com/roman.arguello/or67a_dsim_trio, or available from the corresponding author on reasonable request.

Field-specific reporting

Please select the one below that is the best fit for your research. If you are not sure, read the appropriate sections before making your selection.

☒ Life sciences ☐ Behavioural & social sciences ☐ Ecological, evolutionary & environmental sciences

For a reference copy of the document with all sections, see nature.com/documents/nr-reporting-summary-flat.pdf

Life sciences study design

All studies must disclose on these points even when the disclosure is negative.

Sample size	For electrophsyiology, preliminary experiments were used to assess variance and the adequate sample size. We generally aimed to have ~5-10 replicates. For the population genomic analyses, sample sizes were large and were determined on exiting data for D. melanogaster (# individuals = 84); We generated data for D. simulans and then combined it with an existing data set (# of individuals per gene = 208-210). See additional details in the "Molecular evolution and polymorphism analyses" section of "Methods". For immunohistochemical and in situ stainings, we collected data from multiple independent experiments and aimed for a sample size of 9-12 replicates.
Data exclusions	For the electrophysiology data, several recordings were excluded if the paired solvent recordings were not obtained or if quantification was prevented by "pinching" of spike amplitudes upon neuron firing rate saturation.
Replication	Our replications were successful. Repeated physiology and immunohistochemical experiments remained consistent across days and months.
Randomization	For all experiments, we interleaved genotypes and stimuli when applicable and randomized their order if possible. To control for day effects, we were careful to collect similar sample sizes for each variable on multiple days when possible.
Blinding	Blinding was not used in the study.

Reporting for specific materials, systems and methods

We require information from authors about some types of materials, experimental systems and methods used in many studies. Here, indicate whether each material, system or method listed is relevant to your study. If you are not sure if a list item applies to your research, read the appropriate section before selecting a response.

Materials & experimental systems

n/a	Involved in the study
☐	☒ Antibodies
☒	☐ Eukaryotic cell lines
☒	☐ Palaeontology and archaeology
☐	☒ Animals and other organisms
☒	☐ Human research participants
☒	☐ Clinical data
☒	☐ Dual use research of concern

Methods

n/a	Involved in the study
☒	☐ ChIP-seq
☒	☐ Flow cytometry
☒	☐ MRI-based neuroimaging

Antibodies

Antibodies used	The following antibodies were used in this study (with source and identifier): Rabbit polyclonal anti-GFP, Invitrogen, Cat#A-11122 Mouse monoclonal nc82, Developmental Studies Hybridoma Bank, RRID:AB_2314866 Goat polyclonal anti-mouse Cy5, Molecular Probes, Jackson Immunoresearch, RRID: AB_2338714 Goat polyclonal anti-rabbit Alexa488, Molecular Probes, Jackson Immunoresearch, RRID: AB_2338049 Chicken polyclonal anti-GFP, Abcam, Ab13970 Goat polyclonal anti-chicken Alexa488, Abcam, Ab150169 Please refer to the "Immunohistochemistry" section in the "Methods" for more details.
Validation	All antibodies used were commercially available and had already been established/tested.

Animals and other organisms

Policy information about studies involving animals; ARRIVE guidelines recommended for reporting animal research

Laboratory animals	Lab stocks of Drosophila were used: D. simulans, D. melanogaster, D. mauritiana, and D. sechellia. For physiology experiments, adult males and females were used. For all immunohistochemistry experiments, 3-6 day-old female flies were used. For more details on the strains of each species see "Drosophila Stocks" in the "Methods".
Wild animals	No wild animals were used.
Field-collected samples	No field-caught samples were used.
Ethics oversight	All experiments were conducted in accordance with ethical guidelines from the University of Lausanne.

Note that full information on the approval of the study protocol must also be provided in the manuscript.

CHAPTER 3: Evolution of odor representation and neuromodulation of sensory signals in the antennal lobe

In this chapter I will describe two related projects regarding how olfactory information is represented as neural activity patterns in the antennal lobe of *D. melanogaster* and *D. sechellia*, and how such activity may be differentially modulated between species. While some of this work has been published (manuscript provided below), several lines of investigation were technically difficult to pursue, or deemed to be of lower priority due to progress in other research (notably in Chapter 4). Nevertheless, I provide the context and most important experimental results from these efforts as they may represent a starting point for future investigations.

First, I was interested in studying changes in odor representations in the central brain between the generalist *D. melanogaster* and the noni fruit specialist *D. sechellia*. To do so, I learnt the *in vivo* calcium imaging technique using a widefield microscope and helped with the development of the technique in *D. sechellia*. Calcium imaging is a microscopy technique and a reliable method to study neuron excitability in response to certain stimuli. The most standardized calcium imaging technique in *Drosophila* uses genetically encoded calcium sensing fluorescent proteins (notably GCaMP (GFP-Calmodulin-M13)) that monitors calcium concentration changes in neurons. More specifically, upon stimulation of a neuron (or group of neurons) it will respond, in the form of action potentials, opening cation channels that allow the entrance of ions, such as calcium, contributing to depolarizing the neuron. Calcium will bind to the GCaMP protein leading to a conformational change and increased GFP fluorescence, which can be detected with a camera.

I contributed to the analysis of noni representation in *D. sechellia*'s antennal lobe using the wide field calcium imaging technique. Part of this work was published in Nature (attached below in section 3.1.1 (Auer et al. 2020)), and the other part focuses on two olfactory pathways (Or19a and Or56a projecting to DA1 and DC2 glomeruli, respectively) that exhibit differences in functionality between *D. melanogaster* and *D. sechellia* (sections 3.1.2 and 3.1.3).

In a second approach to gain insights into inter-species differences, I wanted to study species-specific neuromodulation in the *Drosophila* antennal lobe, the first olfactory processing center. To do so, I combined the use of transgenic reporter lines, hybrid crosses and the use of antibodies to describe the expression pattern of a group of selected neuromodulators in both *D. melanogaster* and *D. sechellia*. These findings are described below in this chapter (section 3.2.).

3.1. Comparative physiology in *D. melanogaster* and *D. sechellia*

3.1.1. Olfactory receptor and circuit evolution promote host specialization

Summary of the results

This section describes the result of a collaborative effort from past and current members of the Richard Benton's lab (enclosed publication; Auer, Silbering, Zappia, Álvarez-Ocaña and Arguello), as well as members of other institutions (Khallaf, Ellis, Hansson, Jefferis, Caron and Knaden) (Auer et al. 2020). In this work, we developed *D. sechellia* as a neurogenetic model system and studied the relationship between nervous system structure and function and flies' specialization for noni fruit. Using calcium imaging, we described olfactory pathways responsible for noni attraction in *D. sechellia* and described some

olfactory pathways important for the long-range attraction. Furthermore, we described that the odor tuning of one of these receptors, Or22a, is important for species-specific host-seeking and identified the molecular determinants of this functional change. Through brain circuit tracing we identified species-specific central projection patterns.

My contribution to this work

I helped to developed calcium imaging in *D. sechellia* using widefield microscopy. I compared the neuronal activity patterns in the antennal lobes of *D. melanogaster* and *D. sechellia* when these flies were stimulated with the odors of various juices, including apple vinegar, grape, noni juice and noni fruit extracts. Using diagnostic odors, I localized the relative position of antennal lobe glomeruli of interest, including those mediating noni attraction. Subsequently, I measured the juice-evoked calcium responses in each of the glomeruli and finally quantified the maximum calcium response amplitudes for each animal tested. All these results are compiled in the Extended Data Figure 4a-b of the manuscript included below.

3.1.2. Article: Olfactory receptor and circuit evolution promote host specialization

Olfactory receptor and circuit evolution promote host specialization

https://doi.org/10.1038/s41586-020-2073-7

Received: 13 February 2019

Accepted: 31 January 2020

Published online: 4 March 2020

Check for updates

Thomas O. Auer[1]✉, Mohammed A. Khallaf[2], Ana F. Silbering[1], Giovanna Zappia[1], Kaitlyn Ellis[3], Raquel Álvarez-Ocaña[1], J. Roman Arguello[4], Bill S. Hansson[2], Gregory S. X. E. Jefferis[5], Sophie J. C. Caron[3], Markus Knaden[2] & Richard Benton[1]✉

The evolution of animal behaviour is poorly understood[1,2]. Despite numerous correlations between interspecific divergence in behaviour and nervous system structure and function, demonstrations of the genetic basis of these behavioural differences remain rare[3–5]. Here we develop a neurogenetic model, *Drosophila sechellia*, a species that displays marked differences in behaviour compared to its close cousin *Drosophila melanogaster*[6,7], which are linked to its extreme specialization on noni fruit (*Morinda citrifolia*)[8–16]. Using calcium imaging, we identify olfactory pathways in *D. sechellia* that detect volatiles emitted by the noni host. Our mutational analysis indicates roles for different olfactory receptors in long- and short-range attraction to noni, and our cross-species allele-transfer experiments demonstrate that the tuning of one of these receptors is important for species-specific host-seeking. We identify the molecular determinants of this functional change, and characterize their evolutionary origin and behavioural importance. We perform circuit tracing in the *D. sechellia* brain, and find that receptor adaptations are accompanied by increased sensory pooling onto interneurons as well as species-specific central projection patterns. This work reveals an accumulation of molecular, physiological and anatomical traits that are linked to behavioural divergence between species, and defines a model for investigating speciation and the evolution of the nervous system.

The genetic and neural basis by which animals adapt behaviourally to their ecological niche is largely unknown[1,2]. Insights have previously been gained from investigating intraspecific variation in traditional model organisms, including anxiety behaviours in *Mus musculus*[17] and exploration versus exploitation decisions in *Caenorhabditis elegans*[18]. Interspecific differences are more marked than intraspecific differences. For example, distinct species of *Peromyscus* mice display variations in burrowing and parental care[3,5], and the predatory nematode *Pristionchus pacificus* exhibits feeding behaviours that are divergent from those of *C. elegans*[19]. Defining the molecular basis of interspecific differences is challenging as it requires both that species are comparable in molecular and anatomical terms, and that they can be genetically manipulated.

Drosophilid flies are attractive models for investigating behavioural evolution: *D. melanogaster* offers deep neurobiological knowledge in a numerically relatively simple brain, and closely related drosophilid species show distinct behaviours that are linked to their diverse ecologies[20]. Several of these behavioural traits have previously been correlated to anatomical and/or physiological changes in sensory or central pathways[4,11,13,15,21,22]. One notable drosophilid is *D. sechellia*, which is endemic to the Seychelles and shares a recent common ancestor with the cosmopolitan ecological generalists *D. melanogaster* and *Drosophila simulans*[6,7] (Fig. 1a). *D. sechellia* has evolved extreme specialism for noni fruit (Fig. 1a), and displays olfactory[11–13,15,16], gustatory[14] and reproductive behaviours[8–10] that are unique among known drosophilids. Mapping approaches have located causal loci for some traits specific to *D. sechellia* (typically within large genomic regions[8,10]), and candidate approaches have correlated chemosensory phenotypes with changes in the peripheral sensory pathways of this species[11,14,15].

Despite the potential that *D. sechellia* presents for comparative neuroscience, investigations of the behaviours of *D. sechellia* have been limited by a lack of genetic tools. Here we develop *D. sechellia* into a genetic model system, moving from genotypic–phenotypic correlations to test the role of genetic changes in behavioural evolution.

Specific noni attraction of *D. sechellia*

Noni-derived volatiles are probably the initial cues that guide *D. sechellia* host-seeking[16]. We used two assays to compare the attraction of wild-type strains of *D. sechellia*, *D. simulans* and *D. melanogaster* to noni at distinct spatial scales (Fig. 1b, c, Extended Data Fig. 1). In a long-range wind tunnel assay[23], *D. sechellia* displayed a higher attraction to noni than that of its sister species (Fig. 1b); in a short-range trap assay[15], only *D. sechellia* exhibits a marked preference for noni (Fig. 1c).

[1]Center for Integrative Genomics, Faculty of Biology and Medicine, University of Lausanne, Lausanne, Switzerland. [2]Department of Evolutionary Neuroethology, Max Planck Institute for Chemical Ecology, Jena, Germany. [3]Department of Biology, University of Utah, Salt Lake City, UT, USA. [4]Department of Ecology and Evolution, Faculty of Biology and Medicine, University of Lausanne, Lausanne, Switzerland. [5]Division of Neurobiology, MRC Laboratory of Molecular Biology, Cambridge, UK. ✉e-mail: Thomas.Auer@unil.ch; Richard.Benton@unil.ch

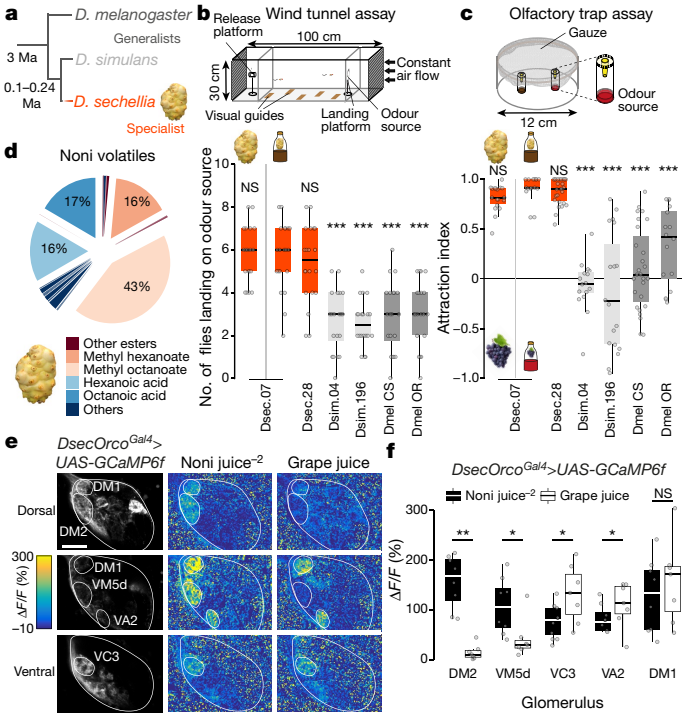

Fig. 1 | Behavioural and physiological responses of *D. sechellia* to noni. **a**, *D. sechellia* specializes on noni fruit, whereas *D. simulans* and *D. melanogaster* are food generalists. Ma, million years ago. **b**, Behavioural responses to noni fruit or juice in a wind tunnel assay of *D. sechellia*, *D. simulans* and *D. melanogaster* wild-type strains ($n = 20$ experiments, with 10 female flies per experiment). Comparisons to the responses of *D. sechellia* 14021-0248.07 flies (Dsec.07) (Supplementary Table 2 provides details of fly strains) to noni juice are shown. Kruskal–Wallis test, Dunn's post hoc correction. **c**, Behavioural responses in a trap assay testing preferences between noni and grape or between noni juice and grape juice, using the same strains as in **b**. $n = 15$–27 experiments, 22–25 female flies per experiment (exact n values are given in the Source Data). Comparisons to the responses of Dsec.07 flies to noni juice are shown. Pairwise Wilcoxon rank-sum test, P values adjusted for multiple comparisons using the Benjamini and Hochberg method. **d**, Odour bouquet of a ripe noni fruit determined by gas chromatography–mass spectrometry (Extended Data Fig. 2, Methods, Supplementary Table 1). **e**, Representative odour-evoked calcium responses in the axon termini of Orco OSNs in the *D. sechellia* antennal lobe (genotype *UAS-GCaMP6f/UAS-GCaMP6f;;DsecOrco*^{Gal4}/+) acquired by two-photon imaging. Three focal planes are shown, revealing different glomeruli (outlined) along the dorsoventral axis. Left, raw fluorescence images. Right and middle, relative increase in GCaMP6f fluorescence ($\Delta F/F$%) after stimulation with noni juice (10^{-2} dilution in H_2O; denoted noni juice^{-2}) or grape juice. Scale bar, 25 µm. **f**, Quantification of responses for the flies represented in **e**. Maximum response amplitudes for each experiment are plotted. $n = 7$–10 female flies. Wilcoxon signed-rank test. All box plots show the median and first and third quartiles of the data, overlaid with individual data points. NS, not significant ($P > 0.05$); *$P < 0.05$; **$P < 0.01$; ***$P < 0.001$.

The behaviour of this species towards noni juice (which represents an odour stimulus that is more reproducible than that of noni fruit) was comparable to that for ripe fruit (Fig. 1b, c), concordant with their qualitatively similar odour bouquets (Fig. 1d, Extended Data Fig. 2a, b, Methods). Assays using other natural odour sources, as previously described in field studies[24], confirmed the unique attractiveness of noni for *D. sechellia* (Extended Data Fig. 1a–e, g).

Noni-sensing olfactory pathways

Drosophilids detect odours using olfactory sensory neurons (OSNs) in sensilla on their antennae and maxillary palps[25]. Most OSNs express a single odorant receptor (Or) or ionotropic receptor (Ir)—which defines odour-tuning properties—along with an obligate co-receptor[26–28]. Neurons that express the same tuning receptor converge onto a discrete glomerulus in the antennal lobe[25]. Previous electrophysiological analyses in *D. sechellia* have identified several OSN populations that respond to individual noni odours[11,13,15,29], but the global representation of the noni bouquet has not been examined.

We generated transgenic *D. sechellia* that express GCaMP6f in the majority of OSNs, under the control of *Gal4* inserted at the *Or co-receptor* (*DsecOrco*) locus (Extended Data Fig. 3). Using wide-field imaging to compare this and an equivalent *D. melanogaster* line (Extended Data Fig. 4a), we did not detect noni-responsive olfactory channels unique to *D. sechellia* but instead found quantitative differences in individual glomerular responses between species (Extended Data Fig. 4b). Two-photon calcium imaging highlighted two glomeruli (DM2 and VM5d) that are distinguished by their very high sensitivity to noni compared to grape juice in *D. sechellia* (Fig. 1e, f, Extended Data Fig. 4b–d). These glomeruli are innervated by OSNs that are housed in the same antennal basiconic sensillum class (ab3) and that respond electrophysiologically to individual noni odours[11,13].

Genetic targeting of olfactory receptors

We determined the electrophysiological responses of noni-sensitive olfactory channels to a range of noni odours (Fig. 2a, b, Extended Data Figs. 4e, 5, 6), and mutated candidate olfactory receptors (Extended Data Figs. 5, 6). In wild-type ab3 sensilla, the larger-spiking ab3A neuron responded most strongly to methyl esters and the smaller-spiking ab3B neuron was highly stimulated by 2-heptanone and 1-hexanol (Fig. 2a). All of these responses were lost in *DsecOrco* mutants, (Fig. 2a), which indicates that these responses are dependent on Or signalling.

The *D. melanogaster* ab3A neuron expresses the *Or22a* and *Or22b* genes[30], whereas *D. sechellia* possesses only *DsecOr22a*[11]. Targeted mutation of this latter locus abolished the odour-evoked responses of the ab3A, but not the ab3B, neuron (Fig. 2a). The receptor in the *D. melanogaster* ab3B neuron is thought to be Or85b[25,31], but *D. sechellia* neurons with a mutation in *DsecOr85b* retained some sensitivity to noni odours (Fig. 2a). Deletion of *DsecOr85b* and the neighbouring *DsecOr85c*—transcripts of which have previously been detected in an antennal transcriptome[32]—led to complete loss of responses of ab3B neurons, arguing for partial receptor redundancy (Fig. 2a).

In *D. sechellia*, Ir75b neurons in antennal coeloconic 3I (ac3I) sensilla have evolved a sensitivity to hexanoic acid that does not exist in *D. melanogaster* or *D. simulans*[15]. Mutations in *DsecIr75b* or *DsecIr8a* (which encodes an Ir co-receptor[27]) led to a selective loss of responses to hexanoic acid and butyric acid in the ac3I sensillum (Fig. 2b, Extended Data Fig. 6). Mutation of *DsecOr35a* (expressed in the paired neuron) diminished responses to all odours except these acids, consistent with the broad tuning of this receptor in *D. melanogaster*[33].

Odorant receptors for long-range attraction

We used the receptor mutants to determine the behavioural role of individual olfactory pathways. In the long-range assay, *DsecOrco* mutants exhibited no attraction to the odour source (Fig. 2c). Notably, flies with a mutation in *DsecOr22a* or in *DsecOr85c* and *DsecOr85b* (hereafter, *DsecOr85c/b*) both displayed similar, strong defects (Fig. 2c). By contrast, *DsecOr35a* mutants were not impaired (Fig. 2c). Loss of Ir8a also led to a significant decrease in long-range attraction in *D. sechellia* (Fig. 2c). This does not appear to be primarily due to defects in the hexanoic-acid-sensing pathway, as *DsecIr75b* mutants had either no or milder defects than *DsecIr8a* mutants (Fig. 2c). Loss of DsecIr64a—which is broadly tuned to acids in *D. melanogaster*[34], and responded to noni in *D. sechellia* (Extended Data Fig. 4f,g)—had no effect on this behaviour.

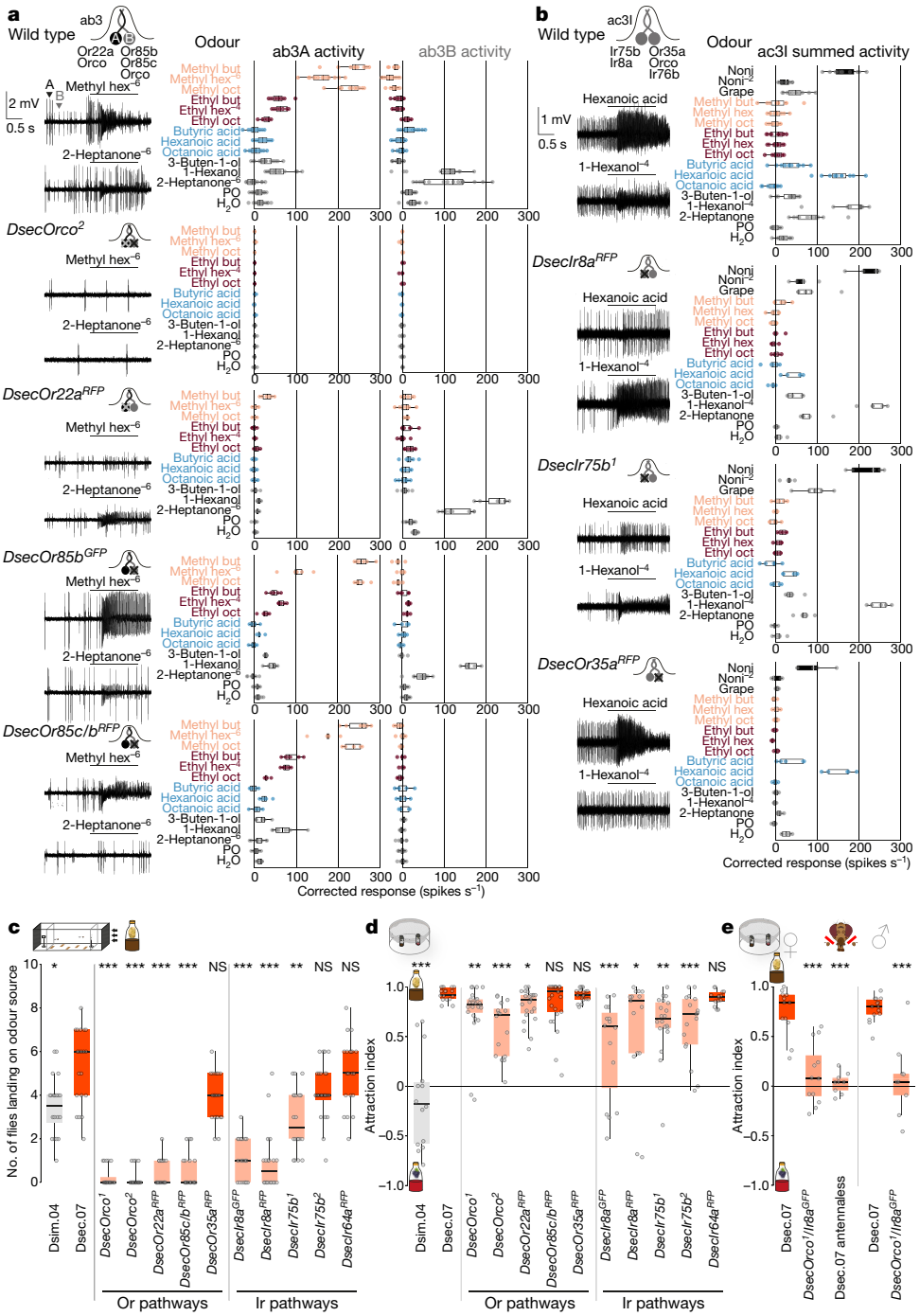

Fig. 2 | Olfactory receptor contributions to noni-sensing.
a, Electrophysiological responses of neurons of the ab3 sensillum to noni odours ($n = 5–20$, female flies, Supplementary Table 7 provides exact n values and mean spike counts) in wild-type and receptor-mutant *D. sechellia* (schematized in the cartoons), with representative traces for methyl hexanoate (hex) and 2-heptanone. Data points are the solvent-corrected activities of individual neurons (arrowheads in the wild-type trace). Odours are coloured according to chemical class: methyl esters (salmon), ethyl esters (dark red), acids (light blue) and others (black). Odorants were used at 10^{-2} dilution (v/v) in double-distilled water or paraffin oil (PO) (see 'Electrophysiology' in the Methods for details), unless indicated otherwise in superscript (for example, methyl hex^{-6} denotes methyl hexanoate at 10^{-6} dilution (v/v)). But, butanoate; hex, hexanoate; oct, octanoate. **b**, Responses of neurons of the ac3I sensillum to noni juice, grape juice and noni odours ($n = 5–11$, female flies) in wild-type and receptor-mutant *D. sechellia*, with representative traces for hexanoic acid and 1-hexanol. Data points are the summed solvent-corrected activities of both neurons. **c**, Behavioural responses to noni juice in the wind tunnel assay ($n = 20$ experiments). Comparisons to the response of Dsec.07 flies are shown. Kruskal–Wallis test, Dunn's post hoc correction. In **c**–**e**, red denotes no significant difference, and salmon denotes a significantly different responses of the *D. sechellia* genotypes. **d**, Behavioural responses in the trap assay testing preference for noni juice or grape juice ($n = 13–25$ experiments). Comparisons to responses of Dsec.07 flies are shown. **e**, Behavioural responses in the trap assay testing preference for noni juice or grape juice, using wild-type *D. sechellia*, *DsecOrco*^{1} *Ir8a*^{GFP} double mutants and antennaless *D. sechellia* ($n = 9–15$ experiments, 22–25 female or male (as indicated) flies per experiment). Average attraction indices for *DsecOrco*^{1} *Ir8a*^{GFP} and antennaless flies are not significantly different from zero. In **d**, **e**, pairwise Wilcoxon rank-sum test, P values adjusted for multiple comparisons using the Benjamini and Hochberg method. NS, not significant ($P > 0.05$); *$P < 0.05$; **$P < 0.01$; ***$P < 0.001$.

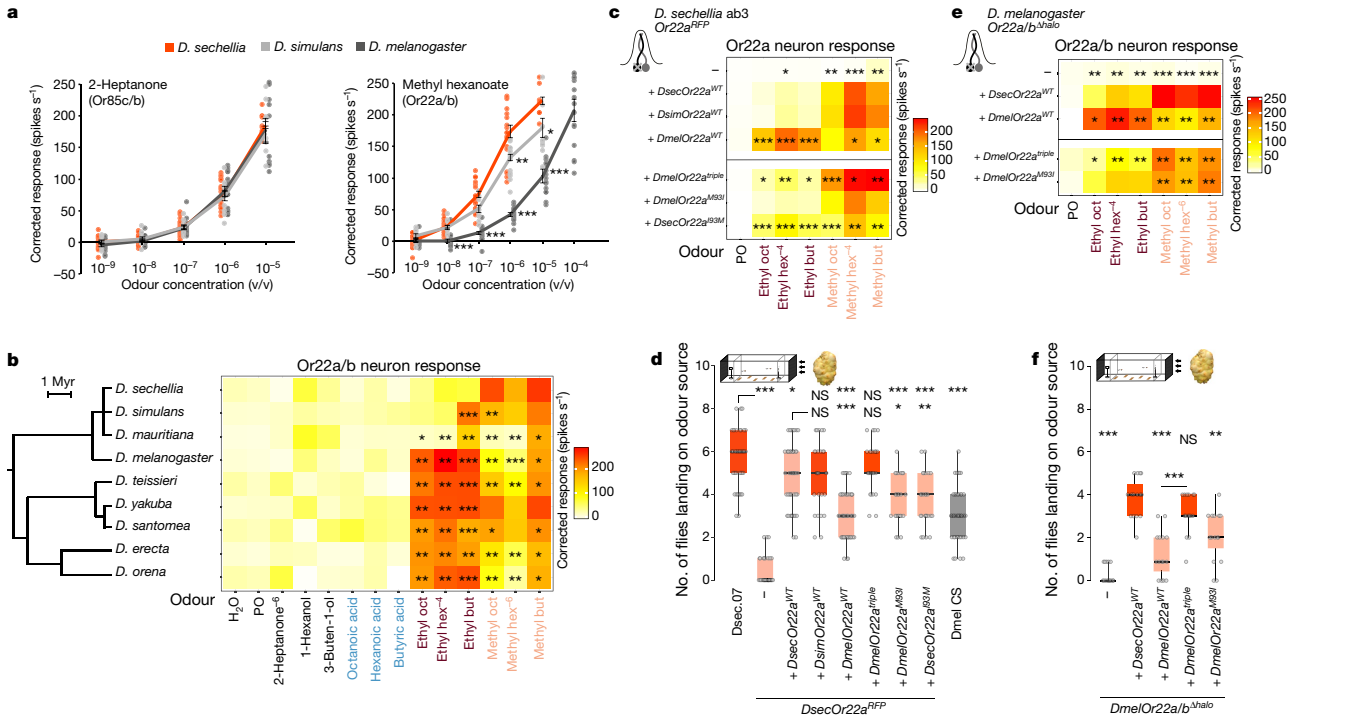

Fig. 3 | Tuning of Or22a is important for attraction to noni. **a**, Dose-dependent responses of Or85c/b (left) and Or22a/b (right) neurons in Dsec.07, Dsim.04 and Dmel CS to 2-heptanone and methyl hexanoate, respectively. Mean ± s.e.m. and individual data points; $n = 5–20$, female flies. Significant differences to responses of *D. sechellia* are shown. In **a**–**c**, **e**, pairwise Wilcoxon rank-sum test, *P* values adjusted for multiple comparisons using the Benjamini and Hochberg method. **b**, Responses of Or22a/b neurons to noni odours across the *D. melanogaster* species subgroup of drosophilids. In all instances, '*D.*' denotes *Drosophila*. Myr, million years. $n = 5–20$, female flies. Data for *D. sechellia* responses are replotted from Fig. 2a. Significant differences to responses of *D. sechellia* to esters are shown. **c**, Responses of Or22a neurons from *D. sechellia* expressing wild-type (top) or mutant (bottom) versions of *Or22a* inserted at the *Or22a* locus ($n = 10–18$, female flies). Significant differences to the responses of $DsecOr22a^{WT}$ flies are shown (**c**, **e**). Responses to methyl hexanoate are a 10^{-4} dilution (v/v) in this panel compared with a 10^{-6} dilution in **b**, **e**. Superscript 'triple' denotes mutations that give rise to Or22a(I45V/I67M/M93I). **d**, Behavioural responses to noni fruit in the wind tunnel assay. $n = 25–45$ experiments. Comparisons to responses of Dsec.07 (top line of *P* values) and $DsecOr22a^{WT}$ (bottom line of *P* values) flies responses are shown. In **d**, **f**, Kruskal–Wallis test, Dunn's post hoc correction. Salmon, *D. sechellia* genotypes with significantly different responses to that of Dsec.07 flies. **e**, Responses of *D. melanogaster Or22a/b*-mutant neurons expressing wild-type (top) or mutant (bottom) versions of *Or22a*. $n = 5–7$, female flies. Box plots of data in **b**, **c**, **e** are shown in Extended Data Fig. 8g, h, i, respectively. **f**, Behavioural responses to noni fruit in the wind tunnel assay. $n = 20$ experiments. Comparisons to responses of $DsecOr22a^{WT}$ (top line of *P* values) and $DmelOr22a^{WT}$ (bottom line of *P* values) flies are shown. Salmon, genotypes with significantly different responses to that of $DsecOr22a^{WT}$ flies. NS, not significant ($P > 0.05$); $^{*}P < 0.05$; $^{**}P < 0.01$; $^{***}P < 0.001$.

In the short-range assay, *DsecOrco* mutants displayed a reduced, but not abolished, preference for noni (Fig. 2d). Flies with mutations in individual Or pathways had very slight (*DsecOr22a*) or no (*DsecOr85c/b* and *DsecOr35a*) defects in this behaviour (Fig. 2d, Extended Data Fig. 7). *DsecIr8a* or *DsecIr75b* (but not *DsecIr64a*) mutants displayed a reduced preference for noni, with notable frequent preference reversals in several trials (Fig. 2d). Flies with mutations in both *DsecOrco* and *DsecIr8a*, as well as antennaless flies, displayed no noni preference (Fig. 2e, Extended Data Fig. 7c, d), indicating that this short-range behaviour depends on multiple partially redundant olfactory inputs. Consistent with these observations, individual noni odours promoted a strong preference at short range, whereas they triggered no or little flight attraction at long range[11,13,15] (Extended Data Fig. 7f, g). The relative contribution of individual channels to these behaviours may be related to their detection thresholds (Extended Data Fig. 2c) and/or differential diffusion of cognate odours within each assay (Extended Data Fig. 2d, e).

Tuning of Or22a affects behaviour

Given the crucial role of Or22a and Or85c/b in long-range attraction, we explored the evolution of these pathways. Or85c/b neurons displayed an indistinguishable sensitivity across species to their best agonist, 2-heptanone. By contrast, Or22a neurons of *D. sechellia*, and Or22a and Or22b (hereafter, Or22a/b) neurons of *D. simulans*, exhibited increased sensitivity to methyl hexanoate, compared to that of *D. melanogaster*[11,29] (Fig. 3a, Extended Data Fig. 8a). Broader profiling of Or22a/b neurons in the *D. melanogaster* species subgroup of drosophilids (Fig. 3b, Extended Data Fig. 8g) revealed that *D. sechellia* was the only species with selective and high sensitivity to methyl esters; other species—including *D. simulans*—also responded to ethyl esters (Fig. 3b). This suggests that changes in the tuning sensitivity and/or breadth of Or22a (but not Or85c/b) contribute to the differences in behaviour of *D. sechellia* relative to *D. melanogaster*.

We next reintroduced wild-type *DsecOr22a* ($DsecOr22a^{WT}$), *DsimOr22a*^{WT} or $DmelOr22a^{WT}$ into the *DsecOr22a* endogenous locus (Extended Data Fig. 8b). Expression of $DsecOr22a^{WT}$ or $DmelOr22a^{WT}$ restored electrophysiological-response profiles similar to those of the native neuronal responses, indicating that the receptor is key for the species-specific tuning of neurons (Fig. 3c top). Introducing $DsimOr22a^{WT}$ conferred sensitivity to methyl esters, but not to ethyl esters (Fig. 3b, c, Extended Data Fig. 8h); genetic analysis in *D. simulans* indicated that the detection of ethyl esters by the endogenous Or22a/b neurons depends on the coexpressed Or22b (Extended Data Fig. 8c–f).

Concordant with their physiological properties, DsecOr22a^{WT} and DsimOr22a^{WT}—but not DmelOr22a^{WT}—rescued long-range behavioural responses to almost wild-type levels (Fig. 3d). Reciprocally, the expression of DsecOr22a^{WT} in the neurons of *D. melanogaster* flies with *Or22a/b*

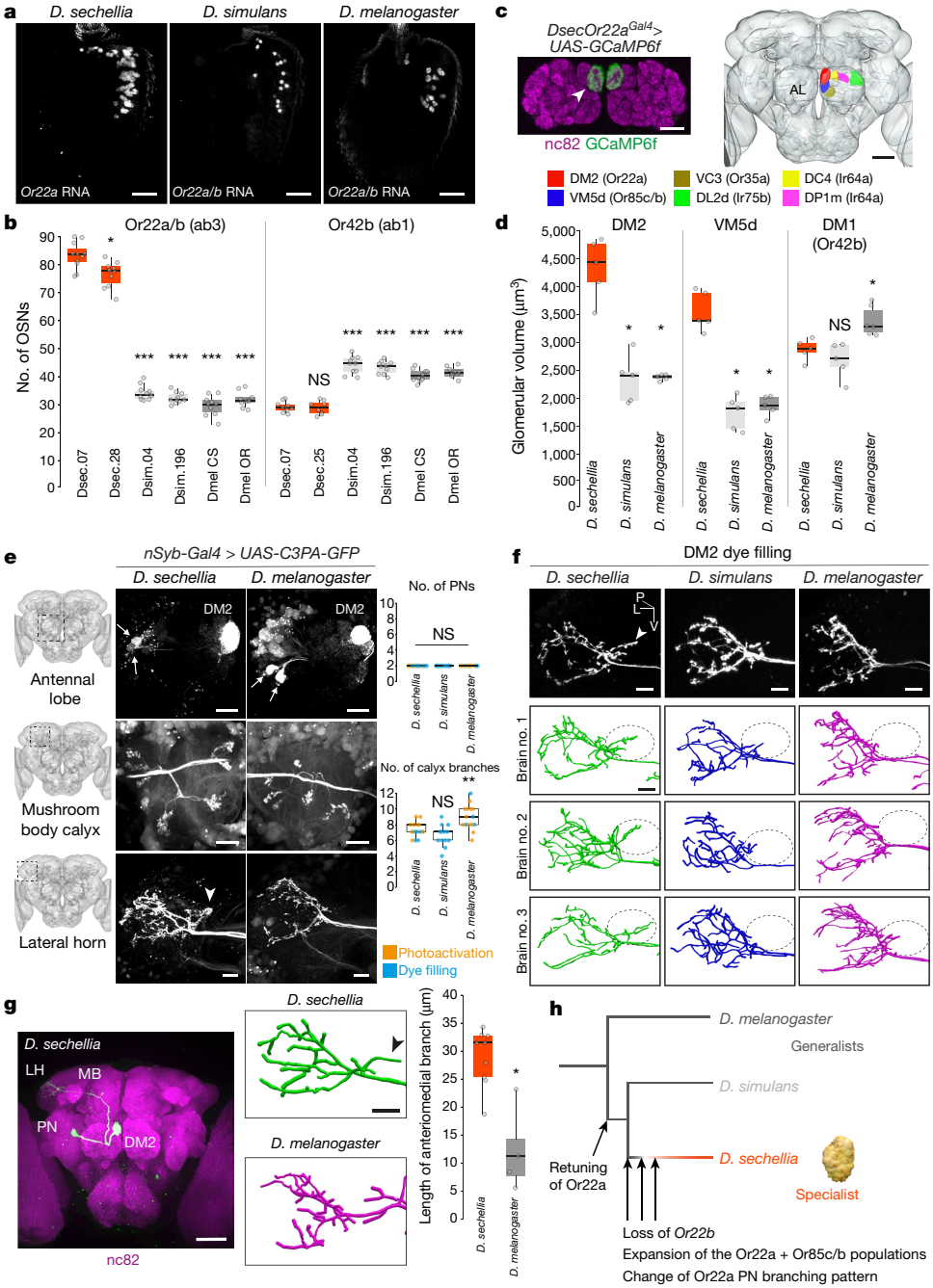

Fig. 4 | Neuroanatomy of noni-sensing olfactory pathways. a, Antennal *Or22a/b* RNA expression in different species. Scale bars, 25 μm. **b**, Quantification of Or22a/b or Or42b OSNs. $n = 8–11$, female flies. Comparisons to Dsec.07 flies are shown. In **b**, **d**, **e**, pairwise Wilcoxon rank-sum test, *P* values adjusted for multiple comparisons using the Benjamini and Hochberg method. **c**, Left, *Or22a*^{Gal4}-driven GCaMP6f expression in DM2 (arrowhead); neuropil visualized with nc82 (magenta). Scale bar, 25 μm. Right, antennal lobe (AL) glomerular segmentation in *D. sechellia* (Extended Data Fig. 3). Scale bar, 50 μm. **d**, Quantification of DM2, VM5d and DM1 volumes. $n = 5$ female flies of each species indicated. **e**, DM2 projection neurons (PNs) labelled via photoactivation in *D. sechellia* (*DsecnSyb-Gal4/UAS-C3PA-GFP*) and *D. melanogaster* (*UAS-SPA-GFP/UAS-C3PA-GFP;nSyb-Gal4/UAS-C3PA-GFP*). Left, image acquisition site. Middle two panels show antennal lobe with labelled projection neurons (arrows) and DM2 glomerulus (scale bar, 20 μm) (top) and projection-neuron innervation of mushroom body calyx (middle) and lateral horn (bottom). Scale bars, 10 μm. Arrowhead in **e**–**g** indicates the extra anteriomedial branch in *D. sechellia*. Right, quantification of DM2 projection neurons (top) and calyx branches (bottom). $n = 14–17$ female flies. **f**, Top row, lateral horn arbours of dye-filled DM2 projection neurons. Genotypes of *D. sechellia* and *D. melanogaster* are as in **e**; genotype of *D. simulans* is *DsimOr22a-GFPnls*. Bottom three rows, representative lateral-horn DM2 arbour traces. Ovals, location of branch specific to *D. sechellia*. P, posterior; L, lateral; V, ventral. Scale bars, 10 μm. **g**, Left, single dye-filled DM2 projection neuron in *D. sechellia*. MB, mushroom body; LH, lateral horn. Scale bar, 50 μm. Middle, representative lateral horn arbour traces of DM2 projection neurons in *D. sechellia* and *D. melanogaster*. Scale bar, 10 μm. Right, quantification of anteriomedial branch length. $n = 4–9$ female flies. Pairwise Wilcoxon rank-sum test. NS, not significant ($P > 0.05$); *$P < 0.05$; **$P < 0.01$; ***$P < 0.001$. **h**, Evolution of structural and physiological changes in the Or22a pathway.

mutations (Fig. 3e top) conferred higher noni sensitivity and long-range attraction than that associated with DmelOr22a^{WT} (Fig. 3f, Extended Data Figs. 8i, 9a).

Molecular basis of Or22a tuning changes

We next sought the molecular basis of the differences in the tuning of Or22a. Expression of chimeric versions of wild-type DsecOr22a

and DmelOr22a in Or22a/b neurons in *D. melanogaster* (Extended Data Fig. 9c) indicated that high sensitivity and selectivity for methyl esters are determined by the N-terminal 100 amino acids of DsecOr22a (chimaera C) (Extended Data Fig. 9b, c, e). Within these amino acids, three positions (I45, I67 and M93) differ between DmelOr22a and its orthologues in species that display a narrowed tuning for methyl esters (Extended Data Fig. 9b). Exchange of these residues to produce DmelOr22a(I45V/I67M/M93I) narrowed the responsiveness to methyl esters, similar to DsecOr22a^{WT} (Fig. 3c, e bottom, Extended Data Fig. 9d, f). Individual mutations revealed that DmelOr22a(M93I) most closely recapitulated the higher sensitivity of this receptor to methyl esters over ethyl esters (Fig. 3c, e bottom, Extended Data Fig. 9d–g). Conversely, DsecOr22a(I93M) exhibited a broadened sensitivity to both classes of ester (Fig. 3c bottom, Extended Data Fig. 9g).

In the long-range olfactory-behaviour assay, expression of DmelOr22a(I45V/I67M/M93I) in Or22a neurons of *D. sechellia* restored an attraction to noni similar to that of wild-type *D. sechellia*, whereas both DmelOr22a(M93I) and DsecOr22a(I93M) displayed levels of attraction intermediate between those of the wild-type-receptor rescues (Fig. 3d). Similarly, expression of DmelOr22a(I45V/I67M/M93I) in *D. melanogaster* conferred noni attraction at levels equivalent to those of DsecOr22a^{WT}, and DmelOr22a(M93I) supported intermediate levels of attraction (Fig. 3f). These results provide evidence that the molecular differences in Or22a orthologues contribute to species-specific olfactory behaviours.

Sensory representation of Or22a

The functional similarity of Or22a orthologues in *D. sechellia* and *D. simulans* (Fig. 3c, d) indicates that additional changes have occurred during the speciation of *D. sechellia*. Concordant with ab3 sensilla counts[11,29], *D. sechellia* exhibits a threefold increase in the number of Or22a neurons (recapitulated in rescue experiments shown in Extended Data Fig. 10a) and the paired Or85c/b neurons, but not several other classes of neurons[15] (Fig. 4a, b, Extended Data Figs. 5d, 10b).

To analyse OSN projections in *D. sechellia*, we inserted *Gal4* at the corresponding receptor loci and combined these with *UAS-GCaMP6f* as an anatomical marker (Extended Data Fig. 3). Extending single-neuron dye-filling analyses[11,13,15], OSN glomerular innervation patterns were indistinguishable between *D. sechellia* and *D. melanogaster* (Fig. 4c, Extended Data Fig. 3c, d). However, the glomerular targets of Or22a and Or85c/b neurons (DM2 and VM5d, respectively) were nearly doubled in volume in *D. sechellia* compared to *D. melanogaster* or *D. simulans*[11,13] (Fig. 4d).

Differences in Or22a circuit wiring

To visualize higher-order elements of the Or22a pathway, we combined a pan-neuronal driver (Extended Data Fig. 10c) with a photoactivatable *GFP* transgene to selectively photolabel DM2 projection neurons. Analysis with analogous genetic reagents in *D. melanogaster*—as well as targeted electroporation of a lipophilic dye[35] into this glomerulus in *D. simulans*, *D. sechellia* and *D. melanogaster*—permitted cross-species comparisons. Two DM2 projection neurons were consistently labelled in all three drosophilids (Fig. 4e).

Projection neurons innervate the mushroom body (which is required for learning and memory) and the lateral horn (which is implicated in innate olfactory responses)[36]. Within the former, the number and arrangement of projection-neuron axonal branches were similar between species (Fig. 4e). In the lateral horn, global anatomy was conserved, with the main tract bifurcating into dorsal and ventral branches. However, dorsal to the bifurcation, *D. sechellia* DM2 projection neurons had a prominent branch innervating an area that was not targeted by the homologous *D. melanogaster* or *D. simulans* neurons (Fig. 4e, f). Using successive photo- and dye-labelling to visualize single DM2 projection neurons in *D. sechellia* and *D. melanogaster*, we confirmed quantitatively the presence of a branch specific to *D. sechellia* (Fig. 4g); this was also detected in flies lacking a functional DsecOr22a receptor (Extended Data Fig. 10d, e), indicating its independence of sensory input. These data raise the possibility that changes in the central circuit that are specific to *D. sechellia* form part of the olfactory specialization of this species towards noni.

Discussion

We have developed *D. sechellia* as a model to link genetic and neural-circuit changes to behaviours relevant for its ecology. The characterization of the Or22a pathway and comparison of the functional and structural properties of this circuit across closely related species provides several insights into behavioural evolution (Fig. 4h).

The *Or22a* allele-transfer experiments provide evidence that olfactory receptor tuning contributes to species-specific odour-evoked behaviour. Our definition of determinants of Or22a retuning also informs the molecular basis of odour–receptor interactions. When mapped onto a presumed homologous Orco structure[37], the key change (M93I) falls within a putative ligand-binding pocket, and may be a 'hotspot' for functional evolution (Extended Data Fig. 11a–c).

Although functional differences in Or22a are important, they cannot explain the behavioural differences of *D. sechellia* and *D. simulans*, as these receptors are interchangeable for supporting noni attraction. We note that the responses of native Or22a neurons in *D. sechellia* and Or22a/b neurons in *D. simulans* are not identical (Fig. 3a, b); the loss of *Or22b* in *D. sechellia* led to a narrowed (and possibly slightly increased) sensitivity to methyl esters, which could be behaviourally relevant. The expansion of this population of neurons specifically in *D. sechellia* is probably a key additional evolutionary innovation, although alone it is insufficient to restore host attraction similar to that of *D. sechellia* when expressing DmelOr22a. The difference in *D. sechellia* projection neuron axon innervations suggests that changes in central-circuit connectivity form part of the adaptation of this species to noni. Future studies are necessary to understand the genetic bases and behavioural importance of these neuroanatomical differences.

The critical role of Or22a in host attraction in *D. sechellia* may account for the rapid molecular evolution of this locus[38–40] (Extended Data Fig. 11d–h). *Drosophila erecta*—a specialist on *Pandanus* fruit—also exhibits expansion of this OSN population[21]. However, a second noni-adapted drosophilid (*D. yakuba mayottensis*)[41] does not share the receptor or OSN number changes that we describe here (Extended Data Fig. 11i–m) which implies it has developed an independent evolutionary solution to locate a common host fruit.

Finally, other olfactory channels are important for noni attraction. These include Or85c/b neurons (which have conserved physiology but increase in number in *D. sechellia* relative to other drosophilids) and Ir75b neurons, which have both changed in function and number in *D. sechellia* while apparently preserving the anatomy of partner projection neurons[15]. Future application of the *D. sechellia* genetic toolkit should offer further fundamental insights into how genes and neurons control behaviour and enable the evolution of novel traits.

Online content

Any methods, additional references, Nature Research reporting summaries, source data, extended data, supplementary information, acknowledgements, peer review information; details of author contributions and competing interests; and statements of data and code availability are available at https://doi.org/10.1038/s41586-020-2073-7.

1. Arguello, J. R. & Benton, R. Open questions: tackling Darwin's "instincts": the genetic basis of behavioral evolution. *BMC Biol.* **15**, 26 (2017).
2. Bendesky, A. & Bargmann, C. I. Genetic contributions to behavioural diversity at the gene–environment interface. *Nat. Rev. Genet.* **12**, 809–820 (2011).

3. Bendesky, A. et al. The genetic basis of parental care evolution in monogamous mice. *Nature* **544**, 434–439 (2017).
4. Ding, Y., Berrocal, A., Morita, T., Longden, K. D. & Stern, D. L. Natural courtship song variation caused by an intronic retroelement in an ion channel gene. *Nature* **536**, 329–332 (2016).
5. Weber, J. N., Peterson, B. K. & Hoekstra, H. E. Discrete genetic modules are responsible for complex burrow evolution in *Peromyscus* mice. *Nature* **493**, 402–405 (2013).
6. Garrigan, D. et al. Genome sequencing reveals complex speciation in the *Drosophila simulans* clade. *Genome Res.* **22**, 1499–1511 (2012).
7. Schrider, D. R., Ayroles, J., Matute, D. R. & Kern, A. D. Supervised machine learning reveals introgressed loci in the genomes of *Drosophila simulans* and *D. sechellia*. *PLoS Genet*. **14**, e1007341 (2018).
8. Amlou, M., Moreteau, B. & David, J. R. Genetic analysis of *Drosophila sechellia* specialization: oviposition behavior toward the major aliphatic acids of its host plant. *Behav. Genet*. **28**, 455–464 (1998).
9. Cobb, M., Burnet, B., Blizard, R. & Jallon, J. M. Courtship in *Drosophila sechellia* – its structure, functional aspects, and relationship to those of other members of the *Drosophila melanogaster* species subgroup. *J. Insect Behav*. **2**, 63–89 (1989).
10. Coyne, J. A. Genetics of sexual isolation in females of the *Drosophila simulans* species complex. *Genet. Res.* **60**, 25–31 (1992).
11. Dekker, T., Ibba, I., Siju, K. P., Stensmyr, M. C. & Hansson, B. S. Olfactory shifts parallel superspecialism for toxic fruit in *Drosophila melanogaster* sibling, *D. sechellia*. *Curr. Biol.* **16**, 101–109 (2006).
12. Higa, I. & Fuyama, Y. Genetics of food preference in *Drosophila sechellia*. I. Responses to food attractants. *Genetica* **88**, 129–136 (1993).
13. Ibba, I., Angioy, A. M., Hansson, B. S. & Dekker, T. Macroglomeruli for fruit odors change blend preference in *Drosophila*. *Naturwissenschaften* **97**, 1059–1066 (2010).
14. Matsuo, T., Sugaya, S., Yasukawa, J., Aigaki, T. & Fuyama, Y. Odorant-binding proteins OBP57d and OBP57e affect taste perception and host-plant preference in *Drosophila sechellia*. *PLoS Biol.* **5**, e118 (2007).
15. Prieto-Godino, L. L. et al. Evolution of acid-sensing olfactory circuits in Drosophilids. *Neuron* **93**, 661–676 (2017).
16. R'Kha, S., Capy, P. & David, J. R. Host-plant specialization in the *Drosophila melanogaster* species complex: a physiological, behavioral, and genetical analysis. *Proc. Natl Acad. Sci. USA* **88**, 1835–1839 (1991).
17. Yalcin, B. et al. Genetic dissection of a behavioral quantitative trait locus shows that *Rgs2* modulates anxiety in mice. *Nat. Genet.* **36**, 1197–1202 (2004).
18. Bendesky, A., Tsunozaki, M., Rockman, M. V., Kruglyak, L. & Bargmann, C. I. Catecholamine receptor polymorphisms affect decision-making in *C. elegans*. *Nature* **472**, 313–318 (2011).
19. Bumbarger, D. J., Riebesell, M., Rödelsperger, C. & Sommer, R. J. System-wide rewiring underlies behavioral differences in predatory and bacterial-feeding nematodes. *Cell* **152**, 109–119 (2013).
20. Markow, T. A. & O'Grady, P. Reproductive ecology of *Drosophila*. *Funct. Ecol.* **22**, 747–759 (2008).
21. Linz, J. et al. Host plant-driven sensory specialization in *Drosophila erecta*. *Proc. R. Soc. Lond. B* **280**, 20130626 (2013).
22. Seeholzer, L. F., Seppo, M., Stern, D. L. & Ruta, V. Evolution of a central neural circuit underlies *Drosophila* mate preferences. *Nature* **559**, 564–569 (2018).
23. Dweck, H. K. et al. Olfactory channels associated with the *Drosophila* maxillary palp mediate short- and long-range attraction. *eLife* **5**, e14925 (2016).
24. Matute, D. R. & Ayroles, J. F. Hybridization occurs between *Drosophila simulans* and *D. sechellia* in the Seychelles archipelago. *J. Evol. Biol.* **27**, 1057–1068 (2014).
25. Vosshall, L. B. & Stocker, R. F. Molecular architecture of smell and taste in *Drosophila*. *Annu. Rev. Neurosci.* **30**, 505–533 (2007).
26. Larsson, M. C. et al. *Or83b* encodes a broadly expressed odorant receptor essential for *Drosophila* olfaction. *Neuron* **43**, 703–714 (2004).
27. Abuin, L. et al. Functional architecture of olfactory ionotropic glutamate receptors. *Neuron* **69**, 44–60 (2011).
28. Benton, R., Sachse, S., Michnick, S. W. & Vosshall, L. B. Atypical membrane topology and heteromeric function of *Drosophila* odorant receptors in vivo. *PLoS Biol.* **4**, e20 (2006).
29. Stensmyr, M. C., Dekker, T. & Hansson, B. S. Evolution of the olfactory code in the *Drosophila melanogaster* subgroup. *Proc. R. Soc. Lond. B* **270**, 2333–2340 (2003).
30. Dobritsa, A. A., van der Goes van Naters, W., Warr, C. G., Steinbrecht, R. A. & Carlson, J. R. Integrating the molecular and cellular basis of odor coding in the *Drosophila* antenna. *Neuron* **37**, 827–841 (2003).
31. Couto, A., Alenius, M. & Dickson, B. J. Molecular, anatomical, and functional organization of the *Drosophila* olfactory system. *Curr. Biol.* **15**, 1535–1547 (2005).
32. Shiao, M. S. et al. Expression divergence of chemosensory genes between *Drosophila sechellia* and its sibling species and its implications for host shift. *Genome Biol. Evol.* **7**, 2843–2858 (2015).
33. Yao, C. A., Ignell, R. & Carlson, J. R. Chemosensory coding by neurons in the coeloconic sensilla of the *Drosophila* antenna. *J. Neurosci.* **25**, 8359–8367 (2005).
34. Ai, M. et al. Acid sensing by the *Drosophila* olfactory system. *Nature* **468**, 691–695 (2010).
35. Ruta, V. et al. A dimorphic pheromone circuit in *Drosophila* from sensory input to descending output. *Nature* **468**, 686–690 (2010).
36. Grabe, V. & Sachse, S. Fundamental principles of the olfactory code. *Biosystems* **164**, 94–101 (2018).
37. Butterwick, J. A. et al. Cryo-EM structure of the insect olfactory receptor Orco. *Nature* **560**, 447–452 (2018).
38. Aguadé, M. Nucleotide and copy-number polymorphism at the odorant receptor genes *Or22a* and *Or22b* in *Drosophila melanogaster*. *Mol. Biol. Evol.* **26**, 61–70 (2009).
39. Goldman-Huertas, B. et al. Evolution of herbivory in Drosophilidae linked to loss of behaviors, antennal responses, odorant receptors, and ancestral diet. *Proc. Natl Acad. Sci. USA* **112**, 3026–3031 (2015).
40. Nozawa, M. & Nei, M. Evolutionary dynamics of olfactory receptor genes in *Drosophila* species. *Proc. Natl Acad. Sci. USA* **104**, 7122–7127 (2007).
41. Yassin, A. et al. Recurrent specialization on a toxic fruit in an island *Drosophila* population. *Proc. Natl Acad. Sci. USA* **113**, 4771–4776 (2016).

Methods

Data reporting

Preliminary experiments were used to assess variance and determine adequate sample sizes in advance of acquisition of the reported data; no statistical methods were used to predetermine sample size. Several experiments were carried out repeatedly, because they served as controls for different genetic manipulations. In particular, we ran wild-type controls in parallel with mutant analyses in behavioural assays and therefore replicated them multiple times. In the wind tunnel assay, the number of possible samples per day is rather low, leading to testing of flies of different genotypes on different days. In these cases, experiments were started at the same time of the day under stringently controlled conditions of temperature, humidity, light and age of flies. For electrophysiological recordings, data were collected from multiple flies on multiple days in randomized order, interleaving wild-type and mutant genotypes. Within datasets, the same odour dilutions were used for acquisition of the dataset. In all cases, the results were reliable and robust over the course of the many years it took to complete this study. For olfactory trap assays, the experiments were conducted with the experimenter blinded to the genotype. The experimenter was not blinded to the genotype of flies in the wind tunnel assay or physiological experiments. All replicates are biological replicates.

Volatile collection, gas chromatography and mass spectrometry

Volatiles were collected from 1 ml of fruit juice or 13 g of noni fruit at different ripening stages in capped 15-ml glass vials with poly-tetrafluoroethylene-lined silicone septa (Sigma, 23242-U). After penetrating the septum of the cap with a solid phase microextraction (SPME) fibre holder, the SPME fibre (grey hub plain, coated with 50/30 µm divinylbenzene/carboxen on polydimethylsiloxane on a StableFlex fibre (Sigma, 57328-U)) was exposed to the head space of each vial for 30 min at room temperature. For collection of head spaces in the trap assay, a single noni juice trap was placed in the arena and odours were collected with SMPE for 5 min at 0 h, 5 h and 10 h after placement. For collection of head spaces in the wind tunnel assay, samples were captured with SPME for 10 min at the landing platform and the release platform directly after application of noni juice. After each odour collection, the SPME fibre was retracted and immediately inserted into the inset of a gas chromatography–mass spectrometry (GC–MS) system (Agilent 7890B fitted with MS 5977A unit) for desorption at 260 °C in split mode (split ratio 100:1). The gas chromatograph was operated with a HP-INNOWax column (Agilent 19091N-133UI). Samples were injected at an initial oven temperature of 50 °C; this temperature was held for 1 min and gradually increased (3 °C min^{-1}) to 150 °C before holding for 1 min. Subsequently, the temperature was increased (20 °C min^{-1}) to 260 °C and held for 5 min. The mass spectrometry transfer line was held at 260 °C, the mass spectrometry source at 230 °C, and the mass spectrometry quad at 150 °C. Mass spectra were taken in EI-mode (70 eV) in a 29–350 *m/z* range. Between different collections, the SPME fibre was conditioned at 270 °C for 15 min. All chromatograms were processed using MSD ChemStation F.01.03.2357 software. Volatile compounds were identified using the NIST library and matched to standards of the Max Planck Institute for Chemical Ecology library. For quantification, peak areas were measured for three replicates for each sample. SPME allows only for a qualitative analysis of odour compositions as well as for an estimate of changing ratios of odours across different samples. Vapour pressure values for hexanoic acid, methyl hexanoate and 2-heptanone have previously been described (www.thegoodscentscompany.com)[42,43].

Drosophila strains

Drosophila stocks were maintained on standard wheat flour–yeast–fruit-juice medium under a 12-h light:12-h dark cycle at 25 °C. For all *D. sechellia* strains, a few grams of formula 4-24 instant *Drosophila* medium, blue (Carolina Biological Supply) soaked in noni juice (nu3) were added on top of the standard food. Wild-type *Drosophila* strains are described in Supplementary Table 2. These strains do not show intraspecific sequence variation in Or22a or Ir75b for known odour-specificity-determining residues (Extended Data Fig. 12), suggesting that other polymorphisms (or nongenetic factors) underlie the observed minor intraspecific behavioural differences (Fig. 1b, c). The mutant and transgenic lines used and generated in this study are listed in Supplementary Table 2.

CRISPR–Cas9-mediated genome engineering

Single guide RNA expression vectors. For expression of individual single guide (sg)RNAs, oligonucleotide pairs (Supplementary Table 3) were annealed and cloned into BbsI-digested pCFD3-dU6-3gRNA (Addgene no. 49410), as previously described[44]. To express multiple sgRNAs from the same vector backbone, oligonucleotide pairs (Supplementary Table 4) were used for PCR and inserted into pCFD5 (Addgene no. 73914) via Gibson Assembly, as previously described[45].

Donor vectors for homologous recombination. To generate an eGFP-expressing donor vector (pHD-Stinger-attP), the fluorophore was excised from pStinger[46] with NcoI/HpaI and used to replace the *DsRed* sequence in NcoI/HpaI-digested pHD-DsRed-attP (Addgene plasmid no. 51019)[47]. Homology arms (1–1.6 kb) for individual target genes were amplified from *D. sechellia* (*Drosophila* Species Stock Center (DSSC) 14021-0248.07), *D. simulans* (DSSC 14021-0251.195) or *D. melanogaster* (Research Resource Identifier Database: Bloomington *Drosophila* Stock Center (RRID:BDSC)_58492) genomic DNA and inserted either into pHD-DsRed-attP or pHD-Stinger-attP via restriction cloning. Details and oligonucleotide sequences are available from the corresponding authors upon request.

Transgenic source of Cas9. pBac(nos-Cas9,3×P3-YFP) (a gift of D. Stern) was integrated into *D. sechellia* (DSSC 14021-0248.07) via *piggyBac* transgenesis. The insertion was mapped to the fourth chromosome using TagMap[48].

Transgene construction

Oligonucleotides for each cloning step are listed in Supplementary Table 5.

attB-nSyb-Gal4,miniW. The 1.9-kb upstream sequence of the *neuronal Synaptobrevin* (*nSyb*) gene was amplified from *D. sechellia* genomic DNA (DSSC 14021-0248.07) and inserted into pGal4attB[49] via restriction cloning using NotI and KpnI.

attB-Gal4,3×P3-Stinger. We first generated an *eGFPnls-SV40* fragment via PCR (using pHD-Stinger-attP as template) and fused it to a minimal *attB40* site[50,51] before insertion into pCR-Blunt II-TOPO (Thermo Fisher). We added a *3×P3-Stinger* fragment amplified from pHD-Stinger via restriction cloning using EcoRV and SalI. Subsequently, we placed a *loxP* site downstream of the initial *SV40* sequence via oligonucleotide annealing and SpeI/KpnI restriction cloning, to produce pCR-TOPO-loxP-attB40-eGFPnlsSV40rev-3×P3:Stinger. We replaced the *eGFPnls-SV40* sequence with an *hsp70-Gal4-SV40* fragment via PCR amplification of the vector backbone and *Gal4* from pGal4attB[49] and subsequent Gibson Assembly resulting in attB-Gal4,3×P3-Stinger.

attB-Or22a^{WT},3×P3-Stinger. In the pCR-TOPO-loxP-attB40eGFPnls SV40rev-3×P3-Stinger plasmid described in 'attB-Gal4,3×P3-Stinger', the *eGFPnlsSV40* fragment was flanked by EcoRV and SalI sites, which were used to integrate the *D. sechellia* or *D. melanogaster Or22a* open reading frame (ORF) + 3′ untranslated region (UTR) after PCR amplification from cDNA, or the *D. simulans Or22a* ORF + 3′UTR (synthesized by Eurofins Genomics), to produce attB-DsecOr22a^{WT},3×P3-Stinger,

attB-DmelOr22a^{WT},3×P3-Stinger and attB-DsimOr22a^{WT},3×P3-Stinger, respectively.

***Or22a* chimaeras.** Chimeric sequences of *D. sechellia* and *D. melanogaster Or22a* were generated by PCR amplification and fusion using the *Or22a* gene templates of the respective species. After subcloning into pCR-Blunt II-TOPO and sequence confirmation, the chimaeras were integrated into pCR-TOPO loxP attB40eGFPnlsSV40rev-3×P3-Stinger via restriction cloning.

***Or22a* site-directed mutant constructs.** Point mutations were introduced via site-directed mutagenesis following standard procedures.

attB-UAS constructs. *DsecOr22a^{WT}*, *DmelOr22a^{WT}*, *DmelOr22a^{triple}* and *DmelOr22a^{M93I}* were amplified by PCR incorporating flanking EcoRI and SalI restriction sites using the constructs described in 'attB-Or22a^{WT},3×P3-Stinger' as template, and integrated into the EcoRI/XhoI-digested pUAST-attB[52].

pDONR221-MCS. A pDONR221 entry vector carrying a multiple cloning site (MCS) was generated by amplification of the MCS of pCR-Blunt II-TOPO incorporating flanking *attB1/2* sites and the PCR fragment integrated into pDONR221 via a BP reaction (Gateway, Thermo Fisher Scientific).

pDONR221-DsimOr22a. A 5.7-kb promoter region upstream of the *Or22a* start codon was amplified from *D. simulans* (DSSC 14021-0251.195) genomic DNA, subcloned into pCR-Blunt II-TOPO and transferred to pDONR221-MCS via BamHI/EcoRV restriction cloning.

pDEST-Hemmar-eGFPnls. The *eGFPnls* fragment of pStinger[46] was amplified by PCR incorporating XhoI and SpeI restriction sites and integrated into the XhoI/XbaI-digested vector pDEST-HemmarG[53] to replace *eGFP*.

pDsimOr22a-eGFPnls. pDONR221-DsimOr22a and pDEST-Hemmar-eGFPnls were combined using LR recombination (Gateway, Thermo Fisher Scientific).

Drosophila microinjections

Transgenesis of *D. sechellia*, *D. simulans* and *D. melanogaster* was performed in-house following standard protocols (http://gompel.org/methods), except for *DsimOr22a-GFPnls* (generated by Rainbow Transgenic Flies). For the *D. sechellia* egg-laying agar plates, grape juice was replaced with noni juice and a few grams of formula 4-24 instant *Drosophila* medium, blue (Carolina Biological Supply) soaked in noni juice (nu3) were added on the surface . Embryos were manually selected for the appropriate developmental stage before alignment and injection. All *D. sechellia* transgenic and mutant lines were generated in the Dsec.07 genetic background. For *piggyBac* transgenesis, a *piggyBac* vector (300 ng μl^{-1}) was injected together with the *piggyBac* helper plasmid[54] (300 ng μl^{-1}). For CRISPR–Cas9-mediated homologous recombination, a mix of an sgRNA-encoding construct (150 ng μl^{-1}), donor vector (400 ng μl^{-1}) and pHsp70-Cas9 (400 ng μl^{-1}) (Addgene no. 45945) was injected[55]. The DsRed fluorescent marker was destroyed in *DsecnSyb-Gal4* and *DsecUAS-C3PA-GFP* via injection of an sgRNA construct targeting *DsRed* (150 ng μl^{-1}) and pHsp70-Cas9 (400 ng μl^{-1}). Injections into *Dsecnos-Cas9* were of a mix of an sgRNA construct (150 ng μl^{-1}) and donor vector (500 ng μl^{-1}). Site-directed integration into *attP* sites was achieved by coinjection of an *attB*-containing vector (400 ng μl^{-1}) and either p3xP3-EGFP.vas-int.NLS (400 ng μl^{-1}) (Addgene no. 60948)[56] or pBS130 (encoding φC31 integrase under control of a heat shock promoter (Addgene no. 26290)[57]). All concentrations are given as final values in the injection mix.

Wind tunnel assay

Long-range attraction experiments were performed in a wind tunnel as previously described[23] with a flight arena of 30-cm width, 30-cm height and 100-cm length. The airstream in the tunnel (0.3 m s^{-1}) was produced by a fan (Fischbach), and filtered through an array of 4 activated charcoal cylinders (14.5-cm diameter × 32.5-cm length) (Camfil). The wind tunnel was maintained within a climate chamber at 25 °C and 50–55% relative humidity under white light. Flies were starved for approximately 20 h; to ensure the flight ability of assayed flies, flies were first released into a mesh cage (50 × 50 × 50 cm, maintained at the same conditions as the wind tunnel) and female flies escaping from the food vial were collected with an aspirator. For each assay, ten 4–6-day-old female flies were released from a plastic tube (with a mesh covering one end and the open end facing the landing platform) fixed horizontally in the centre of the first 5–10 cm of the downwind end of the tunnel. The landing platform was built using a filter paper (3 × 3 cm) charged with either 100 μl of juice (noni (nu3), grape (Beutelsbacher Fruchtsaftkelterei), pineapple (Andros) or mango (Migros)), apple cider vinegar (Migros) or about 100 μl of homogenized ripe fruit (noni or fig) and fixed on a metal holder. Fruit homogenization was performed by blending 10 g of ripe fruit in 20 ml of distilled water; fruit particles were pelleted by centrifugation and the supernatant collected for experiments. In two-choice assays, two identical landing platforms were positioned with equal distance (7.5 cm) from the centre of the air stream alternating the position of noni fruit and apple cider vinegar between assays. The fly tube was placed within the centre of the airstream and 85-cm downwind of the odour source. An experimenter observed the landing platform(s) for the entire duration of the assay; flies arriving and staying on the landing platform(s) within the first 10 min after release were counted.

Olfactory trap assay

The two-choice olfactory trap assay was performed essentially as previously described[15]. For each experiment, traps contained 300 μl of juice (noni (nu3), grape (Beutelsbacher Fruchtsaftkelterei), pineapple (Andros) or mango (Migros)) or apple cider vinegar (Migros). When using fruits as stimuli (noni, grape, papaya, banana and fig), ripe fruits were peeled (banana and papaya) or used whole, homogenized with pestles and each trap was filled with a spatula of the mix (to about 300 μl). Single odours (see 'Electrophysiology' for CAS numbers) were used at a 10^{-2} dilution in grape juice. Triton X-100 (final concentration 0.2%) was added to all traps containing single odours and respective control traps to drown trapped flies. Twenty-two to twenty-five fed, mated, ice-anaesthetized female flies (3–5 days old) were used for each experiment. *D. sechellia* flies were transferred to standard food without noni supplement 24 h before the start of the assay, unless stated otherwise. The distribution of flies was scored after 24 h at 25 °C under red light at 60% relative humidity; experiments with >25% dead flies in the arena after 24 h were discarded. The attraction index was calculated as follows: (number of flies in treatment (for example, noni juice) trap − number of flies in control (for example, grape juice) trap)/number of trapped and untrapped flies alive. For the trap assay quantifications in Fig. 2e, all untrapped flies (including those that died during the assay) were counted owing to the high mortality rate in these experiments (Extended Data Fig. 7c).

The multiple-choice olfactory trap assay was performed using eight traps containing mango, pineapple, noni and grape juices, apple cider vinegar and fig, banana and papaya fruits. Traps were placed equidistantly in a circle in random order for each experiment and conditions were as described for the two-choice assay. The percentage of flies per trap was calculated as follows: (number of flies in trap/number of trapped and untrapped flies alive) × 100. Experiments with >25% dead flies in the arena after 24 h were discarded.

Two-photon calcium imaging

Flies were mounted and dissected as previously described[58], and images were acquired using a commercial upright two-photon microscope (Zeiss LSM 710 NLO). In detail, an upright Zeiss AxioExaminer Z1 was fitted with a Ti:Sapphire Chameleon Ultra II infrared laser (Coherent) as excitation source. Images were acquired with a 20× water-immersion objective (W Plan-Apochromat 20×; NA 1.0, VIS-IR DIC), with a resolution of 128 × 128 pixels (1.1902 pixels μm^{-1}) and a scan speed of 12.6 µs $pixel^{-1}$. The excitation wavelength was set to 920 nm at a laser output of 64.1–70.2 mW measured at the exit of the objective. Emitted light was filtered with a 500–550-nm band-pass filter, and photons were collected by an external nondescanned detector. Each measurement consisted of 50 images acquired at 4.13 Hz, with stimulation starting about 5 s after the beginning of the acquisition and lasting for 1 s. Fly antennae were stimulated using a custom-made olfactometer as previously described[59], with minor modifications. In brief, the antennae of the fly were permanently exposed to air flowing at a rate of 1.5 l min^{-1} and with 55% relative humidity obtained by combining a main stream of humidified room air (0.5 l min^{-1}) and a secondary stream (1 l min^{-1}) of normal room air. Both air streams were generated by vacuum pumps (KNF Neuberger AG) and the flow rate was controlled by two independent rotameters (Analyt). The secondary air stream was guided through either an empty 2-ml syringe or, to generate an odour pulse, a 2-ml syringe containing 20 µl of odour or solvent on a small cellulose pad (Kettenbach). Solvents were either double-distilled water (for noni juice and apple cider vinegar) or paraffin oil (for methyl hexanoate (CAS 106-70-7), 2-heptanone (CAS 110-43-0), 2,3-butanedione (CAS 431-03-8), ethyl propionate (CAS 105-37-3) and 1-hexanol (CAS 111-27-3)). To switch between control air and odour stimulus delivery, a three-way magnetic valve (The Lee) was controlled using Matlab via a VC6 valve controller unit (Harvard Apparatus). Data were processed using Fiji[60] and custom-written scripts in Matlab and R as previously described[59]. Because bleaching was very strong at the beginning of each acquisition, the first 1.5 s were not considered for the analysis, and bleach correction was not applied. Colour-coded images and box plots show the peak response calculated as the mean relative change in fluorescence ($\Delta F/F$%) of 3 frames around the maximum during frames 19–30.

Wide-field calcium imaging

Flies were mounted and dissected as previously described[58]. Images were acquired with a charge-coupled device camera (CoolSNAP-HQ2 Digital Camera System) mounted on a fluorescence microscope (upright fixed stage Carl Zeiss Axio Examiner D1) equipped with a 20× water-immersion objective (W Plan-Apochromat 20× ; NA 1.0, VIS-IR DIC) (Extended Data Fig. 4a) or 40× water-immersion objective (W Plan-Apochromat 40× ; NA 1.0 VIS-IR DIC) (Extended Data Fig. 4f). Excitation light of 470 nm was produced with an LED light (Cool LED pE-100, VisiChrome, intensity 1.8–3.9%). Light was guided through a filter block consisting of a 450–490-nm excitation filter, a dichroic mirror (T495LP) and a 500–550-nm emission filter (Chroma ET). Binned image size was 400 × 300 pixels (Extended Data Fig. 4a) or 266 × 200 pixels (Extended Data Fig. 4f) on the chip, corresponding to 465 × 349 µm (Extended Data Fig. 4a) or 149 × 112 µm (Extended Data Fig. 4f) in the preparation. Exposure time varied between 30 and 100 ms to adjust for different basal fluorescence values across preparations. Films (12.5-s duration) were recorded with an acquisition rate of 4 Hz. Metafluor software (Visitron) was used to control the camera, light, data acquisition and onset of odour stimulation. Odour stimulation and data analysis were otherwise performed as described for two-photon calcium imaging.

Electrophysiology

Single sensillum electrophysiological recordings were performed as previously described[61]. The noni and grape juice stimuli are as described in 'Wind tunnel assay' and 'Olfactory trap assay'; other chemicals of the highest purity are available from Sigma Aldrich. Odorants were used at 10^{-2} (v/v) in all experiments unless noted otherwise in the figures or figure legends. Solvents were either double-distilled water (for noni juice, butyric acid (CAS 107-92-6), hexanoic acid (CAS 1821-02-9)) or paraffin oil (for octanoic acid (CAS 124-07-2), methyl butanoate (CAS 623-42-7), methyl hexanoate (CAS 106-70-7), methyl octanoate (CAS 111-11-5), ethyl butanoate (CAS 105-54-4), ethyl hexanoate (CAS 123-66-0), ethyl octanoate (CAS 106-32-1), 2-heptanone (CAS 110-43-0), 1-hexanol (CAS 111-27-3) and 3-buten-1-ol (CAS 627-27-0)). Odours for sensilla stimulation were used for a maximum of five consecutive trials. If noni juice or noni fruit extract (see 'Wind tunnel assay') were used, odours were renewed after 2 stimulations or, for 10^{-4}, 10^{-3} and 10^{-2} dilutions, after each stimulation. Corrected responses were calculated as the number of spikes in a 0.5-s window at stimulus delivery (200 ms after stimulus onset to take account of the delay due to the air path) subtracting the number of spontaneous spikes in a 0.5-s window 2 s before stimulation, multiplied by 2 to obtain spikes s^{-1}. The solvent-corrected responses shown in the figures were calculated by subtracting from the response to each diluted odour the response obtained when stimulating with the corresponding solvent. Recordings were performed on a maximum of three sensilla per fly. Exact *n* values and mean spike counts for all experiments are provided in Supplementary Table 7.

Immunohistochemistry

RNA fluorescent in situ hybridization (FISH) using digoxigenin- or fluorescein-labelled RNA probes and immunofluorescence on whole-mount antennae were performed essentially as previously described[59,62]. *D. sechellia* probe templates were generated by amplification of regions of genomic DNA (DSSC 14021-0248.07) using primer pairs listed in Supplementary Table 6; these were cloned into pCR-Blunt II-TOPO and sequenced. *D. sechellia* Or22a antibodies were raised in rabbits against the peptide epitope PHISKKPLSERVKSRD (amino acids 7–22), affinity-purified (Proteintech Group) and diluted 1:250. Other antibodies used were: guinea pig anti-Ir75b (RRID: AB_2631093)[63] 1:200, rabbit anti-Ir64a (RRID: AB_2566854)[34] 1:100, rabbit anti-Orco[28] 1:200, guinea pig anti-Ir8a (RRID: AB_2566833)[27] 1:500, rabbit anti-Ir25a (RRID: AB_2567027) 1:500[64] and rabbit anti-GFP 1:500 (Invitrogen). Immunofluorescence on adult brains was performed as previously described[65] (except for the *D. sechellia* reference brain samples; see '*D. sechellia* reference brain') using mouse monoclonal antibody nc82 1:10 (Developmental Studies Hybridoma Bank), rat monoclonal anti-Elav 1:10 (Developmental Studies Hybridoma Bank) and rabbit anti-GFP 1:500 (Invitrogen). Alexa488-, Cy3- and Cy5-conjugated goat anti-guinea pig, goat anti-mouse, goat anti-rat and goat anti-rabbit IgG secondary antibodies (Molecular Probes, Jackson Immunoresearch) were used at 1:500.

D. sechellia reference brain

D. sechellia (DSSC 14021-0248.07) brains (2–7-day-old flies) were stained with nc82 and imaged as previously described[66]. From 88 brains imaged from female flies, 26 high-quality confocal stacks of the midbrain were selected for averaging on a selected 'seed' brain, essentially as previously described[67,68]. Similarly, a reference brain for a male fly (not shown) was constructed, using 20 high-quality confocal stacks (from 87 brains initially imaged). Reciprocal bridging registrations between *D. melanogaster* and *D. sechellia* reference brains were also generated to permit comparison of homologous neurons within a common template, essentially as previously described[68]. The reference brains (*D. sechellia* female and *D. sechellia* male), bridging registrations and associated code are available for download via http://jefferislab.org/si/auer2019.

Image acquisition and processing

Confocal images of antennae and brains were acquired on an inverted confocal microscope (Zeiss LSM 710) equipped with an oil immersion 40× objective (Plan Neofluar 40× oil immersion DIC objective; 1.3 NA),

unless stated otherwise. Images were processed in Fiji[60]. *D. sechellia* brains were imaged and registered to a *D. sechellia* reference brain using the Fiji CMTK plugin (https://github.com/jefferis/fiji-cmtk-gui), as previously described[69]. For segmentation of individual glomeruli of the antennal lobe, glomerular identity was confirmed by location and labelling with *Gal4* reporters (Extended Data Fig. 3) and segmentation performed using Amira 6.5 (Thermo Fisher Scientific). Glomerular volumes were calculated following segmentation with the Segmentation Editor plugin of Fiji using the 3D Manager Plugin. OSN numbers were counted using the Cell Counter Plugin in Fiji or Imaris (Bitplane). Projection-neuron morphologies were reconstructed and measured in neuTube 1.0z[70].

Projection-neuron labelling

Photoactivation was performed as previously described[35] on 3–5-day-old female flies. Brains were dissected in saline[71] (low carbonate; 2 mM Mg^{2+} pH 7.2) and treated with collagenase (2 mg ml^{-1}, 45 s). Dissected brains were initially imaged at 925 nm to identify the DM2 glomerulus based on anatomical position. Photoactivation was achieved through multiple cycles of exposure to 710-nm laser light with a 15-min rest period between each cycle to allow diffusion of the photoactivated fluorophore within the neuron. Photoactivation and imaging was performed on an Ultima two-photon laser scanning microscope (Bruker) equipped with galvanometers driving a Chameleon XR laser (Coherent). Emitted photons were collected with a GaAsP photodiode detector (Bruker) or a PMT detector through a 60× objective (Olympus 60× water immersion; 0.9 NA).

Projection neuron dye-fillings were performed as previously described[35] with some modifications. Brains were dissected in saline, briefly treated with collagenase (2 mg ml^{-1}, 45 s), washed and pinned with fine tungsten wires to a Sylgard sheet (World Precision Instruments) in a 35-mm Petri dish (Falcon) filled with saline. Pulled-glass electrodes were backfilled with Texas Red Dextran (3000, lysine fixable, Thermo Scientific). The electrode was targeted to the DM2 glomerulus using as a guide either basal expression of the pan-neuronal, photoactivatable GFP (*D. sechellia* and *D. melanogaster*) or DM2-specific labelling (*D. simulans*; that is, the *DsimOr22a-GFPnls* strain, in which trace GFP levels were detected in OSN axon termini). The dye was electroporated by applying voltage pulses (30 V) until it became visible in distal neural processes of the projection neuron, and left to diffuse for 60 min. Brains were subsequently imaged by two-photon microscopy, as described.

To label single projection neurons, the DM2 glomerulus was first subjected to one cycle of exposure to 710-nm laser light to identify the cell bodies of DM2 projection neurons. Subsequently, the filled-glass electrode was placed in the centre of the soma of one DM2 projection neuron and the dye was electroporated by applying voltage pulses (30 V) until it became visible in distal neural processes. The dye was left to diffuse for 60 min, before the brains were fixed with 2% paraformaldehyde for 45 min and subjected to immunofluorescence using nc82 (1:20) and anti-mouse Alexa488 (1:500), as described in 'Immunohistochemistry'. Images were acquired on a Zeiss LSM 880 Airy scan confocal microscope using a 40× objective (Plan Neofluar 40× oil immersion DIC objective; 1.3 NA).

Molecular evolution and polymorphism analyses

The *Or22a/b* gene tree was inferred using annotations after manual verification by BLASTing Or22a/b protein sequences (using tblastn with default settings, BLAST+ v.2.7.1[72]) to the genomes of *D. simulans* (r2.01), *Drosophila mauritiana* (r1), *D. yakuba* (r1.04), *D. sechellia* (r1.3) and *D. erecta* (r1.3). Genomic regions were annotated using Wise2 (v.2.4.1)[73], with the protein sequences of *D. melanogaster* as guides. All genes appeared intact and consistent with existing models, with one exception: *D. mauritiana Or22b* is truncated by about 240 bp owing to a gap in the reference genome. The cDNAs were frame-aligned using TranslatorX[74]. The gene tree based on these alignments was inferred using MrBayes (v.3.2.6)[75] with the following settings: rate variation = invariable+gamma, number of substitutions = 6, substitution model = default, number of generations = 10, sample frequency = 10, burn-in = 250.

The *Or22a/b* topology outputted from MrBayes was used for PAML (v.4.8)[76] CodeML branch tests of protein evolution-rate change. Seven models were tested, one with a freely varying ω value and six other models with 1, 4, 5, 7, 8 and 9 ω values (CodeML parameters were all set to zero except for the following: seqtype = 1, CodonFreq = 2, ndata = 1, model = 2, kappa = 2, omega = 0.4, fix_alpha = 1, ncatG = 5, getSE = 1, Small_Diff = 5e-7, cleandata = 1). Nested comparisons between these models using likelihood ratio tests identified a model with 5 ω values to provide the best fit (Extended Data Fig. 11d, Supplementary Table 8).

Polymorphism data for *Or22a/b* was extracted from previously published data. The *D. simulans*, *D. sechellia* and *D. melanogaster* datasets were from previous publications[7,77–79]. VCFtools (v.0.1.17)[80] was used to extract variable sites from the respective VCF files, as well as to output allele frequencies. Variant calling in one of the *D. simulans* datasets[7] was based on a subversion of the *D. simulans* r2 genome, which is slightly different to r2 on FlyBase. This subversion is available at https://github.com/kern-lab/FILET/blob/master/simSechResults/dsimV2-Mar2012_chrsonly.fa.bz2.

Statistics and reproducibility

Data were analysed and plotted using Excel and R (v.3.2.3; R Foundation for Statistical Computing, www.R-project.org).

Reporting summary

Further information on research design is available in the Nature Research Reporting Summary linked to this paper.

Data, availability

All relevant data supporting the findings of this study are available from the corresponding authors upon request or, for behavioural experiments, are included with the paper as Source Data for Figs. 1b, c, 2c–e, 3d, f, Extended Data Figs. 1c, e, f, g, h, 7e–g. Supplementary Table 7 lists the exact *n* and mean values for all electrophysiological data.

Code availability

Code used for analyses and all unique biological materials generated in this study (for example, mutant and transgenic *Drosophila* strains) are available from the corresponding authors upon request.

42. Ambrose, D., Ellender, J. H., Lee, E. B., Sprake, C. H. S. & Townsend, R. Thermodynamic properties of organic oxygen compounds XXXVIII. Vapour pressures of some aliphatic ketones. *J. Chem. Thermodyn.* **7**, 453–472 (1975).
43. Daubert, T. E. & Danner, R. P. *Physical and Thermodynamic Properties of Pure Chemicals: Data Compilation* (Taylor & Francis, 1997).
44. Port, F., Chen, H. M., Lee, T. & Bullock, S. L. Optimized CRISPR/Cas tools for efficient germline and somatic genome engineering in *Drosophila*. *Proc. Natl Acad. Sci. USA* **111**, E2967–E2976 (2014).
45. Port, F. & Bullock, S. L. Augmenting CRISPR applications in *Drosophila* with tRNA-flanked sgRNAs. *Nat. Methods* **13**, 852–854 (2016).
46. Barolo, S., Carver, L. A. & Posakony, J. W. GFP and β-galactosidase transformation vectors for promoter/enhancer analysis in *Drosophila*. *Biotechniques* **29**, 726–732 (2000).
47. Gratz, S. J. et al. Highly specific and efficient CRISPR/Cas9-catalyzed homology-directed repair in *Drosophila*. *Genetics* **196**, 961–971 (2014).
48. Stern, D. L. Tagmentation-based mapping (TagMap) of mobile DNA genomic insertion sites. Preprint at bioRxiv https://doi.org/10.1101/037762 (2017).
49. Croset, V. et al. Ancient protostome origin of chemosensory ionotropic glutamate receptors and the evolution of insect taste and olfaction. *PLoS Genet*. **6**, e1001064 (2010).
50. Bateman, J. R. & Wu, C. T. A simple polymerase chain reaction-based method for the construction of recombinase-mediated cassette exchange donor vectors. *Genetics* **180**, 1763–1766 (2008).
51. Groth, A. C., Olivares, E. C., Thyagarajan, B. & Calos, M. P. A phage integrase directs efficient site-specific integration in human cells. *Proc. Natl Acad. Sci. USA* **97**, 5995–6000 (2000).

52. Bischof, J., Maeda, R. K., Hediger, M., Karch, F. & Basler, K. An optimized transgenesis system for *Drosophila* using germ-line-specific φC31 integrases. *Proc. Natl Acad. Sci. USA* **104**, 3312–3317 (2007).
53. Han, C., Jan, L. Y. & Jan, Y. N. Enhancer-driven membrane markers for analysis of nonautonomous mechanisms reveal neuron–glia interactions in *Drosophila*. *Proc. Natl Acad. Sci. USA* **108**, 9673–9678 (2011).
54. Arnoult, L. et al. Emergence and diversification of fly pigmentation through evolution of a gene regulatory module. *Science* **339**, 1423–1426 (2013).
55. Gratz, S. J. et al. Genome engineering of *Drosophila* with the CRISPR RNA-guided Cas9 nuclease. *Genetics* **194**, 1029–1035 (2013).
56. Zhang, X., Koolhaas, W. H. & Schnorrer, F. A versatile two-step CRISPR- and RMCE-based strategy for efficient genome engineering in *Drosophila*. *G3 (Bethesda)* **4**, 2409–2418 (2014).
57. Gohl, D. M. et al. A versatile *in vivo* system for directed dissection of gene expression patterns. *Nat. Methods* **8**, 231–237 (2011).
58. Knecht, Z. A. et al. Distinct combinations of variant ionotropic glutamate receptors mediate thermosensation and hygrosensation in *Drosophila*. *eLife* **5**, e17879 (2016).
59. Silbering, A. F. et al. Complementary function and integrated wiring of the evolutionarily distinct *Drosophila* olfactory subsystems. *J. Neurosci.* **31**, 13357–13375 (2011).
60. Schindelin, J. et al. Fiji: an open-source platform for biological-image analysis. *Nat. Methods* **9**, 676–682 (2012).
61. Benton, R. & Dahanukar, A. Electrophysiological recording from *Drosophila* olfactory sensilla. *Cold Spring Harb. Protoc.* **2011**, 824–838 (2011).
62. Saina, M. & Benton, R. Visualizing olfactory receptor expression and localization in *Drosophila*. *Methods Mol. Biol.* **1003**, 211–228 (2013).
63. Prieto-Godino, L. L. et al. Olfactory receptor pseudo-pseudogenes. *Nature* **539**, 93–97 (2016).
64. Benton, R., Vannice, K. S., Gomez-Diaz, C. & Vosshall, L. B. Variant ionotropic glutamate receptors as chemosensory receptors in *Drosophila*. *Cell* **136**, 149–162 (2009).
65. Sánchez-Alcañiz, J. A., Zappia, G., Marion-Poll, F. & Benton, R. A mechanosensory receptor required for food texture detection in *Drosophila*. *Nat. Commun.* **8**, 14192 (2017).
66. Ostrovsky, A., Cachero, S. & Jefferis, G. Clonal analysis of olfaction in *Drosophila*: immunochemistry and imaging of fly brains. *Cold Spring Harb. Protoc.* **2013**, 342–346 (2013).
67. Jefferis, G. S. et al. Comprehensive maps of *Drosophila* higher olfactory centers: spatially segregated fruit and pheromone representation. *Cell* **128**, 1187–1203 (2007).
68. Manton, J. D. et al. Combining genome-scale *Drosophila* 3D neuroanatomical data by bridging template brains. Preprint at bioRxiv https://doi.org/10.1101/006353 (2014).
69. Cachero, S., Ostrovsky, A. D., Yu, J. Y., Dickson, B. J. & Jefferis, G. S. Sexual dimorphism in the fly brain. *Curr. Biol.* **20**, 1589–1601 (2010).
70. Feng, L., Zhao, T. & Kim, J. neuTube 1.0: a new design for efficient neuron reconstruction software based on the SWC format. *eNeuro* **2**, ENEURO.0049-14.2014 (2015).
71. Caron, S. J., Ruta, V., Abbott, L. F. & Axel, R. Random convergence of olfactory inputs in the *Drosophila* mushroom body. *Nature* **497**, 113–117 (2013).
72. Camacho, C. et al. BLAST+: architecture and applications. *BMC Bioinformatics* **10**, 421 (2009).
73. Birney, E., Clamp, M. & Durbin, R. GeneWise and Genomewise. *Genome Res.* **14**, 988–995 (2004).
74. Abascal, F., Zardoya, R. & Telford, M. J. TranslatorX: multiple alignment of nucleotide sequences guided by amino acid translations. *Nucleic Acids Res.* **38**, W7–W13 (2010).
75. Ronquist, F. et al. MrBayes 3.2: efficient Bayesian phylogenetic inference and model choice across a large model space. *Syst. Biol.* **61**, 539–542 (2012).
76. Yang, Z. PAML 4: phylogenetic analysis by maximum likelihood. *Mol. Biol. Evol.* **24**, 1586–1591 (2007).
77. Signor, S. A., New, F. N. & Nuzhdin, S. A large panel of *Drosophila simulans* reveals an abundance of common variants. *Genome Biol. Evol.* **10**, 189–206 (2018).
78. Grenier, J. K. et al. Global diversity lines – a five-continent reference panel of sequenced *Drosophila melanogaster* strains. *G3 (Bethesda)* **5**, 593–603 (2015).
79. Huang, W. et al. Natural variation in genome architecture among 205 *Drosophila melanogaster* genetic reference panel lines. *Genome Res.* **24**, 1193–1208 (2014).
80. Danecek, P. et al. The variant call format and VCFtools. *Bioinformatics* **27**, 2156–2158 (2011).
81. Grabe, V. et al. Elucidating the neuronal architecture of olfactory glomeruli in the *Drosophila* antennal lobe. *Cell Rep.* **16**, 3401–3413 (2016).
82. Pellegrino, M., Steinbach, N., Stensmyr, M. C., Hansson, B. S. & Vosshall, L. B. A natural polymorphism alters odour and DEET sensitivity in an insect odorant receptor. *Nature* **478**, 511–514 (2011).
83. Adams, M. D. et al. The genome sequence of *Drosophila melanogaster*. *Science* **287**, 2185–2195 (2000).

Acknowledgements We thank Y. Bellaïche, B. Deplancke, K. S. Douglas, S. Lavista-Llanos, K. O'Connor-Giles, J. Posakony, V. Ruta, D. Stern, G. Suh, A. Yassin, the Bloomington *Drosophila* Stock Center (National Institute of Health (NIH) P40OD018537) and the Developmental Studies Hybridoma Bank (NICHD of the NIH, University of Iowa) for reagents, B. Prud'homme for instruction on *Drosophila* microinjections, B. Sutcliffe and S. Cachero for advice on the generation of reference brains, I. Alali and K. Weniger for technical assistance, J. Simpson for details of the *nSyb* promoter construct; P. C. Chai for assistance with glomerular identification; and I. Rentero Rebollo, J. Sánchez-Alcañiz, L. Prieto-Godino and members of the Benton laboratory for discussions and comments on the manuscript. T.O.A. is supported by a Human Frontier Science Program Long-Term Fellowship (LT000461/2015-L). M.A.K., B.S.H. and M.K. are supported by the Max Planck Society. K.E. and S.J.C.C. are supported by a NIH Award (1 R01 NS 167970) and a Eunice Kennedy Shriver National Institute of Child Health & Human Development Award of the NIH (5 T32 HD 007491). J.R.A. is supported by a Swiss National Science Professorship Grant (PP00P3 176956). G.S.X.E.J. is supported by an ERC Consolidator Grant (649111) and the MRC (MC_U105188491). Research in R.B.'s laboratory is supported by ERC Consolidator and Advanced Grants (615094 and 833548, respectively), the Swiss National Science Foundation and the Fondation Herbette.

Author contributions T.O.A. and R.B. conceived the project. All authors contributed to experimental design, analysis and interpretation of results. T.O.A. generated all molecular reagents, and new drosophilid mutants and transgenic lines. Other experimental contributions were as follows: T.O.A. contributed to experiments shown in Figs. 1c, 2a, b, d, e, 3a–c, e, 4a–d, g, Extended Data Figs. 1a–f, 2c, 3, 4c, e, 5, 6, 7a–f, 8, 9, 10a–d, 11f–m, 12; M.A.K., with input from B.S.H. and M.K., contributed to experiments shown in Figs. 1b, d, 2c, 3d, f, Extended Data Figs. 1f–h, 2a, b, d, e, 7g, Supplementary Table 1; G.Z. contributed to experiments shown in Figs. 1c, 2d, 4b, Extended Data Figs. 1a, b, 3b, 5c, e, g, 6, 7a, b, f, 10b, 11k; A.F.S. contributed to experiments shown in Fig. 1e, f, Extended Data Fig. 4d, f, g; K.E., with input from S.J.C.C., contributed to experiments shown in Fig. 4e–g, Extended Data Fig. 10e; R.Á.-O. contributed to experiments shown in Extended Data Fig. 4a, b; J.R.A. contributed to experiments shown in Extended Data Fig. 11d, e; G.S.X.E.J. contributed to experiments shown in Fig. 4c; and R.B. contributed to experiments shown in Fig. 4c. T.O.A. and R.B. wrote the paper with input from all other authors.

Competing interests The authors declare no competing interests.

Additional information

Supplementary information is available for this paper at https://doi.org/10.1038/s41586-020-2073-7.

Correspondence and requests for materials should be addressed to T.O.A. or R.B.

Peer review information *Nature* thanks Lindy McBride and the other, anonymous, reviewer(s) for their contribution to the peer review of this work.

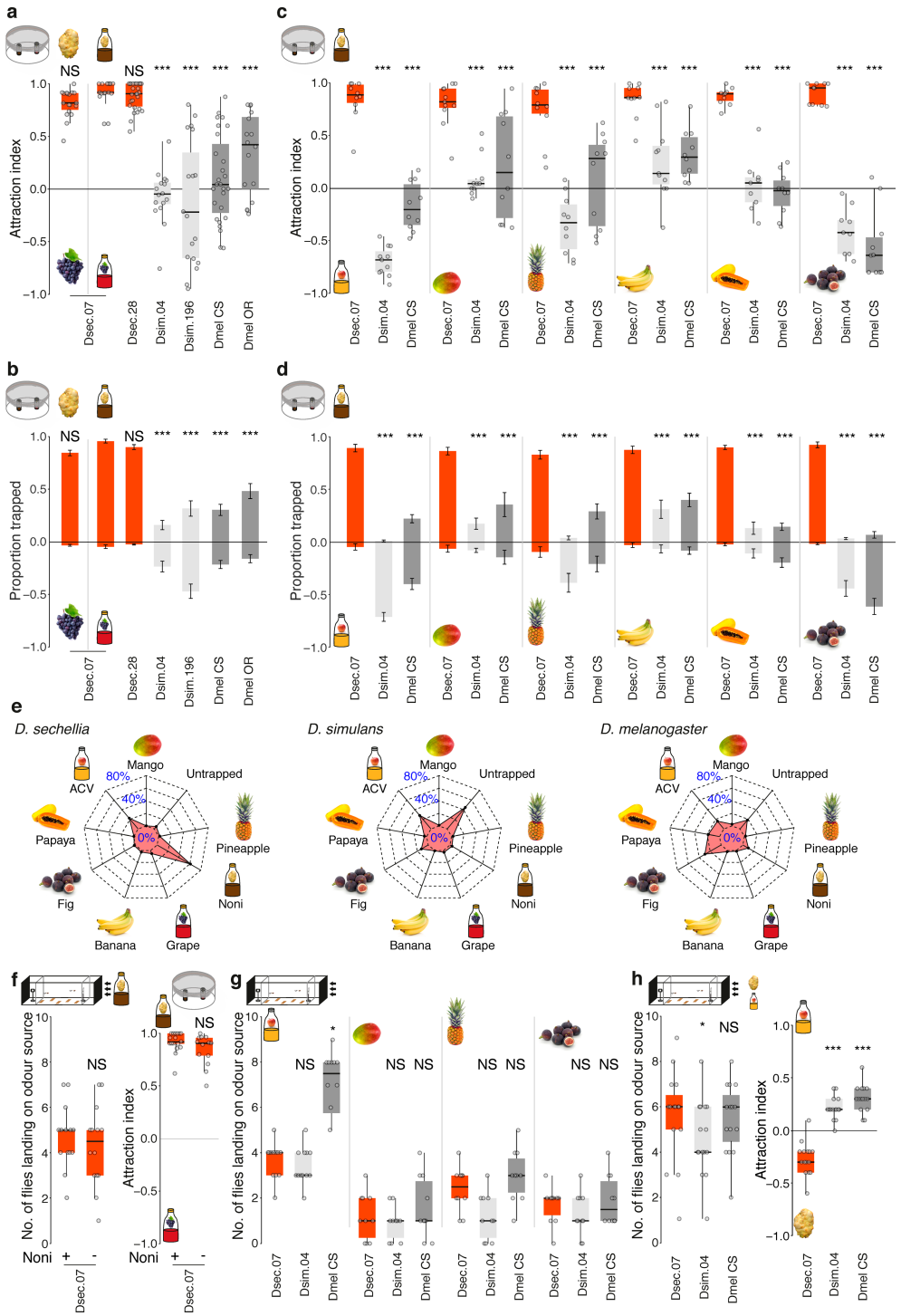

Extended Data Fig. 1 | See next page for caption.

Extended Data Fig. 1 | Species-specific short- and long-range behavioural responses to diverse fruit stimuli. a, Data reproduced from Fig. 1c. Behavioural responses in a trap assay testing preferences between noni and grape, or between noni juice and grape juice. $n = 15–27$ experiments, 22–25 female flies per experiment. Comparisons to responses of Dsec.07 flies to noni juice are shown. In **a**–**d**, **h** (right), pairwise Wilcoxon rank-sum test and *P* values adjusted for multiple comparisons using the Benjamini and Hochberg method. **b**, Proportion of flies (mean ± s.e.m.) in each stimulus trap for the assays shown in **a**. Comparisons to responses of Dsec.07 flies are shown. **c**, Behavioural responses in a trap assay testing preferences between noni juice and diverse fruit juices or fruits for *D. sechellia*, *D. simulans* and *D. melanogaster*. $n = 9–11$ experiments, 22–25 female flies per experiment. Comparisons to responses of Dsec.07 flies are shown. **d**, Proportion of flies (mean ± s.e.m.) in each stimulus trap for the assays shown in **c**. Comparisons to responses of Dsec.07 flies are shown. **e**, Radar plot showing the mean percentage of flies per trap in a multiple-choice trap assay with eight different stimuli for *D. sechellia*, *D. simulans* and *D. melanogaster*. $n = 11$ experiments, 22–25 female flies per experiment. ACV, apple cider vinegar. **f**, Left, behavioural responses to noni juice in a wind tunnel assay of *D. sechellia* reared on standard food with (+) and without (–) noni supplement. Kruskal–Wallis test. Right, behavioural responses in a trap assay testing preferences between noni juice and grape juice for *D. sechellia* reared on standard food with (+) and without (–) noni supplement. Pairwise Wilcoxon rank-sum test. **g**, Behavioural responses to apple cider vinegar, mango juice, pineapple or fig in a wind tunnel assay of *D. sechellia*, *D. simulans* and *D. melanogaster*. $n = 10–12$ experiments, 10 female flies per experiment. Comparisons to responses of Dsec.07 flies are shown. In **g**, **h** (left), Kruskal–Wallis test with Dunn's post hoc correction. **h**, Behavioural responses in a wind tunnel assay testing preference between noni fruit and apple cider vinegar of *D. sechellia*, *D. simulans* and *D. melanogaster*. $n = 15$ experiments, 10 female flies per experiment. Left, total number of flies landing on an odour source. Comparisons to responses of Dsec.07 flies are shown. Right, attraction index calculated as: (flies landing on apple cider vinegar – flies landing on noni)/flies landing on either source. Comparisons to responses of Dsec.07 flies are shown. NS, not significant ($P > 0.05$); $^{*}P < 0.05$; $^{***}P < 0.001$.

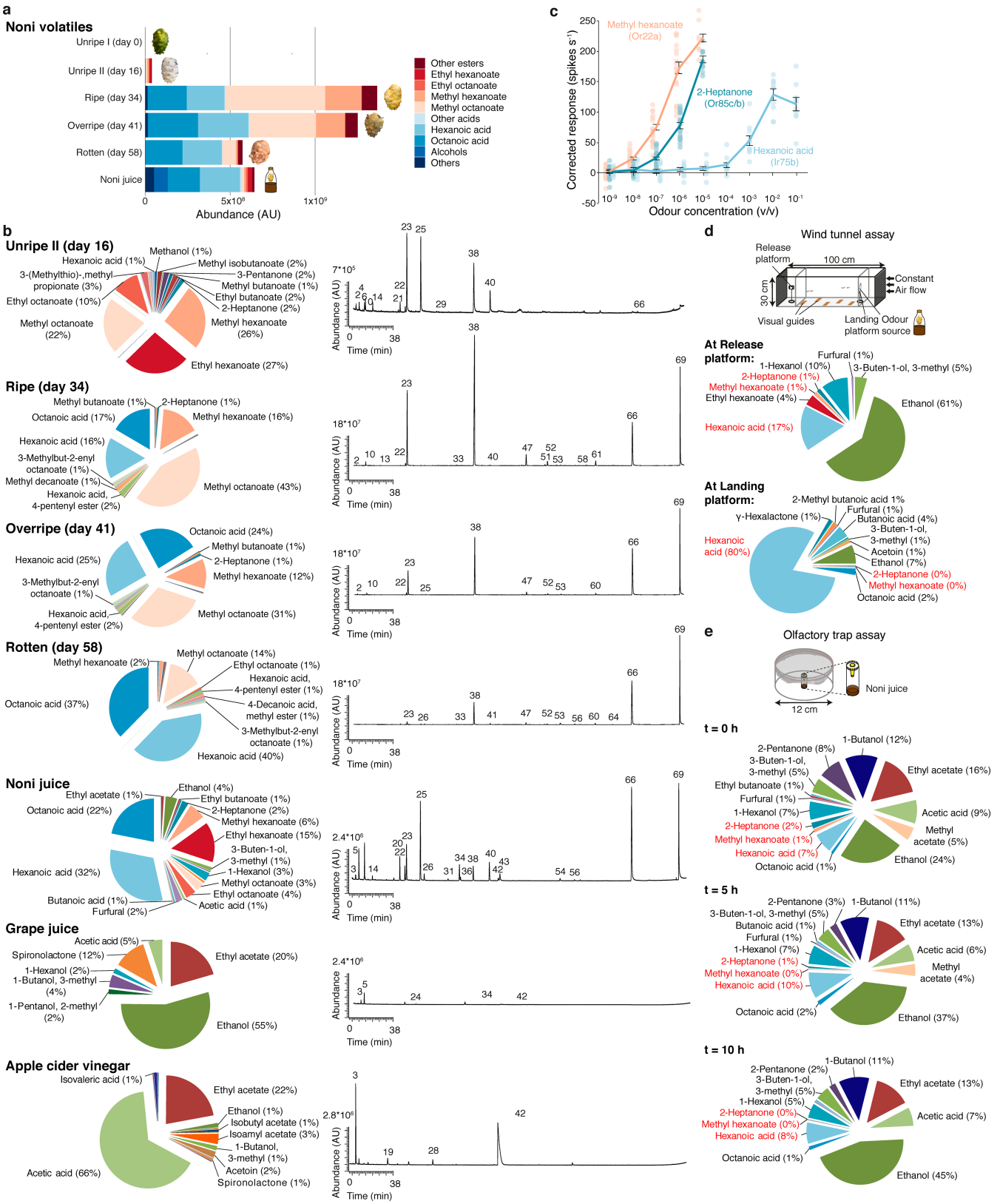

Extended Data Fig. 2 | See next page for caption.

Extended Data Fig. 2 | Chemicals emitted by natural odour sources and odour bouquet changes in behavioural assays. a, Principal constituents of the odour bouquet of noni fruit at different stages of ripening and commercial noni juice, as determined by gas chromatography–mass spectrometry. AU, arbitrary units. **b**, Chemical composition of the odour bouquet of noni fruit at different stages of ripening, noni juice, grape juice and apple cider vinegar. Representative gas chromatograms are shown on the right. Numbers correspond to compounds as listed in Supplementary Table 1 (not all identified peaks are shown). **c**, Dose-dependent electrophysiological responses of Or22a, Or85c/b and Ir75b neurons in Dsec.07 to their best odour agonists. Mean ± s.e.m. and individual data points, $n = 7–20$, female flies. The contribution of Or35a neurons (the spiking of which is difficult to separate from Ir75b neurons in ac3I) to hexanoic-acid responses is likely to be minimal (Fig. 2b). *D. sechellia* Or22a and Or85c/b neuron dose–response data are replotted from Fig. 3a. **d**, Chemical profile of odours collected by SPME at the release and landing platforms in the wind tunnel assay within the first 10 min of noni-juice application. **e**, Chemical profile of odours collected by SPME in the trap assay arena within 5 min of the placement of a trap (that is, $t = 0$ h), and after 5 h and 10 h, using noni juice as stimulus; 0% indicates that only trace proportions of the compound were detected.

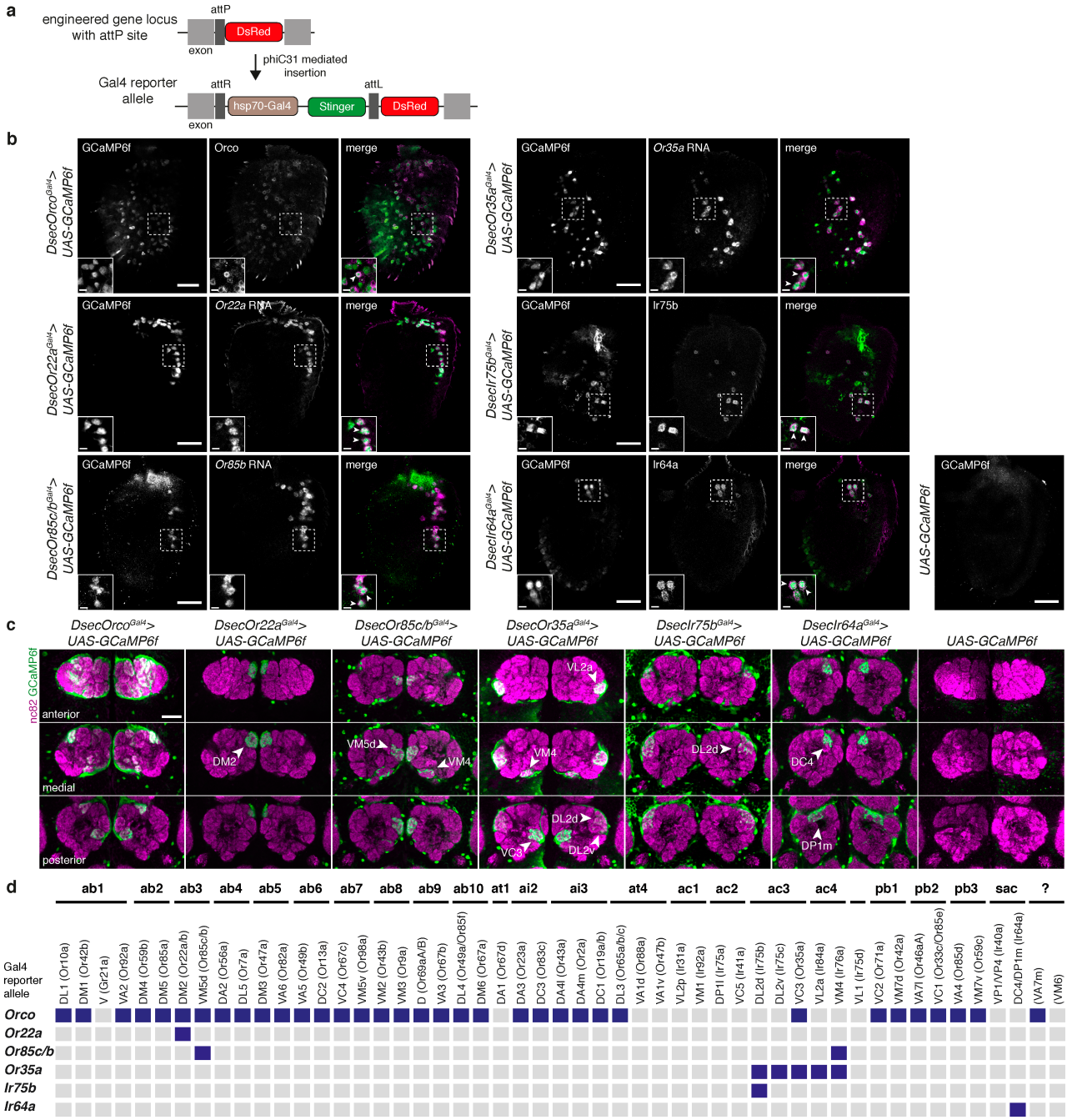

Extended Data Fig. 3 | OSN Gal4 driver lines in *D. sechellia*. **a**, Schematic of the *Gal4* reporter-allele generation strategy, through CRISPR–Cas9-mediated integration of an *attP* site (marked by *3×P3:DsRed*) into the desired Or or Ir gene (Extended Data Figs. 5, 6 provide details of specific alleles), followed by introduction of a *Gal4* ORF via φC31-mediated transgenesis. **b**, Coexpression of the indicated Or^{Gal4}-driven, Ir^{Gal4}-driven or control background GCaMP6f signal (detected by anti-GFP) with the corresponding receptor protein or RNA in whole-mount antennae. Arrowheads point to examples of colabelled cells. Scale bars, 25 µm (main panels), 5 µm (insets). Whereas $DsecOr22a^{Gal4}$ and $DsecIr64a^{Gal4}$ flies completely recapitulate endogenous receptor expression, $DsecOrco^{Gal4}$ and $DsecOr85c/b^{Gal4}$ flies lack expression in some receptor-expressing neurons. $DsecOr35a^{Gal4}$ and $DsecIr75b^{Gal4}$ might be expressed in ectopic cells (as shown in **c**, **d**) or the protein or RNA signal for these receptor genes could be below the detection threshold. **c**, Expression of the indicated Or^{Gal4}-driven, Ir^{Gal4}-driven or control background GCaMP6f signal (detected by anti-GFP) in glomeruli of whole-mount antennal lobes. Three focal planes of the neuropil (visualized with nc82 (magenta)) are shown. Images were registered to a *D. sechellia* reference brain (Methods) for better comparison of antennal lobe structure. Scale bar, 25 µm. **d**, Summary of the glomerular labelling by Or^{Gal4} or Ir^{Gal4} drivers as characterized in **c** (dark blue indicates GCaMP6f signal was detected in at least 3/3 independent brains). Glomeruli are organized by the compartmentalization of the corresponding OSN populations into different classes of sensilla (based on data in *D. melanogaster*[81]). ab, antennal basiconic; at, antennal trichoid; ai, antennal intermediate; ac, antennal coeloconic; pb, palp basiconic; sac, sacculus; ?, OSN population unknown. $DsecOrco^{Gal4}$ is expressed in most—but not all (for example, Or67d DA1)—of the expected OSN populations; $DsecOr35a^{Gal4}$ and $DsecOr85c/b^{Gal4}$ display some ectopic expression, as inferred from their labelling of more than one glomerulus.

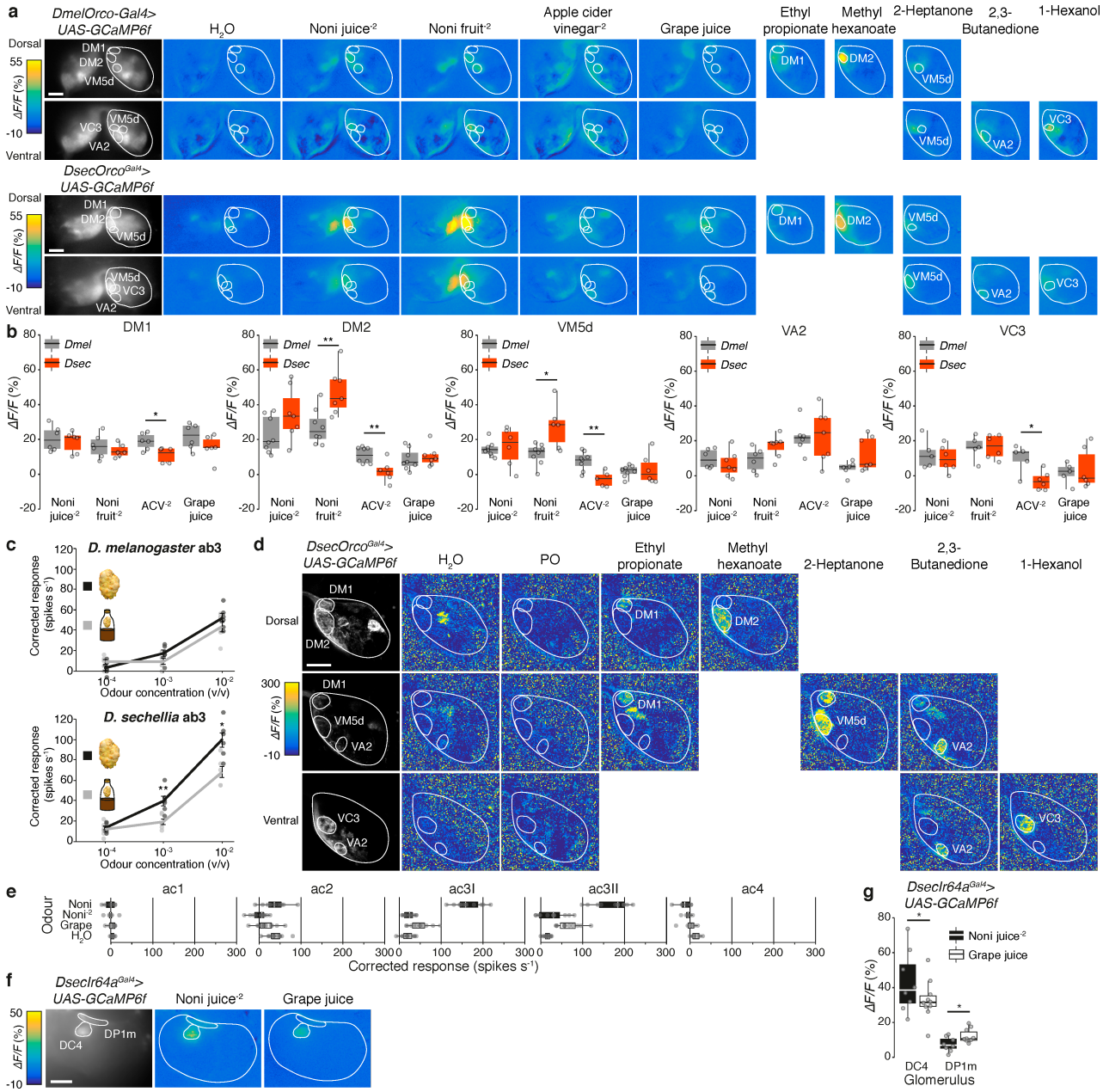

Extended Data Fig. 4 | Comparative olfactory representations of noni in *D. melanogaster* and *D. sechellia*. **a**, Representative odour-evoked calcium responses in the axon termini of Orco OSNs in the antennal lobes of *D. melanogaster* (*Orco-Gal4/Orco-Gal4;UAS-GCaMP6f/UAS-GCaMP6f*) and *D. sechellia* (*UAS-GCaMP6f/UAS-GCaMP6f;;DsecOrco^{Gal4}/+;*), acquired by wide-field imaging. Left, raw fluorescence signals. Right, relative increase in GCaMP6f fluorescence ($\Delta F/F$%) after stimulation with the indicated complex stimuli and single odours. Diagnostic odours: ethyl propionate (10^{-4} dilution (v/v)) for Or42b neurons (innervating DM1); methyl hexanoate (10^{-6} dilution) for Or22a or Or22a/b neurons (DM2); 2-heptanone (10^{-5} dilution) for Or85c/b neurons (VM5d); 2,3-butanedione (10^{-4} dilution) for Or92a neurons (VA2); and 1-hexanol (10^{-4} dilution) for Or35a neurons (VC3). Glomerular boundaries and the entire antennal lobe are outlined. Scale bars, 50 µm. **b**, Quantification of odour-evoked calcium responses for the flies represented in **a**. Maximum calcium-response amplitudes for each experiment are plotted. $n = 5–8$ female flies. Significantly different responses of species to the same stimulus are shown. Wilcoxon signed-rank test. **c**, Combined electrophysiological responses of neurons in the ab3 sensillum in *D. melanogaster* (top) and *D. sechellia* (bottom) upon stimulation with increasing concentrations of noni juice or noni fruit extract. Mean ± s.e.m. and individual data points; $n = 6$, female flies. Significant differences in responses are shown. Pairwise Wilcoxon rank-sum test. Responses of *D. sechellia* are stronger to noni fruit than noni juice, which may reflect the lower abundance of relevant ligands in the juice. **d**, Representative odour-evoked calcium responses in the axon termini of Orco OSNs in the antennal lobe of *D. sechellia* (*UAS-GCaMP6f/UAS-GCaMP6f;;DsecOrco^{Gal4}/+*) acquired by two-photon imaging. Three focal planes are shown, revealing different glomeruli along the dorsoventral axis. Far left column, raw fluorescence images. Other columns show relative increase in GCaMP6f fluorescence ($\Delta F/F$%) after stimulation with diagnostic odours. Scale bar, 25 µm. **e**, Electrophysiological responses in the antennal coeloconic (ac) sensilla classes to the indicated stimuli ($n = 6–11$, female flies) in *D. sechellia* (DSSC 14021-0248.07) representing the summed, solvent-corrected activities of the two or three neurons that they house. **f**, Representative odour-evoked calcium responses in the axon termini of Ir64a OSNs in the *D. sechellia* antennal lobe (*UAS-GCaMP6f/UAS-GCaMP6f;;DsecIr64a^{Gal4}/+*) acquired by wide-field imaging. Left, raw fluorescence signals. Right, relative increase in GCaMP6f fluorescence ($\Delta F/F$%) after stimulation with noni juice (10^{-2} dilution) or grape juice. Scale bar, 25 µm. **g**, Quantification of odour-evoked calcium responses for the flies represented in **f**. Maximum calcium-response amplitudes for each experiment are plotted. $n = 7–10$ female flies. Comparisons of responses to noni (10^{-2} dilution) and grape juice are shown. Wilcoxon signed-rank test. *$P < 0.05$; **$P < 0.01$.

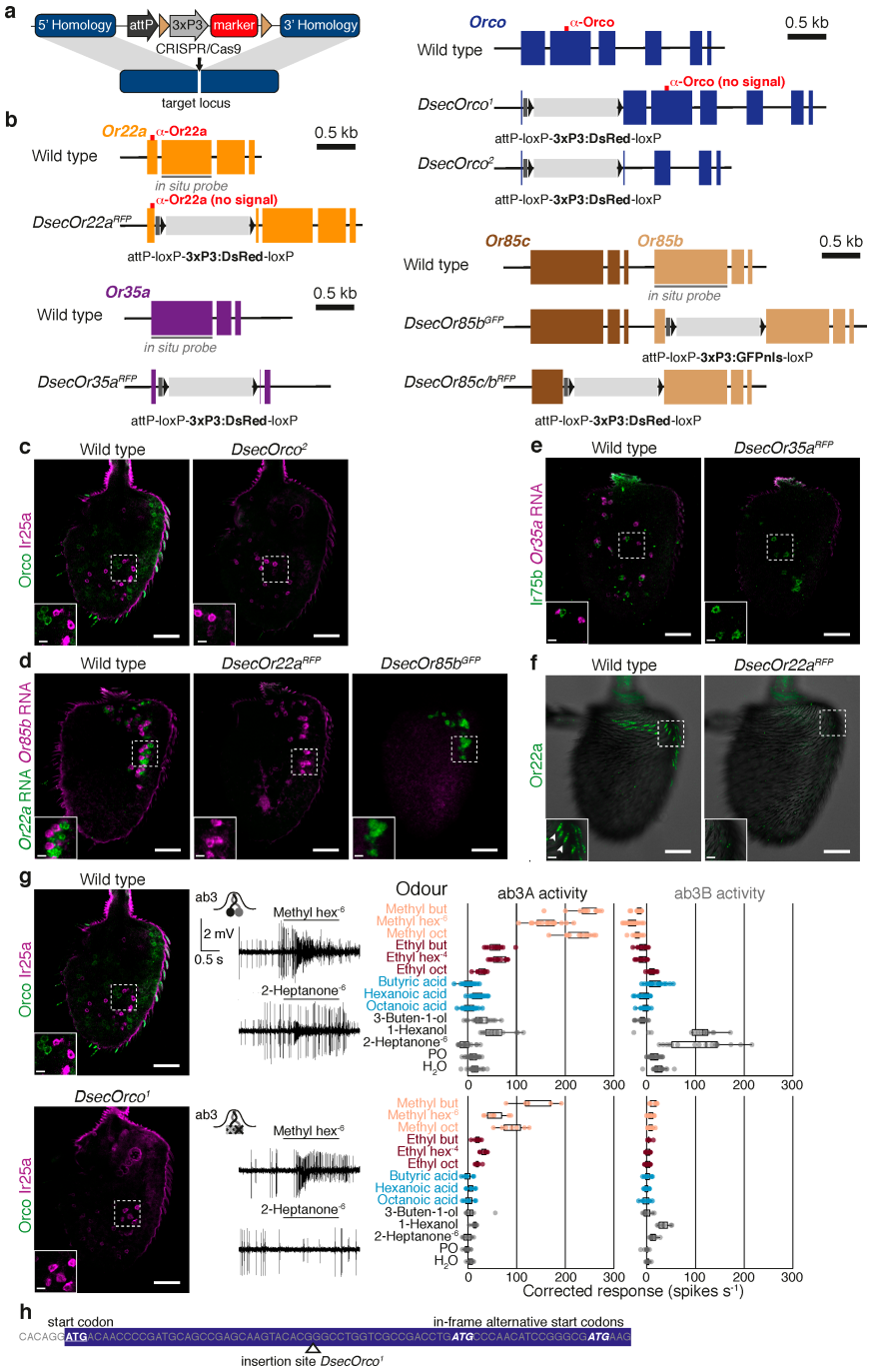

Extended Data Fig. 5 | See next page for caption.

Extended Data Fig. 5 | Generation and validation of loss-of-function alleles of *D. sechellia* Or genes. a, Schematic of the strategy for generating mutant alleles of Or genes, through integration of an eye-expressed fluorescent marker (*3×P3:DsRed* or *3×P3:GFPnls*) into the desired locus via CRISPR–Cas9-cleavage induced homologous recombination. Brown triangles, *loxP* sites for removal of the fluorescent marker via Cre recombination. **b**, Schematics depicting Or gene organization, the structure of mutant alleles and the location of the sequences that encode antibody epitopes. For $DsecOrco^{1}$, the fluorescent marker was integrated into the first coding exon; for $DsecOrco^{2}$, the marker replaces parts of exons 1 and 3 and the whole of exon 2. $DsecOr22a^{RFP}$ carries the fluorescent marker in the first coding exon close to the start codon. $DsecOr35a^{RFP}$ lacks most of exons 1 and 2. For $DsecOr85b^{GFP}$, the marker was integrated into exon 1; for $DsecOr85c/b^{RFP}$, the marker replaces most of the *Or85c* gene and part of exon 1 of *Or85b*. **c**, Immunofluorescence for Orco and Ir25a (as an internal staining control) on whole-mount antennae from wild-type and $DsecOrco^{2}$ flies. Scale bars, 25 µm (**c**–**g**, main panels), 5 µm (**c**–**g**, insets). **d**, RNA FISH for *Or22a* and *Or85b* on whole-mount antennae from wild-type, $DsecOr22a^{RFP}$ and $DsecOr85b^{GFP}$ mutant flies. **e**, Immunofluorescence for Ir75b and RNA FISH for *Or35a* on whole-mount antennae from wild-type and $DsecOr35a^{RFP}$ mutant flies. Arrowheads indicate *Or35a*-expressing cells. Or35a neurons also pair with Ir75c neurons in ac3II sensilla[15], which is reflected in *Or35a*-positive cells that are not paired with Ir75b-expressing cells in wild-type antennae. **f**, Immunofluorescence for Or22a on whole-mount antennae from wild-type and $DsecOr22a^{RFP}$ mutant flies. Arrowheads indicate sensilla that house Or22a neurons. **g**, Far left, immunofluorescence for Orco and Ir25a (as an internal staining control) on whole-mount antennae from wild-type (same image as shown in **c**) (top) and $DsecOrco^{1}$ (bottom) flies. Middle and right, electrophysiological responses in the two neurons of the ab3 sensillum (Fig. 2a) to odours present in noni in wild-type *D. sechellia* and $DsecOrco^{1}$ mutants ($n = 5–20$, female flies). Representative response traces to methyl hexanoate (10^{-6} dilution) and 2-heptanone (10^{-6} dilution) are shown. Data points represent the solvent-corrected activities per neuron. Responses of wild-type *D. sechellia* neurons are replotted from Fig. 2a. Even though Orco expression is undetectable by immunofluorescence, weak electrophysiological responses in ab3 sensilla (and other Orco-dependent sensilla (data not shown)) can be detected. These observations suggest that trace levels of functional Orco are produced from this allele, potentially through use of in-frame start codons downstream of the marker insertion site (as shown in **h**). **h**, Schematic depicting the location of the *Orco* start codon, the fluorescent-marker insertion site of the $DsecOrco^{1}$ allele and downstream potential alternative in-frame start codons.

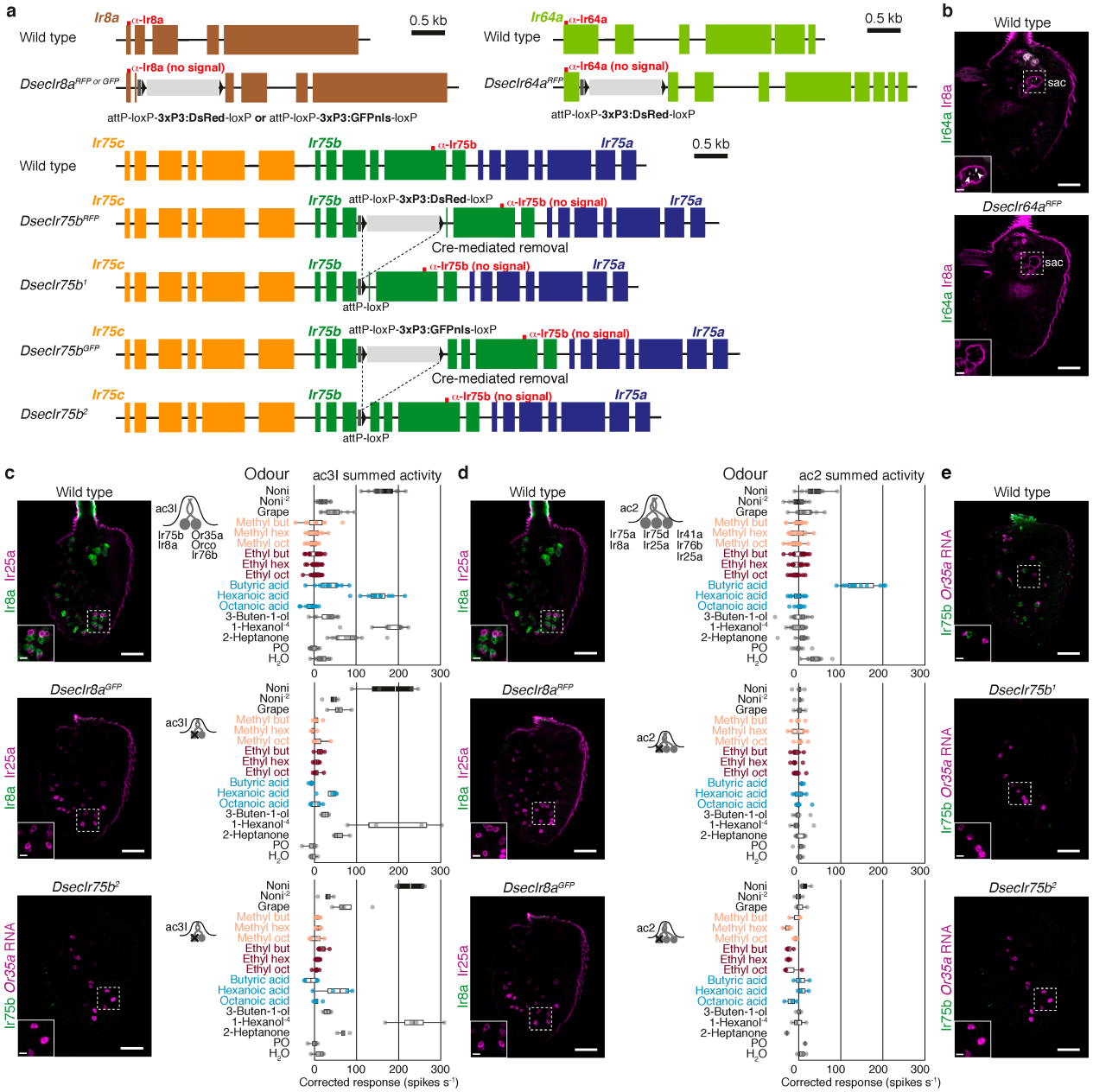

Extended Data Fig. 6 | Generation and validation of loss-of-function alleles of *D. sechellia* Ir genes. a, Schematics depicting organization of Ir genes, the structure of mutant alleles and the sequences that encode antibody epitopes. For *DsecIr8a*^{RFP} or *DsecIr8a*^{GFP}, the fluorescent marker was integrated into the first coding exon. For *DsecIr64a*^{RFP}, the marker replaces parts of exon 2. *DsecIr75b*^{RFP} lacks parts of exons 3 and 4, and for *DsecIr75b*^{GFP} the marker was integrated into exon 3. For both alleles of *Ir75b*, the fluorophore was removed via Cre-mediated recombination to produce *Ir75b*^{1} and *Ir75b*^{2}. **b**, Immunofluorescence for Ir64a and Ir8a (as an internal staining control) on whole-mount antennae from wild-type and *DsecIr64a*^{RFP} mutant flies. Arrowheads indicate the Ir64a-neuron dendrites that innervate sensilla in the sacculus (sac). Scale bars, 25 µm (main panels), 5 µm (insets). **c**, Left, immunofluorescence for Ir8a and Ir25a (as an internal staining control) on whole-mount antennae from wild-type and *DsecIr8a*^{GFP} flies (top and middle). Left, immunofluorescence for Ir75b and RNA FISH for *Or35a* on whole-mount antennae from *DsecIr75b*^{2} mutant flies (bottom). Scale bars, 25 µm (main panels), 5 µm (insets). Right, electrophysiological responses in the ac3I sensillum (neurons housed are indicated in the cartoon) to noni juice, grape juice and odours present in noni (n = 4–11, female flies) in wild-type *D. sechellia* and olfactory-receptor mutants with the Ir75b neuron affected (*DsecIr8a*^{GFP} and *DsecIr75b*^{2}). Data points represent the summed solvent-corrected activities of the sensillum. Responses of wild-type *D. sechellia* are replotted from Fig. 2b. The Or35a neuron exhibits residual responses to hexanoic acid in the *DsecIr8a* and *DsecIr75b* olfactory-receptor mutants (Fig. 2b). **d**, Left, immunofluorescence for Ir8a and Ir25a (as an internal staining control) on whole-mount antennae from wild-type (same image as shown in **c**) and *DsecIr8a*^{RFP} and *DsecIr8a*^{GFP} (same image as shown in **c**) flies. Scale bars, 25 µm (main panels), 5 µm (insets). Right, electrophysiological responses in the ac2 sensillum (neurons housed are indicated in the cartoon) to noni juice, grape juice and odours present in noni (n = 3–11, female flies) in wild-type *D. sechellia* and olfactory-receptor mutants in which the Ir75a neuron is affected (*DsecIr8a*^{RFP} and *DsecIr8a*^{GFP}). Data points represent the summed solvent-corrected neuronal activities of the sensillum. Responses of wild-type *D. sechellia* to noni and grape juice are as shown in Extended Data Fig. 4e. **e**, Immunofluorescence for Ir75b and RNA FISH for *Or35a* on whole-mount antennae from wild-type and *DsecIr75b*^{1} and *DsecIr75b*^{2} (same image as shown in **c**) flies. Scale bars, 25 µm (main panels), 5 µm (insets).

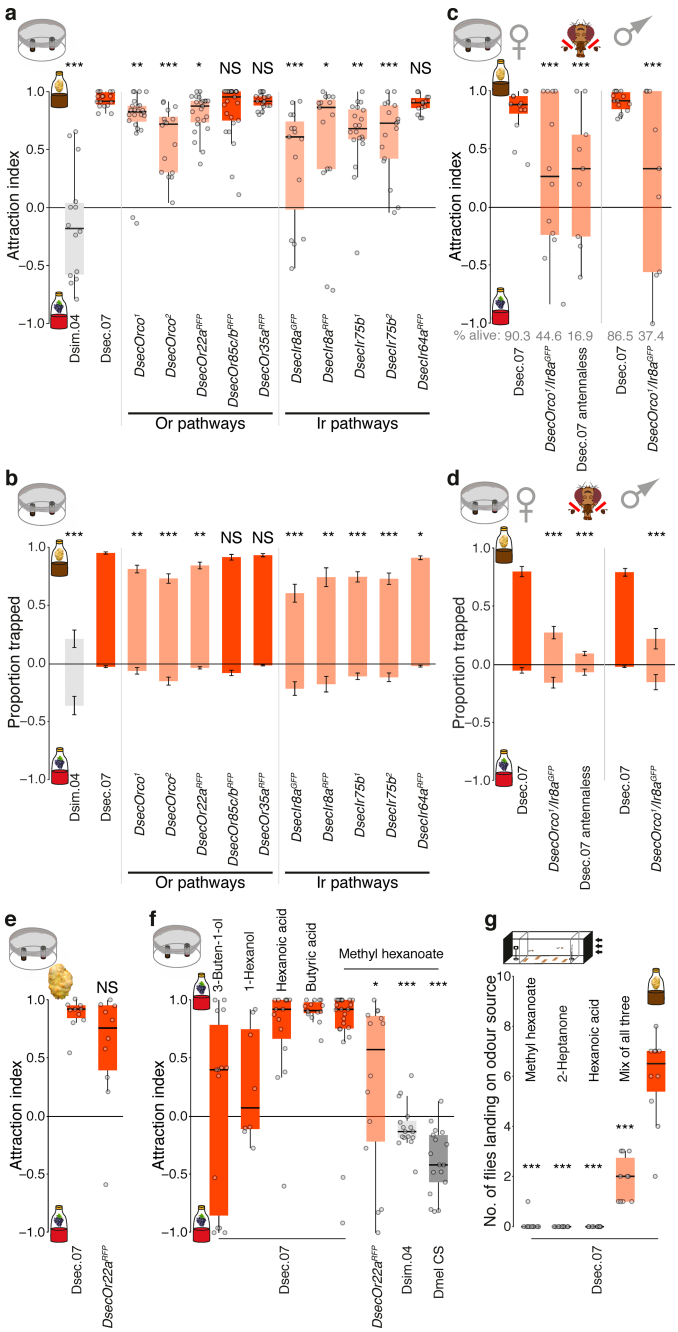

Extended Data Fig. 7 | Genetic and chemical contributions that promote the attraction of *D. sechellia* to noni. a, Data reproduced from Fig. 2d. Behavioural responses in a trap assay testing preference of the indicated genotypes for noni juice or grape juice. $n = 13–25$ experiments, 22–25 female flies per experiment. Comparisons to responses of Dsec.07 flies are shown. In **a**–**d**, **f**, pairwise Wilcoxon rank-sum test and *P* values adjusted for multiple comparisons using the Benjamini and Hochberg method. Red bars, no significant difference; salmon bars, significantly different responses of *D. sechellia* genotypes. **b**, Proportion of flies (mean ± s.e.m.) in each stimulus trap for the assays shown in **a**. Comparisons to responses of Dsec.07 flies are shown. **c**, Olfactory responses in a trap assay testing preferences between noni juice and grape juice of wild-type *D. sechellia*, $DsecOrco^{1}\ Ir8a^{GFP}$ double mutants and wild-type *D. sechellia* with the third antennal segments removed (antennaless). $n = 9–15$ experiments, 22–25 female or male flies (as indicated) per experiment. These data represent the same experiments shown in Fig. 2e, but attraction indices were calculated here taking only alive flies into account. The percentages of flies alive at the end of the assay are indicated below, revealing the high mortality rate of antennaless flies and $DsecOrco^{1}\ Ir8a^{GFP}$ double mutants ($DsecOrco^{2}\ Ir8a^{GFP}$ mutants appeared to be nonviable). Normally, trap assay experiments with >25% fly mortality were discarded (Methods). Comparisons to responses of Dsec.07 flies are shown. **d**, Proportion of flies (mean ± s.e.m.) in each stimulus trap for the assays shown in **c**. Comparisons to responses of Dsec.07 flies are shown. **e**, Behavioural responses in a trap assay testing preferences between noni fruit and grape juice of Dsec.07 and $DsecOr22a^{RFP}$ flies. Comparisons to responses of Dsec.07 flies are shown. Pairwise Wilcoxon rank-sum test. **f**, Behavioural responses in a trap assay testing preferences between grape juice and 10^{-2} dilutions of the indicated odours in grape juice of *D. sechellia*, $DsecOr22a^{RFP}$, *D. simulans* and *D. melanogaster*. Comparisons to responses of Dsec.07 flies to methyl hexanoate are shown. **g**, Behavioural responses in a wind tunnel assay testing attraction of *D. sechellia* to three single noni odours (10^{-2} dilution in water), a mix of all three in the approximate proportions of ripe noni fruit (1:0.04:1, methyl hexanoate:2-heptanone:hexanoic acid) and noni juice. $n = 10$ experiments, 10 female flies per experiment. Comparisons to responses of Dsec.07 flies to noni juice are shown. Kruskal–Wallis test with Dunn's post hoc correction. NS, not significant ($P > 0.05$); $^{*}P < 0.05$; $^{**}P < 0.01$; $^{***}P < 0.001$.

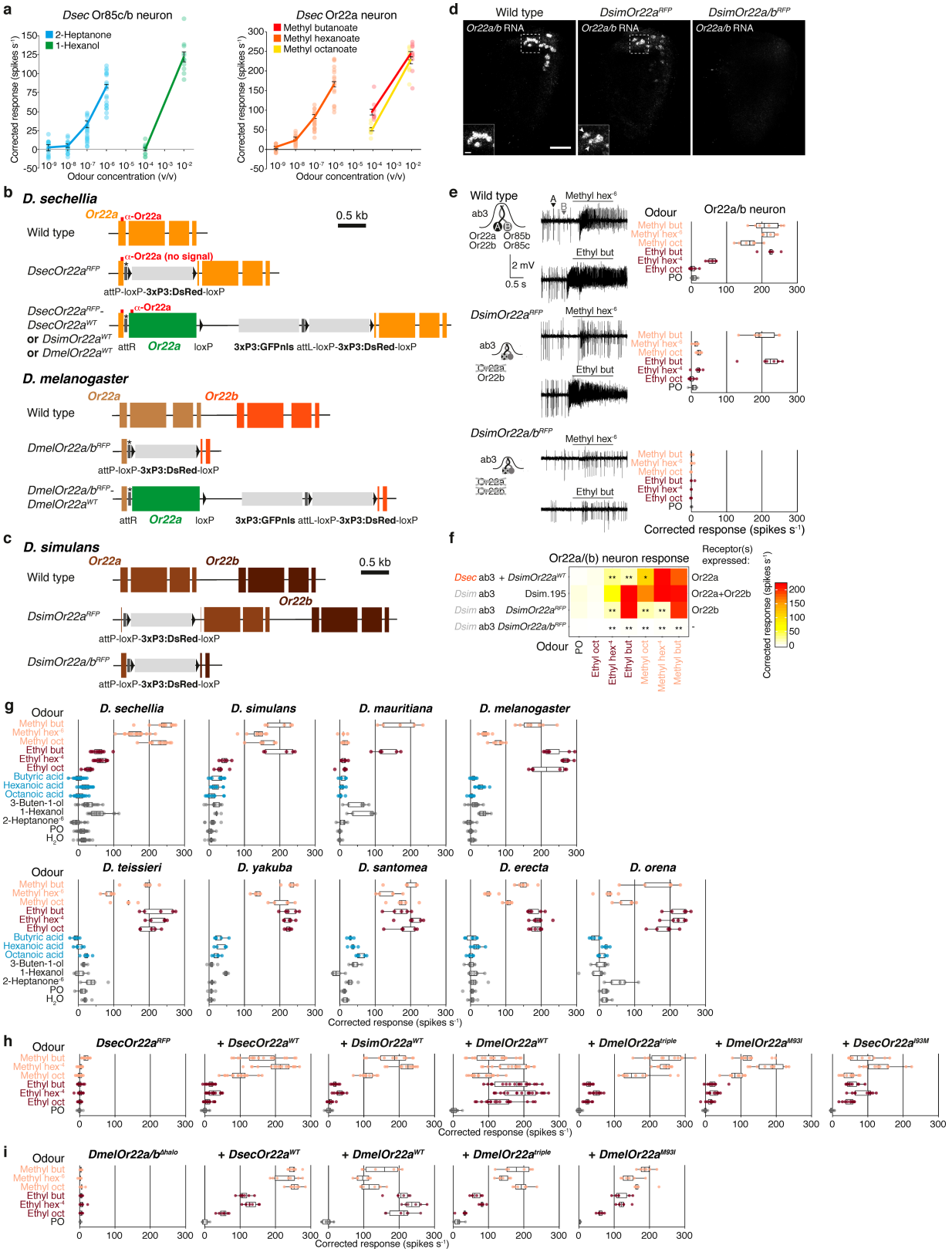

Extended Data Fig. 8 | See next page for caption.

Extended Data Fig. 8 | Odour-tuning properties of drosophilid Or85c/b and Or22a/b neurons, and genomic modifications of the *Or22a/b* loci. a, Left, dose-dependent electrophysiological responses of Or85c/b neurons (ab3B) in Dsec.07 to 2-heptanone and 1-hexanol. Mean ± s.e.m. and individual data points; $n = 11–20$, female flies. Right, dose-dependent electrophysiological responses of Or22a neurons (ab3A) in Dsec.07 to methyl butanoate, methyl hexanoate and methyl octanoate. Mean ± s.e.m. and individual data points; $n = 11–20$, female flies. The dose–response curves for 2-heptanone and methyl hexanoate are replotted from Fig. 3a. **b**, Schematics depicting the arrangement of wild-type, mutant and rescue allele versions of *DsecOr22a* (top) and *DmelOr22a/b* (bottom). Asterisk, stop codon that prevents read-through from the endogenous *Or22a* ORF. **c**, Schematics depicting the arrangement of wild-type and mutant alleles of *DsimOr22a* and *DsimOr22b*. **d**, RNA FISH for *Or22a* on whole-mount antennae from wild-type *D. simulans* (DSSC 14021-0251.195 (Dsim.195)), $DsimOr22a^{RFP}$ and $DsimOr22a/b^{RFP}$ mutant flies. As *Or22a* shares 85% sequence similarity with *Or22b*, the *Or22a* probe hybridizes with transcripts from both genes. Arrowheads indicate *Or22b*-expressing cells in $DsimOr22a^{RFP}$. Scale bar, 25 µm (main panels), 5 µm (insets). **e**, Electrophysiological responses of Or22a/b neurons to different esters in wild-type *D. simulans* and olfactory-receptor mutants ($DsimOr22a^{RFP}$ and $DsimOr22a/b^{RFP}$). $n = 6–10$, female flies. Representative response traces to methyl hexanoate (10^{-6} dilution) and ethyl butanoate (10^{-2} dilution) are shown to the left. **f**, Heat maps of the data shown in **e**, together with the data of the $DsimOr22a^{WT}$ response profile when expressed in $DsecOr22a^{RFP}$ (replotted from Fig. 3c). The receptors expressed in the analysed neurons are listed to the right. Significant differences to responses of wild-type *D. simulans* are shown. Pairwise Wilcoxon rank-sum test and *P* values adjusted for multiple comparisons using the Benjamini and Hochberg method. The equivalent responses to ethyl butanoate of wild-type *D. simulans* and *Or22a*-mutant neurons (but complete loss in *Or22a/b*-mutant neurons) suggests that this odour is detected principally by Or22b. **g**, Box plots with individual data points of the electrophysiological data presented in Fig. 3b. **h**, Box plots with individual data points of the electrophysiological data presented in Fig. 3c. **i**, Box plots with individual data points of the electrophysiological data presented in Fig. 3e. NS, not significant ($P > 0.05$); $^{*}P < 0.05$; $^{**}P < 0.01$; $^{***}P < 0.001$.

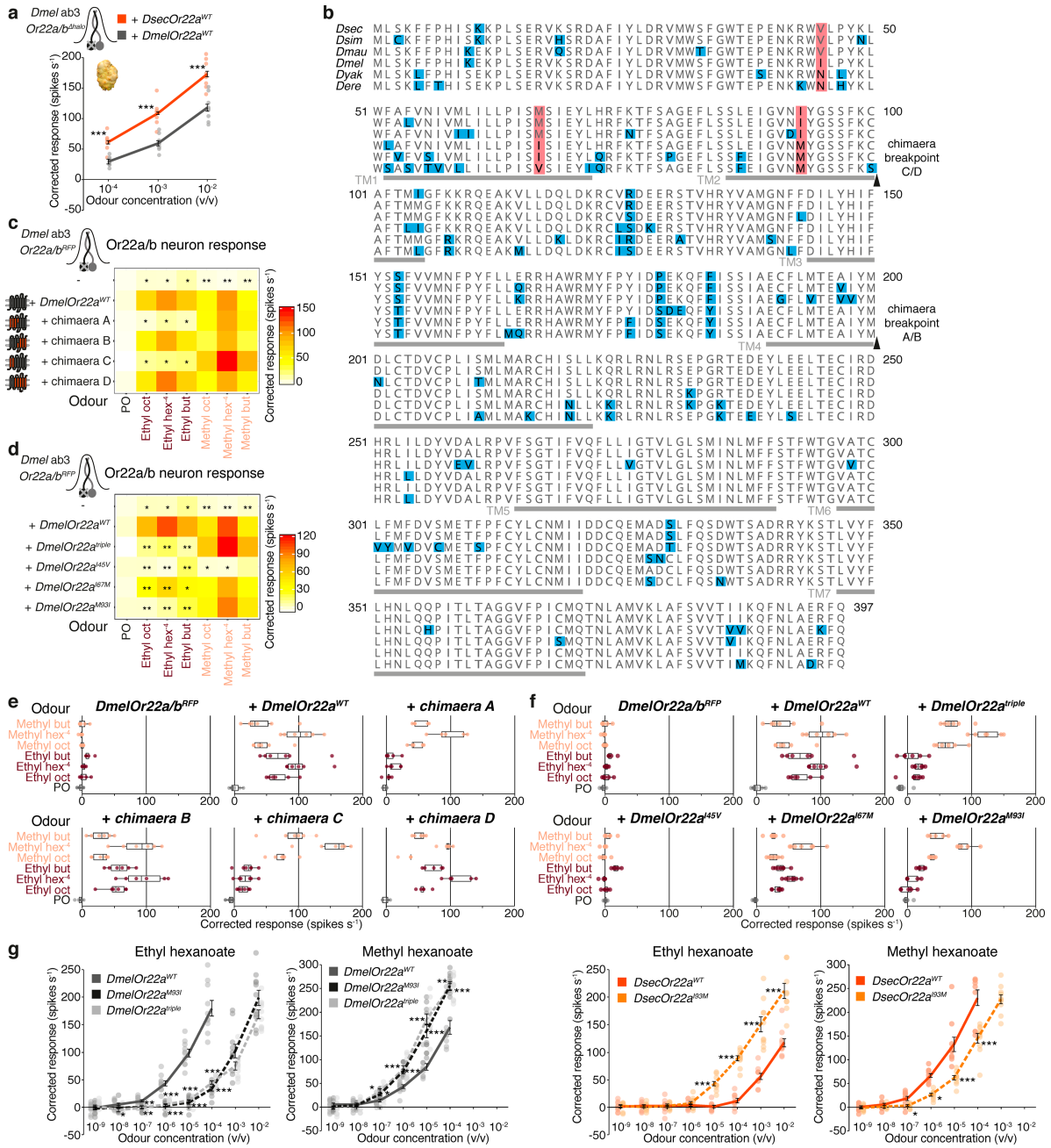

Extended Data Fig. 9 | Mapping of odour-specificity determinants of Or22a. **a**, Electrophysiological responses of *D. melanogaster Or22a/b*-mutant neurons expressing *DsecOr22a*^{WT} or *DmelOr22a*^{WT} upon stimulation with increasing concentrations of noni fruit extract. Mean ± s.em. and individual data points; $n = 9$, female flies. Significantly different values are indicated. Pairwise Wilcoxon rank-sum test. **b**, Protein sequence alignment of Or22a orthologues of six species within the *D. melanogaster* species subgroup of drosophilids. Red shading, amino acid differences between *D. melanogaster*, *D. sechellia*, *D. simulans* and *D. mauritiana* that were analysed by mutagenesis in this study; blue shading, all other sequence differences. Arrowheads, chimaera breakpoints (for chimaeras analysed in **c**). Predicted transmembrane (TM) domains are indicated with grey lines (location as in a previous publication[11]). **c**, Electrophysiological responses to a panel of noni odours conferred by chimeric Or22a proteins encoded by transgenes integrated at the *Or22a/b* locus of *D. melanogaster*. $n = 5–6$, female flies. Schematics on the left indicate the relative proportions of *D. sechellia* (red) and *D. melanogaster* (dark grey) sequences in each chimaera (precise chimaera breakpoints are shown in **b**). Significant differences to responses of *DmelOr22a*^{WT}-expressing neurons are shown. In **c**, **d**, **g**, pairwise Wilcoxon rank-sum test and *P* values adjusted for multiple comparisons using the Benjamini and Hochberg method. **d**, Electrophysiological responses of *D. melanogaster Or22a/b*-mutant neurons expressing different *Or22a* variants. $n = 5–7$, female flies. The location of each mutated residue is indicated in **b**. Data for responses of *Or22a/b*-mutant and *DmelOr22a*^{WT}-expressing neurons are replotted from **c**. Significant differences to responses of *DmelOr22a*^{WT}-expressing neurons are shown. **e**, Box plots with individual data points showing the same data as in **c**. **f**, Box plots with individual data points showing the same data as in **d**. **g**, Dose-dependent electrophysiological responses of *D. sechellia* Or22a neurons that express the indicated transgenes to ethyl or methyl hexanoate. Mean ± s.e.m. and individual data points; $n = 10–11$, female flies. Significant comparisons to the responses of neurons expressing the *DmelOr22a*^{WT} (left) or the *DsecOr22a*^{WT} (right) transgene are shown. NS, not significant ($P > 0.05$); *$P < 0.05$; **$P < 0.01$; ***$P < 0.001$.

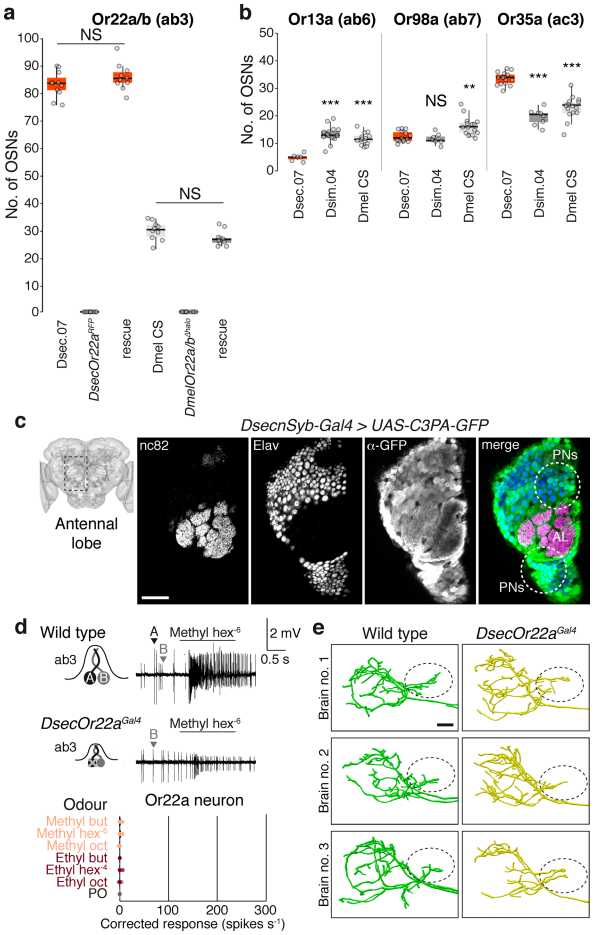

Extended Data Fig. 10 | Changes in the peripheral and central olfactory circuit in *D. sechellia*. **a**, Quantification of the number of OSNs expressing *Or22a/b* in antennae of *D. sechellia* and *D. melanogaster* (data as shown in Fig. 4b), *Or22a/b* mutants in both species and rescue lines expressing *DsecOr22a*^{WT}. $n = 9–11$, female flies. Comparisons of rescue and wild-type genotypes for each species are shown. Pairwise Wilcoxon rank-sum test. No significant differences in Or22a cell number were observed for different rescue transgenes (data not shown). **b**, Quantification of the number of OSNs expressing *Or13a* (ab6), *Or98a* (ab7) or *Or35a* (ac3I/II) in *D. sechellia*, *D. simulans* and *D. melanogaster* ($n = 10–15$, female flies). Comparisons to cell number counts in Dsec.07 flies are shown. Pairwise Wilcoxon rank-sum test and *P* values adjusted for multiple comparisons using the Benjamini and Hochberg method. **c**, Immunofluorescence with nc82 (neuropil), anti-Elav (neurons) and anti-GFP in a *DsecnSyb-Gal4/UAS-C3PA-GFP* transgenic line, which expresses photoactivatable GFP pan-neuronally. The schematic on the left indicates the region of image acquisition. An anterior section through the antennal lobe (AL) is shown to reveal the position of the labelled projection neuron (PN) somas (circled in the right panel). Scale bar, 25 µm. **d**, Electrophysiological responses of the Or22a neuron to odours present in noni in homozygous *DsecOr22a*^{Gal4} (mutant) transgenic flies. $n = 6$, female flies. Data points represent the solvent-corrected activities. Representative response traces to methyl hexanoate (10^{-6} dilution) in wild-type and transgenic flies are shown on top. **e**, Tracing of axonal branches in the lateral horn of dye-filled DM2 projection neurons in wild-type *D. sechellia* and homozygous *DsecOr22a*^{Gal4} mutant flies. Three representative samples are shown. The circles depict the position of the axonal branch specific to *D. sechellia*. Scale bar, 10 µm. Samples could not be discriminated by genotype when presented to six independent researchers blindly. NS, not significant ($P > 0.05$); $^{**}P < 0.01$; $^{***}P < 0.001$.

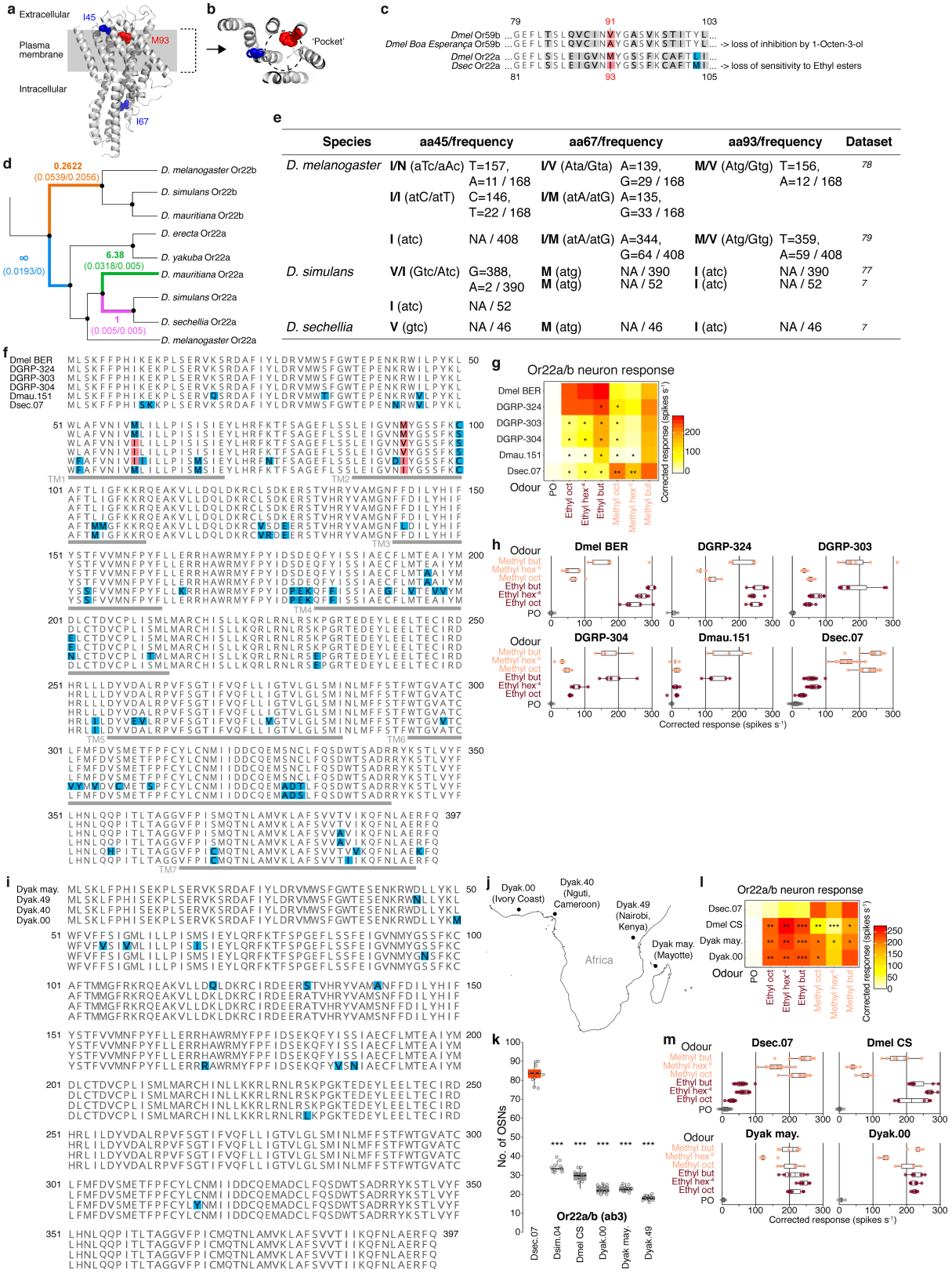

Extended Data Fig. 11 | See next page for caption.

Extended Data Fig. 11 | Phylogenetic and functional analysis of odour-specificity determinants in Or22a. a, Side view of the Orco monomer structure (determined by cryo-electron microscopy[37]); the approximate location of the plasma membrane is indicated. The location of the residues corresponding to the odour-specificity determinants of Or22a analysed in this study (on the basis of previously generated alignments[37]) are highlighted as spheres. **b**, Top view of a cross-section through the putative ligand-binding pocket of the Orco structure shown in **a**. **c**, Partial protein sequence alignment of Or22a and Or59b. The equivalent residue to *D. melanogaster* Or22a M93 in Or59b is V91, which exhibits intraspecific sequence variation that affects odour sensitivity[82]. **d**, Results of branch-based models of molecular evolution that tested for changes in the rates of protein evolution among Or22a and Or22b orthologues (Methods, Supplementary Table 8): the rate of protein changes within the Or22a and Or22b phylogenetic tree highlights dN/dS ratios (ω) that differ from the 'background rate' ($\omega = 0.1772$). Most branches exhibited low ω, arguing for strong purifying selection to maintain protein function over much of the tree. The two ω values that are >1 indicate an excess of protein changes, consistent with positive selection. The branch leading to *D. simulans* and *D. sechellia* Or22a displays nearly equal rates of silent and replacement substitutions, consistent with relaxed constraint during this period. **e**, Allele frequencies within population datasets for *D. melanogaster*[78,79], *D. simulans*[7,77] and *D. sechellia*[7] at the three sites of Or22a that were functionally characterized in this study. The table displays amino acid (aa) positions 45, 67 and 93 of Or22a and the frequencies at which variants within the corresponding codons are segregating (number of alleles with respective variant/number of alleles analysed). NA (not applicable) indicates that positions within the codon are invariant. Datasets analysed are referenced on the right. Selected *Or22a* variants from the *Drosophila melanogaster* Genetic Reference Panel (DGRP)[79] were confirmed by sequencing (**f**) and Or22a-neuron physiology was analysed (**g**, **h**). **f**, Protein sequence alignment of Or22a orthologues of *D. melanogaster*[83], three lines of the DGRP, *D. mauritiana* (DSSC 14021-0241.151 (Dmau.151)) and *D. sechellia*. Red shading, amino acid differences (compared to the other analysed sequences) that are shared by DGRP-303, DGRP-304 and *D. mauritiana* at position 59 and the key odour-specificity determinant at residue 93; blue shading, all other sequence differences. No line within the DGRP with a polymorphism only at position 93 was identified. **g**, Electrophysiological responses of the Or22a/b neuron to odours present in noni ($n = 5–20$, female flies) in the strains shown in **f**. The similarity between the response profiles of DGRP-303, DGRP-304 and *D. mauritiana* suggests that their only shared polymorphism (at position 59) modifies Or22a-response properties in these strains. Comparisons to responses of Dmel BER flies are shown. Pairwise Wilcoxon rank-sum test and *P* values adjusted for multiple comparisons using the Benjamini and Hochberg method. *D. mauritiana* and *D. sechellia* data are replotted from Fig. 3b. **h**, Box plots with individual data points showing the same data as in **g**. *D. mauritiana* and *D. sechellia* data are replotted from Extended Data Fig. 8g. **i**, Protein sequence alignment of Or22a orthologues of the noni-specialized *D. yakuba mayottensis* (Dyak may.)[41] and three other strains of *D. yakuba* (DSSC 14021-0261.00 (Dyak.00), 14021-0261.40 (Dyak.40) and 14021-0261.49 (Dyak.49)). Blue shading, differences between these sequences. **j**, Collection sites of *D. yakuba* strains shown in **i**. **k**, Quantification of the number of OSNs that express *Or22a/b* in *D. sechellia*, *D. simulans*, *D. melanogaster* (data as shown in Fig. 4b) and *D. yakuba*. $n = 10–12$ female flies. Comparisons to cell number counts in Dsec.07 flies are shown. In **k**, **l**, pairwise Wilcoxon rank-sum test and *P* values adjusted for multiple comparisons using the Benjamini and Hochberg method. **l**, Electrophysiological responses to odours present in noni of the Or22a/b neurons in *D. sechellia*, *D. melanogaster* and *D. yakuba* ($n = 5–20$, female flies). Comparisons to responses of Dsec.07 flies are shown. *D. sechellia*, *D. melanogaster* and Dyak.00 data are replotted from Fig. 3b. **m**, Box plots with individual data points showing the same data as in **l**. *D. sechellia*, *D. melanogaster* and Dyak.00 data are replotted from Extended Data Fig. 8g. NS, not significant ($P > 0.05$); $^{*}P < 0.05$; $^{**}P < 0.01$; $^{***}P < 0.001$.

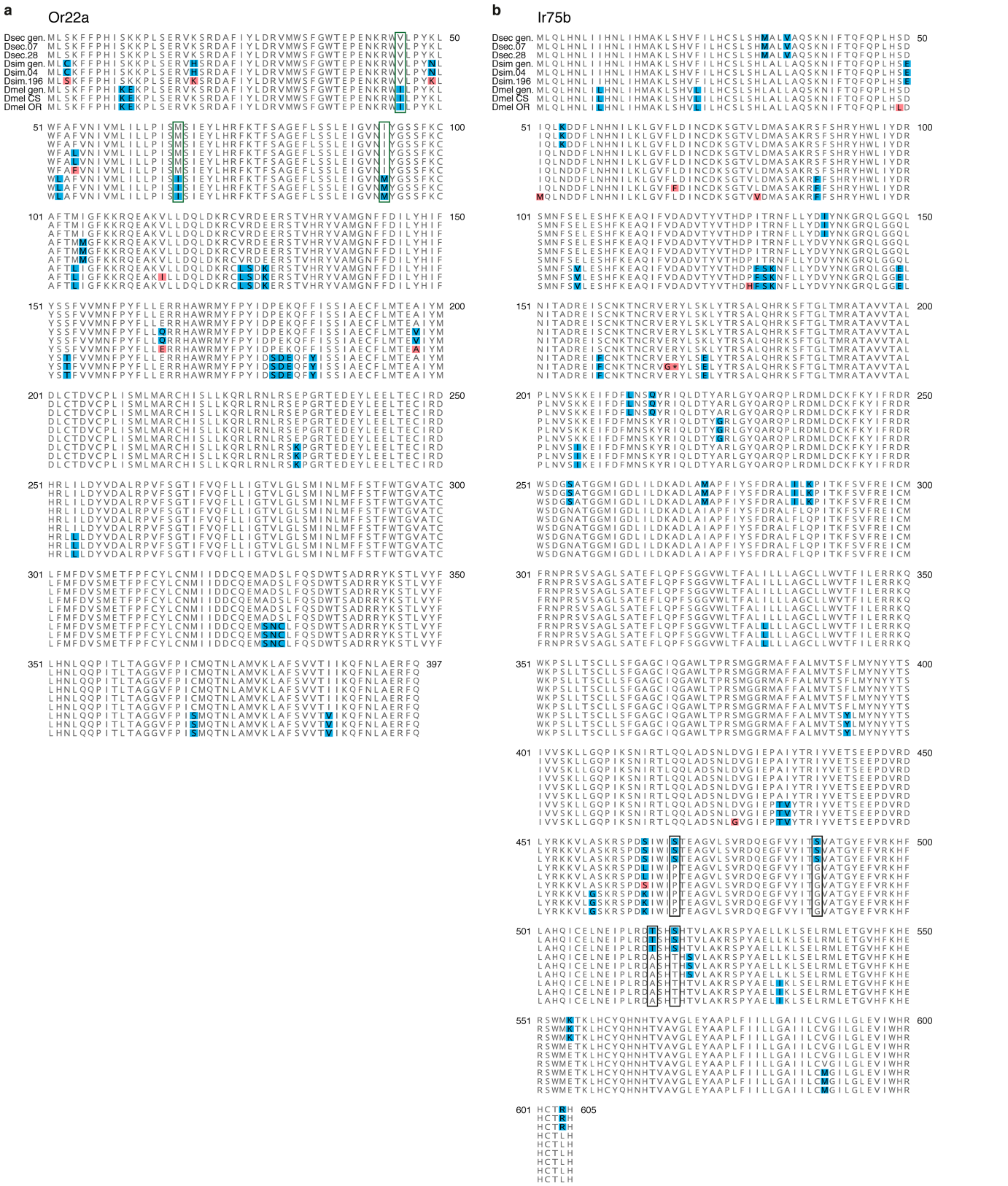

Extended Data Fig. 12 | Protein sequence alignments of Or22a and Ir75b. **a**, Or22a orthologues of strains used for behavioural assays as well as genome-sequenced strains ('gen.') of each species (version: *D. sechellia* (r1.3), *D. simulans* (r2.01) and *D. melanogaster* (r6.28)). Blue or red shading indicates differences between species or strains, respectively. Green boxes, residues tested in this study for their role in defining ester tuning specificity. **b**, Ir75b orthologues of same strains as shown in **a**. Blue or red shading indicates differences between species or strains, respectively. Black boxes, residues predicted to be located within the ligand-binding domain that contributes to odour tuning specificity[63]. The premature stop codon of the Canton-S strain (position 169, marked by an asterisk) does not impair receptor function, as shown in other strains[63].

nature research

Corresponding author(s): Thomas O. Auer, Richard Benton

Last updated by author(s): Feb 25, 2020

Reporting Summary

Nature Research wishes to improve the reproducibility of the work that we publish. This form provides structure for consistency and transparency in reporting. For further information on Nature Research policies, see Authors & Referees and the Editorial Policy Checklist.

Statistics

For all statistical analyses, confirm that the following items are present in the figure legend, table legend, main text, or Methods section.

n/a	Confirmed
☐	☒ The exact sample size (*n*) for each experimental group/condition, given as a discrete number and unit of measurement
☐	☒ A statement on whether measurements were taken from distinct samples or whether the same sample was measured repeatedly
☐	☒ The statistical test(s) used AND whether they are one- or two-sided *Only common tests should be described solely by name; describe more complex techniques in the Methods section.*
☒	☐ A description of all covariates tested
☐	☒ A description of any assumptions or corrections, such as tests of normality and adjustment for multiple comparisons
☐	☒ A full description of the statistical parameters including central tendency (e.g. means) or other basic estimates (e.g. regression coefficient) AND variation (e.g. standard deviation) or associated estimates of uncertainty (e.g. confidence intervals)
☐	☒ For null hypothesis testing, the test statistic (e.g. *F*, *t*, *r*) with confidence intervals, effect sizes, degrees of freedom and *P* value noted *Give P values as exact values whenever suitable.*
☒	☐ For Bayesian analysis, information on the choice of priors and Markov chain Monte Carlo settings
☒	☐ For hierarchical and complex designs, identification of the appropriate level for tests and full reporting of outcomes
☒	☐ Estimates of effect sizes (e.g. Cohen's *d*, Pearson's *r*), indicating how they were calculated

Our web collection on statistics for biologists contains articles on many of the points above.

Software and code

Policy information about availability of computer code

Data collection	Matlab was used for two-photon calcium imaging and Metamorph for widefield calcium imaging. Electrophysiological recordings were performed with AutoSpike. For Gas Chromatography/Mass Spectrometry analysis we used MSD ChemStation F.01.03.2357. For more details refer to the respective sections of the "Methods".
Data analysis	Calcium imaging data were analysed with Matlab and ImageJ and other imaging data with ImageJ, neuTube, Imaris (Bitplane) and Amira 6.5 (Thermo Scientific). Electrophysiological data were analysed in AutoSpike and Excel. Statistical analyses were performed in R.

For manuscripts utilizing custom algorithms or software that are central to the research but not yet described in published literature, software must be made available to editors/reviewers. We strongly encourage code deposition in a community repository (e.g. GitHub). See the Nature Research guidelines for submitting code & software for further information.

Data

Policy information about availability of data

All manuscripts must include a data availability statement. This statement should provide the following information, where applicable:

- Accession codes, unique identifiers, or web links for publicly available datasets
- A list of figures that have associated raw data
- A description of any restrictions on data availability

The datasets generated and/or analysed during the current study are available from the corresponding authors on reasonable request, or are provided in Source Data.

Field-specific reporting

Please select the one below that is the best fit for your research. If you are not sure, read the appropriate sections before making your selection.

☒ Life sciences ☐ Behavioural & social sciences ☐ Ecological, evolutionary & environmental sciences

For a reference copy of the document with all sections, see nature.com/documents/nr-reporting-summary-flat.pdf

Life sciences study design

All studies must disclose on these points even when the disclosure is negative.

Sample size	Preliminary experiments were used to assess variance and determine adequate sample sizes in advance of conducting the experiment. Generally, these were n=~15-20 in behavioural assays and 5-10 in physiological experiments. We used similar sample sizes for all experiments where a single variable (e.g., genotype, species, or stimulus) was being compared.
Data exclusions	In olfactory trap assays, assays with more than 25% of flies not surviving the experimental period were excluded from analysis. See "Olfactory trap assay" section in the "Methods". For the analysis of dose response curves in electrophysiological recordings, we excluded some samples at high stimulus concentrations when pinching of the spike amplitude prevented accurate quantification.
Replication	All attempts at replication were successful. Several experiments were carried out repeatedly due to the fact that they served as controls for different experimental manipulations. In particular we ran wild-type control experiments in parallel with mutant analysis in behavioural experiments and replicated them multiple times. In the wind tunnel assay the number of possible samples per day is rather low leading to testing of flies of different genotypes on different days. In these cases experiments were started at the same time of the day under stringently controlled conditions of temperature, humidity, light, and age of flies. For electrophysiological recordings, data were collected from multiple flies on several experimental days in randomised order interleaving wild-type and mutant genotypes. Within datasets the same odour dilutions were used for acquisition of the dataset. In all cases the results were reliable and robust over the course of the many years it took to complete this study.
Randomization	For all experiments, we interleaved genotypes and stimuli when applicable and randomised if possible their order. To control for potential variations in experimental conditions across days, we were careful to collect if possible a similar sample size for each variable every day the experiment was conducted and performed each experiment on multiple days.
Blinding	For olfactory trap assays, the experiments were conducted with the experimenter blinded to the genotype that was variable in a given experiment and unblinded only after analysis of the assay. The experimenter was not blinded to the genotype of flies in the wind tunnel assay or in physiological experiments.

Reporting for specific materials, systems and methods

We require information from authors about some types of materials, experimental systems and methods used in many studies. Here, indicate whether each material, system or method listed is relevant to your study. If you are not sure if a list item applies to your research, read the appropriate section before selecting a response.

Materials & experimental systems

n/a	Involved in the study
☐	☒ Antibodies
☒	☐ Eukaryotic cell lines
☒	☐ Palaeontology
☐	☒ Animals and other organisms
☒	☐ Human research participants
☒	☐ Clinical data

Methods

n/a	Involved in the study
☒	☐ ChIP-seq
☒	☐ Flow cytometry
☒	☐ MRI-based neuroimaging

Antibodies

Antibodies used	Antibodies used were: rabbit α-Ir75a (RRID:AB_2631091) 1:100, guinea pig α-Ir75b (RRID: AB_2631093) 1:200, rabbit α-Ir64a 1:100, rabbit α-Orco 1:200, guinea pig α-Ir8a (RRID:AB_2566833) 1:500, rabbit α-Ir25a (RRID:AB_2567027) 1:500, rabbit α-GFP 1:500 (Invitrogen). Immunofluorescence on adult brains was performed using mouse monoclonal antibody nc82 1:10 (Developmental Studies Hybridoma Bank), rat monoclonal α-Elav 1:10 (Developmental Studies Hybridoma Bank) and rabbit α-GFP 1:500 (Invitrogen). Alexa488-, Cy3- and Cy5-conjugated goat α-guinea pig, goat α-mouse, goat α-rat and goat α-rabbit IgG secondary antibodies (Molecular Probes; Jackson Immunoresearch) were used at 1:500. See the "Immunohistochemistry" section in the "Methods" for further details.
Validation	We generated an antibody against the D. sechellia Or22a protein by immunisation of rabbits against the peptide epitope PHISKKPLSERVKSRD (amino acids 7-22). Sera were affinity-purified (Proteintech Groups, Inc) and diluted 1:250 before use. We

validated this antibody by comparing the detected protein expression to previously reported data on Or22a expression in D. melanogaster, and by demonstration that immunoreactivity is lost in D. sechellia Or22a mutants.

Animals and other organisms

Policy information about studies involving animals; ARRIVE guidelines recommended for reporting animal research

Laboratory animals	All flies used for behavioural, functional and immunohistochemical analysis were females and between 3-6 days old except for experiments in Figure 2e where we also used 3-6 day-old male flies. For calcium imaging experiments, all flies were females and 7-10 days old. Please refer to Supplementary Table 2 and the "Methods" for further description of research animals.
Wild animals	This study did not involve wild animals.
Field-collected samples	This study did not involve samples collected from the field.
Ethics oversight	All experiments were conducted in accordance with ethical guidelines from the University of Lausanne.

Note that full information on the approval of the study protocol must also be provided in the manuscript.

3.1.3. Comparative calcium imaging responses in *Drosophila*'s antennal lobe: Or19a (DC1) olfactory sensory pathway

As described below in the comparative analysis of neuropeptide expression in the antennal lobe of drosophilids, I observed that the DC1 glomerulus in *D. sechellia* (but not in *D. melanogaster*) had higher levels of sNPF neuropeptide, prompting my interest in the physiological properties of this olfactory pathway. *D. melanogaster* DC1 glomerulus is innervated by Or19a OSNs which are specifically activated by terpenes present in the skin of citrus, such as valencene and limonene (Couto et al. 2005, Dweck et al. 2013, Grabe et al. 2016). These terpenes act both as strong oviposition attractants in *D. melanogaster* and repel endoparasitoid wasps, thereby protecting *Drosophila* larvae (Dweck et al. 2013). Therefore, the proper identification and localization of these volatiles could be determinant for *Drosophila*'s offspring survival.

As different levels of sNPF across drosophilids' DC1 glomerulus could imply different neuromodulation, I set out to perform calcium imaging in Or19a axon terminals and possibly find alternative excitatory patterns between species. In *D. melanogaster*, OSNs and PNs elicit calcium responses in the presence of valencene (Dweck et al. 2013). I confirmed this result in *D. melanogaster* with different valencene concentrations (Figure 1A). However, *D. sechellia*'s DC1 barely responded to valencene, and the response became unspecific (as several glomeruli were activated) at the highest concentration of valencene (Figure 1A). Through the heterologous expression of *Dsec*Or19a in *D. melanogaster* Or22a OSNs to perform single sensillum recordings further supported the calcium imaging results as neither valencene, nor any other terpene present in the citrus

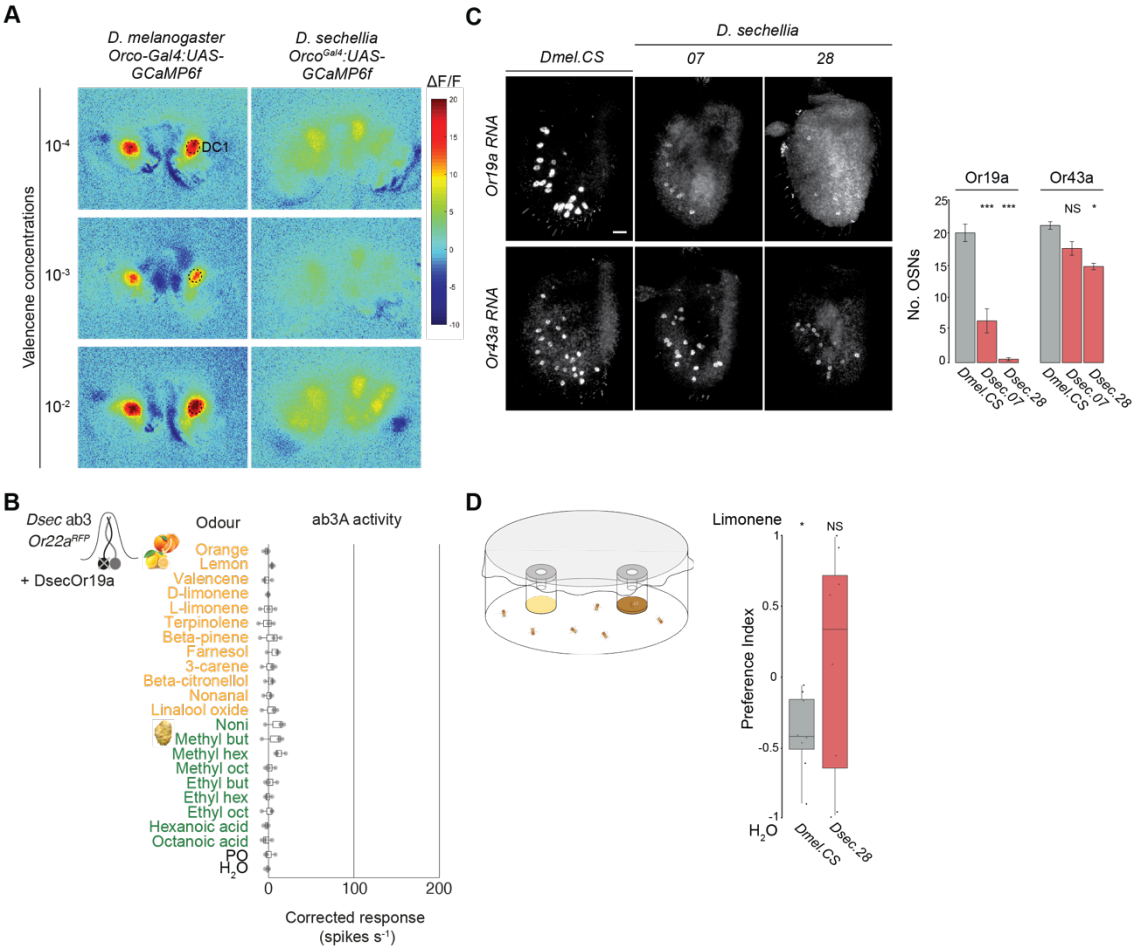

Figure 1. Or19a (DC1) OSN population architecture and physiology in *D. melanogaster* and *D. sechellia*. **A**, Representative odor-evoked calcium responses in the axon termini of Orco OSNd in the antennal lobes of *D. melanogaster* (*Orco:Gal4;UAS:GCaMP6f*) and *D. sechellia* (*Orco^{Gal4}:UAS-GCaMP6f*). The images show the relative increase in GCaMP6f fluorescence (ΔF/F%) after stimulation with different concentrations of valencene. **B**, Antennal electrophysiological responses of *D. sechellia* Or22a/b mutant neurons expressing *DsecOr19a*. **C**, Antennal FISH using *Or19a* (top) and *Or43a* (bottom) mRNA probes. *Or43a* is expressed by the neighboring neuron of Or19a in ac1 sensilla. We used this probe to control for ac1 physical distribution in the antenna between species. The average number of Or19a or Or43a cells in the antenna are shown in the right-hand panel. Error bars represent s.e.m. Comparisons to *DmelCS* are shown (Kruskal-Wallis rank sum test with Nemeyi post-hoc test). Scale bars represent 15μm. **D**, Behavioral responses in the olfactory trap assay testing preference for 1% limonene using wild type *D. melanogaster CS* and *D. sechellia 28*. Preference Indexes compared to 0 (no preference) are shown (one-sample Wilcoxon test with Bonferroni correction). ****P<0.001; **P<0.01; *P<0.05*; NS, Not Significant.

spectrum, elicited responses in *D. sechellia*'s Or19a (Figure 1B, performed by Thomas Auer).

The lack of physiological responses towards terpenes in *D. sechellia* suggested either 1) a re-tuning of the Or19a OSNs or 2) the absence of Or19a

OSNs in *D. sechellia*'s antenna. To test the second hypothesis, I performed RNA FISH using an *Or19a* probe. In fact, *D. sechellia*'s Or19a OSNs numbers were drastically reduced (Figure 1C).

To test if *D. sechellia* maintains a behavioral response towards citrus terpenes despite the strong reduction in Or19a OSN population (maybe overtaken by a different olfactory pathway), I ran behavioral trap assays to test fly's attraction (or aversion) towards limonene, a volatile that strongly attracts and promotes oviposition in *D. melanogaster* (Dweck et al. 2013). Surprisingly, in this behavioral set up, *D. melanogaster* significantly avoided traps containing limonene (Figure 1D) while *D. sechellia* seemed indifferent in the presence of this volatile (Figure 1D). While the inability to reproduce previous behavioral data in *D. melanogaster* (Dweck et al. 2013) makes it difficult to theorize about the role of citrus-related terpenes in oviposition performance across drosophilids, my latest results suggest altogether a less prominent (or missing) role of the Or19a pathway in *D. sechellia*. Ultimately, these observations stimulated my interest in understanding what chemical cues promote oviposition in *D. sechellia*, motivating the major piece of work presented in Chapter 4.

3.1.4. Comparative calcium imaging responses in *Drosophila*'s antennal lobe: Or56a (DA2) olfactory sensory pathway

The interspecific differences that affect Or19a OSNs made me wonder if other labeled olfactory pathways, previously described in *D. melanogaster*, such as Or56a (DA2) had also been targets of species-specific changes. Or56a OSNs are activated exclusively by geosmin, a microbial-derived chemical that alerts flies of the presence of harmful microorganisms on food substrates (Mattheis and Roberts 1992, Stensmyr et al. 2012). In fact, the addition of geosmin to attractive

feeding substrates, such as apple vinegar, reduced attraction of flies to apple cider vinegar (Becher et al. 2010).

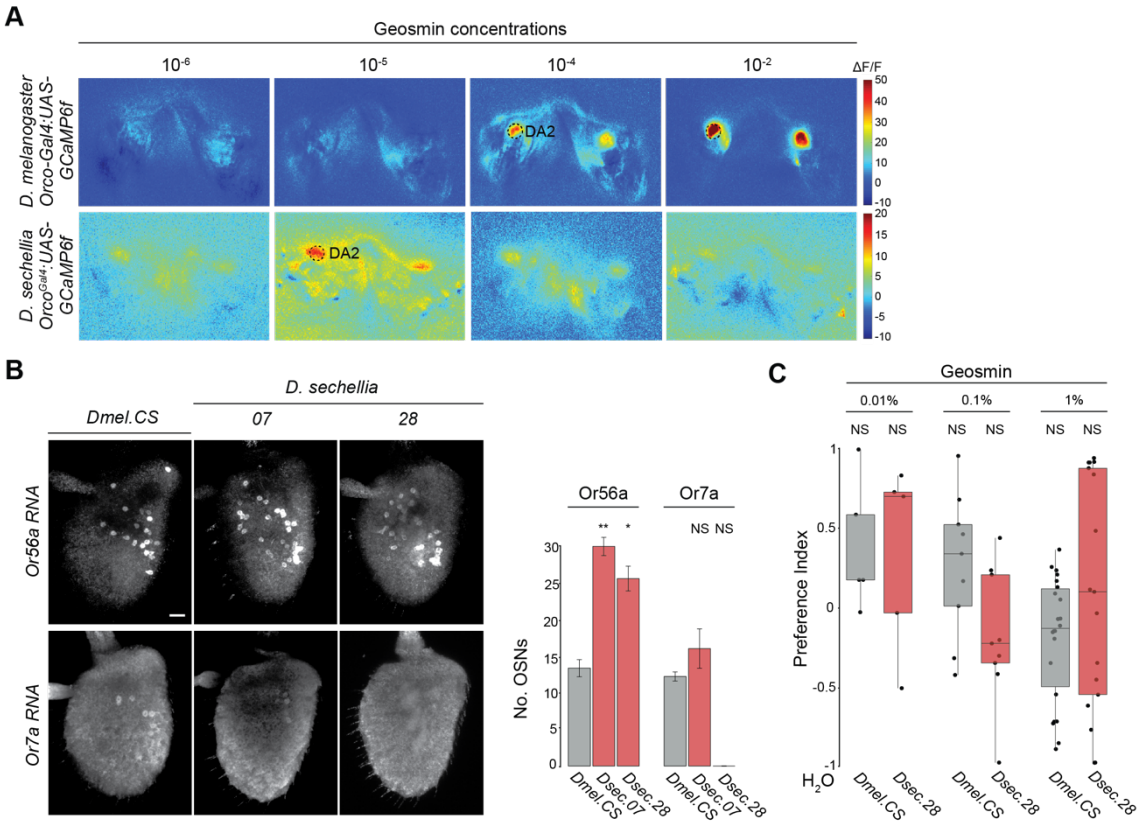

Figure 2. Or56a (DA2) OSN population architecture and physiology in *D. melanogaster* and *D. sechellia*. **A**, Representative odor-evoked calcium responses in the axon termini of Orco OSNd in the antennal lobes of *D. melanogaster* (*Orco:Gal4;UAS:GCaMP6f*) and *D. sechellia* (*Orco^{Gal4}:UAS-GCaMP6f*). The images show the relative increase in GCaMP6f fluorescence (ΔF/F%) after stimulation with different concentrations of geosmin. **B**, Antennal FISH using *Or56a* (top) and *Or7a* (bottom) mRNA probes. *Or7a* is expressed by the neighboring neuron of Or56a in ab4 sensilla. We used this probe to control for ab4 physical distribution in the antenna between species. The average number of Or19a or Or43a cells in the antenna are shown in the right-hand panel. Error bars represent s.e.m. Comparisons to *DmelCS* are shown (Kruskal-Wallis rank sum test with Nemeyi post-hoc test). Scale bars represent 15μm. **C**, Behavioural responses in the olfactory trap assay testing preference for 0.01%, 0.1% and 1% geosmin using wild type *D. melanogaster CS* and *D. sechellia 28*. Preference Indexes compared to 0 (no preference) are shown (one-sample Wilcoxon test with Bonferroni correction). ****P<0.001; **P<0.01; *P<0.05*; NS.

In *D. sechellia* Or56a OSNs, low concentrations of geosmin elicited stronger responses in DA2 glomerulus compared to *D. melanogaster* DA2 glomerulus (Figure 2A). Furthermore, *D. sechellia* antennae harbored twice the number of Or56a OSNs compared to *D. melanogaster* (Figure 2B). However, in an odor trap

assay, neither *D. sechellia* nor *D. melanogaster* were repelled by geosmin (Figure 2C). The failure to reproduce previously described geosmin-elicited aversion in *D. melanogaster* (Stensmyr et al. 2012) made it difficult to further study the ecological role (if any) of geosmin in *D. sechellia*.

3.2. Comparative neuromodulation in the *Drosophila* brain

Innate behaviors depend on genetically hardwired neural circuits and are crucial for animal's survival. However, innate behaviors can also be modulated, and this flexibility is determined by a subset of neurotransmitters and neuromodulators, such as neuropeptides or hormones. Neurotransmitters are chemical compounds necessary for neuron-to-neuron or glial cell-to-neuron communication, whereas neuromodulators are chemicals that adjust neurotransmission in a whole group of neurons. Neuromodulators can be released and exert their function locally as a neurotransmitter, or either diffused throughout the neural tissue with the purpose of regulating neuronal excitability depending on the organism's internal and external contexts (such as feeding or mating state or the food resources and mating substrates availability) (Kim et al. 2017).

The best example of neuromodulation in *D. melanogaster* is the regulation of its food-seeking behavior in fed and starved animals. This adaptive behavior is orchestrated by the parallel action of short neuropeptide F (sNPF) and sNPF receptor (sNPFR) and tachykinin (DTK) and DTK receptor (DTKR) (Ko et al. 2015, Root et al. 2011). In fed flies, apple cider vinegar rarely elicits attraction, and very low concentrations of this juice are indicative of substrates with a low nutritional value (Root et al. 2011). However, during starvation, a stronger

olfactory sensitivity makes flies accepting even lower value food sources in order to fulfill their feeding requirements. Insulin is the chief metabolic regulator, whose levels rise after feeding and decrease upon starvation. Reduce insulin signaling is necessary and sufficient for the upregulation of sNPFR1 in OSNs, such as Or42b neurons (DM1 glomerulus) (Root et al. 2011). Then, sNPF is locally released and binds sNPFR1 promoting facilitation in OSNs that mediate odor-guided attraction (Kim et al. 2015, Root et al. 2011). In parallel, DTK neuropeptide and DTKR upregulation mediate the desensitization of odor-guided rejection of Or85a OSNs (DM5 glomerulus) (Ko et al. 2015, Semmelhack and Wang 2009). A combined action of these two neuromodulatory pathways is crucial for a proper feeding-state adjustment in *D. melanogaster* (Kim et al. 2017, Ko et al. 2015). Other neuromodulatory hormones, such as adipokinetic hormone (AKH), have been also described in feeding modulatory roles. Upon starvation, insulin levels fall whereas AKH levels increase. These metabolic signals modulate the activity of the interoceptive sensory neurons (ISNs) in the subesophageal zone (SEZ) to promote feeding and suppress drinking (Bharucha, Tarr and Zipursky 2008, Kim et al. 2015).

Although there are several neurotransmitters and neuropeptides acting as neuromodulators, here I focus on characterizing two main neurotransmitters, dopamine and GABA, and one neuropeptide, sNPF, whose functions have been well described in *D. melanogaster*.

3.2.1. Dopamine

In a preliminary analysis, I studied the expression pattern of dopamine and its connectome in *D. melanogaster* and *D. sechellia*. The motivation for this study

relays on previous published data (Lavista-Llanos et al. 2014) that suggested increased dopamine levels but reduced L-DOPA (DA precursor) in *D. sechellia*. This was due to a mutation in the gene *Catsup* (encoding the protein Catecholamines up, functioning as a negative regulator of the tyrosine hydroxylase activity (Stathakis et al. 1999)). The L-DOPA deficit was suggested to be responsible for impaired egg production capacity and smaller egg size. However, supplementing flies with L-DOPA, but not tyrosine (another DA precursor) or dopamine itself, could revert this phenotype and promote resistance towards octanoic acid, an abundant volatile present in noni fruit known for its high toxicity across *Drosophila* species, excluding *D. sechellia*.

To study this phenomenon further, I performed immunostainings using the Tyrosine Hydroxylase (TH) antibody and compared its expression pattern across *D. melanogaster* and *D. sechellia* brains. Dopaminergic cell bodies were mainly located in the mushroom bodies and lateral horn (Figure 3A). Several cell bodies were also bilaterally present surrounding the antennal lobes (4 to 8 cell bodies) and the SEZ (4 cell bodies) (Figure 3A), possibly exerting a modulatory function on sensory neurons. Future analysis using transgenic reagents that label TH^+ populations across species will help clarify if inter-species differences exit.

3.2.2. $GABA_BR2$

I also examined the expression of the inhibitory neurotransmitter GABA and its receptor $GABA_BR2$. GABA and $GABA_BR2$ roles have been described in *D. melanogaster* but very little (or nothing) is known about their mechanism of action in *D. sechellia*.

$GABA_BR2$ is a metabotropic receptor present in the cell membrane of multiple neuron types, including OSNs. In *D. melanogaster*, the expression levels of $GABA_BR$ vary among OSN types. The population of Gr21a/Gr63a OSNs that sense CO_2 (Jones et al. 2007, Kwon et al. 2007) do not express $GABA_BR$ and, therefore, they do not show presynaptic inhibition (Root et al. 2008). CO_2 is a harmful volatile for flies and its detection mediates avoidance. The lack of $GABA_BR$ in CO_2-sensing OSNs must be, consequently, important to maintain high sensitivity towards this molecule. Conversely, OSNs involved in pheromone detection show high levels of presynaptic inhibition mediated by $GABA_BRs$ (Root et al. 2008). Since GABA is the chief inhibitory neurotransmitter in the nervous system (Enell et al. 2007), their levels and the levels of its receptor will determine to a large extent the excitability of the neurons in the presence of an action potential (Root et al. 2008).

GABA and $GABA_BR2$ expression was previously studied in *D. melanogaster* by using both GABA antibody and *$GABA_BR2$:Gal4* transgenic reporter (Root et al. 2008). Since the $GABA_BR2$ antibodies were no longer available, I decided to develop *D. sechellia $GABA_BR2$* transcriptional reporters.

I designed and made a P2A-based endogenous tag for *$GABA_BR2$* gene for both *D. melanogaster* and *D. sechellia*. The P2A approach consists in the utilization of a self-cleaving peptide-based multi-gene expression system initially described in *Bombyx mori* that allows endogenous gene targeting without affecting protein stability and function (Daniels et al. 2014, Wang et al. 2015). Unfortunately, the transgenesis with these DNA constructs never worked. An alternative approach was to clone the GFP sequence downstream the *$GABA_BR2$*

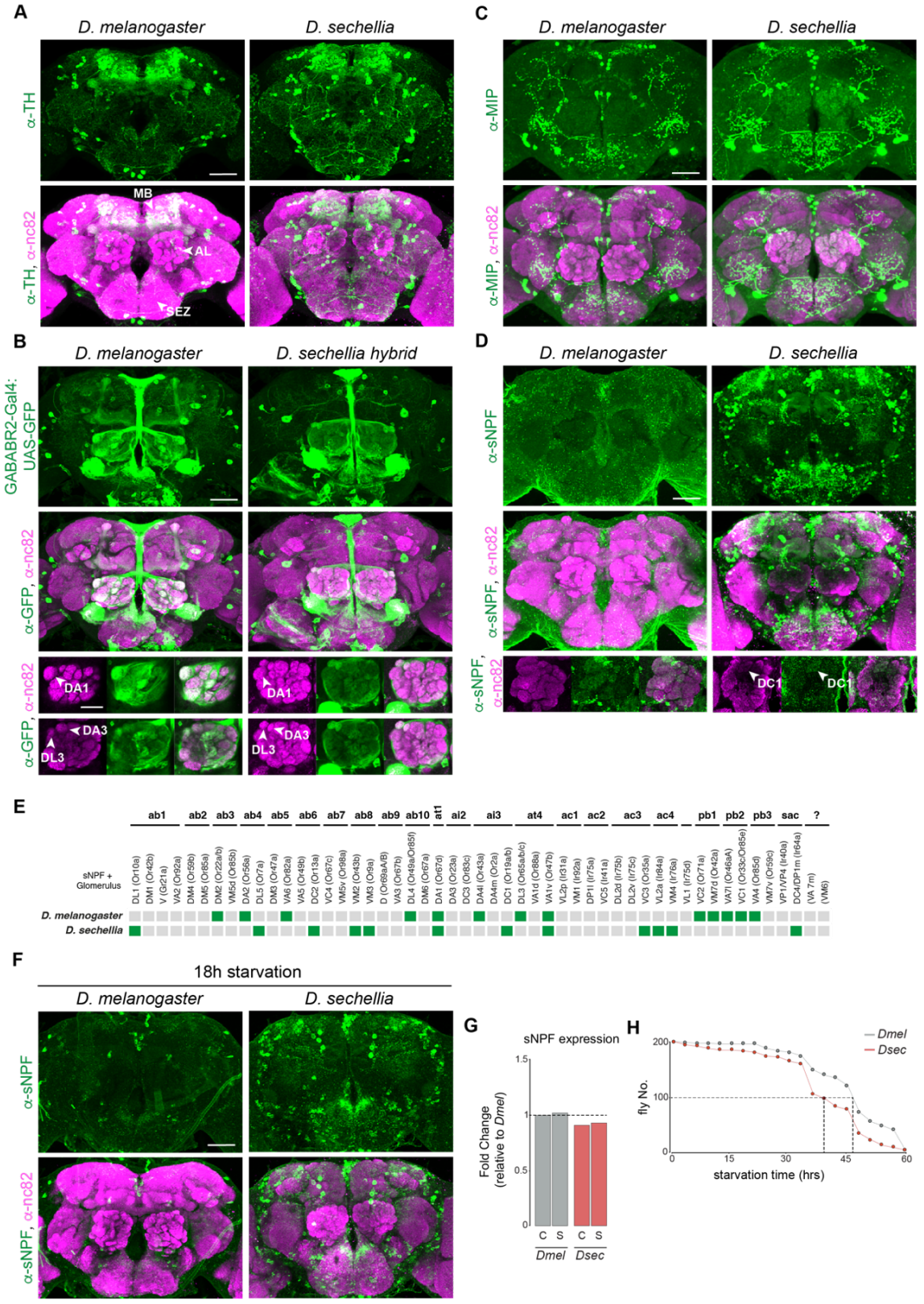

Figure 3. Comparative expression of neuromodulator and neuropeptide *D. melanogaster* and *D. sechellia*. **A-D**, Whole-mount brains expressing the indicated antibodies or transgenic construct (in green). Brain structures are labeled using nc82 antibody (magenta). In B and D inter-species differences of neuromodulator expression in the antennal lobe are highlighted in the zoom ins. **E**, Summary of the glomerular labelling with sNPF (α-RLRW) antibody characterized in *D. melanogaster* and *D. sechellia*. **F**,

Whole-mount brains expressing sNPF antibody (green) after 18h of starvation. **G**, sNPF mRNA levels quantification by qRT-pcr in fed or 4h starved flies. **H**, *Drosophila* resistance to starvation during 60h. Notice the higher resistance of *D. melanogaster* (grey) compared to *D. sechellia* (red). Whole-mount scale bars represent 20μm. Antennal lobe zooms in scale bars represent 30μm.

promoter in both species, which I did. However, these were very weakly expressed (data not shown).

I then decided to analyze *Dmel-GABA$_B$R2:Gal4* expression pattern in *Dmel/Dsec* hybrid flies. The DA1 (Or67d) glomerulus is robustly labeled by *GABA$_B$R2:Gal4;UAS-GFP* in *D. melanogaster* (Root et al. 2008). However, *Dmel/Dsec* hybrids' DA1 was not (Figure 3B). By contrast, neighboring DL3 (Or65a/b/c) and DA3 (Or23a) glomeruli were labeled in *Dmel/Dsec.* hybrids but not in *D. melanogaster* (Figure 3B). While these observations are intriguing, there are several caveats to analyzing reporter transgenes in hybrids, such as ectopic expression of trans-species reporters.

Although these data are preliminary, they suggest that GABA$_B$R2 expression in the antennal lobe might be different across species. In *D. melanogaster*, Or67d (DA1) and Or65a (DL3) bind the pheromone cVA, which is produced by males and fulfills a primary role in sexual and social communication (Kurtovic, Widmer and Dickson 2007, Liu et al. 2011, Symonds and Wertheim 2005). However, the close relative *D. suzukii* has lost the ability to produce cVA and, therefore, the presence of the aphrodisiac pheromone reduces copulation rate in this species (Dekker et al. 2015). Whether *D. sechellia* has also evolved different mating behaviors is unknown, but my data might indicate an alternative modulation of the cVA pathway. In the future, it would be interesting to study the different excitability of DA1 (Or67d) and DL3 (Or65a) glomeruli between *D.*

melanogaster and *D. sechellia* as well as to better understand the role of GABA in *D. sechellia*'s glomerular excitability.

3.2.3. Neuropeptide expression in the *Drosophila* brain

At least 42 genes that encode precursors of neuropeptides have been described in *D. melanogaster* (Hewes and Taghert 2001, Li et al. 2008, Nassel and Winther 2010, Roller et al. 2008, Yew et al. 2009). Of these, 8 are expressed in the antennal lobe and mushroom bodies: Amnesiac-derived (Amn), Allatostatin-A (AstA), Mioinhibitory peptide (MIP), Myosuppressins (DMS), IFamide (SIFa), IPNamide (IPNa), short Neuropeptide F (sNPF) and Tachykinin-related peptides (DTK) (Nassel and Winther 2010).

In a first approach, I established hybrid transgenic lines with the Gal4:UAS expression system using *D. melanogaster neuromodulatorX-Gal4:UAS-GFP*. I then analyzed the fluorescent reporter expression (GFP) in *D. melanogaster* and *Dmel/Dsec* hybrid backgrounds. This comparison provided a quick initial way to determine whether there may be species-specific differences in neuromodulators expression. Preliminary data suggested a conserved MIP reporter expression pattern across species, where cell bodies were clustered along the mushroom bodies, antennal lobes and SEZ (data not shown). These results were also confirmed using MIP antibody (Figure 3C) (Carlsson et al. 2010). However, most of the results obtained through the use of transcriptional reporters were inconclusive since some of the transgenic lines, such as DTK, did not recapitulate the published expression pattern in *D. melanogaster* (data not shown) (Nassel and Winther 2010).

3.2.4. sNPF

To analyze sNPF expression in the fly brain I initially tested two antibodies (α-sNPF and α-RLRW) that bind alternative isoforms of the sNPF neuropeptide. Both antibodies recapitulated sNPF expression (data not shown), but α-RLRW gave a stronger signal and therefore I decided to pursue the analysis with it. The high level of sNPF sequence conservation across species allowed me to use the same antibodies in *D. sechellia*.

D. melanogaster flies showed very low levels and absence of specific staining across their brain (Figure 3D). On the other hand, *D. sechellia* flies displayed a significantly brighter staining highlighting multiple cell bodies throughout the brain (Figure 3D). The increased presence of sNPF in *D. sechellia* suggested the existence of nutritional deficits in their diet giving rise to more "hungry" brains. To test this hypothesis, I performed survival assays to measure species' resistance to starvation (Figure 3H). The results from this experiment suggested a lower tolerance to starvation in *D. sechellia*, where the population was reduced to half after 37h (Figure 3H). A previous study reported differences in the amount of ingested food between wild type *D. melanogaster* and *D. sechellia* in laboratory conditions (Watanabe et al. 2019). In the future, it would be interesting to analyze the repercussion that a fly food laboratory diet has on *D. sechellia*'s starvation resistance compared to a natural noni fruit diet.

sNPF expression pattern in the antennal lobe was different between species. Consistent with previous observations (Carlsson et al. 2010), *D. melanogaster* expressed high levels of sNPF in 13 different glomeruli of the antennal lobe (Figure 3E). However, this expression distribution was not conserved in *D. sechellia* (Figure 3E). Intriguingly, *D. sechellia*'s DC1 glomerulus,

but not *D. melanogaster*'s DC1, expressed high levels of sNPF (Figure 3D). This result was confirmed with the second antibody α-sNPF (data not shown). This observation prompted my interested in the corresponding olfactory pathways (Or19a neurons), as described above.

Previous qRT-PCR results showed that sNPF levels rise as soon as 4h after starvation in *D. melanogaster* (Lee et al. 2009, Lee et al. 2008, Lee et al. 2004, Root et al. 2011). To analyze inter- and intra-specific differences in sNPF expression pattern, I performed immunostainings in 18h starved fly brains (expecting that more prolonged periods of starvation would accentuate sNPF expression levels variations). *D. melanogaster* sNPF staining slightly increased compared to fed conditions (Figure 3D,F). However sNPF levels remained unchanged in starved *D. sechellia* (Figure 3D,F). To confirm these observations, I performed qRT-PCRs in *D. melanogaster* and *D. sechellia* heads either fed or after 4h of starvation. Preliminary data showed no variation across conditions, nor across fly species (Figure 3G). Although this experiment should be repeated exclusively using fly brains (since peripheral head tissues might be masking the levels of sNPF in the brain), the differences between protein and mRNA expression could be due to differential post-transcriptional regulatory mechanisms.

3.3. Materials and methods

Drosophila strains

Drosophila stocks used for Fluorescent *In Situ* Hybridization (FISH) or Immunohistochemistry were maintained at room temperature (~23ºC) on standard corn flour, yeast and agar medium. *D. sechellia* stocks were supplemented with noni paste (*Morinda* (noni) juice (Raab Vitalfood) and a few

grams of Formula 4-24® instant *Drosophila* medium). The following strains were used: *D. melanogaster Canton-S*, *D. sechellia 07* and *28* (*Drosophila* species stock center of San Diego [DSSC]).

Drosophila stocks used for calcium imaging experiments and behavioral assays were maintained at 25ºC on standard corn flour, yeast and agar medium, or supplemented with instant medium and noni juice in the case of *D. sechellia* flies, under 12h light and 12h dark cycle. The following stocks were used for calcium imaging: *Dmel-Orco-Gal4:UAS-GCaMP6f/CyO* and *Dsec-UAS-GCaMP6f/UAS-GCaMP6f;;Orco^{Gal4}/+*.

Antenna dissection and fixation

For antenna dissection, 3-4 days old flies were used and separated by sex. Flies were anesthetized with CO_2, disposed inside a sieve with a metal mesh (250nm diameter, Scienceware^{TM}), and flash-frozen in liquid nitrogen for 5 seconds. Antennae were harvested and fixed in 2 mL of 1xPBS-PFA (4%), Triton-X-100 (3%) for 3 h at 4ºC. After fixation, samples were washed 3 times in 1xPBS Triton-X-100 (3%) and once in 1xPBS Triton-X-100 (0,1%) and then used for experiments. Antennae for storage were washed 2 times in cold Methanol and placed at -20ºC.

Adult brain fixation and dissection

For adult brain dissection, 2-3 days old flies were used and separated by sex. Flies were fixed in 2 mL of 1xPBS-PFA (4%) plus Triton-X-100 (0.2%) for 3 h at 4ºC. After fixation, brains were dissected using forceps. Finally, brains were washed 4 times using 1xPBS Triton-X-100 (0,2%).

Immunohistochemistry (IHC)

Immunofluorescence on adult brains was performed as described (Sanchez-Alcañiz 2017) using mouse monoclonal antibody nc82 1:10 (Developmental Studies Hybridoma Bank), rabbit α-GFP 1:500 (Invitrogen) and chicken α-GFP 1:500 (Abcam). Alexa488- and Cy5-conjugated goat α-rabbit and goat α-mouse IgG (Molecular Probes; Jackson Immunoresearch) and Alexa488-conjugated goat α-chicken (Abcam) secondary antibodies were used at 1:500.

Confocal imaging and image processing

For microscopy, a LSM710 laser scanning confocal microscope (Zeiss) was used to obtain the images of the antenna (40X) and brain (20X). Images were processed using Fiji, Adobe Illustrator CC 2015 and Adobe Photoshop CC 2015 software.

Wide-field calcium imaging

Fly preps were performed as described in (Silbering et al. 2012). Briefly, 4-12 days old flies were immobilized in a Plexiglas chamber with the help of a cactus spine and UV-glue and a window would be opened on top of the fly's head by removing the cuticle with a scalpel allowing the visualization of the antennal lobes. During the imaging, the fly's brain is hydrated using Ringer, a buffer based on distilled water and ions that mimic fly's interstitial medium. For the stimulation, a constant current of compressed air from a tank would pass through a system of Teflon tubes and a glass bottle filled with distilled water in order to humidify the air up to 90% RH. The air current is directed to the fly's antennae from approximately 0,5 cm. 20 mL of odor mixtures of interest were supplied in a 1 x

0,5 cm filter paper contained in a plastic syringe, that is placed 38 cm away from the tube exit. The opening of the valve that allows the release of the odor solution is controlled from a computer using the MetaFluor software (Visitron) injecting 1 ml (1 ml/s) of odor per stimulus. Odors were obtained from Sigma and the dilutions were prepared every month for each set of experiments. More details can be found in the figure legends.

Data processing

Flies showing consistent calcium responses throughout the experiment and low or moderate responses to paraffin oil or water were selected for data analysis. First, each set of images would be opened in Fiji (Fiji is just Image J) and corrected for lateral movement, in case this was necessary, taking as references different anatomical structures. The resulting movies would be saved as .tiff files. The .tiff files were opened using MatLab and the relative calcium change was calculated for each frame *i* as $(\Delta F/F)I\ (\%) = (F(i) - F0)/F0\ X\ 100$, where $F(i)$ is the absolute fluorescence of the *i*th and $F0$ the average fluorescence of the four frames before stimulus onset. Regions of interest were selected with a circumference of 10 pixels of diameter in order to obtain activity traces of desired glomeruli. These traces were transformed into color-gradient images. The numeric values for each experiment were exported in excel file for their statistical analysis.

qRT-PCR

40 female flies belonging to control (fed) or experimental (4h starvation) groups were introduced in 1.5 ml Eppendorf tubes and the heads were collected

after flash-freezing in liquid nitrogen for 5''. For RNA extraction, the RNeasy kit (QIAGEN) was used. The reverse transcription was performed using SuperScript III First-Strand Synthesis System (ThermoFisher). Gene expression was measured in a final volume of 10 μl by qRT-PCR using 5 μl of SYBR Green Master Mix (Applied Biosystems) in a 7500 Fast Light Cycler System (Applied Biosystems). The values showed in Figure 1G come from one replicate. The fold change is quantified compared to the levels of the control gene *actin*. The primers used for the qRT-PCR were the following:

sNPF (97 bp) F: CAAAAAGCGTGGCATACATT, R: AATGTCCGGATTTCAAGGAG

sNPFR1 (77 bp) F: CTGGCCATATCGGACCTACT, R: GGCCAGTACTTGGACAGGAT

actin (109 bp) F: TCTTCCAGCCCTCGTTCC R: TTGTTGGCATACAGGTCCTTAC

Survival assay

For each assay, a total of a 100 of young, mated females per species were separated in 4 different tubes. 24 h before of the starting time of the starvation assay, flies were flipped to fresh tubes provided with enriched food specific for each species: blue paste (instant medium plus water) for *D. melanogaster* or noni paste for *D. sechellia*. During the survival assay flies were maintained at 25ºC in fly incubators with controlled humidity, 12 h light and 12 h dark cycle and provided with a humid tissue. The number of dead flies was annotated every 3 h until the last fly would die.

Olfactory trap assay

The two-choice trap assay was performed as described in (Auer et al. 2020). In brief, traps contained 300 μL of juice (noni or grape (Bio Demeter))

mixed with 0.1% Triton to break the water tension. Different concentrations (indicated in the figure legends) of limonene (Sigma) were added to the solution. During the experiment, 25 young (3-5 days old) fed, mated females were anesthetized on ice were used. Fly choosing was scored after 24 h of experiment at 25ºC and 60% relative humidity in a dark room; experiments with over 25% dead flies were discarded. The attraction index was calculated as follows: (number of flies in trap X – number of flies in trap Y)/number of trapped and untrapped flies alive in the arena.

CHAPTER 4: Odor-gated oviposition behavior in an ecological specialist

Summary of the results

This section describes the result of a collaborative effort from members of the Richard Benton's lab (enclosed publication; Álvarez-Ocaña, Shahandeh, Auer and Benton), as well as members of other institutions (Ray and Gompel) for which a manuscript has been deposited on bioRxiv (Álvarez-Ocaña 2022) and is under review at Nature Communications. In this work, I developed protocols to study fly's oviposition preference with single individuals and in groups to study evolutionary changes that might had happened in the stringent specialist *D. sechellia*. Through the systematic analysis of *D. melanogaster*, *D. simulans* and *D. sechellia* strains, I described *D. sechellia*'s robust preference for noni-containing oviposition substrates. I, with the contribution of Shahandeh, eliminated the role of vision and substrate stiffness in *D. sechellia*'s oviposition preference. Using *D. sechellia* mutants for noni-related olfactory pathways, we studied the role of the olfactory system in this decision making. Moreover, we described that the abundant noni odor hexanoic acid promotes both oviposition preference and motivation in *D. sechellia*, and that mutants for its cognate receptor, Ir75b, lack egg-laying in the sole presence of hexanoic acid enriched substrates. Lastly, we showed that that expression of *DsecIr75b* in *D. melanogaster* is sufficient to switch oviposition preference towards hexanoic acid-containing substrates.

My contribution to this work

During this project, I developed the oviposition assays for single flies and groups of flies employed in this study to analyze oviposition preference. I performed most of the experiments shown in the figures except for those in Figure 2B, Figure 3B and Figure 6D, and I only contributed to set the experiments for Figure S3 together with Shahandeh.

4.1. Article: Odor-gated oviposition behavior in an ecological specialist

Odor-gated oviposition behavior in an ecological specialist

Raquel Álvarez-Ocaña[1], Michael P. Shahandeh[1,#], Vijayaditya Ray[2,#], Thomas O. Auer[1], Nicolas Gompel[2], and Richard Benton[1,*]

[1]Center for Integrative Genomics
Faculty of Biology and Medicine
University of Lausanne
CH-1015
Lausanne
Switzerland

[2]Evolutionary Ecology
Ludwig-Maximilians Universität München
Fakultät für Biologie
Biozentrum
Grosshaderner Strasse 2
82152
Planegg-Martinsried
Germany

[*]Corresponding author:

T: +41 21 692 3932
E: Richard.Benton@unil.ch

[#]M.P.S. and V.R. contributed equally to this work

Abstract

Colonization of a novel ecological niche can require, or be driven by, evolution of an animal's behaviors promoting their reproductive success in the new environment. Little is known about the underlying mechanisms. We have exploited an emerging genetic model for behavioral neuroecology, *Drosophila sechellia* – a close relative of *Drosophila melanogaster* that exhibits extreme specialism for *Morinda citrifolia* noni fruit – to study the evolution and sensory basis of oviposition. *D. sechellia* produces fewer eggs compared to other drosophilids, but lays these almost exclusively on noni substrates, contrasting with avoidance or indifference of noni by generalist species. Visual, textural and social cues do not explain the species-specificity of this preference. By contrast, loss of olfactory input in *D. sechellia*, but not *D. melanogaster*, essentially abolishes egg-laying, suggesting that this sensory modality gates gustatory-driven noni preference. We find the noni bouquet is detected by redundant olfactory pathways. By parsing the fruit's volatile chemicals and genetic perturbation of individual olfactory pathways in *D. sechellia*, we discover a key role for hexanoic acid and its cognate receptor, the Ionotropic receptor Ir75b, in odor-evoked oviposition. Through receptor exchange in *D. melanogaster*, we provide evidence for a causal contribution of odor-tuning changes in Ir75b to the evolution of oviposition behavior during *D. sechellia*'s host specialization.

Introduction

Colonization of, and specialization on, a new ecological niche by an animal can provide many benefits, such as access to new resources, protection from biotic and abiotic threats, and avoidance of competition (Sexton et al., 2017). Niche specialization often requires adaptation of multiple behavioral, physiological and morphological traits to survive and reproduce in a new habitat. Divergence of many traits can potentially lead to reproductive isolation and ultimately speciation, making niche specialization a likely driver of biodiversity (Caillaud and Via, 2000; Rundle and Nosil, 2005; Seehausen, 2006). Many striking examples of adaptations to new niches are known, from the rapid evolution of beak morphology of Darwin's finches as they radiated across the Galápagos archipelago (Grant and Grant, 2005) to visual system loss in Mexican tetra (*Astyanax mexicanus*, blind cave fish) in cave dwellings in the Gulf of Mexico and Rio Grande (Maldonado et al., 2020). While candidate genomic regions and genes have been implicated in some of these adaptations (e.g., (Abzhanov et al., 2004; Lamichhaney et al., 2015)), the restricted genetic tractability of these species – and most other examples in nature – limits our understanding of the mechanistic basis of evolutionary adaptations.

The fly *Drosophila sechellia* provides an exceptional model to investigate the genetic and cellular basis of niche adaptation (Auer et al., 2021; Jones, 2005; Stensmyr, 2009). This species is endemic to the Seychelles archipelago, where it has evolved an extreme specialist lifestyle, feeding and breeding exclusively upon the "noni" fruit of the *Morinda citrifolia* shrub. Adaptation to this niche has occurred in the last few 100,000 years, potentially only since its divergence from a last common ancestor with the cosmopolitan generalist, *Drosophila simulans* (Figure 1A). Importantly, the close phylogenetic proximity of *D. sechellia* to the laboratory model, *Drosophila melanogaster* (Figure 1A), has facilitated the development of genetic tools in this species to explore the mechanistic basis of niche specialization

(Auer et al., 2020; Auer et al., 2021; Combs et al., 2018). Previous work has identified *D. sechellia* Odorant receptors (Ors) essential for long-range detection of noni odors, Or22a and Or85c/b (Auer et al., 2020; Dekker et al., 2006; Ibba et al., 2010), and demonstrated a causal relationship between differences in tuning properties of Or22a in *D. melanogaster* and *D. sechellia* and species-specific noni attraction (Auer et al., 2020).

Long-range olfactory attraction to noni is only one facet of *D. sechellia*'s phenotypic adaptations in this specialized niche (Auer et al., 2021). Notably, the fruit is highly toxic to other drosophilids (and more divergent insects) – predominantly due to its high levels of octanoic acid – indicating the existence of robust (albeit unclear) resistance mechanisms of *D. sechellia* throughout its life cycle (Legal et al., 1994; Legal et al., 1992; R'Kha et al., 1991). Host fruit toxicity has been suggested to relieve *D. sechellia* from interspecific competition and parasitoidization (Salazar-Jaramillo and Wertheim, 2021), providing a potential explanation for the selective advantage of its stringent niche specialization.

Another unique set of phenotypes of *D. sechellia* relates to the production and deposition of eggs. Compared to its generalist cousins, *D. sechellia* ovaries contain ~3-fold fewer ovarioles, with a commensurate reduction in egg number (Coyne et al., 1991; Green and Extavour, 2012; R'Kha et al., 1991). The evolutionary advantage (if any) of reduced fecundity is unclear, but may be linked with the larger size of *D. sechellia* eggs (~50% by volume (Markow et al., 2009)) and the greater tendency of this species to retain fertilized eggs (resulting in facultative ovoviviparity) (Markow et al., 2009). Such observations hint that these traits may be related to more investment of *D. sechellia* in fewer eggs to protect them from the acid-rich noni substrate and/or predators. However, non-adaptive explanations (e.g., pleiotropic effects of mutations in genes underlying other adaptations (Jones, 2004; R'Kha et al., 1997)) cannot be excluded.

Whatever the reason(s) for reduced fecundity of this species, this trait makes the decision of *D. sechellia* females to engage in oviposition particularly important. Previous work has shown that *D. sechellia* depends on the presence of noni for both egg production and laying (Lavista-Llanos et al., 2014; Louis and David, 1986; R'Kha et al., 1991). Furthermore, the most abundant noni chemicals, hexanoic and octanoic acids, can alone induce oviposition (Amlou et al., 1998; Higa and Fuyama, 1993). However, the cognate sensory pathways are unknown, as is the contribution, if any, of other chemosensory or non-chemosensory information to this behavior.

Results

Species-specific oviposition preference and rate

To investigate the neurosensory basis of egg-laying behavior in *D. sechellia*, we first compared the specificity of oviposition site selection of *D. sechellia*, *D. simulans* and *D. melanogaster* in a semi-natural, multi-choice assay in which animals were offered slices of different ripe fruits (noni, banana, apple and grape) within an enclosed arena (Figure 1B). While *D. melanogaster* and *D. simulans* flies avoided using noni fruit as an oviposition substrate (preferring two or three of the other fruits instead), *D. sechellia* laid eggs almost exclusively on noni (Figure 1B).

To systematically test the species-specificity of oviposition behavior and its sensory basis, we next established two-choice group oviposition assays. In these,

egg-laying substrates comprised of commercial juices/vinegar (to ensure consistency of chemical stimulus) mixed in either agarose or Formula 4-24® instant *Drosophila* medium (hereafter, "instant medium"). The latter substrate supported higher egg-laying rate that was important when examining the influence of single odors in subsequent experiments. Two independent strains of each species were tested in all assays to distinguish interspecific from intraspecific differences. *D. melanogaster* and *D. simulans* strains generally exhibited indifference between noni and grape juice substrates, in either agarose or instant medium, with small differences between strains (Figure 1C and Figure S1A). By contrast, *D. sechellia* consistently displayed a strong preference for noni juice-containing substrates (Figure 1C and Figure S1A). Similar, though less marked, differences between species' preferences were observed in assays offering a choice between noni juice and apple cider vinegar in agarose (Figure 1D), but not in instant medium (Figure S1B).

As social interactions can influence drosophilids' oviposition preference (Churchill et al., 2021; Elsensohn et al., 2021), we also established a single-fly oviposition assay (see Methods and Figure S2) (Gou et al., 2016). Using the same combinations of stimuli and substrates as in group assays, we observed even more marked species differences in oviposition site preference: *D. sechellia* laid the vast majority of its eggs on noni juice substrates in all assays (Figure 1E-F and Figure S1C-D), while *D. melanogaster* and *D. simulans* exhibited strong preference for either grape juice or apple cider vinegar in agarose, and variable levels of preference for these counter-stimuli in instant medium (with the exception of one strain of *D. simulans*).

Both group and single-fly assays also confirmed the substantially lower fecundity of *D. sechellia* compared to *D. melanogaster* and *D. simulans* (Figure 1C-F and Figure S1). Quantification of eggs laid by individual flies revealed large variation in egg-laying rate for all species, even within a given assay (Figure 1E-F and Figure S1C-D). However, on average, *D. sechellia* consistently laid a low number of eggs (~5-7 eggs/female/day), while the mean egg-laying frequency for the other species could vary substantially (from ~10 to ~30 eggs/female/day), which may be related to the provision of more or less appealing substrates in different assays.

Together, these results highlight the innate, social-context independent, and robust preference for *D. sechellia* for noni substrates, contrasting with the more context-dependent noni indifference or avoidance exhibited by the generalist drosophilids.

D. sechellia exhibits robust probing of the oviposition substrate

In the oviposition experiments with *D. sechellia* on agarose, we observed many small indentations in the substrate surface at the end of the assay (Figure 2A). Such indentations were only occasionally observed on the agarose substrates where *D. melanogaster* or *D. simulans* had laid eggs (data not shown). (The presence of indentations could not be easily assessed in the instant medium substrate due to its more granular texture). Furthermore, indentations were not observed on agarose exposed only to *D. sechellia* males (data not shown), suggesting that they are not the result of non-sexually dimorphic behaviors such as proboscis probing of the substrate.

The size and shape of the indentations led us to hypothesize that they correspond to the substrate marks formed by the ovipositor during "burrowing" – rhythmic digging of the ovipositor into the substrate prior to egg deposition – described in *D. melanogaster* (Cury and Axel, 2021). To test this hypothesis, we used high-speed imaging to visualize *D. sechellia* oviposition behavior at high spatio-temporal resolution (Bracker et al., 2019). Notably, although the total number of egg-laying events captured was low (precluding detailed quantitative analyses), we observed frequent interactions of the ovipositor with the substrate that did not culminate in egg deposition. These interactions ranged from simple substrate touching or scratching by the ovipositor (Video S1-2; see Methods for classification of behaviors) to more involved digging behaviors (Video S3). In two instances, such digging resulted in the formation of a visible indentation (Figure 2B and Video S4). However, post-hoc observation of the substrate revealed several other examples of indentations that were not captured during the recordings, possibly because they were not visible at the camera angle to the substrate. Conversely, we did not observe any other behaviors of the fly that could explain the formation of the indentations. Very similar ovipositor digging events were observed prior to egg laying (Video S5).

These observations support the hypothesis that indentations represent aborted oviposition events in *D. sechellia*. We reasoned that they provide a relevant complementary measure of oviposition behavior to the numbers of eggs laid. We therefore quantified the number of indentations and eggs for all three species in single-fly two-choice assays (Figure 2C). The total number of indentations and eggs were comparable for *D. sechellia* and *D. simulans* strains, and slightly lower than for *D. melanogaster* (Figure 2D). These observations indicate that, despite the much lower egg number than the generalist species, *D. sechellia* still robustly probes the oviposition substrate (see Discussion).

No evidence for contribution of visual cues to *D. sechellia*'s species-specific oviposition preference

To assess the sensory basis of *D. sechellia*'s strong preference for oviposition on noni substrates, we first tested the contribution of vision as the natural fruits (as well as the artificial substrates) have characteristic colors that might influence decisions on where to lay eggs. In single-fly two-choice assays run in the dark*, D. sechellia* retained very strong, species-specific, preference for laying on noni juice substrates, and no decrease in egg-laying rate was noted (Figure 3A). We extended this analysis to examine whether *D. sechellia* exhibits any unique color preference, reflecting its preference for ripe (dull white/yellow) over unripe (green) fruit. As the noni juice colored the oviposition substrate brown, we tested this possibility using a short-range trap assay (Prieto-Godino et al., 2017), in which identical odor traps – containing noni juice for *D. sechellia* or balsamic vinegar for *D. melanogaster* and *D. simulans* – were enclosed within green or white casings (Figure 3B). Because noni fruit may be found among green foliage, or on the white sandy substrate below *Morinda citrifolia* shrubs (Auer et al., 2021), we reasoned that color contrast may also play an important role in substrate preference, and therefore tested trap preference on a white or green background, as well as in the dark as a control. We observed no preference of any species to enter different colored traps (Figure 3B), suggesting that color is not a critical cue that *D. sechellia* uses to locate host fruit, at least at short-range.

D. sechellia and *D. simulans* prefer softer substrates compared to *D. melanogaster*

Substrate hardness is another potential factor influencing oviposition site preference that might have diverged between species. For example, the pest species *D. suzukii* – which oviposits in various ripe, but not rotten, fruits – exhibits stronger preference for stiffer substrates (that presumably resemble more closely ripe fruit) than *D. melanogaster* (Karageorgi et al., 2017). We compared the texture preference profile of *D. sechellia*, *D. simulans* and *D. melanogaster* through single-fly two-choice assays in which both substrates contain the same attractive chemical stimulus (either noni juice or apple cider vinegar) but different stiffness, obtained by pairing a soft agarose substrate (0.5%) with one ranging from 0.5-2% agarose. Although all three species preferred to oviposit on softer agarose, the discrimination threshold was different: *D. melanogaster* only exhibited such a preference when 0.5% was paired with 1.25% (or higher) agarose, while *D. simulans* and *D. sechellia* discriminated a more subtle difference in texture, preferring 0.5% agarose over 0.75% (Figure 3C-D). Textural discrimination ability of *D. sechellia* therefore cannot explain its ecological specialization. However it is consistent with our observations that on native fruits, *D. sechellia* lays its eggs on the softest part of the fruit: the pedicel cavity in intact fruits (or internal flesh in cut/broken fruits) (Figure 3E), which is much softer that the fruit skin, whose stiffness is approximately equivalent to 0.75% agarose (Figure 3F).

Olfactory pathways required for oviposition and oviposition preference

Having excluded the importance of vision for *D. sechellia*'s egg-laying preference (Figure 3A-B), we reasoned that olfactory cues are likely to be the first sensory signals that *D. sechellia* uses when assessing potential oviposition sites, as these do not require direct contact with the substrate. We first tested near-anosmic double mutant animals for the conserved olfactory co-receptors Orco (required for the function of all Ors) and Ir8a (required for the function of volatile acid-sensing Irs) (Abuin et al., 2011; Auer et al., 2020; Benton et al., 2006; Larsson et al., 2004). Strikingly, in single-fly assays – offering a choice of noni juice and apple cider vinegar in agarose – these flies laid essentially no eggs (Figure 4A-B). Moreover, no indentations were observed on the substrate at the end of the assay (Figure 4B). This lack of oviposition activity is not due to any overt locomotor defects, as these mutant animals display similar levels of activity as wild-type strains (Figure S3). It is also not due to any decrease in egg production, as their ovaries contain a similar number of mature eggs as in wild-type animals (Figure 4C). Importantly, equivalent *D. melanogaster* near-anosmic $Ir8a^{1}$,$Orco^{1}$ double-mutant animals lay many eggs (Figure S4). These observations provide evidence that olfactory input is critical for oviposition behavior in *D. sechellia*, but not *D. melanogaster*.

To test whether olfactory cues are sufficient to promote oviposition, we performed a no-choice oviposition assay in which flies were provided with an agarose/sucrose substrate with a non-accessible source of noni juice or, as control, water (Figure S5). No differences were observed in egg-laying rate of *D. sechellia* (or *D. melanogaster*) strains between these substrates (Figure S5). These results argue that noni odors alone are insufficient to promote egg-laying behavior, which presumably relies also upon gustatory input through multiple contact

chemosensory organs, as is the case in *D. melanogaster* (Chen et al., 2022; Chen and Amrein, 2017; Chen and Dahanukar, 2020).

To further understand the contribution of olfaction to *D. sechellia*'s oviposition behavior, we next tested the *Orco* and *Ir8a* co-receptor mutants singly: both showed a decreased egg-laying rate compared with wild-type controls, but only *Ir8a* mutants displayed reduced preference for noni juice (Figure 4A,4D). Similar phenotypes for these mutants were observed in two-choice assays with grape juice as a counter-stimulus (Figure S6). We went on to screen the phenotypes of mutants lacking genes encoding individual odor-specific "tuning" Ors and Irs (Auer et al., 2020), including Or22a and Or85c/b, which are required for long-range noni attraction (Auer et al., 2020). While these lines displayed variable reductions in egg-laying rate, none of them displayed significantly diminished oviposition preference for noni substrates (Figure 4A,4D and Figure S6). The maintenance of robust oviposition preference towards noni in most of these assays suggested that multiple, partially redundant olfactory signals contribute to oviposition behavior in *D. sechellia*.

Analysis of the effect of individual noni chemicals on oviposition

To characterize the noni chemicals promoting *D. sechellia*-specific oviposition, we tested several candidates in single-fly assays using the different species and three odor concentrations (0.05%, 0.1%, 0.5%) (Figure 5 and Figure S7). Confirming and extending previous group assays (Amlou et al., 1998; Higa and Fuyama, 1993; Matsuo et al., 2007), we found that hexanoic acid promoted very strong preference in *D. sechellia* at all concentrations tested and a higher egg-laying rate (compared to water-only control substrates) at least at intermediate concentrations (Figure 5A-B). *D. melanogaster* and *D. simulans* both display slight preference or indifference at lower concentrations of hexanoic acid and strong aversion at the highest concentration (Figure 5A-B). Octanoic acid has also been described to be an oviposition stimulant/attractant for *D. sechellia* in some (Amlou et al., 1998; Legal et al., 1999; Matsuo et al., 2007), though not all (Markow et al., 2009) reports. In our assays, this acid did not evoke strong oviposition preference of *D. sechellia* at lower concentrations; moreover, egg-laying was largely suppressed at the highest concentration, although the very few eggs laid were found on the octanoic acid substrate (Figure 5A-B). *D. melanogaster* and *D. simulans* found this odor generally aversive (Figure 5A).

We tested two other noni chemicals that are behaviorally-important for long-range noni location: methyl hexanoate (detected by Or22a) and *2*-heptanone (detected by Or85c/b) (Auer et al., 2020; Dekker et al., 2006; Ibba et al., 2010). Methyl hexanoate stimulated a slight enhancement of egg-laying at intermediate concentrations, but flies did not display a strong oviposition site preference for substrates containing this chemical (Figure 5A-B). Similarly, neither *D. melanogaster* nor *D. simulans* exhibited strong preference or aversion to methyl hexanoate-containing substrates. *2*-heptanone had little influence on oviposition-site selection of any species, and was highly toxic for flies at the highest (0.5%) concentration (Figure 5A and data not shown).

Lastly, we tested oviposition stimulants described in *D. melanogaster*, valencene and limonene, which are detected by Or19a neurons (Dweck et al., 2013). *D. sechellia* flies were indifferent to or avoided oviposition on substrates containing either of these chemicals, and egg-laying was suppressed at high

stimulus concentrations (Figure S7). Interpretation of these results must be tempered, however, with our inability to consistently reproduce behavioral effects of these compounds on oviposition reported in *D. melanogaster* (Figure S7) (Dweck et al., 2013), potentially reflecting observations that the behavioral function of this olfactory pathway is context dependent (Chin et al., 2018).

Together these experiments reveal the complex, concentration-dependent influence of different individual chemicals on drosophilid oviposition behavior, which might be due to their detection via both olfactory and gustatory systems. Nevertheless, the robust and *D. sechellia*-specific effect of hexanoic acid on oviposition led us to focus on determining the sensory mechanism by which this noni chemical is detected.

Olfactory detection of hexanoic acid by Ir75b promotes oviposition in *D. sechellia*

To define the sensory mechanisms of volatile hexanoic acid-mediated control of oviposition behavior, we tested our panel of *D. sechellia* olfactory receptor mutants. Loss of either Ir8a or Orco alone led to abolished or greatly diminished egg-laying on hexanoic acid substrates (Figure 6A), suggesting that both Ir and Or pathways contribute. Within the Ir repertoire, Ir75b was an excellent candidate as this receptor has evolved novel sensitivity to hexanoic acid in *D. sechellia* from the ancestral butyric acid sensitivity of the *D. melanogaster* and *D. simulans* orthologs (Prieto-Godino et al., 2017). Indeed, mutation of *Ir75b* in *D. sechellia* led to complete loss of egg-laying on hexanoic acid substrates, a phenotype confirmed in two independent alleles, and a transheterozygous *Ir75b* mutant combination (Figure 6A). Dissection of these flies' ovaries revealed a similar number of eggs as in controls (Figure 6B), suggesting the defect was in egg-laying not production. Consistent with this hypothesis, *DsecIr75b* mutant flies also produced no indentations in these assays (Figure 6C). By contrast, *D. sechellia* lacking the broadly-tuned acid-sensor, Ir64a (Ai et al., 2010), still oviposited, laying almost all eggs on hexanoic acid substrates (Figure 6A).

Amongst the Ors, all three mutants (*DsecOr22a*, *DsecOr35a* and *DsecOr85c/b*) displayed reduced egg-laying rate (Figure 6A). Of the subset of flies that did lay eggs, the *DsecOr35a* and *DsecOr85c/b* mutants maintained strong preference for oviposition on hexanoic acid substrates while *DsecOr22a* mutants no longer discriminated this substrate from the control medium (Figure 6A). Or22a neurons are generally considered to be ester sensors in drosophilids (de Bruyne et al., 2010), but weak Or22a-dependent hexanoic responses have been described in *D. sechellia* (Auer et al., 2020) as well as in *D. melanogaster* (Hallem and Carlson, 2006) (where it is the most sensitive hexanoic acid sensor of this species (Munch and Galizia, 2016)), suggesting that it might be a second olfactory pathway for this oviposition stimulant (see Discussion).

Evolution of Ir75b tuning can explain species-specific behavioral responses

Given the important role of Ir75b for hexanoic acid-stimulated oviposition of *D. sechellia*, we asked if the evolution of the tuning of this receptor might explain species-specific oviposition behavior. In an *Ir75b* mutant of *D. melanogaster* (Mika et al., 2021), we rescued Ir75b function through transgenic expression of either *D. sechellia* Ir75b or, as a control, *D. melanogaster* Ir75b. These flies were offered a

choice to lay eggs on substrates containing hexanoic acid or butyric acid, the preferential ligand of the receptors from *D. sechellia* and *D. melanogaster*, respectively (Prieto-Godino et al., 2017). Egg-laying rate was broadly comparable between all control mutant and both rescue lines (Figure 6D). This result indicates that a functional Ir75b pathway is not important for egg-laying in *D. melanogaster* – consistent with our observation that near-anosmic *D. melanogaster* lay many eggs – thereby permitting assessment of the contribution of the Ir75b pathway to oviposition preference. Rescue flies expressing *D. melanogaster* Ir75b displayed a substrate preference that was not significantly different from parental genotypes (Figure 6D). By contrast, expression of *D. sechellia* Ir75b was sufficient to shift oviposition preference from butyric acid to hexanoic acid substrates compared to controls (Figure 6D). These results are consistent with a causal contribution of *Ir75b* to the evolution of oviposition site preference during *D. sechellia*'s host specialization.

Discussion

Decisions on when and where to lay an egg are critical for all oviparous animals to maximize the chance of survival of their offspring, in particular those lacking parental care (Cury et al., 2019; Rudolf and Rodel, 2005). As such, these decisions are influenced by multiple biotic and abiotic factors in the environment. When species establish themselves within a new ecological niche, changes in these factors can exert selective pressures for novel or modified behavioral responses to sensory cues. It is also possible that chance evolution of traits can permit exploitation of a new niche. Either way, studying such differences between species can provide insight into the relative importance of the plethora of environmental signals, as well as the mechanisms by which nervous systems evolve, changing the relationship between these signals and behavioral outputs. *D. sechellia* offers an excellent opportunity to study oviposition behavioral adaptations, both because its specialist lifestyle likely constrains the set of pertinent sensory cues and because its low fecundity presumably renders the decision to lay an individual egg more important than for highly fertile species. Moreover, the phylogenetic proximity of *D. sechellia* to the generalists *D. melanogaster* and *D. simulans* facilitates comparative behavioral and genetic analyses that might enable reconstruction of the (still-unknown) evolutionary history of this species (Auer et al., 2021; Matsuo, 2008).

Studies in *D. melanogaster* have revealed that oviposition decisions are complex, multisensory-guided behaviors (Cury et al., 2019), and the ultimate choice of egg-laying site is often assay-dependent (e.g., (Schwartz et al., 2012; Yang et al., 2008)). Using several types of behavioral assays, we have confirmed the importance of noni for *D. sechellia* for egg-laying rate and site selection. The latter trait contrasts with the variable preferences of *D. melanogaster* and *D. simulans*. We also discovered an unappreciated feature of oviposition behavior of *D. sechellia*: extensive probing of the substrate surface, resulting in the formation of numerous indentations. These indentations are most likely equivalent to the "burrows" resulting from aborted oviposition events of *D. melanogaster* (Cury and Axel, 2021). One explanation for the high rate of indentations in *D. sechellia* is that females engage in the initiation of the oviposition routine unaware of the low number of eggs they carry. This seems unlikely, however, as it would represent a futile energetic investment for these animals, and *D. melanogaster* mutants that

lack eggs do not make indentations (R.A.-O. and R.B., unpublished). Moreover, high-resolution behavioral observations suggest that the presence of the egg in the ovipositor is integral to penetration of the substrate in *D. melanogaster* (Cury and Axel, 2021) and *D. sechellia*. We favor a hypothesis that extensive indentation formation by *D. sechellia* reflects greater choosiness of this species to deposit eggs only after the female has ascertained to have found the optimal substrate available.

To account for the species-specificity of *D. sechellia* substrate selection, we have been able to exclude several sources of sensory information. Visual input is unimportant (at least at short-range), and *D. sechellia* does not exhibit obvious changes in preference for colors that mimic the choice this species makes in nature. While *D. sechellia* prefers to lay eggs within the softest part of the fruit, and within softer agar, there is no difference in texture preference compared to *D. simulans*, suggesting that this trait is not a key facet of host adaptation, contrasting with the fresh-fruit feeder *D. suzukii* (Karageorgi et al., 2017). Finally, although communal egg-laying is widespread in many invertebrates and vertebrates (Doody et al., 2009), we do not find evidence that this phenomenon contributes to noni preference; if anything, isolated flies lay more eggs with stricter noni preference than those in groups.

Our genetic analysis indicates that olfactory input is essential for egg-laying in *D. sechellia*, as near-anosmic flies fail to lay eggs even in the presence of noni despite normal egg production. Conversely, exposure of flies to noni odors alone, without allowing them to have gustatory sensation of noni juice, does not enhance oviposition rate. Together, these observations suggest that both olfactory and gustatory inputs are important: without olfaction, gustatory signals are insufficient for promoting oviposition, but olfactory signals without gustatory inputs are similarly ineffective. A future priority is to determine how *D. sechellia* detects noni via gustation and if, as in the olfactory system, any gustatory pathways differ between drosophilids.

While loss of the vast majority of olfactory input prevents egg-laying on noni in *D. sechellia*, we found substantial redundancy, as loss of any single tuning Or or Ir (or even Orco) did not strongly diminish noni preference. This observation indicates that multiple distinct odors, acting via several different olfactory receptors, must contribute to short-range behavioral decisions. By simplifying the noni odorscape in our oviposition assays we demonstrate the unique oviposition-promoting role of hexanoic acid and, importantly, define Ir75b and its obligate co-receptor Ir8a, as the cognate sensory receptor. Although hexanoic acid might also be detected by gustatory neurons (based upon studies in *D. melanogaster* (Ahn et al., 2017; Sanchez-Alcaniz et al., 2018; Tauber et al., 2017)), the selective expression of Ir75b and Ir8a in the antenna argues that this is an odor-guided behavior. Moreover, the demonstration that Ir75b is required for this behavior provides an explanation for the evolutionary changes described in this sensory pathway: while *D. melanogaster* (and *D. simulans*) Ir75b are tuned primarily to butyric acid, the *D. sechellia* receptor has evolved novel sensitivity to hexanoic acid, through amino acid substitutions within the ligand-binding domain (Prieto-Godino et al., 2017; Prieto-Godino et al., 2021). In addition, *D. sechellia* exhibits a 2-3-fold increase in number of sensory neurons expressing Ir75b, resulting in increased sensory pooling onto partner interneurons in the brain (Prieto-Godino et al., 2017). Importantly, replacement of *D. melanogaster* Ir75b with the *D. sechellia* receptor induces a small but significant shift in oviposition site preference,

indicating that receptor tuning changes are sufficient alone to confer more *D. sechellia*-like behavior on *D. melanogaster*.

Together with previous work (Auer et al., 2020), our studies of noni-dependent odor-guided behaviors in *D. sechellia* reveal similarities and differences in the coding and evolution of olfactory pathways mediating long-range and short-range detection (Figure 6E). The high redundancy in short-range olfactory signals contrasts markedly with olfactory contributions to long-range noni host-seeking, where loss of single tuning receptors essentially abolished the ability of flies to locate the odor source (Auer et al., 2020). This difference might reflect the complexity of the noni odor blend at different spatial scales: there are likely to be fewer, highly-volatile, compounds reaching behaviorally-relevant concentrations at a distance compared to odors present at short-range (Auer et al., 2020). Concordantly, the behaviorally most-important receptors for long-range (Or22a and Or85c/b) and short-range (Ir75b) noni detection, display differences in sensitivity: Ir75b neurons require several orders of magnitude higher odor stimulus concentration to evoke the same level of neuronal firing as Or22a or Or85c/b neurons (Auer et al., 2020). The segregation of behavioral function of the pathways is, however, not absolute: the long-range olfactory detectors, notably Or22a, also appear to contribute to oviposition behaviors on hexanoic acid substrates, though further genetic analysis will be necessary in future studies.

One striking commonality of all three of these OSN populations is their expansion in *D. sechellia*, although the functional significance of this phenotype is unknown. By contrast, the nature of odor specificity evolution of these pathways is different: Or85c/b neuron sensitivity to *2*-heptanone is unchanged across the drosophilid species (Auer et al., 2020), *D. sechellia* Or22a has enhanced sensitivity to methyl hexanoate compared to the orthologous receptor in *D. melanogaster* (but not in *D. simulans*) (Auer et al., 2020; Dekker et al., 2006), while Ir75b has acquired new sensitivity to hexanoic acid specifically in *D. sechellia* (Prieto-Godino et al., 2017; Prieto-Godino et al., 2021). In addition, methyl hexanoate and *2*-heptanone, but not hexanoic acid, are emitted by a wide range of fruits (Dweck et al., 2018). A model to unify these observations is that the methyl hexanoate and *2*-heptanone act as “habitat odor cues” (Webster and Carde, 2017), attracting *D. sechellia* (but also other species) in the vicinity of noni, while hexanoic acid is a specific “host odor cue” (Webster and Carde, 2017) that, through Ir75b, evokes short-range behaviors only in *D. sechellia*.

In this context, the ecological role of the Ir75b sensory pathway in *D. melanogaster* is unclear, although optogenetic activation experiments have provided evidence for a role in positional attraction and oviposition preference (Prieto-Godino et al., 2017; Wu et al., 2022). Several other olfactory pathways have been implicated in oviposition promotion in *D. melanogaster* (Cury et al., 2019; Dweck et al., 2015; Lin et al., 2015), including Or19a, which detects the citrus odors valencene and limonene (Dweck et al., 2013). Interestingly, *D. sechellia* Or19a neurons appear to have lost sensitivity to these odors (Dweck et al., 2013), which are not reliably detected in noni fruit (Auer et al., 2020). Adaptation of this species might therefore have involved sensory gain or loss in several olfactory pathways to match the pertinent chemical signals in its niche.

Finally, beyond the issues mentioned above, a key future question – in any species – is how olfactory input controls oviposition behavior. Recent studies in *D. melanogaster* have defined circuitry linking mating and egg-laying (Wang et al., 2020); notably, the activity of some of the component neuron populations (i.e.,

ovoENs and ovoINs in the central brain) are activated or inhibited by gustatory and mechanosensory input (Wang et al., 2020). It is possible that olfactory sensory pathways (e.g., downstream of the Ir75b sensory input in *D. sechellia*) impinge on this circuitry (Nojima et al., 2021). Alternatively, olfactory signals might have only an indirect influence, for example, by modulating gustatory inputs to this egg-laying circuitry. Further exploration of the neural basis of oviposition in *D. sechellia* should yield insights into the mechanistic basis of the adaptations of this critical behavior to this species' unique lifestyle.

Methods

Drosophila strains

Drosophila stocks were cultured in a 25ºC incubator under a 12 h light:12 h dark cycle on a standard wheat flour–yeast–fruit juice food. Unless noted otherwise, *D. sechellia* culture vials were supplemented with noni paste, consisting of a few grams of Formula 4-24® instant *Drosophila* medium, blue (Carolina Biological Supply) and noni juice (Raab Vitalfood Bio). All strains used in this study are listed in Table S1 and sources of chemicals are listed in Table S2.

Oviposition assays

We maximized flies' egg-laying capacity by following the protocol of (Gou et al., 2016): prior to the experiments, ~50 1-2 day-old females and males were collected and placed in new fly food tubes enriched with dry yeast (*D. melanogaster* and *D. simulans*) or with dry yeast and noni paste (*D. sechellia*) for 5 days. At this point the food was typically full of crawling larvae, inducing females to retain eggs until transferred to the assay chamber. Unless otherwise stated, oviposition assays were performed at 25ºC, 60% relative humidity and a 12 h light:12 h dark cycle (starting assays in the early afternoon), in either an incubator or behavior room for 22-72 h (depending upon the assay, see below).

Previous work suggested that the low egg-laying rate of *D. sechellia* is due to alterations in dopamine metabolism – which contributes, at least indirectly, to fertility in *D. melanogaster* (Gruntenko and Rauschenbach, 2008; Neckameyer, 1996) – and could be partially compensated by supplementation of food with the dopamine precursor 3,4-dihydroxyphenylalanine (L-DOPA), which is found in noni fruit (Lavista-Llanos et al., 2014). To increase *D. sechellia*'s oviposition rate, we cultivated flies' for five days on noni food supplemented with L-DOPA (1 mg/ml), but did not observe increased egg-laying in either group or single-fly assays compared to control flies given noni paste (Figure S8). Treatment with α-methyl-DOPA (0.4 mM), a non-hydrolysable L-DOPA analog that acts as a competitive inhibitor of DOPA decarboxylase (which converts L-DOPA to dopamine) reduced egg-laying in the single-fly assay but not the group assay (Figure S8). Our inability to fully reproduce the reported effects on oviposition (Lavista-Llanos et al., 2014) – we did not examine other traits investigated in that study, such as egg size and germline cyst apoptosis – might be due to experimental differences in our assays (e.g., use of noni fruit in (Lavista-Llanos et al., 2014)) or the use of more fertile *D. sechellia* strains.

Fruit multiple-choice assay: ripe fruits (apple, banana, grape (all from Migros); noni from *M. citrifolia* plants (University of Zurich Botanical Gardens and Canarius) grown in a greenhouse) were cut into thick (1-2 cm) slices. Fruit pieces were placed in a 5 cm Petri dish (Falcon) inside a plastic chamber (15 cm length × 14 cm width × 5 cm height; Migros). For all species, 50 females and 20 males were anesthetized on ice and introduced into the chamber, which was covered with a fabric gauze. The chambers were placed in a behavioral room in constant darkness for 72 h, after which the number of eggs on each fruit piece was quantified.

Group two-choice assay: agarose (Promega) substrates were prepared as follows: a 1% agarose solution was prepared and let to cool down until it was possible to hold the glass Erlenmeyer flask with bare hands. The 1% agarose preparation was added to juice/odor solution in a 2:1 ratio, resulting in a final concentration of 0.67% agarose. The final mixture was poured up to a 0.5 cm depth into 3 cm Petri dishes (Falcon). Agarose plates were conserved at 4ºC for a maximum of 3 days. Instant medium substrates were prepared by diluting 12 g of instant medium in 100 ml of noni juice (or apple cider vinegar) creating a semi-solid consistency. The instant medium was added into a 3 cm Petri dish until fully covering the bottom of the plate. Instant medium mixes were conserved at 4ºC and used within two weeks. Two Petri dishes containing the desired combination of substrates were placed into the same chamber used for the fruit multiple-choice assay. 10 females and 8-10 males (*D. melanogaster* and *D. simulans*) or 20 females and 15-20 males (*D. sechellia*) were anesthetized with CO_2 and introduced into the chamber for three consecutive days. Due to *D. sechellia*'s low fecundity, through preliminary experiments we considered that the number of eggs laid by 20 *D. sechellia* female flies was sufficient to observe a clear behavioral preference between two conditions. Petri dishes were exchanged with fresh ones every 24 h by quickly lifting the mesh cover. The number of eggs laid per substrate was counted independently on each plate.

Group no-choice odor cue assay: as for the "*Group two-choice assay*" except using a single 3 cm diameter Petri dish containing 0.67% agarose and 150 mM sucrose (Sigma) onto which a non-accessible container covered with a fabric gauze and a perforated cap of a 15 ml Falcon tube (diameter 1 cm, height 2 cm; Techno Plastic Products AG) into which 300 μl of H_2O or noni juice was placed.

Single-fly two-choice assay: 30-cell single-fly chambers were designed and manufactured by Formoplast S.A. following published blueprints (Gou et al., 2016), but using poly(methyl methacrylate) instead of acrylic, and adding a small handle to the top door. Flies were anesthetized in CO_2 and placed in individual egg-laying chambers. Animals were allowed a 30 min period for recovery from anesthetization and acclimation to the chamber, during which time the oviposition substrate was prepared as described above. For single-odor assays, instant medium was dissolved in the desired odor solution diluted in water or juice. The concentration range of odors was defined from preliminary tests and previous studies (Amlou et al., 1998); specified concentrations represent those before adding the instant medium. For agarose substrates, 1 ml of agarose solution (containing the desired stimulus) was added to the bottom slot on one side of the oviposition chamber, which underlies 5 separate cells. For instant medium substrates, the paste was applied to the slot with a spatula. The fly loading slot of the single fly multi-chamber was placed on top of the bottom slot and flies accessed the instant medium. Eggs

were scored on each substrate after 22 h. Preliminary tests of oviposition preferences on different substrates, which informed subsequent experimental design, are shown in Figure S2.

Texture assays: single-fly oviposition assays were performed as described above, but preparing substrates with different final concentrations of agarose.

For all assays, eggs were scored manually under a binocular microscope. The oviposition preference index was calculated as: (number of eggs in substrate X - number of eggs in substrate Y)/total number of eggs only when the number of eggs laid was $\geq$2. Indentations were scored as a small break/holes in the substrate surface; in some cases, the presence of multiple indentations in the same region of the substrate likely led to underestimation of the number of independent indentations.

High-speed imaging of oviposition behavior

D. sechellia flies were cultured on standard cornmeal media. Mated *D. sechellia* females (aged 4-10 day-old in standard cornmeal food vials with or without supplementation with noni paste), were placed in empty vials with hydrated tissue for 14-20 h before the day of the experiment to force egg retention. A group of 2-3 individuals was introduced into a cubical oviposition filming chamber as described (Bracker et al., 2019). A trough on one side of the chamber was filled with a noni juice-agar substrate (1:3 or 1:6 v/v), with a wet pad at its base to limit sagging caused by desiccation. Flies were filmed with an external high-speed camera (JAI RMC-6740 GE, IMACO as detailed in (Bracker et al., 2019) using the custom FlyBehavior software (Bracker et al., 2019), focused on the surface of the agar column, which provided a 1 $\times$ 3 mm oviposition substrate. Recording of the group was performed for several separate 2 h-sessions over the course of one day (from late morning to mid-evening). The following specific behaviors were observed qualitatively by visual inspection of the resulting videos: *Touching* (Video S1) - the ovipositor simply touches the substrate; *Scratching* (Video S2) - the ovipositor brushes against the substrate, giving the impression of gentle scratching; *Digging* (Video S3) - the ovipositor burrows into the substrate surface; *Indentation formation* (Video S4) - the fly digs with its ovipositor at a particular site on the substrate leaving a minor depression (indentation) but no egg; occasionally, we observed that a fly returns to an indentation for egg-laying; *Egg laying* (Video S5) - the fly starts digging into the surface and lays an egg at this site. In many videos, we also observed flies exuding a liquid droplet, possibly from their anal plates (e.g., Video S1, example 4, left-hand animal); this action does not appear to be related to oviposition as it was observed also in virgin female and male flies (V.R. and N.G., unpublished). Video sequences were cropped and assembled in Fiji (Schindelin et al., 2012).

Color preference assays

Color preference was assessed by adapting an olfactory trap assay (Prieto-Godino et al., 2017), in which the arena contained two traps filled with 300 μl of the same attractive odor – noni juice (*D. sechellia*) and balsamic vinegar (Antica Modena) (*D. melanogaster* and *D. simulans*) – masked with different visual cues. To simulate

fruit at a ripe or unripe stage, a trap was covered with a green or white matte table-tennis ball (Lakikey; 40 mm diameter) with two opposing holes cut into it: one large hole on the bottom to insert the trap vial, and a smaller hole on top to allow the flies to enter the trap through a 200 μl pipette tip that was flush with the ball surface. Arenas were lined with either green or white paper (to provide different contrast for the green and white traps), and assays were performed in the light as well as under complete darkness in a behavior room (25ºC and 60% relative humidity). Prior to the assay, flies were kept on standard media without noni supplement for 24 h. Twenty-five fed and mated 3-5 day-old females were introduced into each arena after brief ice anesthesia. The number of flies in each trap (as well as untrapped animals) was counted after 24 h; replicates where >25% of flies died within the experimental period were discarded. The preference index was calculated as: number of flies in white trap - number of flies in green trap/number living flies (trapped and untrapped).

Locomotor activity monitoring

Activity was measured for 5-7 day old mated females at 25ºC under a 12 h light: 12 h dark cycle, staged as for oviposition assays to ensure mating status, in the *Drosophila* activity monitor (DAM) system (Chiu et al., 2010) in incubators with continuous monitoring of light and temperature conditions (TriTech Research DT2-CIRC-TK). In brief, this system uses an infrared beam that bisects a 5 mm glass tube, in which the fly is housed, to record activity as the number of beam crosses per minute. Each tube is plugged with a 5% sucrose/2% agar (w/v) food source at one end and cotton wool at the other. Each DAM was used to record the activity of up to 32 flies simultaneously, and multiple monitors were contained in a single incubator. For all genotypes, we recorded flies over at least 2 technical replicates. Mean activity of an animal was calculated as the average number of beam crosses per minute over three complete days of recording.

Ovary dissection and egg quantification

Females, prepared as for the oviposition assays, were anesthetized with CO_2 and their ovaries dissected with forceps in phosphate buffered saline, using a surgical needle to separate the ovarioles. Mature eggs present in each ovary were counted under a binocular microscope.

Statistical analyses

Oviposition preference indices were calculated compared to the null hypothesis (i.e., preference index = 0) for each strain using a Wilcoxon test with Bonferroni correction for multiple comparisons. Statistical differences across the number of eggs laid per fly per day for multiple comparisons were calculated applying Kruskal-Wallis rank sum test with Nemenyi post-hoc test. For two-sample comparisons, a two-sample t-test was used. The reference strain for multiple or two-sample comparisons is indicated in the figure legends. Error bars show SEM. All statistical values reported on the figures are as follows: NS (not significant) $P > 0.05$; * $P < 0.05$; ** $P < 0.01$; *** $P < 0.001$.

Author contributions

R.A.-O. and R.B. conceived the project. R.A.-O performed all experiments except for those in Figures 3B, S3 and 6D, which were performed by M.P.S., and in Figure 2B and Videos S1-S5, which were performed by V.R., supervised by N.G. T.O.A. generated *D. sechellia* lines and contributed to the establishment of the assays in Figure 1B and 3E. All authors contributed to experimental design and interpretation of results. R.B. and R.A.-O. wrote the manuscript with contributions from all authors. All authors read and approved the final manuscript.

Acknowledgements

We thank Chung-Hui Yang for valuable assistance in establishing the single-fly oviposition assay, Stefano Ceolin for advice on video recordings, René Gerber (University of Zurich Botanical Gardens) for a gift of *M. citrifolia*, Blaise Tissot-Dit-Sanfin for maintenance of *M. citrifolia*, Steeve Cruchet and Liliane Abuin for technical support, and members of the Benton laboratory for discussions and comments on the manuscript. V.R. was supported by the Graduate School of Systemic Neurosciences and by a Deutsche Forschungsgemeinschaft grant (GO 2495/9-1) to N.G. T.O.A. was supported by a Human Frontier Science Program Long-Term Fellowship (LT000461/2015-L) and a Swiss National Science Foundation Ambizione Grant (PZ00P3 185743). Research in R.B.'s laboratory is supported by the University of Lausanne, an ERC Advanced Grant (833548) and the Swiss National Science Foundation.

Availability of data and materials

All materials and data supporting the findings of this study are available from the corresponding author on request.

Competing interests

The authors declare that they have no competing interests.

Figure Legends

Figure 1. *D. sechellia* displays robust, species-specific preference for oviposition on noni substrates.

(A) Phylogeny of the drosophilid species studied in this work. Mya, million years ago.

(B) Fruit multiple-choice oviposition preference assay. Left: image of the assay with noni, banana, apple and grape (clockwise from top left) in the arena. Right: quantification of the number of eggs laid per day (n = 3 assays/species, using 50 flies each for a duration of 3 days). Strains used: *D. melanogaster* Canton S (CS), *D. simulans* 14021-0251.004 (04) and *D. sechellia* 14021-0248.28 (28); see Table S1 for details of all strains used in this work. Mean values ± SEM are shown.

(C) Group oviposition preference assays for noni juice versus grape juice in 0.67% agarose using two strains each of wild-type *D. melanogaster* (*Dmel*: CS and Oregon R (OR)), *D. simulans* (*Dsim*: 04 and 14021-0251.196 (196)) and *D. sechellia* (*Dsec*: 14021-0248.07 (07) and 28). Left: box plots of oviposition preference index in these assays. In these and all other box plots, the middle line represents the median, and the first and third quartiles correspond to the lower and upper hinges, respectively. Individual data points are overlaid on the box-plots, scaled by the total number of eggs laid in an assay (key at top right of the plot); data beyond the whiskers are considered outliers. For these and other box plots statistical differences from 0 (no preference) are indicated: *** $P < 0.001$; ** $P < 0.01$; * $P < 0.05$; NS (not significant) $P > 0.05$ (Wilcoxon test with Bonferroni correction for multiple comparisons); n = 12 (representing 4 group assays, each scored on 3 successive days with fresh oviposition plates each day). Right: bar plots of egg-laying rate per fly per day in these assays. Mean values ± SEM are shown. Statistically-significant differences from the *D. melanogaster* CS strain are indicated: *** $P < 0.001$; ** $P < 0.01$; * $P < 0.05$; NS $P > 0.05$ (Kruskal-Wallis rank sum test with Nemenyi post-hoc test).

(D) Group oviposition preference assays, as in (C), for noni juice versus apple cider vinegar (n = 12, as in (C)).

(E) Single-fly oviposition preference assays for noni juice versus grape juice in agarose for the same strains as in (C). Top: total number of eggs laid in each substrate by each female. Bottom left: oviposition preference index. Statistical differences from 0 (no preference) are indicated as in (C). n = 30-60 flies across 1-2 technical replicates. Bottom right: egg-laying rate. Mean values ± SEM are shown; statistical analysis as in (C).

(F) Single-fly oviposition preference assays, as in (E), for noni juice versus apple cider vinegar. n = 30-90 flies across 1-3 technical replicates.

Figure 2. *D. sechellia* makes frequent substrate indentations during oviposition.

(A) Photo of the noni juice/agarose substrate at the end of a single-fly oviposition assay with *D. sechellia* illustrating the many indentations in the agarose surface and rare eggs.

(B) Still images from high-speed video sequences of *D. sechellia* oviposition behavior illustrating a digging event that does not lead to egg deposition, which results in the formation of a visible indentation on the substrate (left), and digging event that culminates in egg deposition (right). The full videos are provided in Videos S4 and S5.

(C) Quantification of the number of eggs and indentations produced by different species and strain on different substrates in 19-28 single-fly two-choice oviposition assays with noni juice and apple cider vinegar (ACV).
(D) Rate of summed egg-laying and indentations events observed in the experiments in (C). Mean values ± SEM are shown. Statistically-significant differences from the CS strain are indicated: ** $P < 0.01$; * $P < 0.05$; NS $P > 0.05$ (Kruskal-Wallis rank sum test with Nemenyi post-hoc test).

Figure 3. Analysis of visual and textural contributions to *D. sechellia*'s noni preference.
(A) Single-fly oviposition preference assays in the dark for noni juice versus apple cider vinegar in agarose (fly strains as in Figure 1C). Left: oviposition preference index. Statistical differences from 0 (no preference) are indicated: *** $P < 0.001$; ** $P < 0.01$; NS $P > 0.05$ (Wilcoxon test with Bonferroni correction for multiple comparisons); n = 60 flies across 2 technical replicates. Right: egg-laying rate in these assays. Mean values ± SEM are shown (Kruskal-Wallis rank sum test with Nemenyi post-hoc test).
(B) Group color preference assays in which flies are given a choice to enter two traps containing the same chemical stimulus (balsamic vinegar (*D. melanogaster* and *D. simulans*) or noni juice (*D. sechellia*)) and distinguished only by colored casings with different light and background conditions. Statistical differences from 0 (no preference) are indicated: * $P < 0.05$; NS $P > 0.05$ (Wilcoxon test with Bonferroni correction for multiple comparisons); n = 12-24 assays across at least 2 technical replicates.
(C) Single-fly oviposition preference assays testing between the indicate agarose concentrations on the top and 0.5% agarose in the counter-substrate. Both substrates contain apple cider vinegar (*D. melanogaster* and *D. simulans*) or noni juice (*D. sechellia*). Statistical differences from 0 (no preference) are indicated: *** $P < 0.001$; **P < 0.01 * $P < 0.05$; NS $P > 0.05$ (Wilcoxon test with Bonferroni correction for multiple comparisons); n = 30-60 flies across 1-2 technical replicates.
(D) Graph recapitulating data from (C). Dots represent the mean values and the bars represent ±SEM. The statistical values represent the most similar strains of the different species: *** $P < 0.001$; ** $P < 0.01$; NS $P > 0.05$ (Kruskal-Wallis rank sum test with Nemenyi post-hoc test).
(E) Close-up image of noni fruit illustrating the concentration of *D. sechellia* eggs in the pedicel cavity (where the fruit was attached to the stem) and in the flesh exposed by a skin break. Flies were placed in a group assay oviposition chamber containing whole noni fruits during 72 h.
(F) Graph of stiffness of substrates of different agarose concentrations (in noni juice), overlaid with the stiffness ranges of unripe and ripe noni fruits (illustrated in the photos) within the pedicel cavity or on the external skin. Measurements were made using Semmes-Weinstein Monofilaments following the procedure described in (Sanchez-Alcaniz et al., 2017).

Figure 4. Olfactory pathways required for *D. sechellia* oviposition.
(A) Single-fly oviposition preference assays for noni juice versus apple cider vinegar in agarose for the indicated genotypes (Table S1). The plots show the number of eggs laid per fly (n = 30-60 flies across 1-2 technical replicates). *Dsecir75b*$^{1/2}$ is a transheterozygous mutant combination.
(B) Quantification of the number of eggs and indentations on different substrates

of the indicated genotypes (n = 30 (*Dsec* 07) and 58 (*DsecIr8a^{RFP},Orco^{1}*) across 1-2 technical replicates).
(C) Mean number of mature eggs per fly (i.e., a pair of ovaries) of the indicated genotypes. Mean values ± SEM are shown. NS $P > 0.05$ (two-sample t-test); n = 9-10 flies.
(D) Left: oviposition preference index for the assays shown in (A). Statistical differences from 0 (no preference) are indicated: *** $P < 0.001$; ** $P < 0.01$; * $P < 0.05$; NS $P > 0.05$ (Wilcoxon test with Bonferroni correction for multiple comparisons); n = 30-60 flies across 1-2 technical replicates. *Dsec* 07 and *DsecIr8a^{RFP}* show statistical difference *(*$P = 0.0328$; Wilcoxon test with Bonferroni adjustment). Right: egg-laying rate. Mean values ± SEM are shown. Statistically-significant differences from the *Dsec* 07 strain are indicated: *** $P < 0.001$; * $P < 0.05$; NS $P > 0.05$ (Kruskal-Wallis rank sum test with Nemenyi post-hoc test). The non-significant PI for the *DsecIr8a^{RFP},Orco^{1}* double mutant was calculated from the 4/60 animals that laid >2 eggs.

Figure 5. Analysis of the effect of individual noni chemicals on oviposition.
(A) Single-fly oviposition assays of the indicated strains testing different odors and concentrations in an instant medium substrate. Oviposition preference index. Statistical differences from 0 (no preference) are indicated: *** $P < 0.001$; ** $P < 0.01$; * $P < 0.05$; NS $P > 0.05$ (Wilcoxon test with Bonferroni correction for multiple comparisons); n = 30-60 flies across 1-2 technical replicates. For *Dsec* 07 assays with *2*-heptanone (indicated with a white rectangle), the low number of flies laying eggs prevented calculation of a preference index.
(B) Egg-laying rate of the assays in (A). Mean values ± SEM are shown. Statistical comparisons of the effect of odors on egg-laying rate were performed across strains: *** $P < 0.001$; ** $P < 0.01$; * $P < 0.05$; NS $P > 0.05$ (Kruskal-Wallis rank sum test with Nemenyi post-hoc test).

Figure 6. *D. sechellia* Ir75b is required for hexanoic acid responses and sufficient to shift oviposition preference in *D. melanogaster*.
(A) Single-fly oviposition assays testing H_2O versus 0.1% hexanoic acid and H_2O versus 0.5% hexanoic acid in instant medium. Left: oviposition preference indices are only shown for genotypes that laid 2 or more eggs in these assays. Statistical differences from 0 (no preference) are indicated: *** $P < 0.001$; ** $P < 0.01$; NS $P > 0.05$ (Wilcoxon test with Bonferroni correction for multiple comparisons); n = 30-83 flies, 1-3 assays. Right: egg-laying rate. Mean values ± SEM are shown. *** $P < 0.001$; * $P < 0.05$; NS $P > 0.05$ (Kruskal-Wallis rank sum test with Nemenyi post-hoc test).
(B) Average number of mature eggs per pair of ovaries per fly. Mean values ± SEM are shown. NS $P > 0.05$ (two-sample t-test); n = 9 flies.
(C) Quantification of the number of eggs and indentations on different substrates of the indicated genotypes (n = 30 flies in one technical replicate).
(D) Single-fly oviposition assays testing 0.05% hexanoic acid versus 0.05% butyric acid of *D. melanogaster Ir75b* mutant and rescue genotypes. Left: egg-laying rate for *Ir75b-Gal4* control (*w;Ir75b-Gal4/+;Ir75b^{DsRed}*), *UAS-DmelIr75b* control (*w;UAS-DmelIr75b/+;Ir75b^{DsRed}*), *UAS-DsecIr75b* control (*w;UAS-DsecIr75b/+;Ir75b^{DsRed}*), *DmelIr75b* rescue (*w;Ir75b-Gal4/UAS-DmelIr75b;Ir75b^{DsRed}*), and *DsecIr75b* rescue (*w;Ir75b-Gal4/UAS-DsecIr75b;Ir75b^{DsRed}*). *DmelIr75b* and *DsecIr75b* rescue strains showed a significant reduction in the number of eggs compared to

DmelIr75b-Gal4 control. Right: oviposition preference indices for these genotypes. No significant differences were detected between *Ir75b-Gal4* control, *UAS-DmelIr75b* control and *DmelIr75b* rescue strains. The *DsecIr75b* rescue strain showed a significant shift in preference toward 0.05% hexanoic acid compared to both *DmelIr75b-Gal4* and *UAS-DsecIr75b* controls. *** $P < 0.001$; ** $P < 0.01$; $P < 0.05$ (Wilcoxon tests with Bonferroni correction for multiple comparisons). N = 28-55 flies per genotype measured across at least 2 technical replicates.
(E) Schematic summarizing the contributions of different olfactory pathways to niche specialization in *D. sechellia*.

Supplementary Data

Figure S1. Oviposition preference assays using instant medium-based substrates.
(A) Group oviposition preference assays for noni juice versus grape juice in instant medium 10g/100mL, using the same strains as in Figure 1C. Left: box plots of oviposition preference index. Statistical differences from 0 (no preference) are indicated (as in Figure 1C); n = 12 (representing 4 assays of 40-80 flies, each scored on 3 successive days with fresh oviposition plates each day). Right: bar plots of egg-laying rate. Statistically-significant differences from the *D. melanogaster* CS strain are indicated (as in Figure 1C).
(B) Group oviposition preference assay, as in (A) for noni juice versus apple cider vinegar. n = 12 (representing 4 assays of 40-80 flies, each scored on 3 successive days with fresh oviposition plates each day).
(C) Single-fly oviposition preference assay for noni juice versus grape juice in instant medium for the same strains as in (A). Top: total number of eggs laid in each substrate by each female. Bottom left: oviposition preference index. Bottom right: egg-laying rate. Mean values ± SEM are shown.
(D) Single-fly oviposition preference assays, as in (C), for noni juice versus apple cider vinegar. n = 43-60 flies across 2 technical replicates.

Figure S2. Establishment of single-fly oviposition assays.
(A) Single-fly oviposition preference assays testing H_2O versus either 150 mM sucrose or noni juice in agarose. Left: oviposition preference index. Statistical differences from 0 (no preference) are indicated: *** $P < 0.001$; * $P < 0.05$; NS $P > 0.05$ (Wilcoxon test with Bonferroni correction for multiple comparisons); n = 30-45 across 1-2 technical replicates. Preference of *D. melanogaster* for the plain the plain substrate resembles previous observations (Gou et al., 2016). To the right of each plot are bar plots of egg-laying rate. Mean values ± SEM are shown. *** $P < 0.001$ (two-sample t-test).
(B) Single-fly oviposition preference assays, as in (A), in instant medium. n = 30-45 across 1-2 technical replicates. The higher egg-laying rate of both species on instant medium compared to agarose substrates might reflect differences in texture and/or humidity; to avoid interfering with juices attraction, the vast majority of experiments were performed using agarose. Instant medium substrates were used in most single-odor experiments as egg-laying rate was very low on agarose substrates.

Figure S3. Locomotor activity levels of olfactory receptor mutants.
Mean activity of *D. sechellia* mutant flies represented by the number of beam

crosses per minute per fly recorded over three complete light-dark cycles. Statistical differences from *Dsec* 07 (the genetic background strain for all mutants) are indicated: * p < 0.05; NS *P* > 0.05 (Wilcoxon test with Bonferroni correction for multiple comparisons); n = 23-46 flies per genotype across at least 2 technical replicates.

Figure S4. Near-anosmic *D. melanogaster* do not display defects in oviposition behavior.
(A) Single-fly oviposition preference assays for apple cider vinegar versus noni juice in agarose for the indicated genotypes. The plots show the number of eggs laid per fly (n = 26-29 flies across 1 technical replicate).
(B) Left: oviposition preference index for the assays shown in (A). Statistical differences from 0 (no preference) are indicated: *** *P* < 0.001 (Wilcoxon test with Bonferroni correction for multiple comparisons). *Dmel* CS and *DmelIr8a^{1}/Orco^{1}* show statistical difference (*P* = 6.334×10^{-5}; Wilcoxon test with Bonferroni adjustment). Right: egg-laying rate. Mean values ± SEM are shown. Statistically-significant differences from the *D. melanogaster* CS strain are indicated: * *P* < 0.05 (Kruskal-Wallis rank sum test with Nemenyi post-hoc test). As the *Ir8a^{1};Orco^{1}* mutant is not in the CS genetic background, it is unclear if the slight increase in preference for ACV and in egg-laying rate in the mutant strain reflects a role for these olfactory co-receptors or an effect of genetic background.

Figure S5. Olfactory cues are not sufficient for noni oviposition preference.
Left: schematic of the one-choice group oviposition assay in the presence of a non-accessible noni juice source (or H_2O control). Agarose plates supplemented with 150 mM sucrose were provided as oviposition substrates. Right: egg-laying rate. Mean values ± SEM are shown. NS *P* > 0.05 (Kruskal-Wallis rank sum test with Nemenyi post-hoc test); n = 12 (representing 4 assays, each scored on 3 successive days with fresh oviposition plates each day).

Figure S6. Olfactory pathways required for *D. sechellia* oviposition.
(A) Single-fly oviposition preference assays for noni juice versus grape juice in agarose for the indicated genotypes. The plots show the number of eggs laid per fly (n = 30-60 flies across 1-2 technical replicates).
(B) Single-fly oviposition assay for the same strains and conditions as in (A). Left: oviposition preference index. Statistical differences from 0 (no preference) are indicated: *** *P* < 0.001; ** *P* < 0.01; * *P* < 0.05 (Wilcoxon test with Bonferroni correction for multiple comparisons); n = 30-60 flies, 1-2 assays. *Dsec 07* and *DsecIr8a^{RFP}* show statistical difference (*p*-value = 0.0223; Wilcoxon test with Bonferroni adjustment). Right: egg-laying rate in these assays. Mean values ± SEM are shown. *** *P* < 0.001; ** *P* < 0.01 (Kruskal-Wallis rank sum test with Nemenyi post-hoc test).

Figure S7. Influence of valencene and limonene on oviposition behavior.
(A) Single-fly oviposition assays for valencene and limonene at the indicated concentrations. Odors were diluted in apple cider vinegar (for *D. melanogaster* and *D. simulans*) or noni juice (for *D. sechellia*) and agarose. For further information about fly strains and statistical meaning refer to the legend for Figure 1C. Statistical differences from 0 (no preference) are indicated: *** *P* < 0.001; ** *P* < 0.01; * *P* < 0.05; NS *P* > 0.05 (Wilcoxon test with Bonferroni correction for multiple

comparisons); n = 30-90 flies, 1-3 assays.
(B) Bar plots of egg laying rates for flies from (A). Mean values ± SEM are shown.
(C) Single-fly oviposition assays of same strains as in (A), with an instant medium substrate. Left: oviposition preference index in control (H_2O versus H_2O) or experimental (0.1% valencene versus H_2O) conditions. Statistical differences from 0 (no preference) are indicated: *** $P < 0.001$; NS $P > 0.05$ (Wilcoxon test with Bonferroni correction for multiple comparisons). n = 30-60 flies, 1-2 assays. Right: egg-laying rate in these assays. Mean values ± SEM are shown. Statistical comparisons of the effect of odors on egg-laying rate were performed across strains: *** $P < 0.001$; ** $P < 0.01$; * $P < 0.05$; NS $P > 0.05$ (two-sample t-test). For some strains (indicated with a white rectangle), the low number of flies laying eggs prevented calculation of a preference index.

Figure S8. Impact of modulation of L-DOPA levels on egg-laying rate of *D. sechellia*
Egg-laying rate of *D. sechellia* cultivated on non-supplemented noni juice food media (green) or supplemented with L-DOPA or α-methyl-DOPA (see Methods). Left: group oviposition assays (representing 2 assays of either 10 (*D. melanogaster* and *D. simulans*) or 20 (*D. sechellia*) flies each, each scored on 3 successive days with fresh oviposition plates each day). Right: single-fly oviposition assays. Mean values ± SEM are shown (statistical differences from the noni juice substrates are shown: *** $P < 0.001$; * $P < 0.05$; NS $P > 0.05$ (Kruskal-Wallis rank sum test with Nemenyi post-hoc test); n = 60 flies across 2 technical replicates.

Video S1. Compilation of video sequences illustrating substrate touching by the ovipositor in *D. sechellia*.

Video S2. Compilation of video sequences illustrating substrate scratching by the ovipositor in *D. sechellia*.

Video S3. Compilation of video sequences illustrating substrate digging by the ovipositor in *D. sechellia*.

Video S4. Compilation of video sequences illustrating indentation formation by the ovipositor in *D. sechellia*.

Video S5. Compilation of video sequences illustrating egg-laying by *D. sechellia*.

Table S1. *Drosophila* strains.

Strain	Source	Identifier
D. melanogaster wildtype Canton-S (CS)		
D. melanogaster wildtype Oregon-R (OR)		
D. melanogaster Ir8a^{1}	(Abuin et al., 2011)	RRID:BDSC_41744
D. melanogaster Orco^{1}	(Larsson et al., 2004)	RRID:BDSC_23130
D. melanogaster Ir75b^{DsRed}	(Mika et al., 2021)	
D. melanogaster Ir75b-Gal4	(Prieto-Godino et al., 2017)	
D. melanogaster UAS-DmelIr75b	(Prieto-Godino et al., 2017)	
D. melanogaster UAS-DsecIr75b	(Prieto-Godino et al., 2017)	
D. simulans wildtype *Dsim* 04	*Drosophila* Species Stock Center [DSSC]	14021-0251.004
D. simulans wildtype *Dsim* 196	DSSC	14021-0251.196
D. sechellia wildtype *Dsec* 07	DSSC	14021-0248.07
D. sechellia wildtype *Dsec* 28	DSSC	14021-0248.28
D. sechellia Orco^{1}	(Auer et al., 2020)	
D. sechellia Or22a^{RFP}	(Auer et al., 2020)	
D. sechellia Or85b/c^{RFP}	(Auer et al., 2020)	
D. sechellia Or35a^{RFP}	(Auer et al., 2020)	
D. sechellia Ir8a^{GFP}	(Auer et al., 2020)	
D. sechellia Ir64a^{RFP}	(Auer et al., 2020)	
D. sechellia Ir75b^{1}	(Auer et al., 2020)	
D. sechellia Ir75b^{2}	(Auer et al., 2020)	

Table S2. Chemicals.

Odor	Supplier	CAS
Agarose	Promega	-
Apple cider vinegar	Migros	-
BACTO Agar	BD	214010
Balsamic vinegar	Antica Modena	-
Butyric acid	Sigma-Aldrich	107-92-6
3,4-dihydroxyphenylalanine (L-DOPA)	Sigma-Aldrich	53587-29-4
Formula 4-24® instant *Drosophila* medium ("instant medium")	Carolina Biological Supply	-
Grape juice	Beutelsbacher Bio	-
2-heptanone	Sigma-Aldrich	110-43-0
Hexanoic acid	Sigma-Aldrich	142-62-1
Limonene	Sigma-Aldrich	5989-27-5
α-methyl-DOPA	Sigma-Aldrich	41372-08-1
Methyl hexanoate	Sigma-Aldrich	106-70-7
Noni juice	Raab Vitalfood Bio	-
Octanoic acid	Sigma-Aldrich	124-07-2
Sucrose	Sigma	57-50-1
Valencene	Sigma-Aldrich	4630-07-3

References

Abuin, L., Bargeton, B., Ulbrich, M.H., Isacoff, E.Y., Kellenberger, S., and Benton, R. (2011). Functional architecture of olfactory ionotropic glutamate receptors. Neuron *69*, 44-60.

Abzhanov, A., Protas, M., Grant, B.R., Grant, P.R., and Tabin, C.J. (2004). Bmp4 and morphological variation of beaks in Darwin's finches. Science *305*, 1462-1465.

Ahn, J.E., Chen, Y., and Amrein, H.O. (2017). Molecular basis of fatty acid taste in *Drosophila*. eLife *6*, e30115.

Ai, M., Min, S., Grosjean, Y., Leblanc, C., Bell, R., Benton, R., and Suh, G.S. (2010). Acid sensing by the *Drosophila* olfactory system. Nature *468*, 691-695.

Amlou, M., Moreteau, B., and David, J.R. (1998). Genetic analysis of *Drosophila sechellia* specialization: oviposition behavior toward the major aliphatic acids of its host plant. Behavior Genetics *28*, 455-464.

Auer, T.O., Khallaf, M.A., Silbering, A.F., Zappia, G., Ellis, K., Alvarez-Ocana, R., Arguello, J.R., Hansson, B.S., Jefferis, G.S.X.E., Caron, S.J.C*., et al.* (2020). Olfactory receptor and circuit evolution promote host specialization. Nature *579*, 402-408.

Auer, T.O., Shahandeh, M.P., and Benton, R. (2021). *Drosophila sechellia*: A Genetic Model for Behavioral Evolution and Neuroecology. Annu Rev Genet *55*, 527-554.

Benton, R., Sachse, S., Michnick, S.W., and Vosshall, L.B. (2006). Atypical membrane topology and heteromeric function of *Drosophila* odorant receptors *in vivo*. PLOS Biol *4*, e20.

Bracker, L.B., Schmid, C.A., Bolini, V.A., Holz, C.A., Prud'homme, B., Sirota, A., and Gompel, N. (2019). Quantitative and Discrete Evolutionary Changes in the Egg-Laying Behavior of Single *Drosophila* Females. Front Behav Neurosci *13*, 118.

Caillaud, M.C., and Via, S. (2000). Specialized Feeding Behavior Influences Both Ecological Specialization and Assortative Mating in Sympatric Host Races of Pea Aphids. Am Nat *156*, 606-621.

Chen, H.L., Motevalli, D., Stern, U., and Yang, C.H. (2022). A functional division of *Drosophila* sweet taste neurons that is value-based and task-specific. Proceedings of the National Academy of Sciences of the United States of America *119*.

Chen, Y., and Amrein, H. (2017). Ionotropic Receptors Mediate *Drosophila* Oviposition Preference through Sour Gustatory Receptor Neurons. Curr Biol *27*, 2741-2750 e2744.

Chen, Y.D., and Dahanukar, A. (2020). Recent advances in the genetic basis of taste detection in *Drosophila*. Cell Mol Life Sci *77*, 1087-1101.

Chin, S.G., Maguire, S.E., Huoviala, P., Jefferis, G., and Potter, C.J. (2018). Olfactory Neurons and Brain Centers Directing Oviposition Decisions in *Drosophila*. Cell Rep *24*, 1667-1678.

Chiu, J.C., Low, K.H., Pike, D.H., Yildirim, E., and Edery, I. (2010). Assaying locomotor activity to study circadian rhythms and sleep parameters in *Drosophila*. J Vis Exp, e2157.

Churchill, E.R., Dytham, C., Bridle, J.R., and Thom, M.D.F. (2021). Social and physical environment independently affect oviposition decisions in *Drosophila*. Behav Ecol *32*, 1391-1399.

Combs, P.A., Krupp, J.J., Khosla, N.M., Bua, D., Petrov, D.A., Levine, J.D., and Fraser, H.B. (2018). Tissue-Specific *cis*-Regulatory Divergence Implicates *eloF* in Inhibiting Interspecies Mating in *Drosophila*. Curr Biol *28*, 3969-3975 e3963.
Coyne, J.A., Rux, J., and David, J.R. (1991). Genetics of morphological differences and hybrid sterility between *Drosophila sechellia* and its relatives. Genet Res *57*, 113-122.
Cury, K.M., and Axel, R. (2021). Decisions in an Innate Behavioral Sequence. bioRxiv, 2021.2004.2003.438315.
Cury, K.M., Prud'homme, B., and Gompel, N. (2019). A short guide to insect oviposition: when, where and how to lay an egg. J Neurogenet *33*, 75-89.
de Bruyne, M., Smart, R., Zammit, E., and Warr, C.G. (2010). Functional and molecular evolution of olfactory neurons and receptors for aliphatic esters across the *Drosophila* genus. J Comp Physiol A Neuroethol Sens Neural Behav Physiol *196*, 97-109.
Dekker, T., Ibba, I., Siju, K.P., Stensmyr, M.C., and Hansson, B.S. (2006). Olfactory shifts parallel superspecialism for toxic fruit in *Drosophila melanogaster* sibling, *D. sechellia*. Curr Biol *16*, 101-109.
Doody, J.S., Freedberg, S., and Keogh, J.S. (2009). Communal egg-laying in reptiles and amphibians: evolutionary patterns and hypotheses. Q Rev Biol *84*, 229-252.
Dweck, H.K., Ebrahim, S.A., Farhan, A., Hansson, B.S., and Stensmyr, M.C. (2015). Olfactory proxy detection of dietary antioxidants in *Drosophila*. Curr Biol *25*, 455-466.
Dweck, H.K., Ebrahim, S.A., Kromann, S., Bown, D., Hillbur, Y., Sachse, S., Hansson, B.S., and Stensmyr, M.C. (2013). Olfactory preference for egg laying on citrus substrates in *Drosophila*. Curr Biol *23*, 2472-2480.
Dweck, H.K.M., Ebrahim, S.A.M., Retzke, T., Grabe, V., Weissflog, J., Svatos, A., Hansson, B.S., and Knaden, M. (2018). The Olfactory Logic behind Fruit Odor Preferences in Larval and Adult *Drosophila*. Cell Rep *23*, 2524-2531.
Elsensohn, J.E., Aly, M.F.K., Schal, C., and Burrack, H.J. (2021). Social signals mediate oviposition site selection in *Drosophila suzukii*. Sci Rep *11*, 3796.
Gou, B., Zhu, E., He, R., Stern, U., and Yang, C.H. (2016). High Throughput Assay to Examine Egg-Laying Preferences of Individual *Drosophila melanogaster*. J Vis Exp, e53716.
Grant, P.R., and Grant, B.R. (2005). Darwin's finches. Curr Biol *15*, R614-615.
Green, D.A.n., and Extavour, C.G. (2012). Convergent evolution of a reproductive trait through distinct developmental mechanisms in *Drosophila*. Dev Biol *372*, 120-130.
Gruntenko, N.E., and Rauschenbach, I.Y. (2008). Interplay of JH, 20E and biogenic amines under normal and stress conditions and its effect on reproduction. J Insect Physiol *54*, 902-908.
Hallem, E.A., and Carlson, J.R. (2006). Coding of odors by a receptor repertoire. Cell *125*, 143-160.
Higa, I., and Fuyama, Y. (1993). Genetics of food preference in *Drosophila sechellia*. I. Responses to food attractants. Genetica *88*, 129-136.
Ibba, I., Angioy, A.M., Hansson, B.S., and Dekker, T. (2010). Macroglomeruli for fruit odors change blend preference in *Drosophila*. Die Naturwissenschaften *97*, 1059-1066.
Jones, C.D. (2004). Genetics of egg production in *Drosophila sechellia*. Heredity (Edinb) *92*, 235-241.

Jones, C.D. (2005). The genetics of adaptation in *Drosophila sechellia*. Genetica *123*, 137-145.
Karageorgi, M., Bracker, L.B., Lebreton, S., Minervino, C., Cavey, M., Siju, K.P., Grunwald Kadow, I.C., Gompel, N., and Prud'homme, B. (2017). Evolution of Multiple Sensory Systems Drives Novel Egg-Laying Behavior in the Fruit Pest *Drosophila suzukii*. Curr Biol *27*, 847-853.
Lamichhaney, S., Berglund, J., Almen, M.S., Maqbool, K., Grabherr, M., Martinez-Barrio, A., Promerova, M., Rubin, C.J., Wang, C., Zamani, N.*, et al.* (2015). Evolution of Darwin's finches and their beaks revealed by genome sequencing. Nature *518*, 371-375.
Larsson, M.C., Domingos, A.I., Jones, W.D., Chiappe, M.E., Amrein, H., and Vosshall, L.B. (2004). *Or83b* encodes a broadly expressed odorant receptor essential for *Drosophila* olfaction. Neuron *43*, 703-714.
Lavista-Llanos, S., Svatos, A., Kai, M., Riemensperger, T., Birman, S., Stensmyr, M.C., and Hansson, B.S. (2014). Dopamine drives *Drosophila sechellia* adaptation to its toxic host. eLife *3*, e03785.
Legal, L., Chappe, B., and Jallon, J.M. (1994). Molecular basis of *Morinda citrifolia* (L.): Toxicity on *Drosophila*. J Chem Ecol *20*, 1931-1943.
Legal, L., David, J.R., and Jallon, J.M. (1992). Toxicity and attraction effects produced by *Morinda citrifolia* fruits on the *Drosophila melanogaster* complex of species. Chemoecology *3*, 125-129.
Legal, L., Moulin, B., and Jallon, J.M. (1999). The Relation between Structures and Toxicity of Oxygenated Aliphatic Compounds Homologous to the Insecticide Octanoic Acid and the Chemotaxis of Two Species of *Drosophila*. Pesticide biochemistry and physiology *65*, 90-101.
Lin, C.C., Prokop-Prigge, K.A., Preti, G., and Potter, C.J. (2015). Food odors trigger males to deposit a pheromone that guides aggregation and female oviposition decisions. eLife *4*, e08688.
Louis, J., and David, J.R. (1986). Ecological specialization in the *Drosophila melanogaster* species subgroup: A case study of *Drosophila sechellia*. Acta Oecol, Oecol gen *7*, 215-229.
Maldonado, E., Rangel-Huerta, E., Rodriguez-Salazar, E., Pereida-Jaramillo, E., and Martinez-Torres, A. (2020). Subterranean life: Behavior, metabolic, and some other adaptations of *Astyanax* cavefish. J Exp Zool B Mol Dev Evol *334*, 463-473.
Markow, T.A., Beall, S., and Matzkin, L.M. (2009). Egg size, embryonic development time and ovoviviparity in *Drosophila* species. J Evol Biol *22*, 430-434.
Matsuo, T. (2008). Genes for host-plant selection in *Drosophila*. J Neurogenet *22*, 195-210.
Matsuo, T., Sugaya, S., Yasukawa, J., Aigaki, T., and Fuyama, Y. (2007). Odorant-binding proteins OBP57d and OBP57e affect taste perception and host-plant preference in *Drosophila sechellia*. PLOS Biol *5*, e118.
Mika, K., Cruchet, S., Chai, P.C., Prieto-Godino, L.L., Auer, T.O., Pradervand, S., and Benton, R. (2021). Olfactory receptor-dependent receptor repression in *Drosophila*. Science advances *7*, eabe3745.
Munch, D., and Galizia, C.G. (2016). DoOR 2.0--Comprehensive Mapping of *Drosophila melanogaster* Odorant Responses. Sci Rep *6*, 21841.
Neckameyer, W.S. (1996). Multiple roles for dopamine in *Drosophila* development. Dev Biol *176*, 209-219.

Nojima, T., Rings, A., Allen, A.M., Otto, N., Verschut, T.A., Billeter, J.C., Neville, M.C., and Goodwin, S.F. (2021). A sex-specific switch between visual and olfactory inputs underlies adaptive sex differences in behavior. Curr Biol *31*, 1175-1191 e1176.

Prieto-Godino, L.L., Rytz, R., Cruchet, S., Bargeton, B., Abuin, L., Silbering, A.F., Ruta, V., Dal Peraro, M., and Benton, R. (2017). Evolution of acid-sensing olfactory circuits in drosophilids. Neuron *93*, 661-676 e666.

Prieto-Godino, L.L., Schmidt, H.R., and Benton, R. (2021). Molecular reconstruction of recurrent evolutionary switching in olfactory receptor specificity. eLife *10*, e69732.

R'Kha, S., Capy, P., and David, J.R. (1991). Host-plant specialization in the *Drosophila melanogaster* species complex: a physiological, behavioral, and genetical analysis. Proceedings of the National Academy of Sciences of the United States of America *88*, 1835-1839.

R'Kha, S., Moreteau, B., Coyne, J.A., and David, J.R. (1997). Evolution of a lesser fitness trait: egg production in the specialist *Drosophila sechellia*. Genet Res *69*, 17-23.

Rudolf, V.H., and Rodel, M.O. (2005). Oviposition site selection in a complex and variable environment: the role of habitat quality and conspecific cues. Oecologia *142*, 316-325.

Rundle, H.D., and Nosil, P. (2005). Ecological speciation. Ecol Lett *8*, 336-352.

Salazar-Jaramillo, L., and Wertheim, B. (2021). Does *Drosophila sechellia* escape parasitoid attack by feeding on a toxic resource? Peerj *9*, e10528.

Sanchez-Alcaniz, J.A., Silbering, A.F., Croset, V., Zappia, G., Sivasubramaniam, A.K., Abuin, L., Sahai, S.Y., Munch, D., Steck, K., Auer, T.O*., et al.* (2018). An expression atlas of variant ionotropic glutamate receptors identifies a molecular basis of carbonation sensing. Nat Commun *9*, 4252.

Sanchez-Alcaniz, J.A., Zappia, G., Marion-Poll, F., and Benton, R. (2017). A mechanosensory receptor required for food texture detection in *Drosophila*. Nat Commun *8*, 14192.

Schindelin, J., Arganda-Carreras, I., Frise, E., Kaynig, V., Longair, M., Pietzsch, T., Preibisch, S., Rueden, C., Saalfeld, S., Schmid, B*., et al.* (2012). Fiji: an open-source platform for biological-image analysis. Nat Methods *9*, 676-682.

Schwartz, N.U., Zhong, L., Bellemer, A., and Tracey, W.D. (2012). Egg laying decisions in *Drosophila* are consistent with foraging costs of larval progeny. PLOS ONE *7*, e37910.

Seehausen, O. (2006). African cichlid fish: a model system in adaptive radiation research. Proc Biol Sci *273*, 1987-1998.

Sexton, J.P., Montiel, J., Shay, J.E., Stephens, M.R., and Slatyer, R.A. (2017). Evolution of Ecological Niche Breadth. Annual Review of Ecology, Evolution, and Systematics, 183-206.

Stensmyr, M.C. (2009). *Drosophila sechellia* as a model in chemosensory neuroecology. Ann N Y Acad Sci *1170*, 468-475.

Tauber, J.M., Brown, E.B., Li, Y., Yurgel, M.E., Masek, P., and Keene, A.C. (2017). A subset of sweet-sensing neurons identified by IR56d are necessary and sufficient for fatty acid taste. PLOS Genet *13*, e1007059.

Wang, F., Wang, K., Forknall, N., Patrick, C., Yang, T., Parekh, R., Bock, D., and Dickson, B.J. (2020). Neural circuitry linking mating and egg laying in *Drosophila* females. Nature *579*, 101-105.

Webster, B., and Carde, R.T. (2017). Use of habitat odour by host-seeking insects. Biol Rev Camb Philos Soc *92*, 1241-1249.
Wu, S.T., Chen, J.Y., Martin, V., Ng, R., Zhang, Y., Grover, D., Greenspan, R.J., Aljadeff, J., and Su, C.Y. (2022). Valence opponency in peripheral olfactory processing. Proceedings of the National Academy of Sciences of the United States of America *119*, e2120134119.
Yang, C.H., Belawat, P., Hafen, E., Jan, L.Y., and Jan, Y.N. (2008). *Drosophila* egg-laying site selection as a system to study simple decision-making processes. Science *319*, 1679-1683.

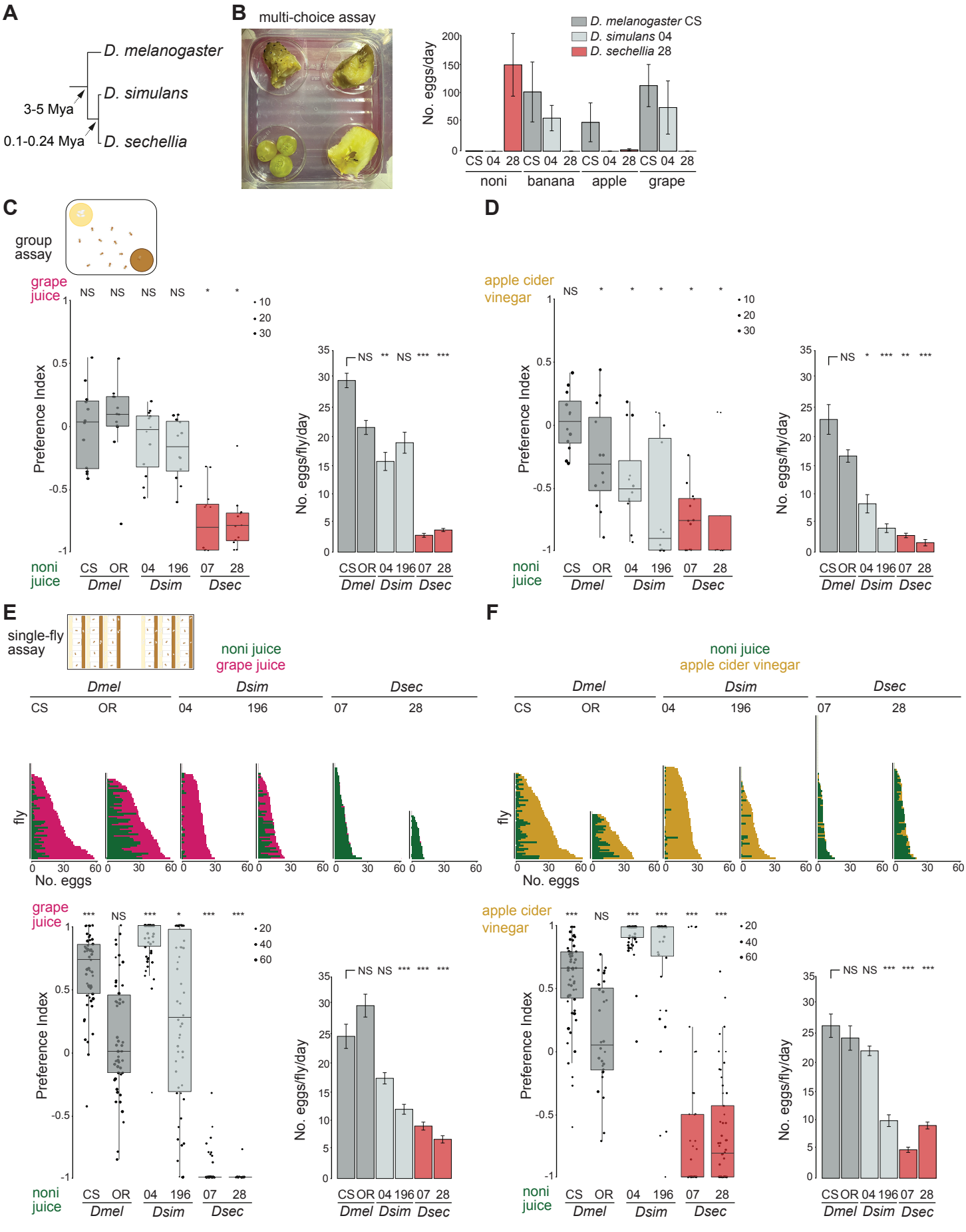
A
D. melanogaster
D. simulans
3-5 Mya
0.1-0.24 Mya
D. sechellia
B
multi-choice assay
D. melanogaster CS
D. simulans 04
D. sechellia 28
No. eggs/day
CS 04 28 CS 04 28 CS 04 28 CS 04 28
noni
banana
apple
grape
C
group assay
grape juice
Preference Index
noni juice
CS OR 04 196 07 28
Dmel Dsim Dsec
No. eggs/fly/day
D
apple cider vinegar
E
single-fly assay
noni juice
grape juice
fly
No. eggs
F
noni juice
apple cider vinegar

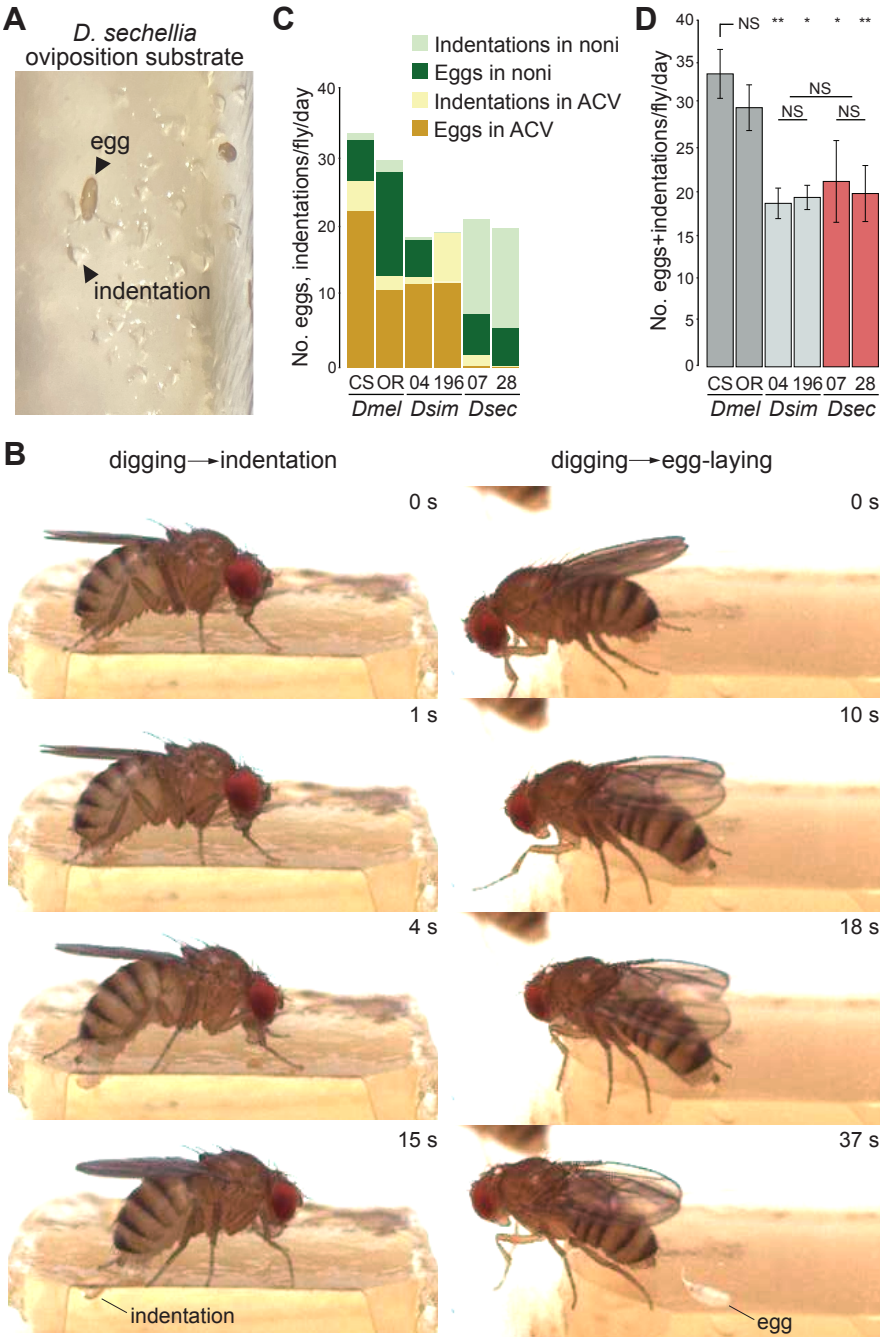
A
D. sechellia
oviposition substrate
egg
indentation
C
Indentations in noni
Eggs in noni
Indentations in ACV
Eggs in ACV
No. eggs, indentations/fly/day
0
10
20
30
40
CS OR 04 196 07 28
Dmel Dsim Dsec
D
NS ** * * **
NS
NS NS
No. eggs+indentations/fly/day
0
5
10
15
20
25
30
35
40
CS OR 04 196 07 28
Dmel Dsim Dsec
B
digging→indentation
digging→egg-laying
0 s
1 s
4 s
15 s
indentation
0 s
10 s
18 s
37 s
egg

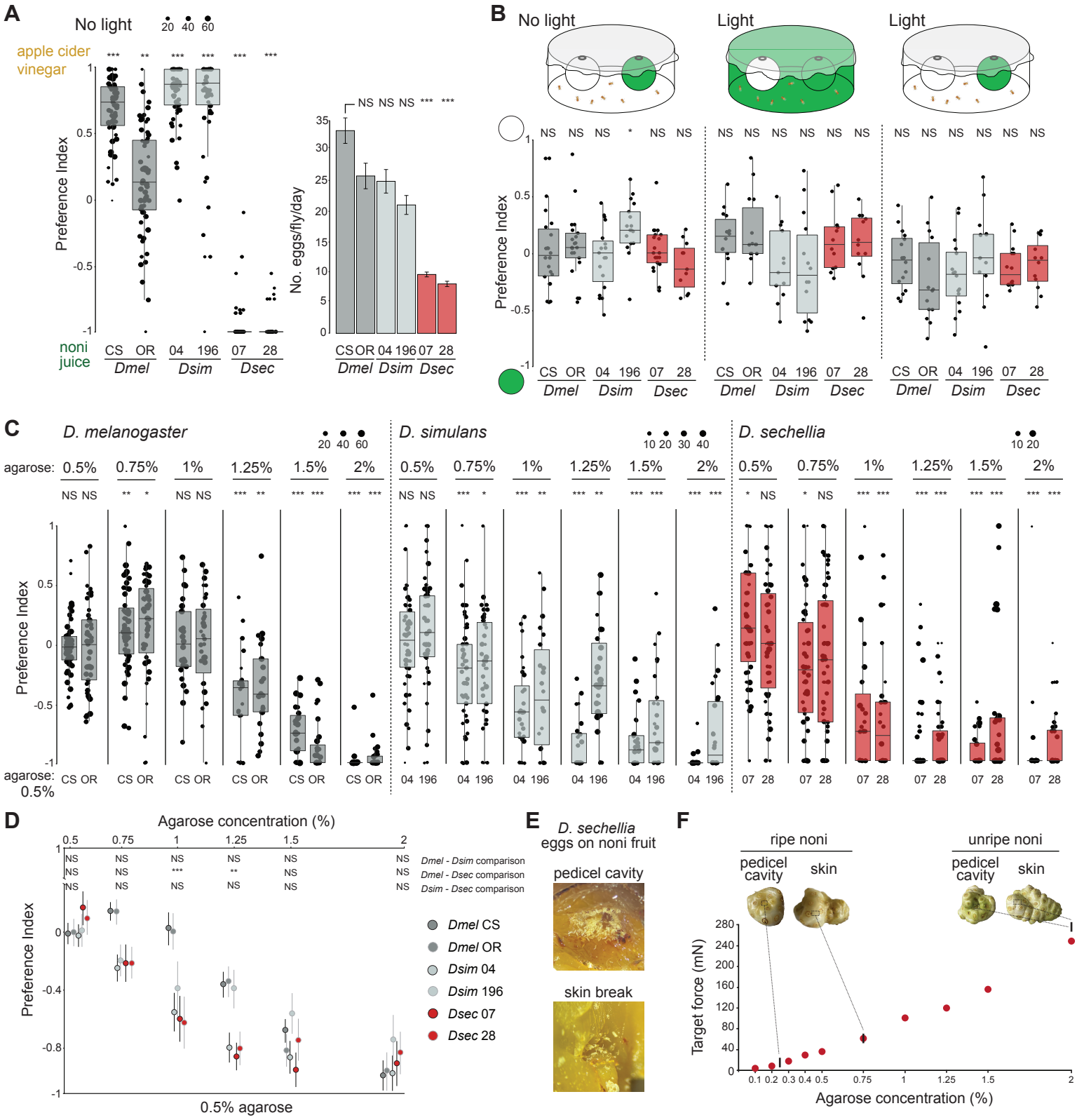
A
No light
20 40 60
apple cider vinegar
Preference Index
noni juice
CS OR 04 196 07 28
Dmel Dsim Dsec
No. eggs/fly/day
NS NS NS *** ***
B
No light
Light
Light
Preference Index
C
D. melanogaster
D. simulans
D. sechellia
agarose: 0.5% 0.75% 1% 1.25% 1.5% 2%
Preference Index
D
Agarose concentration (%)
Preference Index
0.5% agarose
Dmel - Dsim comparison
Dmel - Dsec comparison
Dsim - Dsec comparison
Dmel CS
Dmel OR
Dsim 04
Dsim 196
Dsec 07
Dsec 28
E
D. sechellia
eggs on noni fruit
pedicel cavity
skin break
F
ripe noni
unripe noni
pedicel cavity
skin
Target force (mN)
Agarose concentration (%)

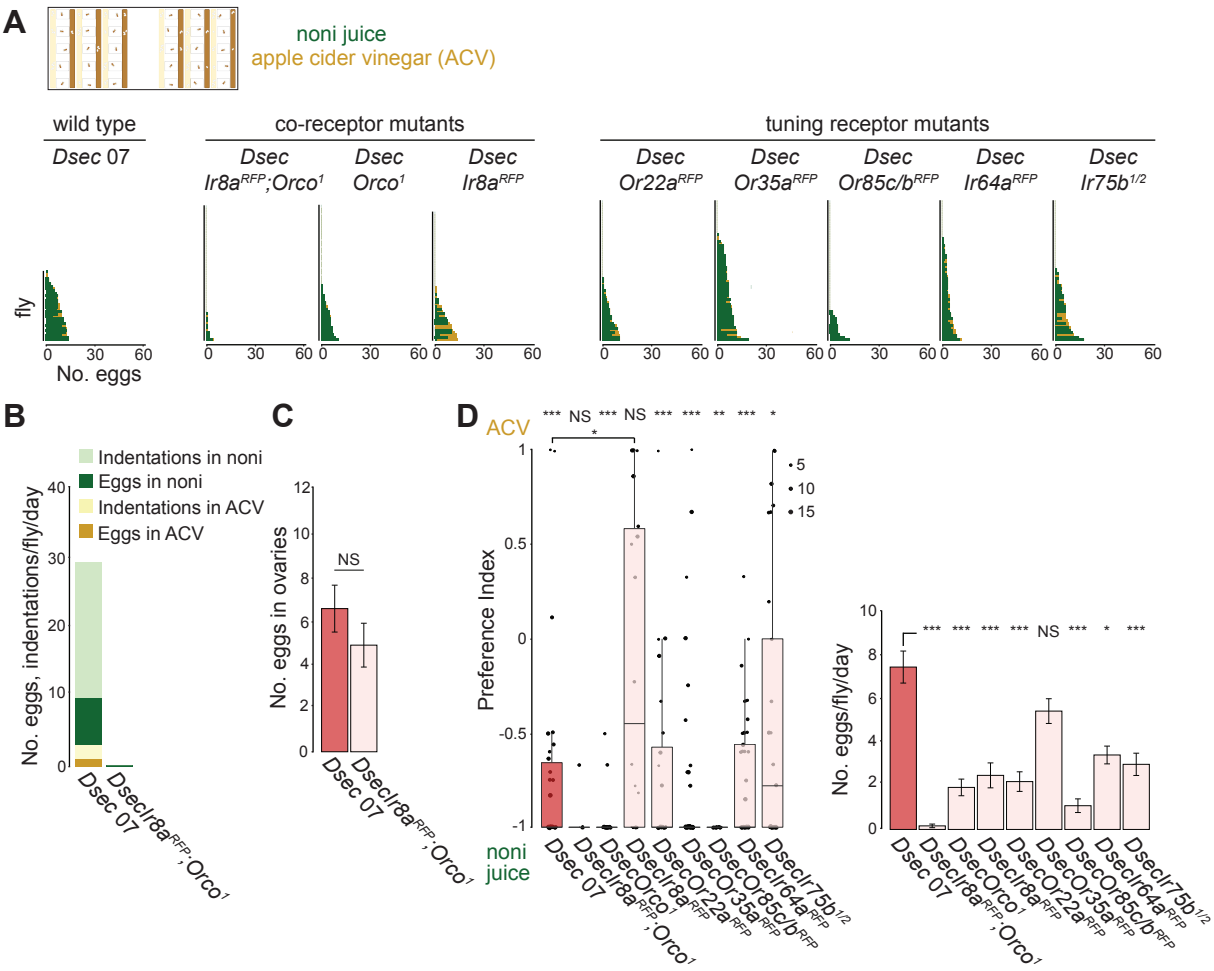
A
noni juice
apple cider vinegar (ACV)
wild type
co-receptor mutants
tuning receptor mutants
Dsec 07
Dsec Ir8aRFP;Orco1
Dsec Orco1
Dsec Ir8aRFP
Dsec Or22aRFP
Dsec Or35aRFP
Dsec Or85c/bRFP
Dsec Ir64aRFP
Dsec Ir75b1/2
fly
No. eggs
B
Indentations in noni
Eggs in noni
Indentations in ACV
Eggs in ACV
No. eggs, indentations/fly/day
C
No. eggs in ovaries
NS
D
ACV
Preference Index
noni juice
No. eggs/fly/day

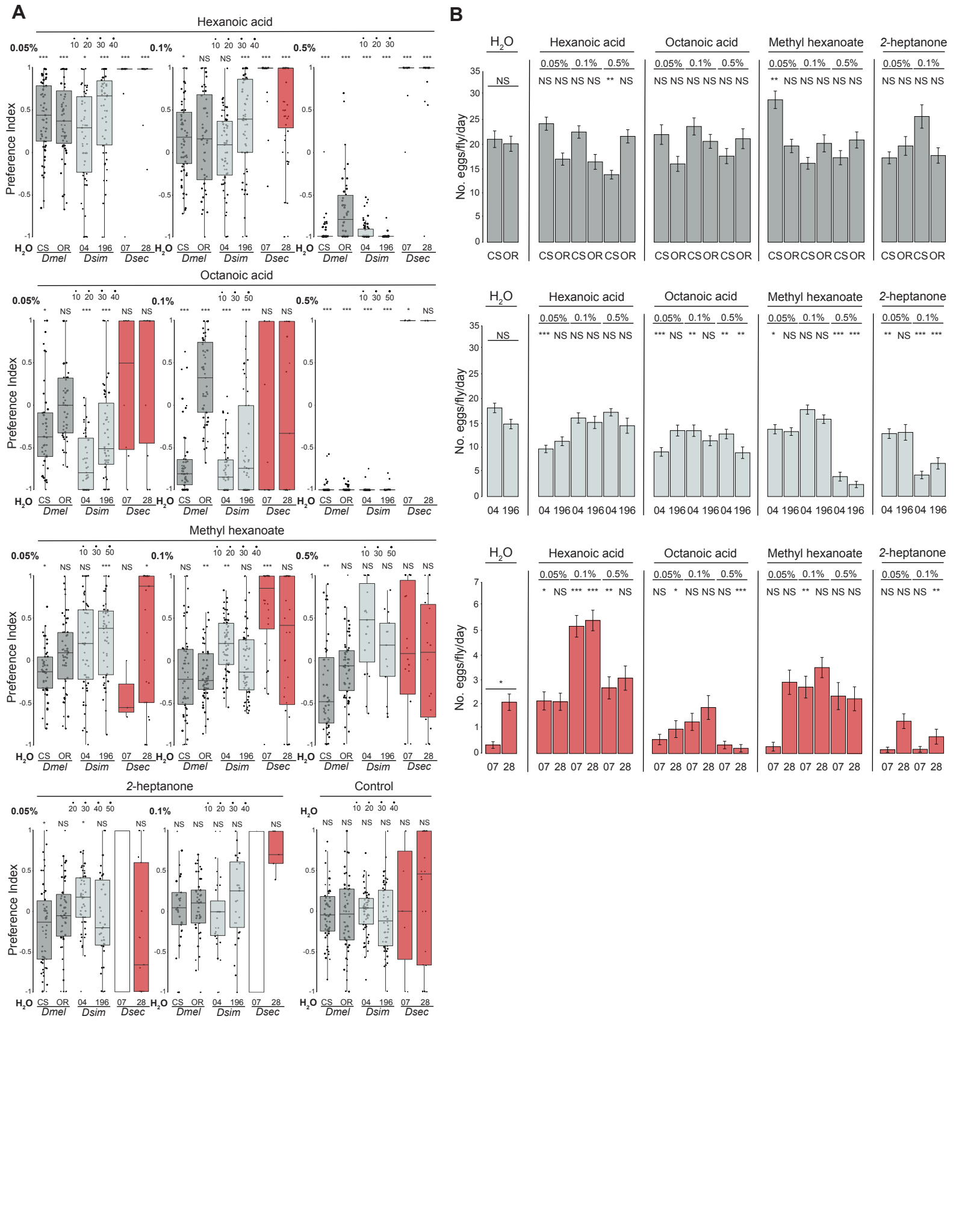
A
Hexanoic acid
Octanoic acid
Methyl hexanoate
2-heptanone
Control
0.05%
0.1%
0.5%
Preference Index
H2O CS OR 04 196 07 28
Dmel Dsim Dsec
B
H2O
Hexanoic acid
Octanoic acid
Methyl hexanoate
2-heptanone
0.05% 0.1% 0.5%
No. eggs/fly/day
CS OR
04 196
07 28

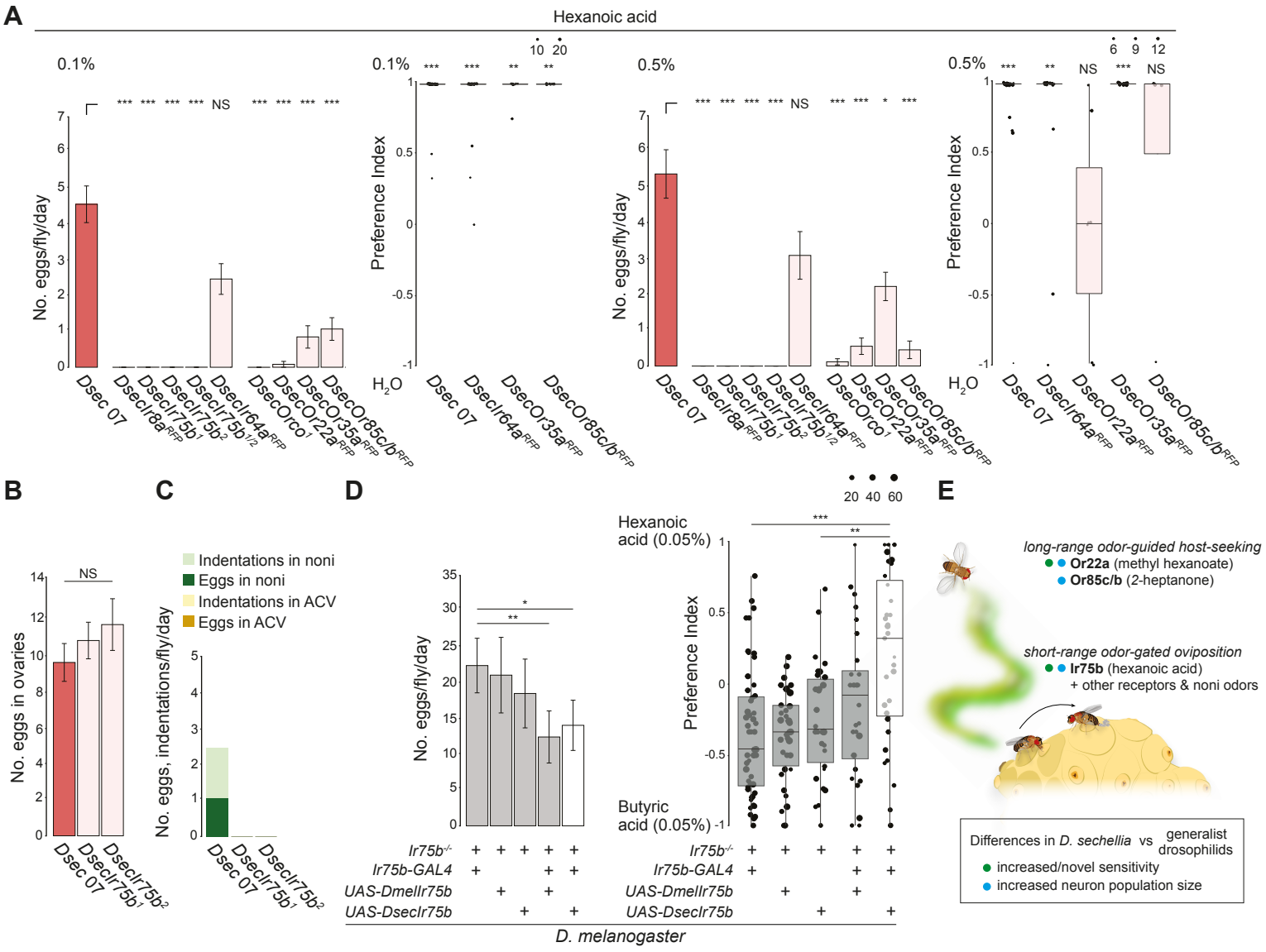
A
Hexanoic acid
0.1%
0.5%
No. eggs/fly/day
Preference Index
H2O
Dsec 07
DsecIr8a^RFP
DsecIr75b^1
DsecIr75b^2
DsecIr75b^1/2
DsecIr64a^RFP
DsecOrco^1
DsecOr22a^RFP
DsecOr35a^RFP
DsecOr85c/b^RFP
NS
B
No. eggs in ovaries
C
Indentations in noni
Eggs in noni
Indentations in ACV
Eggs in ACV
No. eggs, indentations/fly/day
D
No. eggs/fly/day
Hexanoic acid (0.05%)
Butyric acid (0.05%)
Preference Index
Ir75b-/-
Ir75b-GAL4
UAS-DmelIr75b
UAS-DsecIr75b
D. melanogaster
E
long-range odor-guided host-seeking
Or22a (methyl hexanoate)
Or85c/b (2-heptanone)
short-range odor-gated oviposition
Ir75b (hexanoic acid)
+ other receptors & noni odors
Differences in D. sechellia vs generalist drosophilids
increased/novel sensitivity
increased neuron population size

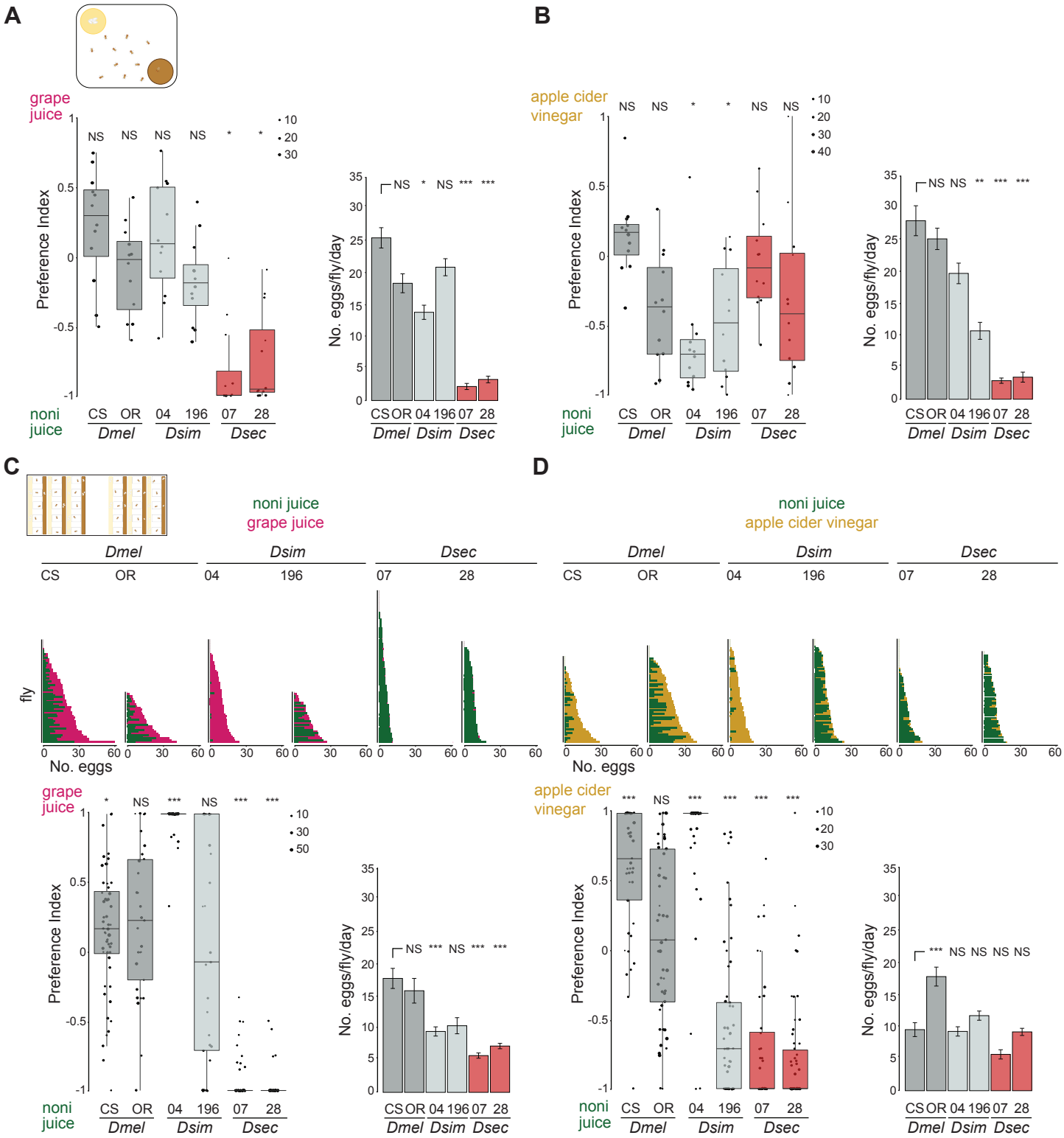
A
grape juice
Preference Index
No. eggs/fly/day
noni juice
CS OR 04 196 07 28
Dmel Dsim Dsec
B
apple cider vinegar
C
noni juice
grape juice
fly
No. eggs
D
noni juice
apple cider vinegar

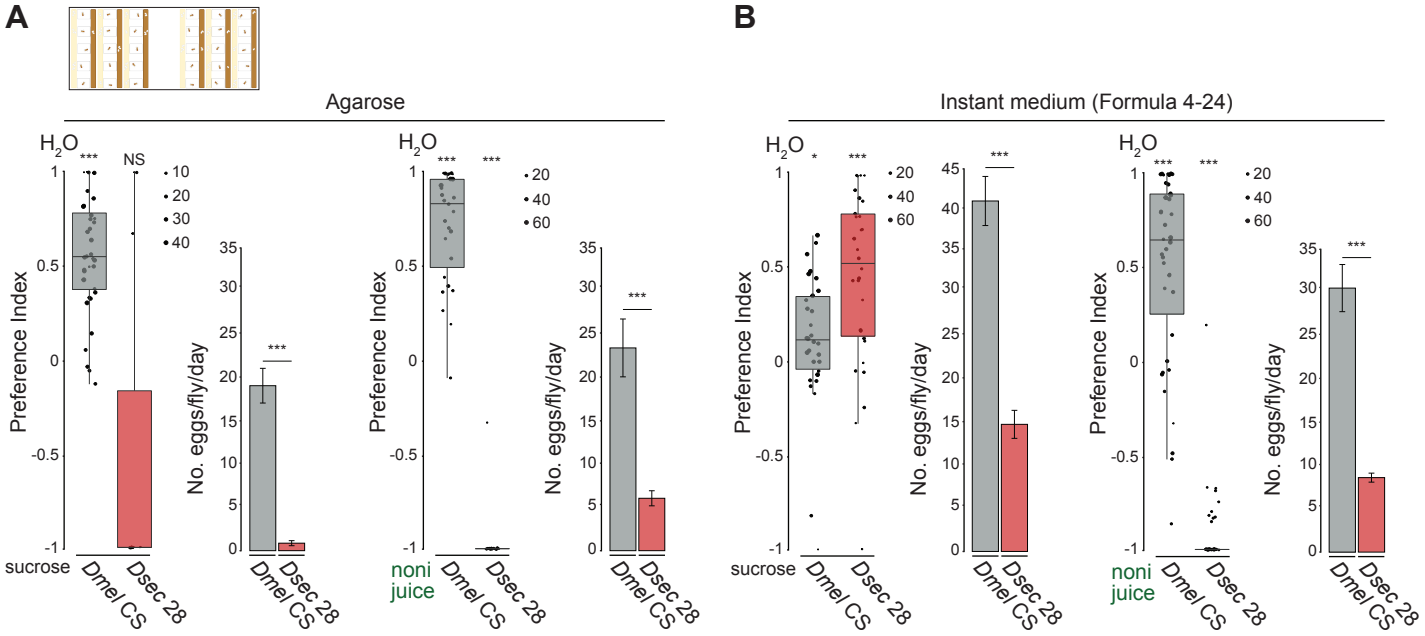
A
Agarose
H2O
sucrose
noni juice
Preference Index
No. eggs/fly/day
***
NS
10
20
30
40
60
Dmel CS
Dsec 28
B
Instant medium (Formula 4-24)
*

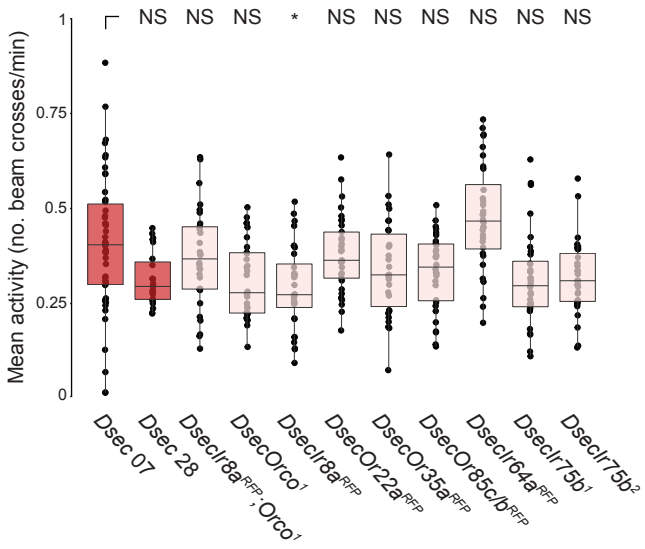
Mean activity (no. beam crosses/min)
1
0.75
0.5
0.25
0
NS
NS
NS
*
NS
NS
NS
NS
NS
NS
Dsec 07
Dsec 28
DsecIr8a^RFP,Orco^1
DsecOrco^1
DsecIr8a^RFP
DsecOr22a^RFP
DsecOr35a^RFP
DsecOr85c/b^RFP
DsecIr64a^RFP
DsecIr75b^1
DsecIr75b^2

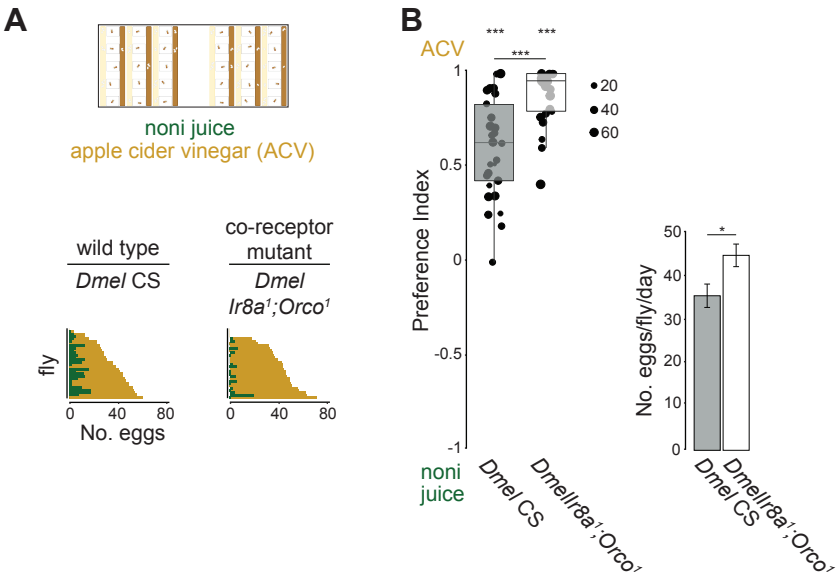
A
noni juice
apple cider vinegar (ACV)
wild type
Dmel CS
co-receptor mutant
Dmel Ir8a1;Orco1
fly
0
40
80
No. eggs
B
ACV
***
***
***
20
40
60
Preference Index
1
0.5
0
-0.5
-1
noni juice
Dmel CS
Dmel Ir8a1;Orco1
No. eggs/fly/day
*
50
40
30
20
10
0
Dmel CS
Dmel Ir8a1;Orco1

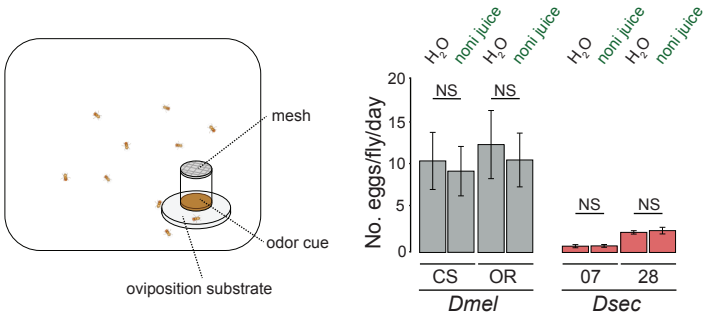
mesh
odor cue
oviposition substrate
H2O
noni juice
H2O
noni juice
H2O
noni juice
H2O
noni juice
No. eggs/fly/day
20
15
10
5
0
NS
NS
NS
NS
CS
OR
07
28
Dmel
Dsec

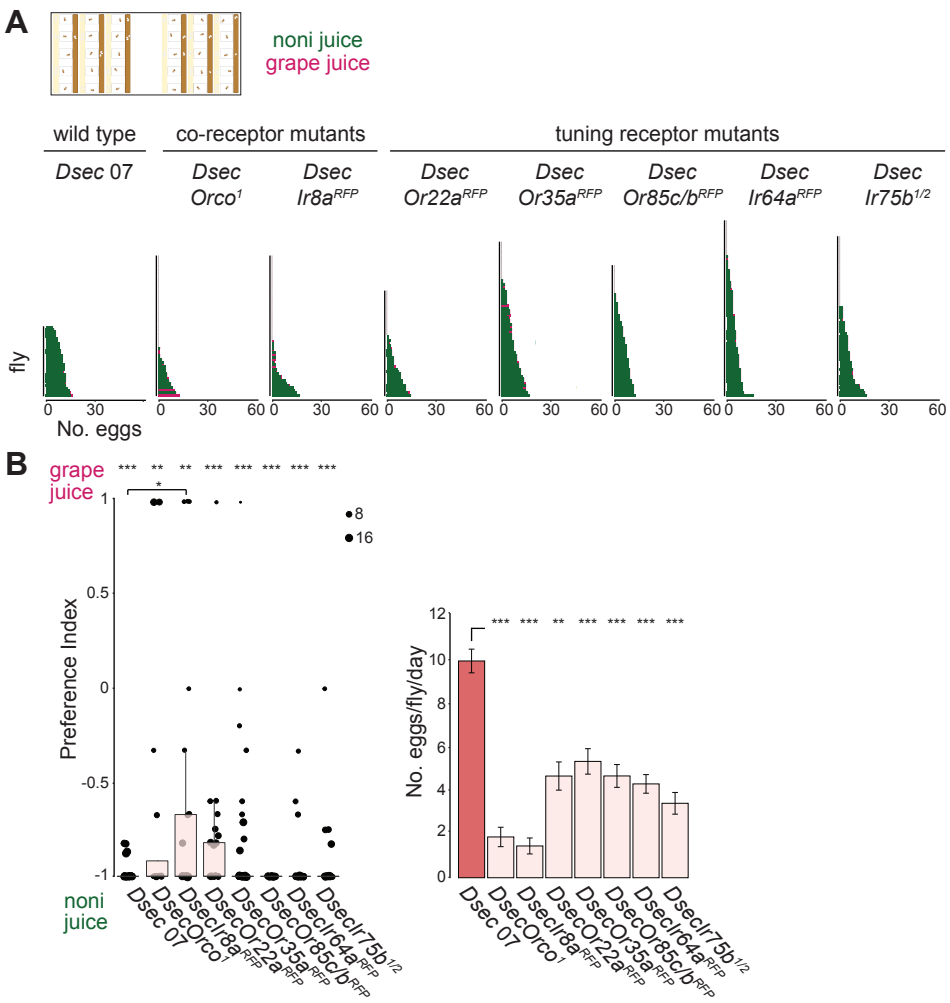
A
noni juice
grape juice
wild type
co-receptor mutants
tuning receptor mutants
Dsec 07
Dsec Orco1
Dsec Ir8aRFP
Dsec Or22aRFP
Dsec Or35aRFP
Dsec Or85c/bRFP
Dsec Ir64aRFP
Dsec Ir75b1/2
fly
No. eggs
B
grape juice
noni juice
Preference Index
No. eggs/fly/day
8
16

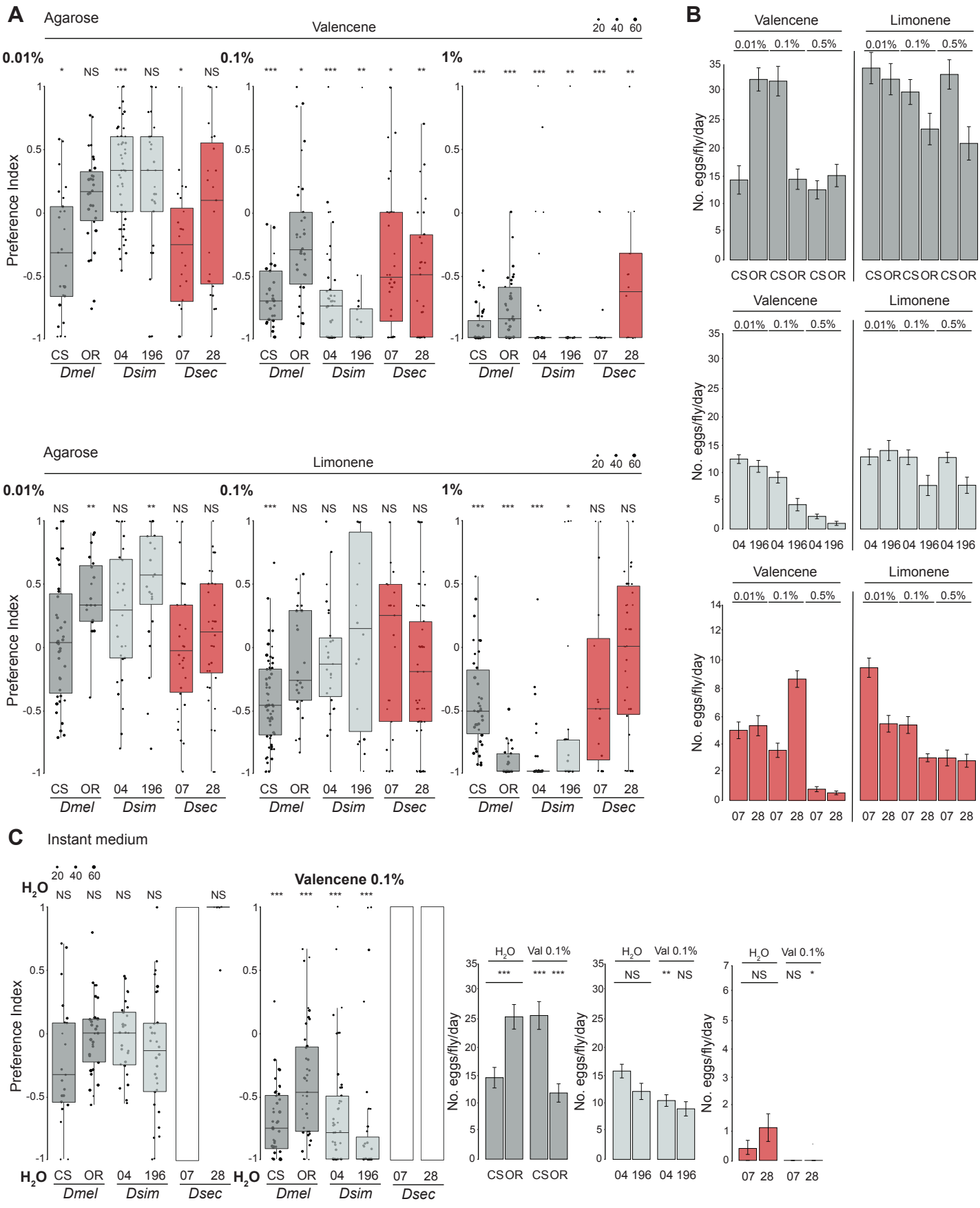
A
Agarose
Valencene
0.01%
0.1%
1%
Preference Index
CS OR 04 196 07 28
Dmel Dsim Dsec
Agarose
Limonene
B
Valencene
Limonene
0.01% 0.1% 0.5%
No. eggs/fly/day
CS OR CS OR CS OR
04 196 04 196 04 196
07 28 07 28 07 28
C
Instant medium
H2O
Valencene 0.1%
Val 0.1%

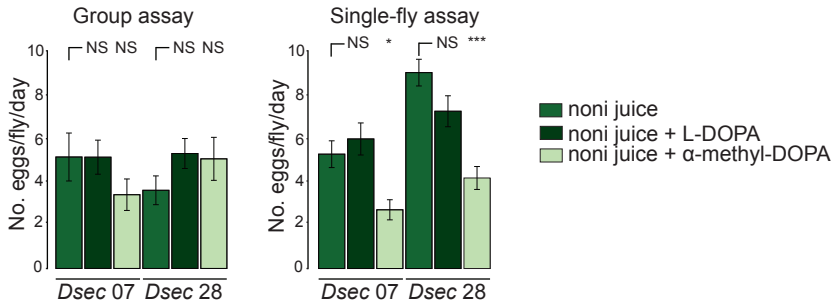
Group assay
Single-fly assay
No. eggs/fly/day
0
2
4
6
8
10
NS NS
NS NS
NS
*
NS
***
Dsec 07
Dsec 28
noni juice
noni juice + L-DOPA
noni juice + α-methyl-DOPA

CHAPTER 5: FINAL DISCUSSION AND CONCLUSIONS

5.1. General discussion

"*Why do we eat what we eat?"* was the title of the Master project offer that brought me to Richard Benton's laboratory in 2016, which involved the study of odorant receptor families' dynamics (expansions or contractions) across drosophilids and their repercussion on fly's ecology. Although the answer to this question remains open due to its complexity, during my thesis I contributed to the better understanding of neuronal evolution using the olfactory system of *D. melanogaster* and some of its close relatives as model systems.

Olfactory systems are formed by complex connectomes that control sophisticated stereotyped behaviors that undergo evolutionary changes at different levels across individuals (see introductory Chapter 1) and I am happy to have brought new mechanisms of olfactory evolution to the scientific community.

First, I presented a novel example of how evolution can shape *Drosophila*'s peripheral olfactory organs by changing odorant receptor tuning through the co-expression of multiple receptors in the same OSN (see Chapter 2). In this study, we described the co-expression of three *Or67a* genes (P, D and 3R, according to their chromosomal localization) in *D. simulans* and *D. mauritiana* and analyzed their electrophysiological response profiles through single sensillum recordings. Using *Or67a*-copies single mutants, we discovered that the encoded receptors had unique but overlapping responses that globally resembled *D. simulans* ab10 sensillum wild type responses. Although other co-expression examples have previously been described in *D. melanogaster* (such the tandem genes Or22a/Or22b (Aguade 2009, Dobritsa et al. 2003, Guo and Kim 2007, McBride 2007) or the highly divergent Or33c and Or85e (Goldman et

al. 2005)), ours is the first study that analyzes the physiological consequences of odorant receptor gene co-expression and opens the door to analyzing other instances of stable receptor co-expression as an adaptive evolutionary mechanism in other insect species. In *D. melanogaster*, Or67a is broadly tuned towards fruit esters (Dweck et al. 2018) and has been indirectly linked to aversive behaviors in odor preference assays (Dweck et al. 2018) and to mediate oviposition site preference through optogenetic activation (Wu et al. 2022). In the future, analyzing the behavioral outputs of Or67a co-expressed receptors would bring new insights into *D. simulans* ecology and adaptation mechanisms.

Second, I contributed to the development of *D. sechellia* as a new genetic model to address evolutionary questions that involve species-specific adaptations (see Chapter 3). During *D. sechellia*'s adaptation to its fruit host, a vast olfactory sensory reorganization has occurred. Using wide field calcium imaging, I described the representation of *D. sechellia*'s noni fruit-elicited responses in the antennal lobe and discovered important differences with *D. melanogaster*: For instance, *D. sechellia*'s DM2 (Or22a) and VM5d (Or85c/b) glomeruli elicit stronger responses to commercial noni juice (although not significant) and noni fruit extract (significant), but weaker responses to apple cider vinegar (significant) compared to *D. melanogaster*. The absence of statistical significance to commercial noni juice could be explained by differences in its odor bouquet compared to real noni fruit extract (Auer et al. 2020), or by a low sensitivity of the wide field calcium imaging technique. Using less diluted noni juice or a – more sensitive – two-photon microscope to perform these experiments could clarify if these are the case. Later, I studied the glomerular representation and the cellular expression of Or19a (DC1) and Or56a (DA2) in

D. sechellia. In previous studies, Or19a OSNs were described to specifically respond to citrus-related terpenes (such as valencene or limonene (Dweck et al. 2013)) and promote oviposition in *D. melanogaster* female flies. On the other hand, through the sensation of geosmin, Or56a OSNs drive oviposition aversion in *D. melanogaster* (Stensmyr et al. 2012). Here, I have shown changes in Or19a (decrease) and Or56a (increase) OSN population size in *D. sechellia* compared to *D. melanogaster*. Furthermore, calcium imaging shows that *D. sechellia*'s DC1 glomerulus fails to respond to valencene (supported by heterologous single sensillum recording *of DsecOr19a* and the lack of phenotype in attraction-trap assays) while *D. sechellia*'s DA2 has developed a stronger sensitivity to geosmin compared to *D. melanogaster*. However, *D. sechellia*'s Or56a does not mediate aversion as flies fail to show behavioral preference at least in the trap assays. If the lack of DC1 responses is related to the low number of Or19a OSN (indicating that this olfactory channel is disappearing in *D. sechellia*) or because we have not found its cognate ligand needs to be determined. Similarly, even though the structures are maintained, the valence of geosmin must have changed in *D. sechellia* flies during its speciation towards noni fruit. Altogether, this work shows how evolutionary adaptations are rarely governed by one single change or mutation, but that they rather are the result of complex and numerous phenotypic changes. Although I did not follow up this line of research further, these results could be the starting point for future studies to connect species-specific olfactory changes to their individual ecologies.

Third, I studied a different aspect of *D. sechellia*'s adaptation focusing on its egg laying behavior on noni fruit (see Chapter 4). Oviposition-related decisions (that might include when and where to lay eggs) are crucial for the reproductive

success and the maintenance of species, and they are even more important for those without parental care (Cury, Prud'homme and Gompel 2019, Rudolf and Rodel 2005). In this regard, environmental factors will determine and modify fly's egg-laying-related decisions, and changes in these factors will exert selective pressures on sensory perception, therefore modifying animals' behaviors. Through single-fly and group oviposition assays, I demonstrated that *D. sechellia*'s olfaction was necessary (although not sufficient) to make egg-laying-related decisions, as near-anosmic flies (*D. sechellia Ir8a*^{1}, *Orco*^{1} double mutants) failed to lay eggs in the presence of noni juice. However, near-anosmic *D. melanogaster* flies succeeded in laying eggs at similar rates as the wild type strains, suggesting that *D. sechellia* has developed a more dependent requirement of its olfactory system to identify its host (at least in an oviposition context). An interesting candidate receptor that could explain *D. sechellia*'s egg-laying adaptation was Ir75b for several reasons. Previous studies showed that Ir75b OSN population increased its size in *D. sechellia* and that Ir75b receptor developed novel ligand-binding properties towards hexanoic acid compared to *D. melanogaster* (Prieto-Godino et al. 2017). Furthermore, hexanoic acid was reported to generate attraction and promote egg-laying in *D. sechellia* but not in *D. melanogaster* nor *D. simulans* (Amlou, Moreteau and David 1998). In fact, *D. sechellia* Ir75b mutants show an egg-laying arrest in the sole presence of hexanoic acid that is not due to a defect in egg production. Unexpectedly, *D. sechellia* Or22a mutants also experience a noticeable reduction in the number of eggs laid in hexanoic acid-enriched substrates. However, *D. sechellia* Ir75b and Or22a mutants did not show a significant reduction in the preference for noni juice. To analyze the possibility of olfactory redundancy, I plan on performing

single-fly oviposition assays testing *D. sechellia Or22a*^{RFP}, *Ir75b*^{1} double mutants' preference for noni juice. If they individually are required for detecting noni-related oviposition-inducing chemicals, mutant flies for these two receptors would potentially show a bigger trend for reduce preference. Alternatively, no-choice odor cue oviposition assays show that noni juice olfactory cues are not sufficient to promote oviposition. Indisputably, this argues towards the prominent role of gustation during the making of oviposition-related decision. In *D. melanogaster*, Irs (Chen and Amrein 2017) and Grs (Joseph and Heberlein 2012) are necessary for oviposition preference and oviposition performance. Future analysis will be necessary to shed light on the role of gustation on *D. sechellia*'s egg-lying behavior. While many question remain, my work explicitly demonstrates distinct genetic contributions underlying *D. sechellia*'s olfactory adaptations to noni fruit.

5.2. Final remarks

Altogether, these studies highlight complex adaptation mechanisms that animals undergo within the course of evolution. One of the main challenges I experienced while working on these topics, was the reduced (although increasing) genetic tool repertoire in non-*melanogaster* species, sometimes enhanced by the less straightforward transgenesis protocols. In fact, this was the main reason why I decided to set aside the comparison of neuromodulators expression across drosophilids (see Chapter 3). In some cases, fly stocks of non-*melanogaster* species (such as *D. sechellia*) are harder to maintain or require more care, which can be very time consuming. In the same line, *D. sechellia*'s fragility difficulted the design of efficient protocols to assess oviposition site preference and overall egg-lying performance of these flies, extending the trouble shooting period to over three months (where different pre-experimental and

oviposition assays' conditions were tested). However, overcoming these limitations and encouraging evo-devo projects will be essential to better understand how neuronal systems are shaped by evolution.

BIBLIOGRAPHY

Aguade, M. (2009) Nucleotide and copy-number polymorphism at the odorant receptor genes Or22a and Or22b in Drosophila melanogaster. *Mol Biol Evol,* 26**,** 61-70.

Akutsu, J. & T. Matsuo (2022) Drosophila suzukii preferentially lays eggs on spherical surfaces with a smaller radius. *Sci Rep,* 12**,** 15792.

Albalat, R. & C. Canestro (2016) Evolution by gene loss. *Nat Rev Genet,* 17**,** 379-91.

Amlou, M., B. Moreteau & J. R. David (1998) Genetic analysis of Drosophila sechellia specialization: oviposition behavior toward the major aliphatic acids of its host plant. *Behav Genet,* 28**,** 455-64.

Arbuthnott, D., T. Y. Fedina, S. D. Pletcher & D. E. L. Promislow (2017) Mate choice in fruit flies is rational and adaptive. *Nature Communications,* 8.

Arguello, J. R., M. Cardoso-Moreira, J. K. Grenier, S. Gottipati, A. G. Clark & R. Benton (2016) Extensive local adaptation within the chemosensory system following Drosophila melanogaster's global expansion. *Nat Commun,* 7**,** ncomms11855.

Atkinson, N. S., G. A. Robertson & B. Ganetzky (1991) A component of calcium-activated potassium channels encoded by the Drosophila slo locus. *Science,* 253**,** 551-5.

Auer, T. O., R. Alvarez-Ocana, S. Cruchet, R. Benton & J. R. Arguello (2022) Copy number changes in co-expressed odorant receptor genes enable selection for sensory differences in drosophilid species. *Nat Ecol Evol,* 6**,** 1343-1353.

Auer, T. O., M. A. Khallaf, A. F. Silbering, G. Zappia, K. Ellis, R. Alvarez-Ocana, J. R. Arguello, B. S. Hansson, G. Jefferis, S. J. C. Caron, M. Knaden & R. Benton (2020) Olfactory receptor and circuit evolution promote host specialization. *Nature,* 579**,** 402-408.

Auer, T. O., M. P. Shahandeh & R. Benton (2021) Drosophila sechellia: A Genetic Model for Behavioral Evolution and Neuroecology. *Annu Rev Genet,* 55**,** 527-554.

Barish, S. & P. C. Volkan (2015) Mechanisms of olfactory receptor neuron specification in Drosophila. *Wiley Interdiscip Rev Dev Biol,* 4**,** 609-21.

Becher, P. G., M. Bengtsson, B. S. Hansson & P. Witzgall (2010) Flying the fly: long-range flight behavior of Drosophila melanogaster to attractive odors. *J Chem Ecol,* 36**,** 599-607.

Benton, R., S. Sachse, S. W. Michnick & L. B. Vosshall (2006) Atypical membrane topology and heteromeric function of Drosophila odorant receptors in vivo. *PLoS Biol,* 4**,** e20.

Benton, R., K. S. Vannice, C. Gomez-Diaz & L. B. Vosshall (2009) Variant ionotropic glutamate receptors as chemosensory receptors in Drosophila. *Cell,* 136**,** 149-62.

Bharucha, K. N., P. Tarr & S. L. Zipursky (2008) A glucagon-like endocrine pathway in Drosophila modulates both lipid and carbohydrate homeostasis. *J Exp Biol,* 211**,** 3103-10.

Carlsson, M. A., M. Diesner, J. Schachtner & D. R. Nassel (2010) Multiple neuropeptides in the Drosophila antennal lobe suggest complex modulatory circuits. *J Comp Neurol,* 518**,** 3359-80.

Chen, Y. & H. Amrein (2017) Ionotropic Receptors Mediate Drosophila Oviposition Preference through Sour Gustatory Receptor Neurons. *Curr Biol,* 27**,** 2741-2750 e4.

Couto, A., M. Alenius & B. J. Dickson (2005) Molecular, anatomical, and functional organization of the Drosophila olfactory system. *Curr Biol,* 15**,** 1535-47.

Cury, K. M., B. Prud'homme & N. Gompel (2019) A short guide to insect oviposition: when, where and how to lay an egg. *J Neurogenet,* 33**,** 75-89.

D'Oliveira Albanus, R., R. J. Siqueira Dalmolin, J. L. Rybarczyk-Filho, M. A. Alves Castro & J. C. Fonseca Moreira (2014) Differential evolutionary constraints in the evolution of chemoreceptors: a murine and human case study. *ScientificWorldJournal,* 2014**,** 696485.

Daniels, R. W., A. J. Rossano, G. T. Macleod & B. Ganetzky (2014) Expression of multiple transgenes from a single construct using viral 2A peptides in Drosophila. *PLoS One,* 9**,** e100637.

Darwin, C. 1859. *On the origin of species by means of natural selection*. Lond.

de Bruyne, M., P. J. Clyne & J. R. Carlson (1999) Odor coding in a model olfactory organ: the Drosophila maxillary palp. *J Neurosci,* 19**,** 4520-32.

Dekker, T., I. Ibba, K. P. Siju, M. C. Stensmyr & B. S. Hansson (2006) Olfactory shifts parallel superspecialism for toxic fruit in Drosophila melanogaster sibling, D. sechellia. *Curr Biol,* 16**,** 101-9.

Dekker, T., S. Revadi, S. Mansourian, S. Ramasamy, S. Lebreton, P. G. Becher, S. Angeli, O. Rota-Stabelli & G. Anfora (2015) Loss of Drosophila pheromone reverses its role in sexual communication in Drosophila suzukii. *Proc Biol Sci,* 282**,** 20143018.

Ding, Y., A. Berrocal, T. Morita, K. D. Longden & D. L. Stern (2016) Natural courtship song variation caused by an intronic retroelement in an ion channel gene. *Nature,* 536**,** 329-32.

Dobritsa, A. A., W. van der Goes van Naters, C. G. Warr, R. A. Steinbrecht & J. R. Carlson (2003) Integrating the molecular and cellular basis of odor coding in the Drosophila antenna. *Neuron,* 37**,** 827-41.

Drosophila 12 Genomes, C., A. G. Clark, M. B. Eisen, D. R. Smith, C. M. Bergman, B. Oliver, T. A. Markow, T. C. Kaufman, M. Kellis, W. Gelbart, V. N. Iyer, D. A. Pollard, T. B. Sackton, A. M. Larracuente, N. D. Singh, J. P. Abad, D. N. Abt, B. Adryan, M. Aguade, H. Akashi, W. W. Anderson, C. F. Aquadro, D. H. Ardell, R. Arguello, C. G. Artieri, D. A. Barbash, D. Barker, P. Barsanti, P. Batterham, S. Batzoglou, D. Begun, A. Bhutkar, E. Blanco, S. A. Bosak, R. K. Bradley, A. D. Brand, M. R. Brent, A. N. Brooks, R. H. Brown, R. K. Butlin, C. Caggese, B. R. Calvi, A. Bernardo de Carvalho, A. Caspi, S. Castrezana, S. E. Celniker, J. L. Chang, C. Chapple, S. Chatterji, A. Chinwalla, A. Civetta, S. W. Clifton, J. M. Comeron, J. C. Costello, J. A. Coyne, J. Daub, R. G. David, A. L. Delcher, K. Delehaunty, C. B. Do, H. Ebling, K. Edwards, T. Eickbush, J. D. Evans, A. Filipski, S. Findeiss, E. Freyhult, L. Fulton, R. Fulton, A. C. Garcia, A. Gardiner, D. A. Garfield, B. E. Garvin, G. Gibson, D. Gilbert, S. Gnerre, J. Godfrey, R. Good, V. Gotea, B. Gravely, A. J. Greenberg, S. Griffiths-Jones, S. Gross, R. Guigo, E. A. Gustafson, W. Haerty, M. W. Hahn, D. L. Halligan, A. L. Halpern, G. M. Halter, M. V. Han, A. Heger, L. Hillier, A. S. Hinrichs, I. Holmes, R. A. Hoskins, M. J. Hubisz, D. Hultmark, M. A.

Huntley, D. B. Jaffe, et al. (2007) Evolution of genes and genomes on the Drosophila phylogeny. *Nature,* 450**,** 203-18.
Dweck, H. K., S. A. Ebrahim, S. Kromann, D. Bown, Y. Hillbur, S. Sachse, B. S. Hansson & M. C. Stensmyr (2013) Olfactory preference for egg laying on citrus substrates in Drosophila. *Curr Biol,* 23**,** 2472-80.
Dweck, H. K., G. J. Talross, W. Wang & J. R. Carlson (2021) Evolutionary shifts in taste coding in the fruit pest Drosophila suzukii. *Elife,* 10.
Dweck, H. K. M., S. A. M. Ebrahim, T. Retzke, V. Grabe, J. Weissflog, A. Svatos, B. S. Hansson & M. Knaden (2018) The Olfactory Logic behind Fruit Odor Preferences in Larval and Adult Drosophila. *Cell Rep,* 23**,** 2524-2531.
Edwards, A. C. & T. F. Mackay (2009) Quantitative trait loci for aggressive behavior in Drosophila melanogaster. *Genetics,* 182**,** 889-97.
Endo, K., T. Aoki, Y. Yoda, K. Kimura & C. Hama (2007) Notch signal organizes the Drosophila olfactory circuitry by diversifying the sensory neuronal lineages. *Nat Neurosci,* 10**,** 153-60.
Endo, K., M. R. Karim, H. Taniguchi, A. Krejci, E. Kinameri, M. Siebert, K. Ito, S. J. Bray & A. W. Moore (2011) Chromatin modification of Notch targets in olfactory receptor neuron diversification. *Nat Neurosci,* 15**,** 224-33.
Enell, L., Y. Hamasaka, A. Kolodziejczyk & D. R. Nassel (2007) gamma-Aminobutyric acid (GABA) signaling components in Drosophila: immunocytochemical localization of GABA(B) receptors in relation to the GABA(A) receptor subunit RDL and a vesicular GABA transporter. *J Comp Neurol,* 505**,** 18-31.
Flint, J. (2003) Analysis of quantitative trait loci that influence animal behavior. *J Neurobiol,* 54**,** 46-77.
Garrigan, D., S. B. Kingan, A. J. Geneva, P. Andolfatto, A. G. Clark, K. R. Thornton & D. C. Presgraves (2012) Genome sequencing reveals complex speciation in the Drosophila simulans clade. *Genome Res,* 22**,** 1499-511.
Golden, J. W. & D. L. Riddle (1984a) ACaenorhabditis elegans dauer-inducing pheromone and an antagonistic component of the food supply. *J Chem Ecol,* 10**,** 1265-80.
--- (1984b) The Caenorhabditis elegans dauer larva: developmental effects of pheromone, food, and temperature. *Dev Biol,* 102**,** 368-78.
Goldman, A. L., W. Van der Goes van Naters, D. Lessing, C. G. Warr & J. R. Carlson (2005) Coexpression of two functional odor receptors in one neuron. *Neuron,* 45**,** 661-6.
Grabe, V., A. Baschwitz, H. K. M. Dweck, S. Lavista-Llanos, B. S. Hansson & S. Sachse (2016) Elucidating the Neuronal Architecture of Olfactory Glomeruli in the Drosophila Antennal Lobe. *Cell Rep,* 16**,** 3401-3413.
Greenspan, R. J. & J. F. Ferveur (2000) Courtship in Drosophila. *Annu Rev Genet,* 34**,** 205-232.
Greenwood, A. K., A. R. Wark, K. Yoshida & C. L. Peichel (2013) Genetic and neural modularity underlie the evolution of schooling behavior in threespine sticklebacks. *Curr Biol,* 23**,** 1884-8.
Guo, S. & J. Kim (2007) Molecular evolution of Drosophila odorant receptor genes. *Mol Biol Evol,* 24**,** 1198-207.
Hansson, B. S. & M. C. Stensmyr (2011) Evolution of insect olfaction. *Neuron,* 72**,** 698-711.
Hardy, J. & A. Singleton (2009) Genomewide association studies and human disease. *N Engl J Med,* 360**,** 1759-68.

Heisenberg, M. (2003) Mushroom body memoir: from maps to models. *Nat Rev Neurosci,* 4**,** 266-75.
Herculano-Houzel, S. (2012) The remarkable, yet not extraordinary, human brain as a scaled-up primate brain and its associated cost. *Proc Natl Acad Sci U S A,* 109 Suppl 1**,** 10661-8.
Hewes, R. S. & P. H. Taghert (2001) Neuropeptides and neuropeptide receptors in the Drosophila melanogaster genome. *Genome Res,* 11**,** 1126-42.
Hu, C. K., R. A. York, H. C. Metz, N. L. Bedford, H. B. Fraser & H. E. Hoekstra (2022) cis-Regulatory changes in locomotor genes are associated with the evolution of burrowing behavior. *Cell Rep,* 38**,** 110360.
Huang, Y. & D. Erezyilmaz (2015) The Genetics of Resistance to Morinda Fruit Toxin During the Postembryonic Stages in Drosophila sechellia. *G3 (Bethesda),* 5**,** 1973-81.
Jallon, J. M. & J. R. David (1987) Variations in Cuticular Hydrocarbons among the Eight Species of the Drosophila Melanogaster Subgroup. *Evolution,* 41**,** 294-302.
Jefferis, G. S., E. C. Marin, R. F. Stocker & L. Luo (2001) Target neuron prespecification in the olfactory map of Drosophila. *Nature,* 414**,** 204-8.
Jefferis, G. S., E. C. Marin, R. J. Watts & L. Luo (2002) Development of neuronal connectivity in Drosophila antennal lobes and mushroom bodies. *Curr Opin Neurobiol,* 12**,** 80-6.
Jefferis, G. S., C. J. Potter, A. M. Chan, E. C. Marin, T. Rohlfing, C. R. Maurer, Jr. & L. Luo (2007) Comprehensive maps of Drosophila higher olfactory centers: spatially segregated fruit and pheromone representation. *Cell,* 128**,** 1187-203.
Jones, W. D., P. Cayirlioglu, I. G. Kadow & L. B. Vosshall (2007) Two chemosensory receptors together mediate carbon dioxide detection in Drosophila. *Nature,* 445**,** 86-90.
Jordan, K. W., T. J. Morgan & T. F. Mackay (2006) Quantitative trait loci for locomotor behavior in Drosophila melanogaster. *Genetics,* 174**,** 271-84.
Joseph, R. M. & U. Heberlein (2012) Tissue-specific activation of a single gustatory receptor produces opposing behavioral responses in Drosophila. *Genetics,* 192**,** 521-32.
Kallman, B. R., H. Kim & K. Scott (2015) Excitation and inhibition onto central courtship neurons biases Drosophila mate choice. *Elife,* 4**,** e11188.
Karageorgi, M., L. B. Bracker, S. Lebreton, C. Minervino, M. Cavey, K. P. Siju, I. C. Grunwald Kadow, N. Gompel & B. Prud'homme (2017) Evolution of Multiple Sensory Systems Drives Novel Egg-Laying Behavior in the Fruit Pest Drosophila suzukii. *Curr Biol,* 27**,** 847-853.
Keesey, I. W., M. Knaden & B. S. Hansson (2015) Olfactory specialization in Drosophila suzukii supports an ecological shift in host preference from rotten to fresh fruit. *J Chem Ecol,* 41**,** 121-8.
Keesey, I. W., J. Zhang, A. Depetris-Chauvin, G. F. Obiero, A. Gupta, N. Gupta, H. Vogel, M. Knaden & B. S. Hansson (2022) Functional olfactory evolution in Drosophila suzukii and the subgenus Sophophora. *iScience,* 25**,** 104212.
Kim, D. R., J. L. Snell, G. C. Ewing & J. O'Reardon (2015) Neuromodulation and antenatal depression: a review. *Neuropsychiatr Dis Treat,* 11**,** 975-82.
Kim, S. M., C. Y. Su & J. W. Wang (2017) Neuromodulation of Innate Behaviors in Drosophila. *Annu Rev Neurosci,* 40**,** 327-348.

Ko, K. I., C. M. Root, S. A. Lindsay, O. A. Zaninovich, A. K. Shepherd, S. A. Wasserman, S. M. Kim & J. W. Wang (2015) Starvation promotes concerted modulation of appetitive olfactory behavior via parallel neuromodulatory circuits. *Elife,* 4.

Kurtovic, A., A. Widmer & B. J. Dickson (2007) A single class of olfactory neurons mediates behavioural responses to a Drosophila sex pheromone. *Nature,* 446**,** 542-6.

Kwon, J. Y., A. Dahanukar, L. A. Weiss & J. R. Carlson (2007) The molecular basis of CO2 reception in Drosophila. *Proc Natl Acad Sci U S A,* 104**,** 3574-8.

Lachaise, D. & J. F. Silvain (2004) How two Afrotropical endemics made two cosmopolitan human commensals: the Drosophila melanogaster-D. simulans palaeogeographic riddle. *Genetica,* 120**,** 17-39.

Lavista-Llanos, S., A. Svatos, M. Kai, T. Riemensperger, S. Birman, M. C. Stensmyr & B. S. Hansson (2014) Dopamine drives Drosophila sechellia adaptation to its toxic host. *Elife,* 3.

Lee, K. S., S. H. Hong, A. K. Kim, S. K. Ju, O. Y. Kwon & K. Yu (2009) Processed short neuropeptide F peptides regulate growth through the ERK-insulin pathway in Drosophila melanogaster. *FEBS Lett,* 583**,** 2573-7.

Lee, K. S., O. Y. Kwon, J. H. Lee, K. Kwon, K. J. Min, S. A. Jung, A. K. Kim, K. H. You, M. Tatar & K. Yu (2008) Drosophila short neuropeptide F signalling regulates growth by ERK-mediated insulin signalling. *Nat Cell Biol,* 10**,** 468-75.

Lee, K. S., K. H. You, J. K. Choo, Y. M. Han & K. Yu (2004) Drosophila short neuropeptide F regulates food intake and body size. *J Biol Chem,* 279**,** 50781-9.

Lee, T., A. Lee & L. Luo (1999) Development of the Drosophila mushroom bodies: sequential generation of three distinct types of neurons from a neuroblast. *Development,* 126**,** 4065-76.

Li, B., R. Predel, S. Neupert, F. Hauser, Y. Tanaka, G. Cazzamali, M. Williamson, Y. Arakane, P. Verleyen, L. Schoofs, J. Schachtner, C. J. Grimmelikhuijzen & Y. Park (2008) Genomics, transcriptomics, and peptidomics of neuropeptides and protein hormones in the red flour beetle Tribolium castaneum. *Genome Res,* 18**,** 113-22.

Li, X., W. Li, H. Wang, D. L. Bayley, J. Cao, D. R. Reed, A. A. Bachmanov, L. Huang, V. Legrand-Defretin, G. K. Beauchamp & J. G. Brand (2006) Cats lack a sweet taste receptor. *J Nutr,* 136**,** 1932S-1934S.

Lin, C. C. & C. J. Potter (2015) Re-Classification of Drosophila melanogaster Trichoid and Intermediate Sensilla Using Fluorescence-Guided Single Sensillum Recording. *PLoS One,* 10**,** e0139675.

Linz, J., A. Baschwitz, A. Strutz, H. K. Dweck, S. Sachse, B. S. Hansson & M. C. Stensmyr (2013) Host plant-driven sensory specialization in Drosophila erecta. *Proc Biol Sci,* 280**,** 20130626.

Liu, W., X. Liang, J. Gong, Z. Yang, Y. H. Zhang, J. X. Zhang & Y. Rao (2011) Social regulation of aggression by pheromonal activation of Or65a olfactory neurons in Drosophila. *Nat Neurosci,* 14**,** 896-902.

Lu, B., A. LaMora, Y. Sun, M. J. Welsh & Y. Ben-Shahar (2012) ppk23-Dependent chemosensory functions contribute to courtship behavior in Drosophila melanogaster. *PLoS Genet,* 8**,** e1002587.

Mackay, T. F., S. Richards, E. A. Stone, A. Barbadilla, J. F. Ayroles, D. Zhu, S. Casillas, Y. Han, M. M. Magwire, J. M. Cridland, M. F. Richardson, R. R. Anholt, M. Barron, C. Bess, K. P. Blankenburg, M. A. Carbone, D. Castellano, L. Chaboub, L. Duncan, Z. Harris, M. Javaid, J. C. Jayaseelan, S. N. Jhangiani, K. W. Jordan, F. Lara, F. Lawrence, S. L. Lee, P. Librado, R. S. Linheiro, R. F. Lyman, A. J. Mackey, M. Munidasa, D. M. Muzny, L. Nazareth, I. Newsham, L. Perales, L. L. Pu, C. Qu, M. Ramia, J. G. Reid, S. M. Rollmann, J. Rozas, N. Saada, L. Turlapati, K. C. Worley, Y. Q. Wu, A. Yamamoto, Y. Zhu, C. M. Bergman, K. R. Thornton, D. Mittelman & R. A. Gibbs (2012) The Drosophila melanogaster Genetic Reference Panel. *Nature,* 482**,** 173-8.

Mansourian, S., A. Enjin, E. V. Jirle, V. Ramesh, G. Rehermann, P. G. Becher, J. E. Pool & M. C. Stensmyr (2018) Wild African Drosophila melanogaster Are Seasonal Specialists on Marula Fruit. *Curr Biol,* 28**,** 3960-3968 e3.

Markow, T. A., S. Beall & L. M. Matzkin (2009) Egg size, embryonic development time and ovoviviparity in Drosophila species. *J Evol Biol,* 22**,** 430-4.

Martelli, C., U. Pech, S. Kobbenbring, D. Pauls, B. Bahl, M. V. Sommer, A. Pooryasin, J. Barth, C. W. P. Arias, C. Vassiliou, A. J. F. Luna, H. Poppinga, F. G. Richter, C. Wegener, A. Fiala & T. Riemensperger (2017) SIFamide Translates Hunger Signals into Appetitive and Feeding Behavior in Drosophila. *Cell Reports,* 20**,** 464-478.

Mattheis, J. P. & R. G. Roberts (1992) Identification of geosmin as a volatile metabolite of Penicillium expansum. *Appl Environ Microbiol,* 58**,** 3170-2.

Matzkin, L. M., T. D. Watts, B. G. Bitler, C. A. Machado & T. A. Markow (2006) Functional genomics of cactus host shifts in Drosophila mojavensis. *Mol Ecol,* 15**,** 4635-43.

McBride, C. S. (2007) Rapid evolution of smell and taste receptor genes during host specialization in Drosophila sechellia. *Proc Natl Acad Sci U S A,* 104**,** 4996-5001.

McBride, C. S., J. R. Arguello & B. C. O'Meara (2007) Five Drosophila genomes reveal nonneutral evolution and the signature of host specialization in the chemoreceptor superfamily. *Genetics,* 177**,** 1395-416.

McGrath, P. T., Y. Xu, M. Ailion, J. L. Garrison, R. A. Butcher & C. I. Bargmann (2011) Parallel evolution of domesticated Caenorhabditis species targets pheromone receptor genes. *Nature,* 477**,** 321-5.

Metz, H. C., N. L. Bedford, Y. L. Pan & H. E. Hoekstra (2017) Evolution and Genetics of Precocious Burrowing Behavior in Peromyscus Mice. *Curr Biol,* 27**,** 3837-3845 e3.

Nassel, D. R. & A. M. Winther (2010) Drosophila neuropeptides in regulation of physiology and behavior. *Prog Neurobiol,* 92**,** 42-104.

Niimura, Y. (2009) Evolutionary dynamics of olfactory receptor genes in chordates: interaction between environments and genomic contents. *Hum Genomics,* 4**,** 107-18.

Niimura, Y., A. Matsui & K. Touhara (2014) Extreme expansion of the olfactory receptor gene repertoire in African elephants and evolutionary dynamics of orthologous gene groups in 13 placental mammals. *Genome Research,* 24**,** 1485-1496.

Prieto-Godino, L. L., R. Rytz, S. Cruchet, B. Bargeton, L. Abuin, A. F. Silbering, V. Ruta, M. Dal Peraro & R. Benton (2017) Evolution of Acid-Sensing Olfactory Circuits in Drosophilids. *Neuron,* 93**,** 661-676 e6.

Prieto-Godino, L. L., A. F. Silbering, M. A. Khallaf, S. Cruchet, K. Bojkowska, S. Pradervand, B. S. Hansson, M. Knaden & R. Benton (2020) Functional integration of "undead" neurons in the olfactory system. *Sci Adv,* 6**,** eaaz7238.

Ramdya, P. & R. Benton (2010) Evolving olfactory systems on the fly. *Trends Genet,* 26**,** 307-16.

Robertson, H. M. (2019) Molecular Evolution of the Major Arthropod Chemoreceptor Gene Families. *Annu Rev Entomol,* 64**,** 227-242.

Robertson, H. M. & K. W. Wanner (2006) The chemoreceptor superfamily in the honey bee, Apis mellifera: expansion of the odorant, but not gustatory, receptor family. *Genome Res,* 16**,** 1395-403.

Roller, L., N. Yamanaka, K. Watanabe, I. Daubnerova, D. Zitnan, H. Kataoka & Y. Tanaka (2008) The unique evolution of neuropeptide genes in the silkworm Bombyx mori. *Insect Biochem Mol Biol,* 38**,** 1147-57.

Root, C. M., K. I. Ko, A. Jafari & J. W. Wang (2011) Presynaptic facilitation by neuropeptide signaling mediates odor-driven food search. *Cell,* 145**,** 133-44.

Root, C. M., K. Masuyama, D. S. Green, L. E. Enell, D. R. Nassel, C. H. Lee & J. W. Wang (2008) A presynaptic gain control mechanism fine-tunes olfactory behavior. *Neuron,* 59**,** 311-21.

Rudolf, V. H. & M. O. Rodel (2005) Oviposition site selection in a complex and variable environment: the role of habitat quality and conspecific cues. *Oecologia,* 142**,** 316-25.

Rytz, R., V. Croset & R. Benton (2013) Ionotropic receptors (IRs): chemosensory ionotropic glutamate receptors in Drosophila and beyond. *Insect Biochem Mol Biol,* 43**,** 888-97.

Sanchez-Gracia, A., F. G. Vieira & J. Rozas (2009) Molecular evolution of the major chemosensory gene families in insects. *Heredity (Edinb),* 103**,** 208-16.

Schlegel, P., A. S. Bates, T. Sturner, S. R. Jagannathan, N. Drummond, J. Hsu, L. Serratosa Capdevila, A. Javier, E. C. Marin, A. Barth-Maron, I. F. Tamimi, F. Li, G. M. Rubin, S. M. Plaza, M. Costa & G. Jefferis (2021) Information flow, cell types and stereotypy in a full olfactory connectome. *Elife,* 10.

Schultzhaus, J. N., S. Saleem, H. Iftikhar & G. E. Carney (2017) The role of the Drosophila lateral horn in olfactory information processing and behavioral response. *J Insect Physiol,* 98**,** 29-37.

Seeholzer, L. F., M. Seppo, D. L. Stern & V. Ruta (2018) Evolution of a central neural circuit underlies Drosophila mate preferences. *Nature,* 559**,** 564-569.

Semmelhack, J. L. & J. W. Wang (2009) Select Drosophila glomeruli mediate innate olfactory attraction and aversion. *Nature,* 459**,** 218-23.

Shiao, M. S., J. M. Chang, W. L. Fan, M. Y. Lu, C. Notredame, S. Fang, R. Kondo & W. H. Li (2015) Expression Divergence of Chemosensory Genes between Drosophila sechellia and Its Sibling Species and Its Implications for Host Shift. *Genome Biol Evol,* 7**,** 2843-58.

Shiraiwa, T. (2008) Multimodal chemosensory integration through the maxillary palp in Drosophila. *PLoS One,* 3**,** e2191.

Silbering, A. F., R. Bell, C. G. Galizia & R. Benton (2012) Calcium imaging of odor-evoked responses in the Drosophila antennal lobe. *J Vis Exp*.

Stathakis, D. G., D. Y. Burton, W. E. McIvor, S. Krishnakumar, T. R. Wright & J. M. O'Donnell (1999) The catecholamines up (Catsup) protein of Drosophila melanogaster functions as a negative regulator of tyrosine hydroxylase activity. *Genetics,* 153**,** 361-82.

Stensmyr, M. C., T. Dekker & B. S. Hansson (2003) Evolution of the olfactory code in the Drosophila melanogaster subgroup. *Proc Biol Sci,* 270**,** 2333-40.

Stensmyr, M. C., H. K. Dweck, A. Farhan, I. Ibba, A. Strutz, L. Mukunda, J. Linz, V. Grabe, K. Steck, S. Lavista-Llanos, D. Wicher, S. Sachse, M. Knaden, P. G. Becher, Y. Seki & B. S. Hansson (2012) A conserved dedicated olfactory circuit for detecting harmful microbes in Drosophila. *Cell,* 151**,** 1345-57.

Stern, D. L. (2014) Identification of loci that cause phenotypic variation in diverse species with the reciprocal hemizygosity test. *Trends in Genetics,* 30**,** 547-554.

Su, C. Y. & J. W. Wang (2014) Modulation of neural circuits: how stimulus context shapes innate behavior in Drosophila. *Curr Opin Neurobiol,* 29**,** 9-16.

Symonds, M. R. & B. Wertheim (2005) The mode of evolution of aggregation pheromones in Drosophila species. *J Evol Biol,* 18**,** 1253-63.

Tabor, H. K., N. J. Risch & R. M. Myers (2002) Candidate-gene approaches for studying complex genetic traits: practical considerations. *Nat Rev Genet,* 3**,** 391-7.

Vieira, F. G. & J. Rozas (2011) Comparative genomics of the odorant-binding and chemosensory protein gene families across the Arthropoda: origin and evolutionary history of the chemosensory system. *Genome Biol Evol,* 3**,** 476-90.

Vosshall, L. B., H. Amrein, P. S. Morozov, A. Rzhetsky & R. Axel (1999) A spatial map of olfactory receptor expression in the Drosophila antenna. *Cell,* 96**,** 725-36.

Vosshall, L. B. & R. F. Stocker (2007) Molecular architecture of smell and taste in Drosophila. *Annu Rev Neurosci,* 30**,** 505-33.

Wang, G. H. & L. M. Wang (2019) Recent advances in the neural regulation of feeding behavior in adult Drosophila. *J Zhejiang Univ Sci B,* 20**,** 541-549.

Wang, Y., F. Wang, R. Wang, P. Zhao & Q. Xia (2015) 2A self-cleaving peptide-based multi-gene expression system in the silkworm Bombyx mori. *Sci Rep,* 5**,** 16273.

Wark, A. R., A. K. Greenwood, E. M. Taylor, K. Yoshida & C. L. Peichel (2011) Heritable differences in schooling behavior among threespine stickleback populations revealed by a novel assay. *PLoS One,* 6**,** e18316.

Wark, A. R., M. G. Mills, L. H. Dang, Y. F. Chan, F. C. Jones, S. D. Brady, D. M. Absher, J. Grimwood, J. Schmutz, R. M. Myers, D. M. Kingsley & C. L. Peichel (2012) Genetic architecture of variation in the lateral line sensory system of threespine sticklebacks. *G3 (Bethesda),* 2**,** 1047-56.

Watanabe, K., Y. Kanaoka, S. Mizutani, H. Uchiyama, S. Yajima, M. Watada, T. Uemura & Y. Hattori (2019) Interspecies Comparative Analyses Reveal Distinct Carbohydrate-Responsive Systems among Drosophila Species. *Cell Rep,* 28**,** 2594-2607 e7.

Weber, J. N., B. K. Peterson & H. E. Hoekstra (2013) Discrete genetic modules are responsible for complex burrow evolution in Peromyscus mice. *Nature,* 493**,** 402-5.

Wu, S. T., J. Y. Chen, V. Martin, R. Ng, Y. Zhang, D. Grover, R. J. Greenspan, J. Aljadeff & C. Y. Su (2022) Valence opponency in peripheral olfactory processing. *Proc Natl Acad Sci U S A,* 119.

Yassin, A., V. Debat, H. Bastide, N. Gidaszewski, J. R. David & J. E. Pool (2016) Recurrent specialization on a toxic fruit in an island Drosophila population. *Proc Natl Acad Sci U S A,* 113**,** 4771-6.

Yew, J. Y., Y. Wang, N. Barteneva, S. Dikler, K. K. Kutz-Naber, L. Li & E. A. Kravitz (2009) Analysis of neuropeptide expression and localization in adult drosophila melanogaster central nervous system by affinity cell-capture mass spectrometry. *J Proteome Res,* 8**,** 1271-84.

Zandawala, M., M. E. Yurgel, M. J. Texada, S. Liao, K. F. Rewitz, A. C. Keene & D. R. Nassel (2018) Modulation of Drosophila post-feeding physiology and behavior by the neuropeptide leucokinin. *PLoS Genet,* 14**,** e1007767.

Zhao, Z. & C. S. McBride (2020) Evolution of olfactory circuits in insects. *J Comp Physiol A Neuroethol Sens Neural Behav Physiol,* 206**,** 353-367.

Ziegler, A. B., M. Berthelot-Grosjean & Y. Grosjean (2013) The smell of love in Drosophila. *Front Physiol,* 4**,** 72.

Zwarts, L., L. Vanden Broeck, E. Cappuyns, J. F. Ayroles, M. M. Magwire, V. Vulsteke, J. Clements, T. F. Mackay & P. Callaerts (2015) The genetic basis of natural variation in mushroom body size in Drosophila melanogaster. *Nat Commun,* 6**,** 10115.